Tectonics, Climate Change, and Landscape Evolution in the southern Sierra Nevada, California

2003 Pacific Cell Friends of the Pleistocene Field Trip
Sequoia and Kings Canyon
October 3 – 5, 2003

Tectonics, Climate Change, and Landscape Evolution in the Southern Sierra Nevada, California

Friends of the Pleistocene Pacific Cell

2003 Fall Field Trip
October 3-5, 2003

Field Trip Guidebook

Guidebook organized and edited by:
Greg Stock

Trip leaders:
Greg Stock, *University of California, Santa Cruz*
William Bull, *University of Arizona*
Gary Weismann, *Michigan State University*
Anthony Caprio, *National Park Service*
Nate Stephenson, *U. S. Geological Survey*
John Wakabayashi, *Consulting geologist*
Bud Burke, *Humboldt State University*
John Tinsely, *U. S. Geological Survey*

Other contributors:
Allen Glazner, *University of North Carolina, Chapel Hill*
Robert Anderson, *University of Colorado, Boulder*
Robert Finkel, *Lawrence Livermore National Laboratory*
James Zachos, *University of California, Santa Cruz*
George Bennett, *Michigan State University*
Graham Fogg, *University of California, Davis*

Sponsored by:
Department of Earth Sciences
University of California, Santa Cruz

Frontispiece. The 1864 field party of the California Geological Survey. From left to right: James T. Gardiner, Richard D. Cotter, William H. Brewer, and Clarence King.

TABLE OF CONTENTS

List of Figures …….. **vi**

Introduction, acknowledgments, and editorial notes ……. **1**

Important items of note ……. **5**

Road log: **Gathering of Friends:**
Thursday, October 2, Visalia to Horse Creek
(Directions to Thursday night campsite) ……. **10**
Day 1:
Friday, October 3, Horse Creek to Crystal Cave …… **11**
Day 2:
Saturday, October 4, Redwood Canyon to Boyden Cave …….. **20**
Day 3:
Sunday, October 5, Hume Lake to the western foothills …… **26**

Appendices: **Appendix 1:**
Wakabayashi, J., and Stock, G. M., 2003, Overview of the Cenozoic geologic history of the Sierra Nevada. …….. **31**

Appendix 2:
Weissmann, G. S., Bennett, G. L., V, and Fogg, G. E., 2003, Stratigraphic sequences of the Kings River alluvial fan formed in response to Sierra Nevada glacial cyclicity. …… **41**

Appendix 3:
Stock, G. M., 2003, Cave formation, geochronology, and rates of river incision in a southern Sierra Nevada stream canyon: Geomorphic studies of Crystal Cave……. **51**

Appendix 4A:
Tinsley, J. C., 2003, Lilburn Cave and the karst of Redwood Canyon: A fleeting overview…….. **57**

Appendix 4B:
Caprio, T., 2003, Holocene fire and climate history from Sierra Nevada tree rings …….. **62**

Appendix 4C:
Stephenson, N. L., 2003, Giant Sequoia ecology and recent glacial retreat: Evidence for Holocene climate change in the southern Sierra Nevada…….. **73**

Appendix 5:
Glazner, A. F., 2003, Volcanic evidence for Pliocene delamination of the Sierra Nevada batholithic root……. **79**

Appendix 6:
Stock, G. M., Anderson, R. S., and Finkel, R. C., 2003, Late Cenozoic evolution of southern Sierra Nevada topography from cosmogenic dating of cave sediments…… **84**

Appendix 7:
Stock, G. M., and Anderson, R. S., 2003, Cave-derived river incision rates from the South Fork Kings River: Complex river response to tectonic and climatic forcing…….. **94**

Appendix 8:
Bull, W. B., 2003, Guide to Sierra Nevada lichenometry……. **100**

Appendix 9A:
Burke, R.M., 2003, A note on the glacial history of the Sequoia – Kings Canyon National Parks region……. **122**

Appendix 9B:
Stock, G. M., and Zachos, J. Z., 2003, Speleothem records of glacial-interglacial cycles in the Sierra Nevada, California…… **128**

Appendix 10:
Stock, G. M., 2003, Buried topography and lack of Tertiary strata in the southern Sierra Nevada foothills……. **135**

National Park Service fee waiver letter……. **139**

LIST OF FIGURES

Road log:
Figure 1: Map of Sequoia and Kings Canyon National Park …… **8**
Figure 2: Field trip route map …… **9**
Figure 3: Range map of Coast Redwood and Giant Sequoia trees……
Figure 4: Map of Crescent Meadow area and High Sierra Trail……... **14**
Figure 5: Glacial geology of the Wolverton and Lodgepole vicinity .. **17**
Figure 6: Glacial termini positions in the southern Sierra Nevada ….. **17**
Figure 7: Canyons of the Middle and South Forks of the Kings River as seen from Junction View …….. **23**
Figure 8: Kaweah and Kings river hydrographs of the January 1,1997 floods …….…….. **27**

Appendix 1:
Figure 1-1: Generalized topography of the Sierra Nevada ……. **32**
Figure 1-2: Paleorelief of the northern and central Sierra Nevada ….. **34**
Figure 1-3: Accumulation rates in the San Joaquin basin …… **35**
Figure 1-4: Generalized topography of the Sierra Nevada prior to late Cenozoic uplift …….. **36**
Figure 1-5: Methods used to estimate late Cenozoic uplift ……
Figure 1-6: Results of U/Th(He) dating of apatites …….… **38**

Appendix 2:
Figure 2-1: Sequence cycles on a stream-dominated alluvial fan …… **43**
Figure 2-2: DEM model for the upper Kings River alluvial fan ……. **44**
Figure 2-3: Stratigraphic column for the Kings River alluvial fan …. **45**
Figure 2-4: Interpreted soil survey of the Kings River alluvial fan …. **46**
Figure 2-5: Cross-sections through the Kings River alluvial fan …… **47**
Figure 2-6: Detail of the soil survey around the incised valley fill …. **47**
Figure 2-7: Block diagram showing the sequence surfaces of the upper Kings River alluvial fan …… **48**

Appendix 3:
Figure 3-1: Plan view of Crystal Cave …… **52**
Figure 3-2: Cave profiles and cave-derived rates of incision for Cascade and Yucca Creeks …….. **55**

Appendix 4A:
Figure 4A-1: Plan and profile view of Lilburn Cave ……. **59**
Figure 4A-2: Photographs of Big Spring during flush …….. **60**
Figure 4A-3: Hydrographs of Big Spring showing ebb and flow cycles …….. **62**

Appendix 4B:
Figure 4B-1: Common signal in Sequoia chronologies……. **63**
Figure 4B-2: Typical high elevation growth form of old trees…….. **63**
Figure 4B-3: Foxtail chronology characteristics at differing elevations **64**
Figure 4B-4: Inferred long-term fluctuations in temperature and precipitation…….. **64**
Figure 4B-5: Decline in foxtail stands on the west slope of the Sierra Nevada…….. **65**

Figure 4B-6: Response of tree ring chronologies to monthly MET station data……. **65**
Figure 4B-7: Tree ring data and climate calibration…… **66**
Figure 4B-8: Reconstructed flow of the San Joaquin River from 942 to 1989 A.D…… **66**
Figure 4B-9: Sequoia ring widths vs. August PDSI……... **66**
Figure 4B-10: Foxtail frost rings……. **67**
Figure 4B-11: Foxtail snag in the upper Mineral King Valley, Sequoia National Park……. **67**
Figure 4B-12: Frost ring chronologies…… **67**
Figure 4B-13: Fire scar dates, Sherman Tree Parking Lot slab…….. **68**
Figure 4B-14: Fire event chronology from the Atwell Grove…… **68**
Figure 4B-15: Change in fire frequency over time……. **69**
Figure 4B-16: Long-term fire and climate patterns…… **69**
Figure 4B-17: Comparison of fire events with estimates of past precipitation…… **70**
Figure 4B-18: Inverse relationship between fire and elevation…….. **71**
Figure 4B-19: Master fire chronologies…….. **71**
Figure 4B-20: Fire climate relationships……. **71**
Figure 4B-21: Managed vs. non-managed fire area …… **71**

Appendix 4C: **Figure 4C-1:** Pollen percentage diagram for Log Meadow Core 1…. **74**
Figure 4C-2: Example of vegetation change due to fire exclusion…. **75**
Figure 4C-3: Recent retreat of the Goddard Glacier……... **77**
Figure 4C-4: Recent retreat of the Darwin Glacier……. **78**

Appendix 5: **Figure 5-1:** Distribution of volcanism in the southern Sierra Nevada region as a function of time…… **80**
Figure 5-2: Potassium index (K1) plotted as a function of time……. **81**

Appendix 6: **Figure 6-1:** Geologic and topographic setting of the central and southern Sierra Nevada…….. **85**
Figure 6-2: River incision history from Sierra Nevada caves…… **87**
Figure 6-3: Reproducibility results for cosmogenic burial dating…. **88**
Figure 6-4: Cave-derived river incision rates for the South Fork Kings Canyon……. **90**

Appendix 7: **Figure 7-1:** View out of a cave entrance high in a cliff above the South Fork Kings River……. **95**
Figure 7-2: Response of the South Fork Kings River to late Cenozoic tectonic and climatic events…….. **97**

Appendix 8: **Figure 8-1:** California location map showing locations of lichenometry sites……. **100**
Figure 8-2: A 1000 year-old lichen growing at the Roaring River site **102**
Figure 8-3: Lichens growing on a rockfall block in the Seaward Kaikoura Range, New Zealand…… **103**
Figure 8-4: Evaluating the quality of a large *Acarospora chlorophana* at the Roaring River site…….. **104**
Figure 8-5: Example of calibration procedure to determine lichen growth rates……. **107**
Figure 8-6: Attempting to date a young moraine at Cirque Peak…… **109**
Figure 8-7: Seismic shaking controls on the formation of moraines.. **110**
Figure 8-8: Frequency distribution of *Rhizocarpon subgenus Rhizocarpon* sizes on the blocks of the youngest Karkerieppe glacial moraine……. **111**
Figure 8-9: Univariate scattergram of *Lecidea atrobrunnea* at the Chickenfoot moraine lichenomtery site…… **112**
Figure 8-10: Histograms of the sizes of the largest *Acarospora chlorophana* lichens on blocks that have fallen off of a volcanic neck……. **113**
Figure 8-11: Times of rockfalls for 10 Sierra Nevada sites…….. **114**
Figure 8-12: Kings Canyon peaks in lichen size distributions……. **116**
Figure 8-13: Variation of density of lichen size measurements…… **117**
Figure 8-14: Distribution of largest lichen maximum diameters on rockfall blocks at the Roaring River site……. **118**

Appendix 9: **Figure 9-1:** Map of maximum extent of Tioga ice in the southern Sierra Nevada…… **125**
Figure 9-2: Sierra Nevada speleothems used to investigate late Pleistocene glacial-interglacial transitions…… **129**
Figure 9-3: Microclimate from two Sierra Nevada caves…….. **131**
Figure 9-4: Stable isotope plots for Sierra Nevada speleothems…… **133**

Appendix 10: **Figure 10-1**: Stratigraphic and geomorphic setting of the south-western Sierra Nevada foothills…….. **136**
Figure 10-2: Expanded view of buried topography in the vicinity of the Kings and Kaweah rivers…….. **137**

Then it seemed to me the Sierra should be called not the Nevada or Snowy Range, but the Range of Light. And after ten years spent in the heart of it, rejoicing and wondering, bathing in the glorious floods of light, seeing the sunbursts of morning among the icy peaks, the noonday radiance on the trees and rocks and snow, the flush of the alpenglow, and a thousand dashing waterfalls with their marvelous abundance of irised spray, it still seems to me above all others the Range of Light, the most divinely beautiful of all the mountain chains I have seen.

- John Muir, The Mountains of California

INTRODUCTION

Welcome to the 2003 Pacific Cell Friends of the Pleistocene field trip! This year's trip brings us to the southern Sierra Nevada, into the dramatic landscapes and stunning scenery of Sequoia and Kings Canyon National Parks and the newly created Giant Sequoia National Monument. These public lands preserve the world's largest giant sequoia grove, one of the deepest canyons in North America, and the highest peak in the lower 48 states. Many of these southern Sierra Nevada icons will be topics for discussion as we explore the tectonic and climatic events that have helped to shape this rugged landscape.

The southern Sierra Nevada has attracted the attention and admiration of geologists for well over a century, and the history of geologic study here includes many preeminent geologists. In fact, this year's trip will be following rather closely the route taken by the first scientific expedition into this part of the Sierra Nevada, the 1864 Whitney Survey of the Geological Survey of California (Frontispiece). The survey party, backed by the Director of the Survey, Josiah Whitney, included William Brewer, party chief, Charles Hoffman, topographer, James Gardiner, geologist, Clarence King, geologist (later to become the first Director of the U. S. Geological Survey), and Richard Cotter, packer. During the 1864 expedition, the party explored much of the southern Sierra Nevada and discovered, mapped, and named many of the loftier peaks in the range, including Mount Brewer, Mount Gardiner, Mount Clarence King, Mount Williamson, Mount Tyndall, and Mount Whitney (Farquhar, 1965). Since this early exploration of the range, many prominent geologists have focused their study on this region, including John Muir, Joseph LeConte, G.K. Gilbert, Waldemar Lindgren, Elliot Blackwelder, and Francois Matthes. Matthes in particular was a great observer of the southern Sierra Nevada landscape, and worked diligently to convey his findings to visitors of Sequoia National Park (e.g., Matthes, 1956; 1965)

More recently, significant advancements in our understanding of the geomorphic evolution of the southern Sierra Nevada were made by the pioneering work of, among others, Clyde Wahrhaftig (e.g., Wahrhaftig, 1965, Bateman and Wahrhaftig, 1966), Brent Dalrymple (Dalrymple, 1964), and King Huber. Huber used tilted volcanic flows along the San Joaquin River to estimate late Cenozoic crestal uplift of the range (Huber, 1981). He deduced some 1.5 to 2 km of crestal uplift in the late Cenozoic, and concluded that uplift was underway by 10 Ma but had increased by 3 Ma. This carefully presented work has become the standard reference on Late Cenozoic uplift of the Sierra Nevada. Since that time, additional lines of evidence have emerged supporting 1.5-2.5 km of crestal uplift via westward tilting in the last ~5 Ma (e.g., Unruh, 1991; Wakabayashi and Sawyer, 2001).

The anomalous late Cenozoic uplift event has received much attention from those wishing to explain the driving mechanisms behind it. In the past decade, both climatically and tectonically based uplift mechanisms have been proposed (e.g., Small and Anderson, 1995; Ducea and Saleeby, 1996). Pliocene delamination of the dense batholithic root from beneath the range crest is an idea supported by a wide variety of geologic evidence (e.g.,

Wernicke et al., 1996; Ducea and Saleeby, 1998; Manley et al., 2000; Farmer et al., 2002) and links many geologic observations of the southern Sierra Nevada. At Stop 5 we will examine a potassic basalt thought to relate to the delamination event which will serve as a backdrop for discussion of this intriguing hypothesis. At the final stop of the trip, Stop 10, we'll discuss the topographic implications of such a "mantle drip" below the western foothills.

Research in the past decade has also advanced our understanding of the late Cenozoic topographic history of the southern Sierra Nevada, but it has also raised fundamental new questions. U/Th(He) dating of paleotopography was interpreted to suggest that many of the modern Sierra river canyons were in place as early as 60-80 Ma, and that the topographic relief of the range had decreased since that time, with little or no Cenozoic uplift (House et al., 1998; 2001). This controversial work has spurred renewed interest in the age of Sierra Nevada river canyons and in the topographic evolution of the range. Wakabayashi and Sawyer (2001) examined late Cenozoic volcanic deposits in the northern and central parts of the range and concluded that the Sierra Nevada may well represent a tale of two uplifts, with major Cretaceous topography decaying throughout the early and mid-Cenozoic, followed by renewed uplift in the Late Cenozoic. However, debate on this issue continues, particularly for the southern Sierra Nevada, where widespread late Cenozoic deposits are lacking. During three stops, Stops 1, 6, and 7, we will attempt to summarize the late Cenozoic topographic history of the southern Sierra Nevada.

Stops 3, 6, and 7 will highlight the often-overlooked cave and karst of the southern Sierra Nevada. During these stops we'll present new rates of river incision based on dated cave deposits. The cave records serve to link many of the data sets and conceptual models put forth regarding the topographic evolution of the Sierra Nevada, but also add intriguing detail not resolvable in previous studies. We will visit an extensive cave during Stop 3.

Landscape evolution in the southern Sierra Nevada is not driven by tectonics alone. Several stops on this year's trip will deal with archives of Quaternary climate change in the southern Sierra Nevada. Stops 2, 4, and 9 will cover the present state of knowledge of Pleistocene glaciation, and will also present new archives of Sierra glacial history, including sequence stratigraphy of alluvial fans in the Central Valley, speleothems, and repeat photography. Stop 4 will also cover Holocene vegetation records, primarily those contained within meadow cores and tree rings, and discuss implications for Holocene climate change. Finally, new advancements in dating of climatic and geomorphic events using lichenometry, presented at Stop 8, provide an important new tool for constraining these events. These diverse archives document significant Quaternary climate variability experienced by the southern Sierra Nevada, and highlight the importance of this variability on rates of geomorphic processes.

The rich history of pioneering work by previous geologists laid the groundwork for much of the research presented during this field trip. While most would agree that now is an exciting time to be studying the Sierra Nevada, perhaps it has always been so. The Sierra Nevada continues to inspire and challenge those who study it - this field trip provides an opportunity to do just that.

Greg Stock
Santa Cruz, CA
September, 2003

ACKNOWLEDGEMENTS

Many people were instrumental in making this trip possible. First of all, thanks go to the trip leaders and guidebook contributors, especially those that traveled across the country on their own nickel, for sharing the results of their work. Organizing an FOP trip entirely within National Parks and Monuments proved a bit challenging, and I thank Joel Despain, Erik Oberg, and Annie Esperanza of Sequoia and Kings Canyon National Parks for encouraging the trip and removing (or at least lowering) many bureaucratic hurdles. Mary Allison and Jennifer White of Sequoia National Forest played an equally valuable role. Abby and Jay Snow of the Sequoia Natural History Association made possible the visit to Crystal Cave. Phil Deffenbaugh and Matt Murphy of the U.S. Army Corps of Engineers provided group camping at Horse Creek. Thanks to Jim Moore, who allowed me to borrow from the road guides published in his wonderful book "Exploring the Highest Sierra" – on sale at a visitor center near you! Thanks also to Doug LaFarge and Christie Rowe for their help with the email list and website. Former FOP leaders John Caskey, Bud Burke, and John Wakabayashi provided helpful advice and encouragement. Finally, thanks to all of the Friends whose incredible enthusiasm for, and commitment to, these events make the whole thing possible.

EDITORIAL NOTES

Following this introduction is a road log for the three days of field trip stops. As with all road logs, there will be some difference between the published mileages and those registered on various vehicle odometers. For this reason, two sets of mileages are given. In bold are shown the mileages for short segments, usually punctuated by major road junctions. Shorter segments tend to reduce the total odometer error that would otherwise propagate over the course of the day. However, I recognize the difficulty in staying current with the odometer resets, and so periodic cumulative mileages for the day are also reported. Note that the cumulative mileages are more prone to total odometer error, and do not include additional miles logged while lost, during beer runs, etc. It is therefore recommended that the individual segment mileages be followed more than the cumulative ones. All mileages are approximate.

We will be passing rather quickly by some interesting geology and spectacular scenery. I have therefore tried to include information on passing sites of interest that are not official trip stops. Many of these sites are worthy of visiting after the trip stops. Detailed discussions of the material presented during formal trip stops are found in the appendices that follow the road log.

Friends of the Pleistocene field trips traditionally examine ongoing or recently completed geologic research, and we continue this year in the tradition. Therefore, some of the work presented during the FOP 2003 field trip and reproduced in this guidebook has been published, some is presently in review, and some remains unpublished. Data may even be available during the trip that was not available during preparation of this guidebook. We (the authors) request/insist that the data presented herein be considered preliminary until formally published in peer-reviewed format. As always, feedback on the research is welcomed. For errors contained within this guidebook (and there will be some), I take full responsibility and offer my apologies, with the explanation that the time to get this to the printer arrived too soon.

REFERENCES CITED

Bateman, P. C., and Wahrhaftig, C., 1966, Geology of the Sierra Nevada, in Bailey, E. H., ed., Geology of northern California, California Division of Mines and Geology Bulletin, v. 190, p. 107-172.

Dalrymple, G. B., 1964, Cenozoic chronology of the Sierra Nevada, California: University of California Publication of Geological Sciences, v. 47, 41 p.

Ducea, M. N., and Saleeby, J. B., 1998, A case for delamination of the deep batholithic crust beneath the Sierra Nevada: International Geology Review, v. 40, p. 78-93.

Farmer, G. L., Glazner, A. F., Manley, C. R., 2002, Did lithospheric delamination trigger late Cenozoic potassic volcanism in the southern Sierra Nevada, California?: Geological Society of America Bulletin, v. 114, p. 754-768.

House, M. A., Wernicke, B. P., and Farley, K. A., 1998, Dating topography of the Sierra Nevada, California, using apatite (U-Th)/He ages: Nature, v. 396, p. 66-69.

House, M. A., Wernicke, B. P., and Farley, K. A., 2001, Paleo-geomorphology of the Sierra Nevada, California, from (U-Th)/He ages in apatite: American Journal of Science, v. 301, p. 77-102.

Huber, N. K., 1981, Amount and timing of Late Cenozoic uplift and tilt of the central Sierra Nevada, California – evidence from the upper San Joaquin river basin: U.S. Geological Survey Professional Paper 1197, 28 p.

Manley, C. R., Glazner, A. F., Farmer, G. L., 2000, Timing of volcanism in the Sierra Nevada of California: Evidence for Pliocene delamination of the batholithic root? Geology, v. 28, p. 811-814.

Matthes, F. E., 1956, Sequoia National Park: A geological album, Fryxell, F., ed., Berkeley, California, University of California Press

Matthes, F. E., 1965, Glacial reconnaissance of Sequoia National Park, California, Fryxell, F., ed., U. S. Geological Survey Professional Paper 504-A, 58 p.

Small, E. E., and Anderson, R. S., 1995, Geomorphically driven Late Cenozoic rock uplift in the Sierra Nevada, California: Science, v. 270, p. 277-280.

Unruh, J. R., 1991, The uplift of the Sierra Nevada and implications for Late Cenozoic epeirogeny in the western Cordillera: Geological Society of America Bulletin, v. 103, p. 1395-1404.

Wahrhaftig, C. W., 1965, Stepped topography of the southern Sierra Nevada, California: Geological Society of America Bulletin, v. 76, p. 1165-1189.

Wakabayashi, J., and Sawyer, T. L., 2001, Stream incision, tectonics, uplift, and evolution of topography of the Sierra Nevada, California: Journal of Geology, v. 109, p. 539-562.

Wernicke, B., Clayton, R., Ducea, M., Jones, C. H., Park, S., Ruppert, S., Saleeby, J., Snow, J. K., Squires, L., Fliedner, M., Jiracek, G., Keller, R., Klemperer, S., Luetgart, J., Malin, P., Miller, K., Mooney, W., Oliver, H., Phinney, R., 1996, Origin of high mountains in the continents: The southern Sierra Nevada: Science, v. 271, p. 190-193.

IMPORTANT ITEMS OF NOTE

Driving: Narrow, steep, winding roads characterize most of the driving during this trip. Please drive slowly and enjoy the scenery, for your own safety as well as that of wildlife. Pay particular attention to avoiding tarantulas and rattlesnakes on the road from Ash Mountain to Giant Forest.

Vehicles: Most roads traveled during this trip are paved, and the few dirt roads have good clearance. 4-wheel drive vehicles are not required. Please note that vehicles longer than 22 feet (read: RV's and trailers) are not recommended on the Generals Highway between Three Rivers and Giant Forest (Day 1). They are not allowed on the Crescent Meadow and Crystal Cave roads (Stops 1 and 3). Carpooling solutions are available so that vehicles exceeding 22 feet are not taken on these roads – see below.

Carpooling: Many of the stops scheduled for this trip have limited parking. Reducing the number of vehicles in the FOP caravan will really help make the stops run smoothly. The route has been designed to encourage a number of carpooling options, even after the trip has begun. For starters, vehicles may be left for the weekend in a secure area at Horse Creek Campground, our campsite for Thursday night. As our three-day trip makes a broad loop through the southern Sierra Nevada, it is possible carpool for the duration of the trip with someone who has space and is heading south when the trip is over – a slight detour back to Horse Creek from Highway 99 will return you to your vehicle.

If you must take your vehicle into the mountains, here is a description of the optimal carpooling scenario in which you leave your vehicle periodically and carpool for a few hours (see Figure 2 map for reference):

- Leave Horse Creek campsite on Friday morning and drive into Sequoia National Park.
- Leave vehicle at the Giant Forest Museum parking lot and carpool to Stops 1, 2, and 3. Pick up vehicle again on way to Friday night campsite.
- Leave campsite on Saturday morning. Leave vehicle at Quail Flat and carpool down into Redwood Canyon for Stop 4. Return to vehicle and head for Saturday night campsite.
- Leave vehicle at Ten Mile Overflow campsite, our campsite for Saturday night. An added advantage of leaving cars here is that it will help establish our presence here for Saturday night camping. Carpool for the rest of the day to Stops 5, 6, and 7. Return to Saturday night campsite.
- Leave campsite and Sunday morning and drive into Kings Canyon. Leave vehicle at Boyden Cave parking lot and carpool to Stops 8 and 9. Return to vehicle and head to Stop 10 and/or home.

Resource protection: A primary goal of this trip is to leave no mark of our passing. We are further encouraged to do this by National Park rangers, who are charged with protecting Park resources and present citations for violations. Please leave no trash, and pick up any you might find. Store food properly (see section on bears below). Stay on trails when possible, and be careful of trampling fragile plants. Inside Crystal Cave, stay on the paved trail and do not touch cave formations. Finally, be careful not to park vehicles on undisturbed ground.

Dogs: Within Sequoia and Kings Canyon National Parks, dogs are not allowed on trails and must be on leashes when not in a vehicle. Therefore, dogs are not allowed to attend Stops 1, 3, and 8 (i.e. they must be in a vehicle), and must be leashed if attending Stops 2, 4, and 9. They are free to roam at the remaining stops, and at all of the campsites.

Bears: There are many black bears within Sequoia and Kings Canyon National Parks, and negative human-bear interactions are a constant problem. Most of these problems stem from inadequate food storage on the part of the humans. Keep a clean campsite, and make sure trash goes in bear-proof trashcans. When not eating, keep food covered up in vehicles. If you see a bear acting naturally, observe it from a distance. If a bear approaches you, wave your arms and make loud noises to scare it off. Almost all black bears can be scared away, but if a bear does get your food, don't try to take it back! Proper food storage will save you from lost food and/or damaged property, but more importantly it will keep a bear from starting down the slippery slope of human interaction, a course of action that often leads to their death.

Weather: Fall weather in the southern Sierra Nevada is typically clear, with warm days and cool nights. However, anything is possible in the mountains at this time, especially at the relatively high elevations (5,000-7,000 ft) where we will be spending much of our time. Snow is not impossible. Bring raingear and layers of warm clothing.

2003 FRIENDS OF THE PLEISTOCENE PACIFIC CELL FALL FIELD TRIP ROAD LOG

Thursday, October 2
Visalia to Horse Creek
(Directions to Thursday night campsite)

Day 1 (Friday, October 3)
Horse Creek to Crystal Cave

Day 2 (Saturday, October 4)
Redwood Canyon to Boyden Cave

Day 3 (Sunday, October 5)
Hume Lake to the western foothills

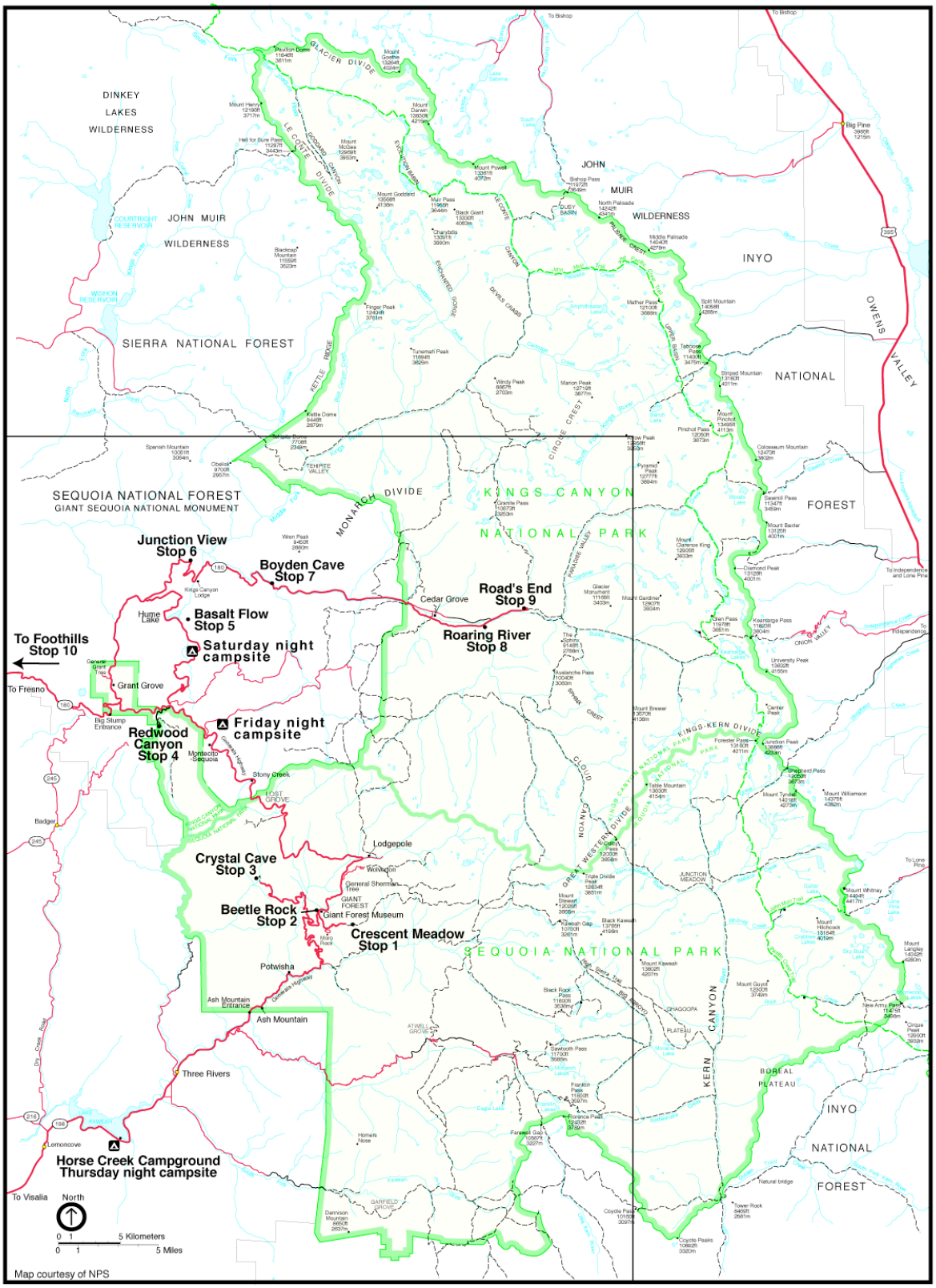

Figure 1. Map of Sequoia and Kings Canyon National Parks, showing major peaks, drainages, trails, and roads. Stop and campsite locations for the 2003 Friends of the Pleistocene Field Trips are shown in bold. Boxed area is enlarged in Figure 2. Note the extensive roadless areas of these National Parks; 85% of Sequoia and Kings Canyon are designated wilderness.

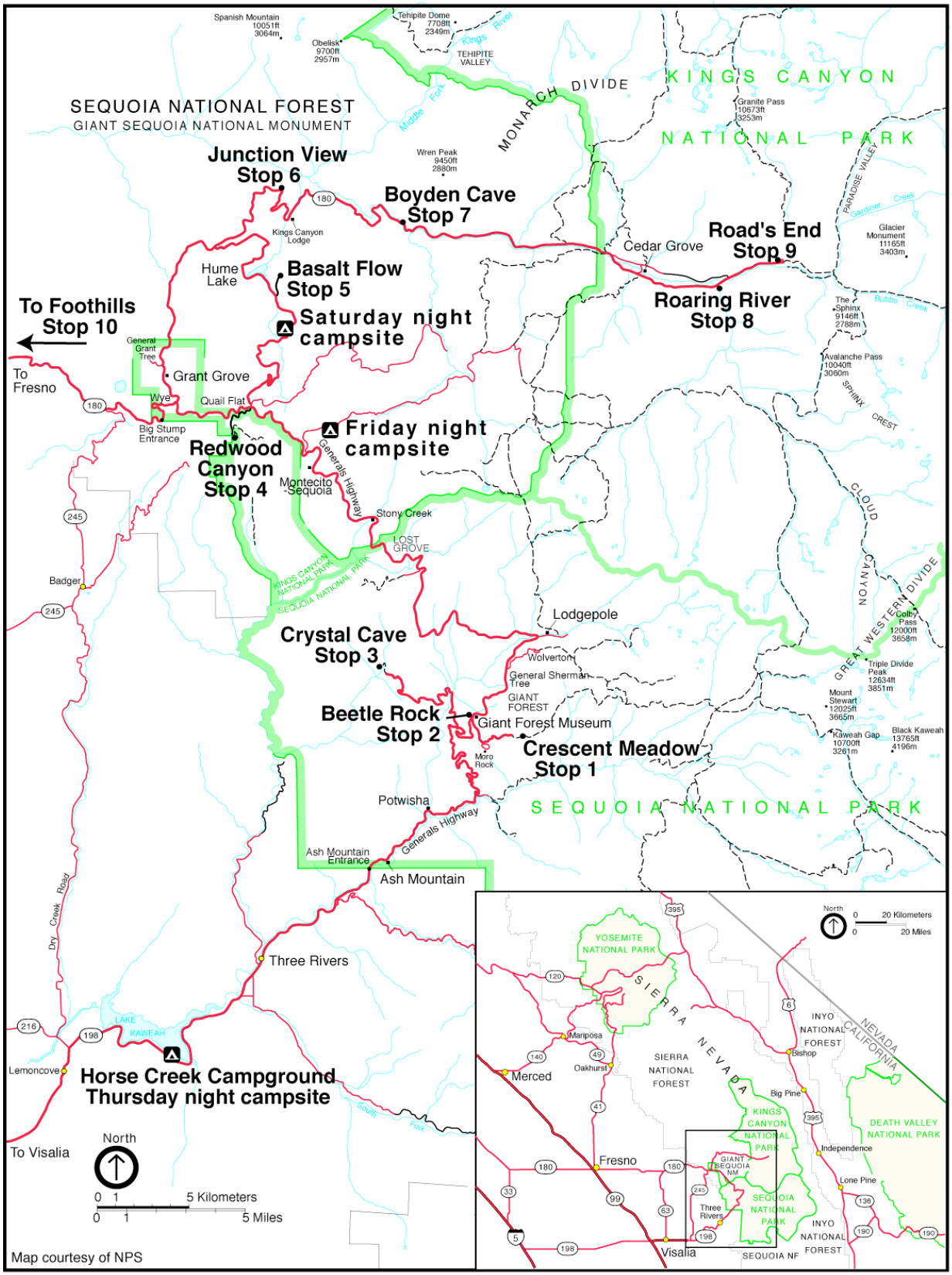

Figure 2. Route map for the 2003 Friends of the Pleistocene Field Trip. Stop and campsite locations are shown in bold. Inset box provides regional setting for Sequoia and Kings Canyon National Parks.

GATHERING OF FRIENDS: (Thursday, October 2)
TRIP REGISTRATION AND THURSDAY NIGHT CAMP SITE

The 2003 Pacific Cell Friends of the Pleistocene field trip will convene on Thursday, October 2nd at the Horse Creek Campground at Lake Kaweah, located in the foothills of the southern Sierra Nevada east of Visalia and west of Sequoia National Park.

Most trip participants will be accessing Sequoia National Park via Highway 99. At Visalia, exit east on Highway 198 and proceed through the city of Visalia. At the far east end, you will encounter two four-way stop signs separated by 1 mile. The second stop sign marks the junction of Highway 198 and Highway 245 (also called North Spruce Road). On your left will be a sign advertising the town of Woodlake just to the north (this sign may not be lit at night).

Reset your odometer at the second stop sign and proceed straight toward Three Rivers and Sequoia National Park.

Segment mileage	Total mileage	
0.0	0.0	**Junction of Highway 198 and Highway 245.**
7.4		**Town of Lemoncove**
		Note: If you are driving this section of Highway 198 with some daylight, notice the odd look of the surrounding topography, with granitic bedrock hills and ridges poking up through Quaternary alluvium of the San Joaquin Valley. This buried topography, which is also found near the outlet of the Kings River, will be the topic of the final stop of the trip (Stop 10).
13.7	13.7	**Left turn into Horse Creek Campground, the campsite for Thursday night. Pick any site in the back campground loop. The registration table will be set up at the far end of the loop beginning at 4 PM.**

Note: Gas stations are infrequent and gasoline expensive over the course of the next three days, so it is suggested that you gas up Thursday evening in Visalia or early Friday morning on our way through Three Rivers.

DAY 1: (Friday, October 3)
HORSE CREEK TO CRYSTAL CAVE

Such a landscape! A hundred peaks in sight over thirteen thousand feet – many very sharp – deep canyons, cliffs in every direction, sharp ridges almost inaccessible to man on which human foot has never trod – all combine to produce a view the sublimity of which is rarely equaled, one which few are privileged to behold.

- William Brewer, Up and Down California

Depart Horse Creek Campground at 08:00.

Reset odometer. Turn left out of Campground onto Highway 198 east toward Three Rivers and Sequoia National Park.

Segment mileage	Total mileage	
0.0	0.0	**Junction of Horse Creek Campground and Highway 198.**
0.8		**Bridge over Horse Creek.**
4.9		**Western limit of Three Rivers.** The town of Three Rivers is established along the Middle Fork of the Kaweah River, near its confluence with the South and North forks of the Kaweah. If you are low on gas, fill up at one of the gas stations in town, as we will be passing only two gas stations during the course of the trip and gas is expensive there.
10.1		**Road to Mineral King. Continue straight on Highway 198.**
11.8		**Bridge over the Middle Fork Kaweah River.**
12.3	12.3	**Ash Mountain Entrance to Sequoia National Park.** Show the Park Service letter printed on the last page of this guidebook to receive an entrance fee waiver. Note that Highway 198 is now called the Generals Highway, which runs through Sequoia National Park and connects to Highway 180. Sequoia National Park was the first National Park in California, created by an act of Congress on September 25, 1890. Five days later on October 1, 1890, a second act created Yosemite National Park and also enlarged Sequoia to include Giant Forest and the General Grant Grove. Adjacent Kings Canyon National Park, which we will visit on Day 3, was founded in 1940 and incorporated Grant Grove into a larger park protecting the headwaters of the Kings and San Joaquin rivers. 85% of Sequoia and Kings Canyon National Parks is administered as wilderness, making these parks especially appealing to backcountry enthusiasts.

13.3 **Ash Mountain Visitor Center.** Elevation 518 m (1,700 ft). There are restrooms here.

14.7 **Tunnel Rock.** The Civilian Conservation Corps built the Generals Highway during the 1930's. Here the Highway was routed underneath a large granodiorite boulder until 1998 when the Park Service finally tired of extracting wedged RV's out from under the rock and rerouted the road around it during a road-widening project.

15.3 **Views of the Great Western Divide.** If the weather is clear, many of the high peaks on the Great Western Divide can be viewed to the east, up the Middle Fork of the Kaweah River. The Great Western Divide is a sub range west of the Sierra Nevada crest that separates the Kaweah River, which is below you, from the glacial trough of the upper Kern River canyon, which is oriented north-south on the east side of the Divide. The triangular peak on the left is Triple Divide Peak (elevation 3,851 m; 12,634 ft), which serves as the headwaters for the Kings, Kaweah, and Kern Rivers. The double-summited peak to the right is Mount Stewart (elevation 3,721 m; 12,205 ft), named for George Stewart, a Visalia newspaperman who orchestrated the campaign leading to the creation of Sequoia National Park in 1890.

16.1 **Bridge over the Marble Fork Kaweah River.**

16.2 **Potwisha Campground.**

17.7 **Views up the Middle Fork Kaweah to Mount Stewart (3,271 m; 12,205 ft).**

18.6 18.6 **Hospital Rock.** There are restrooms here. The large granodiorite boulders at Hospital Rock are believed to have been deposited by major rockfalls off of Moro Rock, the large exfoliation dome that looms above on the north side of the canyon. One of these boulders split after coming to rest, and Wukchumne pictographs of a red iron-oxide compound are painted on the flat joint face of this fracture. It is unknown when these particular boulders fell, but clearly the exfoliation process continues as evidenced by the two white streaks on the slabs northwest of Moro Rock. These streaks trace discrete rockfall events within the last decade.

Get ready for some serious mountain driving, and stop reading this if you get car sick.

19.3 **Quartzite ridge.** The cliff above and west of Hospital Rock is a narrow band of resistant, vertically-bedded quartzite associated with metamorphic rocks of the Sequoia Pendant (Sisson and Moore, 1994). The quartzite may be traced across the Middle Fork Kaweah River, where it forms a prominent knickpoint, and over Paradise Ridge to the southwest.

23.7 **Amphitheater Point.**

25.4 **Deer Ridge.** Just around the corner from Deer Ridge, there are views down into Deep Canyon, a gorge cut by the Marble Fork of the Kaweah River. Several caves are present in the bottom of the canyon, but the upper walls have not been explored. Just upstream of the marble gorge the river profile rises in a series of knickpoints carving into resistant quartzite bands; not far upstream of these waterfalls, the river returns to a low gradient likely influenced by glaciation in nearby Tokopah Valley.

26.3 **Eleven Range Lookout.**

27.3 **Giant Forest.** Giant Sequoias (*Sequoia Gigantea*) grow naturally only on the western slope of the Sierra Nevada, between roughly 1,500 and 2,100 m (5,000 and 7,000 ft) in elevation. However, ancestors of these trees ranged more widely, presumably during wetter climates that favored their growth. There are about 75 groves scattered throughout the range (Fig. 3), but Giant Forest is the one of the largest and perhaps the most impressive - four of the world's five largest trees stand here.

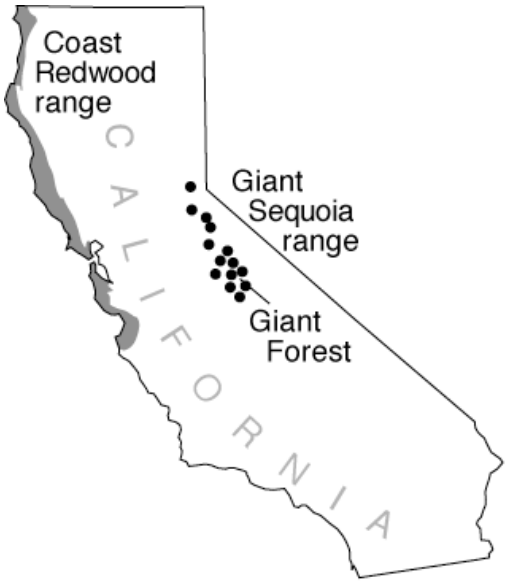

Figure 3. Map of California showing present distribution of Coast Redwood (*Sequoia sempivirens*) and Giant Sequoia (*Sequoia Gigantea*). Giant Sequoias grow only in the Sierra Nevada, at elevations between roughly 1,500 and 2,100 m (5,000 and 7,000 ft). There are about 75 Sequoia groves scattered across the central and southern Sierra Nevada; only the largest groves are shown. Map courtesy of National Park Service.

27.4 **Crystal Cave turnoff.** Continue up the Generals Highway, but note this turnoff, as we will be returning here for Stop 3.

27.9 **Four Guardsmen.** The highways splits and threads between four large Sequoia trees.

29.5 **Left turn into the parking area for the Giant Forest Museum. Those wishing to carpool to Stops 1-3 (and you are encouraged to do so!) may park vehicles here and catch a ride for much of the rest of the day.**

29.6 29.6 **Junction with Moro Rock and Crescent Meadow Road. Turn right toward Moro Rock and Crescent Meadow. The turnoff to this road is just after the parking area for the Giant Forest Museum, and just before the Museum itself.**

30.9 **Veer left at junction with Moro Rock road, heading toward Tunnel Log and Crescent Meadow.**

31.3 **Tunnel Log.** The tunnel was excavated by members of the Civilian Conservation Corps in 1938 after a Giant Sequoia fell across the Crescent Meadow Road. If you *even suspect* that your vehicle is over 8 feet high, take the bypass.

32.4 32.4 **Crescent Meadow parking area. Park vehicles in the lot, and walk 0.5 mile along the High Sierra Trail to a clearing overlooking the Middle Fork Kaweah River (Fig. 4). There are restrooms at the trailhead.**

STOP 1: Viewpoint along the High Sierra Trail (09:30-11:00) Wakabayashi and Stock. See Appendix 1.
Overview of tectonics and geomorphology of the southern Sierra Nevada; pre-late Cenozoic geology; late Cenozoic uplift history.

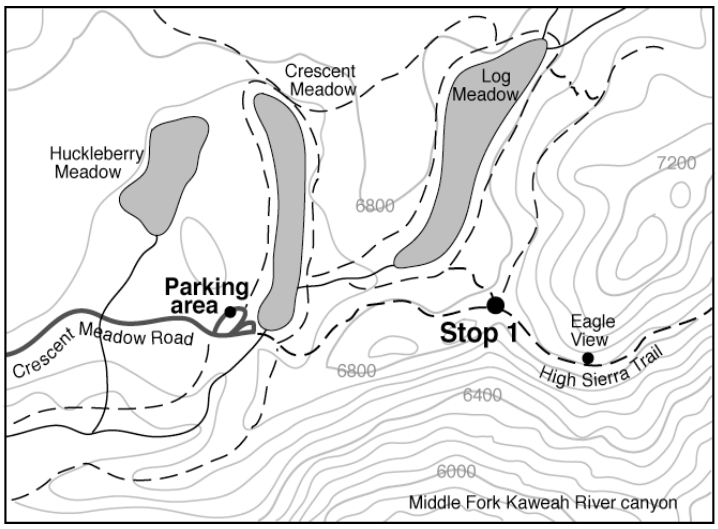

Figure 4. Map of the Crescent Meadow area, showing location of Stop 1, 0.5 mile along the High Sierra Trail. Crescent Meadow, along with Log and Huckleberry meadows, are located at the southern edge of the Giant Forest plateau. This plateau is sharply truncated on the southern edge by the deeply incised Middle Fork Kaweah River canyon. Excellent views of the Great Western Divide are obtained from Eagle View, 0.2 mile along the High Sierra Trail beyond the site of Stop 1.

Crescent Meadow is one of the largest meadows in Sequoia National Park, and sits on the edge of the Giant Forest plateau, near the rim of the deeply incised Middle Fork Kaweah River canyon. It also marks the start of the High Sierra Trail, which connects Giant Forest with Mount Whitney on the Sierra Nevada crest. Our first stop is 0.5 mi out on the High Sierra Trail, at a site overlooking

both the Middle Fork Kaweah River canyon and Log Meadow. After the overview discussion, you may wish to hike an additional 0.4 mile to Eagle View, a point on the High Sierra Trail with great views of Castle Rocks and the Great Western Divide. An alternative route back to the cars can be taken along Log Meadow (Fig. 4). Pollen abundances in meadow cores from Log Meadow record mid- to late-Holocene expansion of sequoias (see Figure 4C-1, Appendix 4C).

Return to vehicles. Backtrack to the Generals Highway and turn left, toward Three Rivers. Go only ~0.1 mile and turn right into parking area for Giant Forest Museum and Beetle Rock. Follow the signs to the overflow parking area, which is set back slightly from the main parking lot. Park here and follow the short trail out to Beetle Rock. There are restrooms at the overflow parking area.

STOP 2: Beetle Rock (11:30-12:00). Weissmann. See Appendix 2.
Stratigraphic sequences of the Kings River alluvial fan formed in response to Sierra Nevada glacial cyclicity.

Beetle Rock is composed of ~100 Ma Giant Forest Granodiorite (Sisson and Moore, 1994). Cosmogenic nuclide concentrations in slabs from this rock indicate that it is eroding at a rate of ~0.003 mm yr^{-1} (Stock et al., in review).

Return to Generals Highway and reset odometer. Turn right toward Crystal Cave turnoff.

0.0 35.4 **Junction of Giant Forest Museum parking lot and Generals Highway.**

2.2 37.6 **Turnoff to Crystal Cave. Turn right onto Crystal Cave Road.**

4.0 **Bridge over the Marble Fork of the Kaweah River.**

5.4 **View southwest into Deep Canyon, a gorge cut through vertically-bedded marble by the Marble Fork Kaweah River.**

9.1 44.5 **Crystal Cave parking lot. We'll probably take some time for lunch here before heading to the cave. The steep 0.6 mile long trail to the cave begins at the north end of the parking lot. There are no restrooms at the cave, so use the porta-potties in the parking lot before heading to the cave.**

STOP 3: Crystal Cave (13:00-16:00) Stock. See Appendix 3.
Origin and morphology of Sierra Nevada caves; geochronology of cave deposits; caves as recorders of river incision in the southern Sierra Nevada.

Crystal Cave is chilly at 10°C (48°F); warm clothes and a flashlight are recommended. No dogs are allowed on the trail to the cave or loose in the

parking lot. Please leave rock hammers and tripods in vehicles. Within the cave, stay on the paved trail and refrain from touching cave surfaces, particularly calcite speleothems. No eating, drinking, or smoking is allowed within the cave.

The trail to Crystal Cave descends into a steep canyon carved by Cascade Creek, a tributary of the North Fork of the Kaweah River. Along the trail, narrow marble lenses are visible across the canyon; these marble outcrops contain numerous caves. Note the prominent knickpoints in the Cascade Creek profile. We will stop briefly at the cave entrance for a description of the cave morphology and an explanation of the cosmogenic nuclide burial dating technique used to constrain cave ages. We will then be free to wander through the cave (on the paved trail only!) for the next 1-1.5 hours, examining various aspects of cave geology.

Return to vehicles. Backtrack along the Crystal Cave Road to its junction with the Generals Highway. Reset odometer and turn left toward Giant Forest and Friday night camp.

0.0 53.6 **Junction of Crystal Cave Road and General's Highway.**

2.1 **Giant Forest Museum parking area. Pick up your vehicle here if you have been carpooling the Stops 1-3.**

2.2 55.8 **Road to Moro Rock and Crescent Meadow.**

2.9 **Recently fallen sequoia.** A sequoia tree toppled over here in August of this year, crushing an SUV while its occupants were hiking.

4.5 **General Sherman Tree.** Based on volume, the General Sherman Tree is the world's largest living tree. It stands 84 m (275 ft) tall and has a basal diameter of 11 m (36.5 ft). It weighs an estimated 1,385 tons. A single branch measures 2 m (7 ft) in diameter. The General Sherman Tree is estimated to be approximately 2,150 years old (Stephenson, 2000). Though not a formal stop, it is definitely worth a quick visit if you haven't seen it before.

5.1 **Wolverton Road turnoff.** Nearby Wolverton Creek once flowed directly into Tokopah Valley to the north, but is now deflected southward by the extensive south lateral moraines deposited by the large glaciers that occupied Tokopah Valley during the Tahoe and Tioga stage glaciations (Fig. 5; Wahrhaftig, 1984). These moraines are well-exposed in roadcuts on the south side of the Highway about 1 mile past Wolverton Creek, between the Wolverton Road turnoff and the Lodgepole visitor center. These are among the best-preserved moraines on the western slope of the southern Sierra Nevada.

6.4 **View up Tokopah Valley.** Granitic boulders on the south (right) side of the Generals Highway mark the left lateral moraines occupying Tokopah Valley during Tahoe and Tioga times. Moraine crests indicate that during the Tahoe glaciation the glacier in Tokopah Valley was approximately 230-300 m (750-1000 ft) thick (Fig. 5). The western terminus of the Tahoe glacier was about 3 km west of the Lodgepole Visitor Center, at an elevation of approximately 1830 m (Fig. 6) (Wahrhaftig, 1984; Moore, 2000).

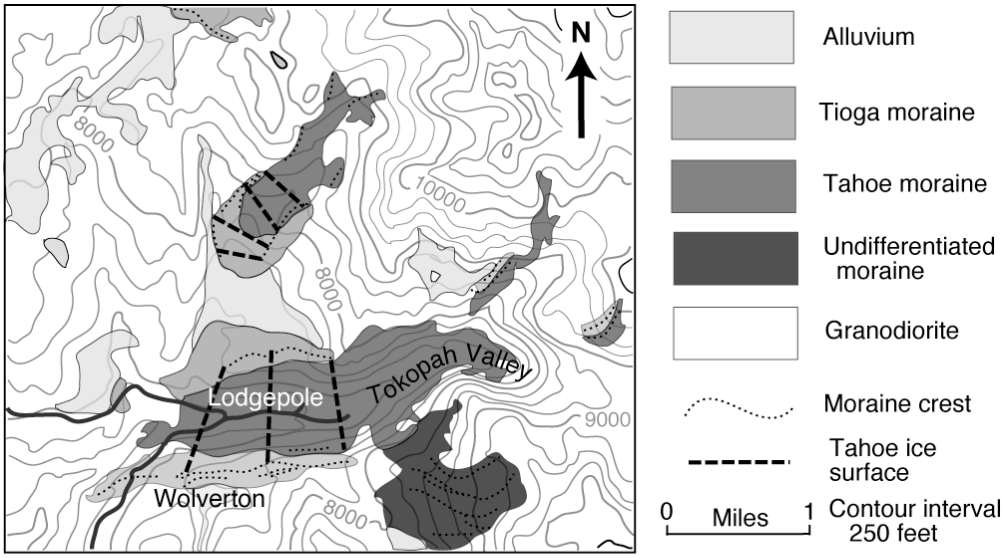

Figure 5. Map of glacial deposits in the vicnity of Wolverton and Lodgepole. Large glaciers descended down Tokopah Valley (now occupied by the Marble Fork of the Kaweah River) during Tahoe and Tioga times.The bold dashed lines, representingthe top of the Tahoe ice as determined by the height of Tahoe moraine crests, indicate that during Tahoe glaciation the ice at Lodgepole was 750-100 ft (230-300 m) thick. Modified from Moore (2000).

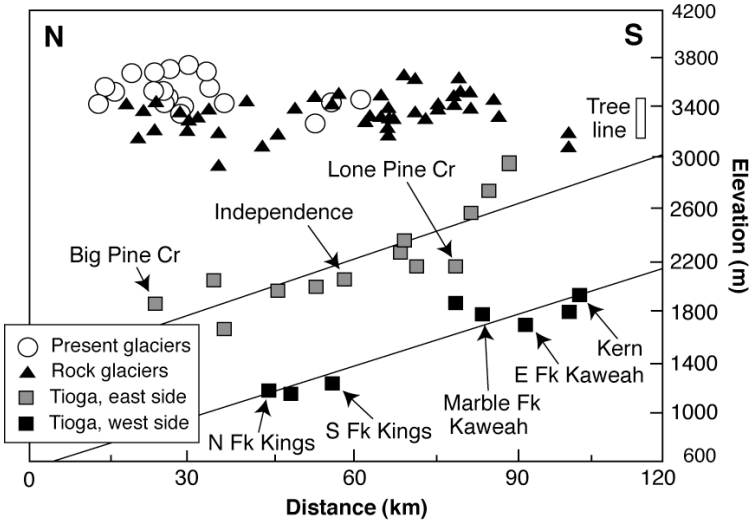

Figure 6. Elevation of glacier termini positions in the southern Sierra Nevada. Present-day glaciers lie in northern Kings Canyon National Park and generally occur above 3,600 m but do extend down to 3,300 m. Active rock glaciers lie at the same or slightly lower elevations. The lower limit of Tioga glaciers was lower on the western side of the range than on the eastern side, presumably due to greater precipitation and larger contributing areas on the western slope. Modified from Figure 9.3, Moore (2000).

6.8 60.4 **Lodgepole Visitor Center.** Elevation 2,048 m (6,720 ft). Lodgepole is situated in the bottom of Tokopah Vally, through which the Marble Fork of the Kaweah now flows. You may find restrooms here, as well as a store with ice, a good selection of beer, and other grocery items.

6.9 **Bridge over the Marble Fork Kaweah River.**

7.7 **Bridge over Clover Creek.**

10.7 **Bridge over Halstead Creek.** Recent erosion due to a poorly-placed culvert has exposed a many-meters thick section of meadow stratigraphy on the west (left) side of the Highway.

11.3 **Bridge over Suwanee Creek.** Just after the bridge over Suwanee Creek there are nice sphereoidally weathered granitic boulders in roadcuts on the north (right) side of the Highway.

13.9 **Little Baldy Saddle. Highest elevation attained during this trip: 2,236 m (7,335 ft.)**

18.3 **Lost Grove.**

19.0 **Sequoia National Park boundary.** You are now leaving Sequoia National Park, administered by the National Park Service, and entering Giant Sequoia National Monument, created in April, 2000 and administered by the U.S. Forest Service. The change in land managers means a change in rules; dogs are now allowed on trails, and camping is no longer restricted to established campgrounds.

20.2 **Stony Creek Campground.**

24.6 **Montecito – Sequoia Resort.** Those not wanting to camp may find a room here.

25.6 79.2 **Turn right onto the Big Meadows - Horse Corral Meadow Road. A sign indicating distances to Big Meadows, Buck Rock Lookout, and Horse Corral Meadow marks the road.**

27.2 80.8 **Friday night campsite –dispersed camping. For the next 0.5 mile there are many parking and camping sites, mostly on the south (right) side of the road. Please do not drive vehicles beyond "No vehicle" signs. Those wishing for quieter, more private camping should head for additional campsites further east, either at the nearby Buck Rock or Big Meadows campgrounds.**

The granitic domes around Friday night's campsite are composed of the ~100 Ma Big Meadows granite (Sisson and Moore, 1994). Cosmogenic nuclide concentrations in similar granitic domes nearby indicate that these surfaces are eroding slowly, at ~0.015 mm yr^{-1} (Stock et al., in review). Visible to the south are peaks of the Mineral King area, including Vandever Mountain (3,642 m; 11,947 ft) and Florence Peak (3,790 m; 12,432 ft).

Historical note: The 1864 Whitney Survey party traveled from the Sierra foothills up to Grant Grove, and then worked their way through this area. From Big Meadows they climbed a peak on the Kings-Kaweah divide, which they named Mount Silliman. From here, they descended Sugarloaf Creek to Roaring River and made camp at the base of a fine conical peak. Brewer noted: "Hofmann and I climbed this cone. The view was wilder than we have ever seen before. Such a landscape! A hundred peaks in sight over thirteen thousand feet – many very sharp – deep canyons, cliffs in every direction, sharp ridges almost inaccessible to man on which human foot has never trod – all combine to produce a view the sublimity of which is rarely equaled, one which few are privileged to behold" (Farquhar, 1965). From this vantage point, which was scaled again the following day and named Mount Brewer in honor of the party chief, several high peaks on the main Sierra Nevada crest about 14 km to the east were mapped and named, including Mount Whitney, Mount Williamson, and Mount Tyndall (Farquhar, 1965).

DAY 2: (Saturday, October 4)
REDWOOD CANYON TO BOYDEN CAVE

In the vast Sierra wilderness, far to the southward of the famous Yosemite Valley, there is yet a grander valley of the same kind. It is situated on the south fork of the Kings River, above the most extensive groves and forest of the Giant Sequoia, and beneath the shadows of the highest mountains in the range, where canyons are the deepest and the snow-laden peaks are crowded most closely together.

- John Muir, A Rival to the Yosemite – The Canyon of the South Fork Kings River

Depart campsite at 08:00. Backtrack the 1.5 miles to the Generals Highway. Reset odometer and turn right.

Segment mileage	Total mileage	
0.0	0.0	**Junction of Big Meadows Road with the Generals Highway.**
0.2		**Big Baldy Trailhead.**
2.2		**Buena Vista Dome Trailhead.**
2.3		**Kings Canyon Overlook.**
3.3	3.3	**Quail Flat. Turn left onto somewhat inconspicuous dirt road. You are now entering Kings Canyon National Park. For those wishing to carpool, it is possible to park cars at Quail Flat, a big paved parking lot across the Generals Highway from the turnoff to Redwood Canyon. We will be returning here after Stop 4.**
5.2		**Turn left into large dirt parking area at the Redwood Canyon trailhead.**
5.3		**Redwood Canyon trailhead. Park close together so that all vehicles may fit in the parking area. It may be necessary to double park. There are restrooms at the trailhead.**

STOP 4: Redwood Canyon Trailhead (08:30-11:00) Tinsley, Caprio, and Stephenson. See Appendices 4A, 4B, and 4C.

Hydrology and sedimentology of Lilburn Cave; Holocene climate and fire history from tree rings; Giant Sequoia fire history; recent deglaciation.

Redwood Canyon is the largest undisturbed Giant Sequoia grove in the world. ~8 km (5 mi) down the canyon from the trailhead, Redwood Creek sinks into a northwest-trending marble lens mantled by granitic colluvium/alluvium. For the next ~5.5 km (3.3 mi) the creek flows underneath an extensive sinkhole plain through cave passages that have not yet been accessed. Eventually the creek appears in the upstream end Lilburn Cave, a complex maze cave that is the largest cave in California at 32 km (20 mi). After flowing through Lilburn

Cave, the creek resurges from Big Spring, a unique ebb and flow spring (see Appendix 4A).

Retrace 2.0 miles up dirt road to junction with the Generals Highway. Reset odometer. Proceed straight across Generals Highway to big paved lot (Quail Flat). At far end of lot veer left on Ten Mile Road (Hume Lake Road) toward Hume Lake.

0.0 7.3 **Junction of Redwood Canyon Road and Generals Highway.**

5.5 **Bridge over Ten Mile Creek. Ten Mile Campground.**

6.0 13.3 **Ten Mile Overflow Campground. This is our campsite for Saturday night. Those wishing to carpool from this point are encouraged to leave a vehicle here and join someone with an extra seat. As always, carpooling is encouraged, particularly because parking for Stop 6 is limited.**

6.9 **Landslide Campground.**

8.1 **Logger Flat Group Campground.**

8.2 15.5 **Turn right onto dirt road with sign reading "Road Closed Ahead 7 Miles".**

8.6 **Outcrops of Pliocene potassium-rich basalt resting unconformably on granodiorite.**

9.1 16.4 **Park in large dirt turnout on left. Some 4-wheel drive vehicles may park in smaller turnouts on the right. If (when) this space fills, there is another large turnout on the left 0.1 mile further up the road.**

STOP 5: Basalt near Hume Lake (11:30-12:00) Stock (Glazner). See Appendix 5.
Volcanic evidence for Pliocene delamination of the Sierra Nevada batholithic root.

17.4 **Return to junction with Ten Mile Road. Turn right toward Hume Lake.**

10.7 **Bridge over Ten Mile Creek. Veer left toward Hume Lake and Highway 180.**

11.8 **Hume Lake.** Hume Lake Christian Camp. There is gasoline and ice (but no beer) available at the small general store.

13.3 **Stay left at junction, heading toward Highway 180 and Cedar Grove.**

13.9 **First views into the canyons of the Middle and South Forks of the King River.**

16.1 23.4 **Junction with Highway 180. Reset odometer. Turn right (east) towards Cedar Grove.**

0.0 **Junction of Ten Mile Road (Hume Lake Road) and Highway 180.**

1.6 **Tertiary basalt in roadcut.** An outcrop of olivine basalt is exposed in a roadcut on the west (left) side of the Highway. The basalt contains phenocrysts of olivine, pyroxene, and plagioclase along with fine-grained minerals of olivine, pyroxene, plagioclase, K-feldspar, apatite, opaques, and rare biotite. This basalt is thought to be similar in age to that viewed at Stop 5 (approximately 3.4 Ma), but is considerably less potassic in composition (Moore and Dodge, 1980). The basalt rests on 2 m of granitic sand and ash and lapilli that in turn rest on weathered granodiorite.

The views north and east from this point include Middle Palisade (4,280 m; 14,040 ft) and University Peak (4,156 m; 13,632 ft) on the main Sierra Nevada crest, and Mount Gardiner (3,935 m; 12,907 ft) and Mount Cotter (3,878 m; 12,721 ft) on King Spur.

4.9 28.3 **Junction View turnout. There are three medium-sized turnouts on the left (north) side of the road, and all vehicles must fit in them. Please park as close together as possible. It's going to be tight - double parking may be necessary. Be very careful crossing the oncoming lane of traffic, as visibility is about nil. We will try to have someone on the shoulder controlling traffic.**

STOP 6: Junction View (13:00-14:00) Stock. See Appendix 6.
Late Cenozoic topographic evolution in the southern Sierra Nevada; Pre-Pliocene paleorelief; Late-Pliocene and Quaternary rates of river incision.

Visible far below Junction View turnout is the confluence of the Middle and South Forks of the Kings River, separated by the Monarch Divide (Fig 7). Upstream of the confluence, the canyons of the Middle and South Fork have nearly 2 km of local relief. Just downstream of this confluence the canyon is the deepest in the Sierra Nevada, and one of the deepest in North America, dropping 2,391 m (7,842 ft) from the north rim at Spanish Mountain to the river. Points visible from north to south are: Deer Ridge, Spanish Mountain (3,046 m; 10,051 ft), Tombstone Ridge, Tehipite Valley, Monarch Divide, Wren Peak (2,864 m; 9450 ft) and University Peak (4,131 m; 13,632 ft) on the Sierra Nevada crest.

Historical note: The 1864 Whitney Survey party spend many days exploring the rugged headwaters of the Kings River visible from this spot. After gaining the summit view of Mount Brewer, Clarence King set his sights on Mount Whitney, thought to be the highest peak in the range. He begged Brewer to allow him to try to reach its summit, and Brewer reluctantly

consented. The following day Brewer and Cotter set out on a six-day journey across some of the most rugged terrain of the High Sierra. Though they failed to reach the summit, their traverse across the maze of canyons and ridges ushered in a new era in American mountaineering. After rejoining the main party near Mount Brewer, the group returned to Big Meadow and worked down Roaring River to the canyon of the South Fork of the Kings River near the present site of Cedar Grove.

This was the first in a series of epic misadventures for King, in which he was routinely thwarted from the summit of Mount Whitney and twice scaled the wrong peaks (Mounts Tyndall and Langley) in his effort to be the first to the top of the range. He did finally reach the summit of Mount Whitney in September of 1873 only to find evidence of the first ascent party, a group of fishermen from Lone Pine who had scaled the peak just one month prior (Farquhar, 1965). However, these mishaps did not keep King from attaining fame for his book "Mountaineering in the Sierra Nevada". King went on to become the first director of the U.S. Geological Survey.

Figure 7. Canyons of the Middle (left) and South (right) forks of the Kings River as seen from Junction View. Local relief here is ~2 km. Highway 180 is visible on the right, leading up into Kings Canyon. Photograph by Greg Stock.

4.9 **Turn left out of turnout and continue east on Highway 180 toward Cedar Grove.**

7.1 **Bridge over Ten Mile Creek.**

7.2 **Kings Canyon Resort.** There is gasoline and a grocery store here. Those not wanting to camp may find a room here.

8.4 **Yucca Point.** A trail leads down from this point to the confluence of the South and Middle Forks of the Kings River.

12.5 **Convict Flat Campground.** The anomalous flat and knob toward the river may be the result of a landslide originating on the steep slope east of the highway (Moore, 2000). Convicts worked on the construction of this part of the Kings Canyon Highway during the 1930's and were housed near this site.

12.7 **Horseshoe Bend.** This prominent bend in the river is near the central part of a well-bedded, well-sorted, and vertically oriented quartzite bed. This quartzite is a unit of the Boyden Cave roof pendant, one part of the Kings Terrane (Moore and Nockleberg, 1991). The other part of the Kings Terrane is the Goddard roof pendant, composed chiefly of metavolcanic rocks. The two parts are separated by the Kings River Suture. The Boyden Cave roof pendant consists of highly deformed quartzites, calc-schist, phyllite biotite schist, and marble. Sparse fossils indicate a Jurassic age. Northwest of Horseshoe Bend the various units of the western part of the Boyden Cave roof pendant are spectacularly exposed on the southern slopes of Monarch Divide, particularly near-vertical cliffs of marble. The quartzite at Horseshoe Bend is comprised of >90% quartz, and is therefore quite resistant to erosion. This likely causes the steep cliffs and narrow inner gorge in this vicinity, and also creates a prominent step in the river profile here (see Appendix 7).

13.2 **View up canyon of the marble cliffs above Boyden Cave.**

14.0 37.4 **Boyden Cave parking lot. Park in the parking lot or in one of the nearby turnouts both before and after the bridge. There are restrooms in the parking lot.**

STOP 7: Boyden Cave (14:30-16:30) Stock. See Appendix 7.
Cave record of river incision in the South Fork Kings River canyon; temporal trends in river incision rates; summary of new insights regarding late Cenozoic landscape evolution.

The towering cliffs on either side of the Boyden Cave parking lot, named the Windy Cliffs, are composed of a vertically oriented, massive, blue-gray marble of Jurassic age. In terms of weathering, this large lens of marble is the most resistant unit of the Boyden Cave metamorphic pendant, resulting in the prominent ridgelines and nearly vertical cliffs. However, we have seen that marble is prone to chemical dissolution, and numerous caves are found within this rugged landscape. Boyden Cave, discovered in 1907, is situated in the southern wall of the gorge 42 m above the river, and is open to the public in the summer and early fall. Boyden Cave is hydrologically (though not

physically) connected to nearby Church Cave, the third longest cave in California at approximately 6 km in length. Several small caves are presently forming at river level just downstream of the bridge, and portions of the river flow through them, depositing granitic sediment. These caves are modern analogues for the development of many of the caves visible in the cliffs high above the river. Dating of granitic sediment within these caves provides a downcutting history for this gorge (Stock et al., in review).

Time permitting, there are several options for the late afternoon. Those wishing to explore one of the small caves near the river may do so. Bear Cave is just across the bridge on the left in a roadcut through marble. Kings River Cave is at river level in the opposite wall of the canyon, about 100 m downstream of the bridge. Headlamps or flashlights are necessary. If exploring Kings River Cave, be prepared to get wet. Wear shorts and sandals and be very careful crossing the river – if the river is high the crossing is not recommended. Another option is to investigate an interesting sedimentary deposit in a north (left) side roadcut 5.7 miles up the canyon beyond Boyden Cave. This is presumably a glacial outwash deposit, but deserves more careful consideration. There is space for only 8-10 cars at this site, and crossing the highway is hazardous. Finally, you may simply want to relax by the river and have a cold beverage. From here the plan is to backtrack to our campsite near Ten Mile Creek, just beyond Hume Lake.

Reset your odometer at Boyden Cave. Turn left onto Highway 180 (towards Grant Grove and Fresno) and backtrack 14 miles to the junction of Ten Mile Road (Hume Lake Road).

0.0 37.4 **Boyden Cave parking lot.**

14.0 51.4 **Junction of Ten Mile Road (Hume Lake Road) and Highway 180. Turn left toward Hume Lake.**

4.1 **Hume Lake.** There is gasoline and ice (but no beer) available at the small general store.

9.9 47.3 **Turn right onto somewhat inconspicuous dirt road. This is Ten Mile Overflow Campground, our campsite for Saturday night. Camping space is a little bit tight here - those wishing for more space and/or quieter camping might want to head for Ten Mile Campground, 0.5 miles further down the road.**

The Annual Business Meeting will commence around the campfire around 8:00 PM.

DAY 3: (Sunday, October 5)
HUME LAKE TO THE WESTERN FOOTHILLS

True appreciation of landscape comes when one is alive to both its beauty and its meaning.
- Fritiof Fryxell

Depart campsite at 09:00. Reset odometer. Turn left onto Ten Mile Road (Hume Lake Road) and follow to Highway 180, retracing route from Day 2.

Segment mileage	Total mileage	
0.0	0.0	**Ten Mile Overflow Campground.**
10.6	10.6	**Junction with Highway 180. Turn right toward Cedar Grove.** See Saturday road log for a description of sites between here and Boyden Cave.
24.6	24.6	**Boyden Cave. You may leave vehicles here and carpool to stops 8 and 9. There are restrooms in the Boyden Cave parking lot.**
24.6		**Bridge over South Fork of the Kings River.** During the last two days of December in 1996, a warm tropical storm moved across California, dumping several inches of rain on an already substantial winter snowpack. The resulting river discharges on January 1, 1997 were among the highest in recorded history (Fig. 8). Pine Flat Reservoir downstream measured peak hourly inflow at 87,000 cfs! For comparison, the discharge now (mid-October) is probably a few hundred cfs. Much of the road along the South Fork Kings river was washed out during this flood, and visitor facilities in upper Kings Canyon were closed for much of the spring and early summer. Large logs stranded on the bridge near Boyden Cave provide a minimum estimate of the peak discharge height.
25.2		**Chevron folds in phyllite.** On the north (left) side of the highway there is a spectacular and photogenic exposure of chevron folds in a roadcut through interlayered calcium silicate phyllite. These folds illustrate the multiple periods of deformation experienced by metamorphic rocks of the Boyden Cave Pendant (Moore, 2000).
25.3		**Boulder Creek enters from the south (right).**
26.8		**Impressive yellow-green lichen growth on vertically bedded schist of the Boyden Cave metamorphic pendant.**

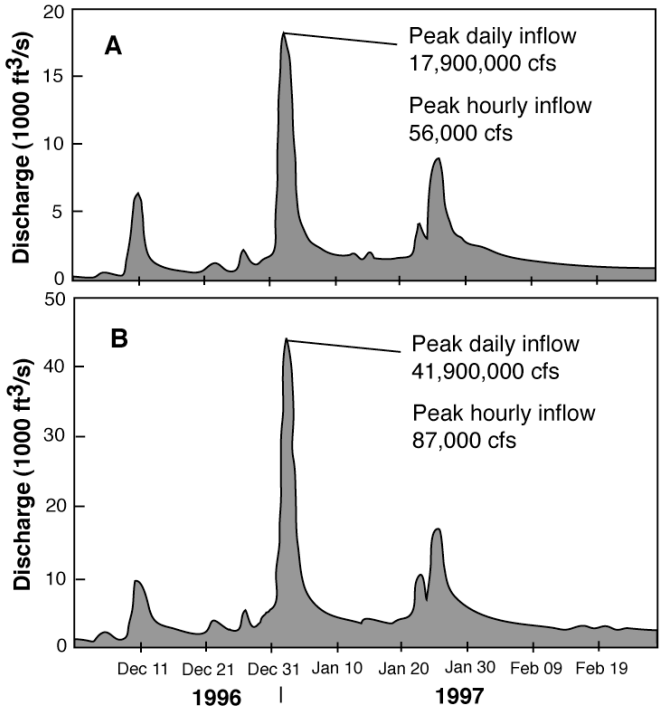

Figure 8. Hydrographs showing daily inflows into Lake Kaweah (A) and Pine Flat (B) reservoirs during the period December 1 to February 28, 1996-97. A warm rain on an already thick snowpack created some of the largest river discharges in historical record. Peak daily inflow (and thus peak daily discharge) for the Kings River was 41,900 cfs, and peak hourly inflow (and thus peak hourly discharge) was 87,000 cfs. For comparison, typical fall (October) discharges above Pine Flat Reservoir are ~650 cfs. Hydrographs courtesy of US Army Corps of Engineers.

30.3 **Glacial outwash(?).** On the north (left) side of the highway an impressive sedimentary deposit is preserved in a stream/road cut. This stratified mix of sand and boulders is presumably glacial outwash, as the main trunk glacier which occupied the South Fork Canyon during the larger Pleistocene advances extended down to just upstream of this point (see Fig. 9A-1). This exposure provides some measure of the amount of aggradation of the fluvial system associated with glaciation upstream. Please be careful if you choose to stop here; parking is limited to 8-10 cars and crossing the highway is hazardous.

30.7 **Grizzly Creek.** A small (by Sierra standards) waterfall results where the slightly hanging valley of Grizzly Creek enters the South Fork river canyon. Grizzly Creek is generally considered the point marking the transition from predominantly fluvial to predominantly glacial erosion. Upstream of this point the canyon changes from a steep, narrow V-shaped canyon to a less steep, U-shaped canyon reminiscent of Yosemite Valley.

32.8 32.8 **Entrance to Kings Canyon National Park..**

33.5 **Bridge over the South Fork of the Kings River.**

34.3 **Sheep Creek.** Notice that the road climbs up to cross Sheep Creek, and descends again after crossing it. It seems that Sheep Creek has created a steep sided alluvial fan as it debouches into Kings Canyon, and is currently held on the apex of the fan by boulder levees.

34.5 34.5 **Turnoff to Cedar Grove.** Elevation 1,412 m (4,635 ft). Restrooms, grocery store.

35.5 **Moraine Campground.** There are many Tioga age recessional moraines in this area.

35.6 **Canyon View Overlook.** View up canyon of the U-shaped cross section of upper Kings Canyon.

37.9 37.9 **Parking area for Roaring River Falls. The paved parking lot is too small to accommodate all vehicles, but there are turnouts on the same (south) side of the road both before and beyond the main parking lot. Please park close together to ensure that there is space for all vehicles. If parking gets tight, we may arrange a shuttle based out of Road's End, 2.5 miles up the road.**

STOP 8: Roaring River Falls (10:00-12:00) Bull. See Appendix 8.
Lichenometry dating of paleoseismic, geomorphic, and climatic events

Historical note: The 1864 Whitney Survey party entered Kings Canyon via Roaring River and subsequently made several attempts to explore the region to the north. They made their way up Copper Creek to Granite Basin and from the crest of the divide near Granite Pass (elevation 3,250 m; 10,673 ft) found that their pack animals could not descend into the steep canyon of the Middle Fork of the Kings River. From the crest, they mapped and named Mount Goddard on the San Joaquin-Kings divide, the Palisades on the main Sierra Nevada crest, and three nearby peaks on Kings Spur: Mount Gardiner, Mount Cotter, and Mount Clarence King. Returning to the South Fork Canyon, they worked their way east up Bubbs Creek to Kearsarge Pass and down to Owens Valley, ending their explorations in this area (Farquhar, 1965).

38.2 **Bridge over South Fork Kings River.**

38.7 **Highway cuts through a small Tioga (Tenaya?) recessional moraine.**

39.5 **Zumwalt Meadow. There are restrooms in the parking lot here.** North Dome (2,658 m; 8,717 ft) towers above the meadow to the north.

40.4 40.4 **Road's End. Continue around the loop and turn right into the last parking area. If this lot fills, go around the loop a second time and park in one of the earlier, long-term parking areas. There are restrooms here.**

STOP 9: Road's End (12:30-13:30) Burke and Stock. See Appendices 9A and 9B.
Late Pleistocene and Holocene glaciation in the Sierra Nevada; speleothem records of glacial-interglacial transitions.

The prominent cliff on the south wall of Kings Canyon here is the Grand Sentinel. John Muir explore Kings Canyon during 1875-1877 and wrote of the Grand Sentinel: "Beyond the Gable Group, and separated slightly from it by the beautiful Avalanche Canyon and Cascades, stand the bold and majestic mass of the Grand Sentinel, 3,300 feet high, with a split vertical front presented to the valley, as sheer and nearly as extensive as the front of Yosemite Half Dome. Projecting out into the valley from the base of this sheer front is the Lower Sentinel, 2,400 feet high; and on either side, the West and East Sentinels, about the same height, forming altogether the boldest and most massively sculpted group in the valley" (Muir, 1891). Muir, a keen observer of nearly all aspects of Sierra Nevada natural history, was a strong advocate of a glacial origin for the deep U-shaped canyons of the High Sierra, but his ideas were ridiculed at the time by many of the leading California geologists, including Clarence King and Josiah Whitney. Most would now agree that Muir was correct – glacial striations and polish on the walls of the above Road's End indicate that Pleistocene glaciers were hundreds of meters thick at this point.

Road's End is only 24 km (15 mi) from trailheads on the eastern side of the Sierra Nevada west of Independence, and is situated two-thirds of the way across the range. Naturally, there were those folks who wanted to continue the road up Bubbs Creek and over Kearsarge Pass to Independence, but their efforts were stymied in 1965 when the Sierra Club and others fought to end the road here. Road's End is now a popular trailhead for the rugged backcountry of the upper South and Middle Fork Kings Rivers.

Return to vehicles, and backtrack west on Highway 180 toward Grant Grove and Fresno.

71.2 71.2 **Hume Lake turnoff. Continue straight on Highway 180 toward Grant Grove and Fresno.**

72.7 **Impressively grussified granite in roadcuts.**

76.2 **Entrance to Kings Canyon National Park.**

77.4 **Turnoff to General Grant Tree.**

77.5 **Grant Grove Visitor Center.** Elevation 2,008 m (6,589 ft).

79.1 79.1 **The Wye. This is the junction between Highway 180 and the General's Highway. Reset odometer and bear right towards Fresno.**

0.0 79.1 **Junction of Highway 180 and Generals Highway.**

1.1 **Big Stump Picnic Area.** Restrooms are here.

1.7 80.8 **Kings Canyon Entrance Station. Leaving Kings Canyon National Park.** Show the Park Service letter on the last page of this guide for an access fee waiver.

7.9 **Late Tertiary basalt in roadcut.** This is another of the many small remnants of potassium-rich basalt scattered about the southern Sierra Nevada. This lava contains phenocrysts of olivine, biotite, and augite, and fine-grained minerals of augite, biotite, luecite, K-feldspar, apatite, and opaque minerals. About 2 km south, a second basalt remnant capping Stony Flat has a whole-rock K-Ar age of 3.4 Ma (Moore and Dodge, 1980).

15.4 **Boundary of Giant Sequoia National Monument.**

21.9 **Bridge over Mill Creek.**

24.3 **Town of Squaw Valley.**

29.2 108.3 **Large turnout on left (south) side of Highway 180. Turn left into turnout and park close together. It may be necessary to double park. Be careful crossing the lane of oncoming traffic – it is difficult to see around the corner. We will try to have someone on the shoulder controlling traffic.**

STOP 10: Foothills east of Fresno (15:00-15:30) Stock. See Appendix 10.
Buried topography and lack of exposed Tertiary strata in the southern Sierra Nevada foothills.

This is the final stop of the 2003 FOP trip. Drive safely, and see you next year!

REFERENCES CITED

Farquhar, F., P., 1965, History of the Sierra Nevada: Berkeley, University of California Press, 262 p.

Moore, J. G., 2000, Exploring the Highest Sierra, Stanford University Press, Stanford, California, 427 p.

Moore, J. G., and Dodge, F. C. W., 1980, Late Cenozoic volcanic rocks of the southern Sierra Nevada, California: I. Geology and petrology: Geological Society of America Bulletin, v. 91, p. 515-518.

Moore, J. G., and Nockleberg, W. J., 1991, Geologic map of the Tehipite Dome Quadrangle, Fresno County, California: U.S. Geological Survey map GQ-1676.

Muir, J., 1891, A rival of the Yosemite: The canyon of the South Fork Kings River, California: Century, v. 43, p. 77-91.

Sisson, T., W., and Moore, J. G., 1994, Geologic map of the Giant Forest Quadrangle, Tulare County, California: U.S. Geological Survey Map GQ-1751

Stephenson, N. L., 2000, Estimated ages of some large Giant Sequoias: General Sherman keeps getting younger: Madrono, v. 47, p. 61-67.

Stock, G. M., Anderson, R. S., and Finkel, R. C., in review, Pace of landscape evolution in the Sierra Nevada, California, revealed by cosmogenic dating of cave sediments

Wahrhaftig, C., 1984, Geomorphology and glacial geology – Wolverton and Crescent Meadow areas and vicinity, Sequoia National Park, California: U. S. Geological Survey Open-File Report 84-400, 52 p.

APPENDIX 1: OVERVIEW OF THE CENOZOIC GEOLOGIC HISTORY OF THE SIERRA NEVADA

John Wakabayashi *1329 Sheridan Lane, Hayward, CA 94544 wako@tdl.com*
Greg M. Stock *University of California, Santa Cruz, Santa Cruz, CA 95060 gstock@es.ucsc.edu*

INTRODUCTION

The ~650 km long Sierra Nevada is the most prominent mountain range in California, with peak elevations that exceed 2000 m over a distance of 500 km, and 3000 m over a distance of 350 km. Crestal elevations increase systematically from north to south, reaching their maximum in eastern Sequoia and Kings Canyon National Parks. Mount Whitney, located at the headwaters of the Kern River, marks the highest point of the range (and also the highest point in the lower 48 states) at 4,419 m (14,495 ft). South of Mount Whitney, crestal elevations decrease rapidly. From the crest, the range slopes gently westward in a broad, low-relief surface punctuated by deeply incised river canyons. In the northern part of the range, the western slope has a relatively uniform low-angle slope, whereas in the southern part of the range, in the Sequoia-Kings Canyon region, it slopes gently west of the crest and steepens in the western foothills. In contrast, the eastern slope drops steeply, leading to a distinct asymmetry to the range. The height of the eastern escarpment varies from about 1,000 m in the northernmost part of the range to nearly 3,300 m below Mount Whitney.

The Sierra Nevada and the adjacent Central Valley are part of the Sierra Nevada microplate, an element of the broad Pacific-North American plate boundary (Argus and Gordon, 1991). The microplate is bounded on the west by an active fold and thrust belt that marks the eastern margin of the Coast Range province, and on the east by prominent eastern escarpment that marks the Sierra Nevada Frontal Fault System, a zone of normal, normal dextral, and dextral faulting (e.g., Beanland and Clark, 1995). Internal deformation of the microplate is minor compared with deformation along its boundaries.

PRE-LATE CENOZOIC HISTORY OF THE SIERRA NEVADA

Although our focus is on late Cenozoic topographic development of the Sierra Nevada, it is necessary to also understand some of the pre-late Cenozoic history, because the earlier history of the range contributed substantially to the present topography. The geologic units of the Sierra Nevada comprise late Cretaceous (~85 Ma) and older granitoids and assorted metamorphic rocks intruded by them (called "basement" herein), that are uncomformably overlain by sedimentary and volcanic strata that are predominantly Eocene and younger (Bateman and Wahrhaftig, 1966). Sierra Nevada topography appears to be a product of late Cenozoic uplift and relief generation superimposed on pre-existing topography (Wakabayashi and Sawyer, 2001). The amount of paleorelief (relief that predates late Cenozoic uplift) is much larger in the southern than northern Sierra (Fig. 1-1). In the northern Sierra Nevada, late Cenozoic volcanic rocks cap the ridges, and only a few isolated basement highs rise above the late Cenozoic deposits. In contrast, in the Tuolumne River drainage, late Cenozoic deposits are inset hundreds of meters below basement ridgetops (Wakabayashi and Sawyer, 2001). The reconstruction of the 10 Ma paleo-San Joaquin River channel suggests paleorelief that exceeds 1000 m in parts of that drainage (Huber, 1981). The difference in

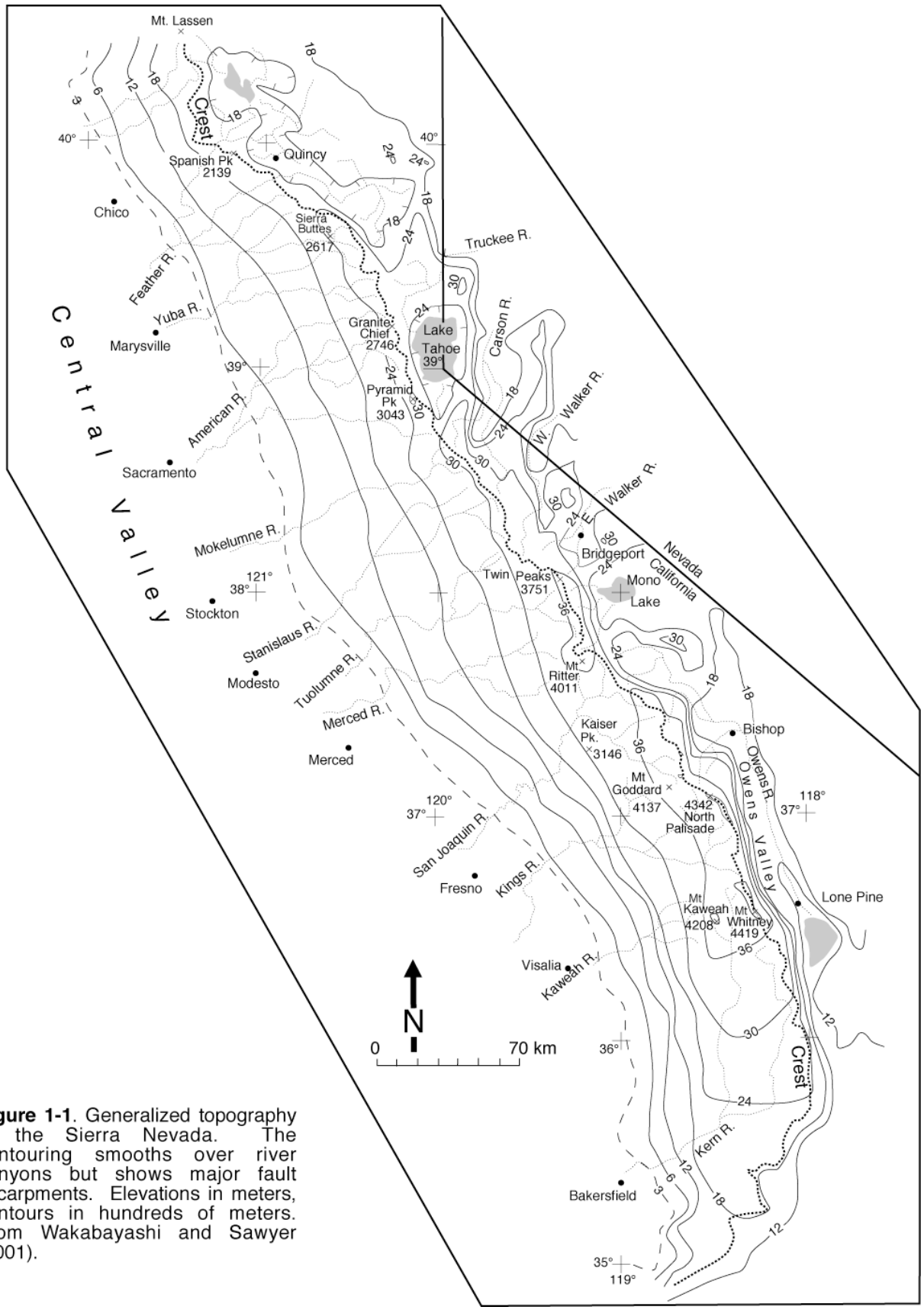

Figure 1-1. Generalized topography of the Sierra Nevada. The contouring smooths over river canyons but shows major fault escarpments. Elevations in meters, contours in hundreds of meters. From Wakabayashi and Sawyer (2001).

paleorelief from north to south appears to coincide with the difference in present peak elevations, as well as the different cross-sectional topographic shape of the northern and southern part of the range (Fig. 1-2) (Wakabayashi and Sawyer, 2001).

The channeling of Mio-Pliocene and Oligocene units into or through Eocene deposits is minimal, suggesting minimal Eocene to Miocene-Pliocene incision (≤150 m, and mostly <60 m) at extremely low time-averaged rates (<0.007 mm yr^{-1}, and mostly <0.003 mm yr^{-1}). This contrasts starkly with post Miocene-Pliocene incision of as much as 1 km at time-averaged (5 Ma to present) rates of up to 0.2 mm yr^{-1}. The lack of Eocene to Miocene-Pliocene incision and erosion is consistent with low sedimentation rates (≤0.02 mm yr^{-1}) in the Great Valley, where much of the eroded material from the Sierra was deposited (Wakabayashi and Sawyer, 2001) (Fig. 1-3). For comparison, sedimentation rates averaged over the last 5 Ma are as high as 0.16 mm yr^{-1}, and pre-Eocene rates are as high as 0.52 mm yr^{-1}.

Plutons of 100 Ma age were emplaced at depths of 11 to 15 km (Ague and Brimhall, 1988) were exhumed and locally covered by Eocene gravels. The Eocene gravels have a rather wide range of age estimates associated with them, but, based on the sedimentation record in the Great Valley, it is likely that major exhumation and erosion were complete by the beginning of the Eocene. Because the style of deformation in the Sierra Nevada in the late Cretaceous-early Tertiary was transpressional (e.g., Renne et al., 1993; Tobisch et al., 1995), exhumation was essentially equal to erosion (for extensional or transtensional deformation exhumation can be much greater than erosion because of tectonic removal of overlying material). Exhumation of the 100 Ma plutons by the beginning of the Eocene requires erosion rates that averaged 0.26-0.35 mm yr^{-1} from 100 to 57 Ma (Wakabayashi and Sawyer, 2001).

Apparently pre-Eocene erosion rates were higher in the Sierra than they have been in the last 5 Ma and much higher than the rates from 57 to 5 Ma. Accordingly, it is likely that paleorelief in the Sierra is largely relict from a pre-Eocene episode of uplift. What peak elevation the range attained during this earlier phase of uplift is difficult to estimate because there are no preserved markers of paleoelevation. The spatial distribution of (U-Th)/He cooling ages has been used to estimate relief that existed in late Cretaceous time and by comparison to modern relief, estimate elevation (House et al., 1998), but these estimates are dependent on an assumption of laterally constant thermal gradients. This assumption may not be valid, considering that the sampling transect crosses several different plutons of different ages and different intrusion depths (Ague and Brimhall, 1988). The cooling rate of the plutons indicated by the apatite and sphene fission track data of Dumitru (1990) suggest that the age and age difference of the plutons may significantly impact (U-Th)/He cooling ages.

An estimate for peak paleoelevations of the range prior to late Cenozoic uplift can be made by subtracting late Cenozoic uplift estimates from the present elevations of the range. Such an exercise results in estimated peak paleoelevations of 2500 m or higher in the southern Sierra Nevada (Kings River drainage) to less than 1000 m in the northern Sierra (Wakabayashi and Sawyer, 2001) (Fig. 1-4). Erosion rates of bedrock summit and interfluve surfaces in the Sierra Nevada are low (0.002-0.020 mm yr^{-1}; Small et al., 1997; Stock et al., in review), so the amount of elevation loss since 5 Ma of these surfaces should be fairly low (<75m). In addition, because Eocene-Miocene erosion in the Sierra appears to have been fairly minor, it is likely that the range did not stand much higher at 57 Ma than it did at 5 Ma. The range may have been much higher in the late Cretaceous as a result of transpressional deformation and the construction of large arc volcanoes, but, as noted previously, estimation of peak elevations during this time is uncertain.

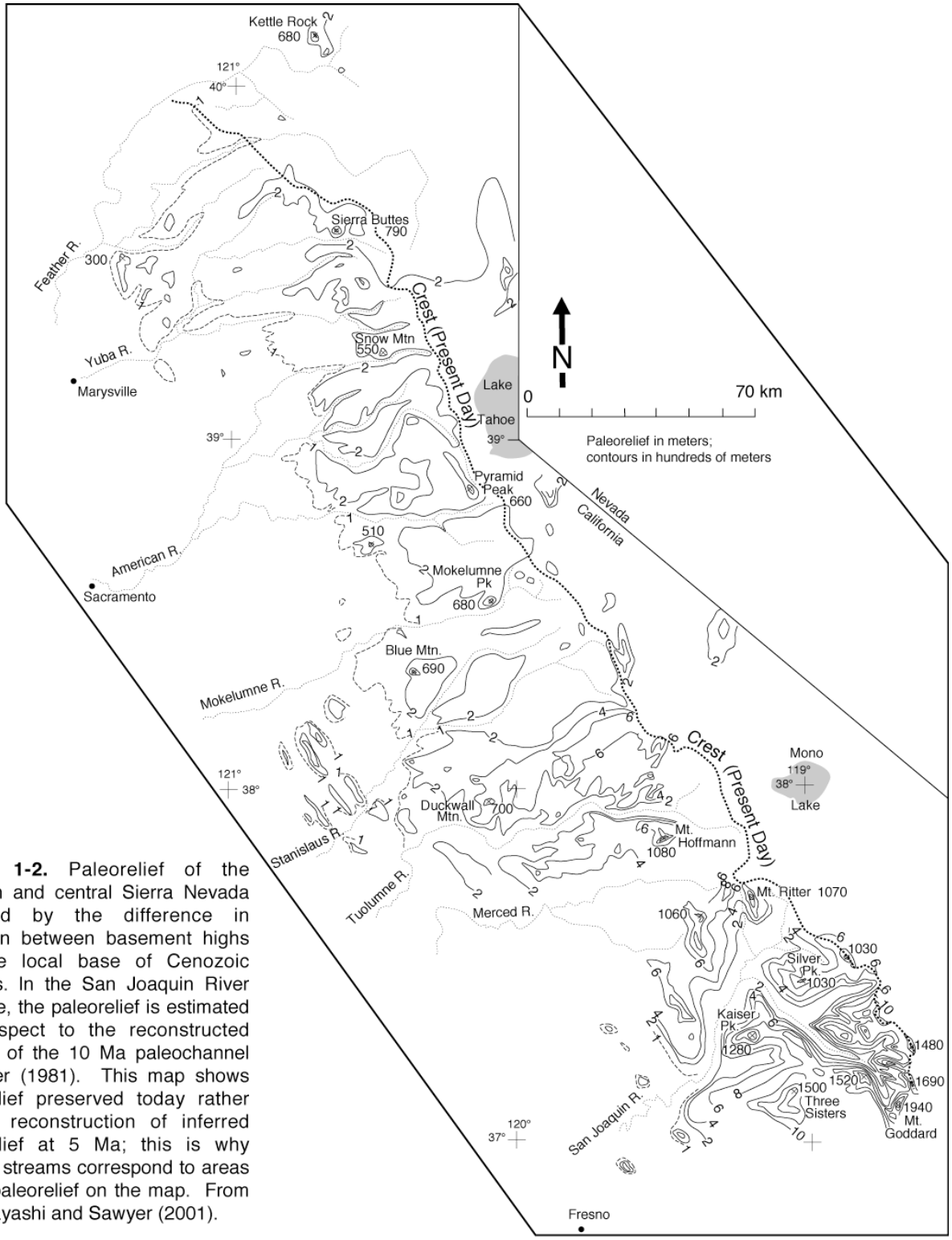

Figure 1-2. Paleorelief of the northern and central Sierra Nevada recorded by the difference in elevation between basement highs and the local base of Cenozoic deposits. In the San Joaquin River drainage, the paleorelief is estimated with respect to the reconstructed position of the 10 Ma paleochannel of Huber (1981). This map shows paleorelief preserved today rather than a reconstruction of inferred paleorelief at 5 Ma; this is why modern streams correspond to areas of low paleorelief on the map. From Wakabayashi and Sawyer (2001).

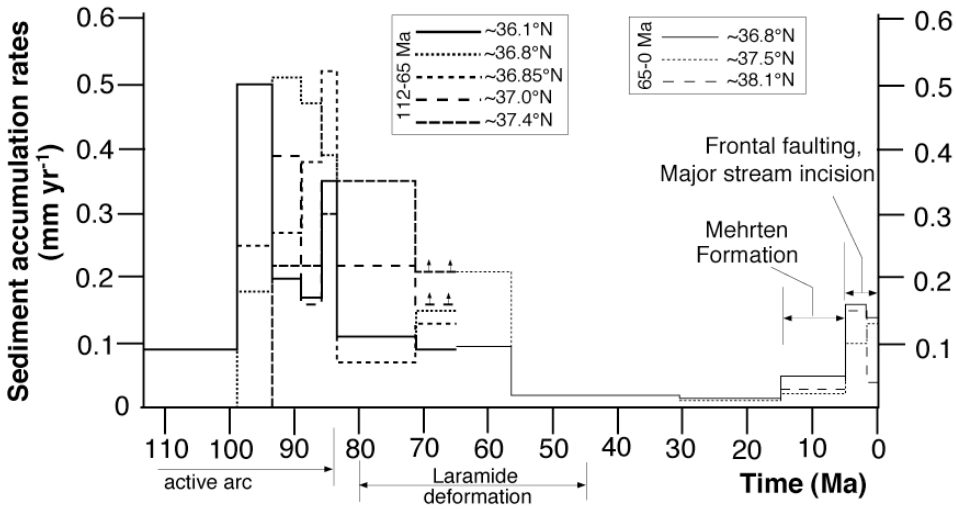

Figure 1-3. Accumulation rates in the San Joaquin basin. Rates are calculated from unit thicknesses of Moxon (1988) for Cretaceous deposits and of Bartow (1985) for Cenozoic deposits, and timescales of Gradstein et al. (1995) for the Cretaceous and of Berggren et al. (1995) for the Cenozoic. Upward pointing arrows above accumulation rate lines denote minimum rates. The Cretaceous part of the diagram is restricted to the San Joaquin basin, and the Cenozoic part is restricted to the eastern part of the northern San Joaquin basin, because sediment sources other than the Sierra may contribute to other parts of the Great Valley basin (the Klamath Mountains for the Cretaceous Sacramento Valley basin and the Tehachapi Mountains and Coast Ranges for the southern and western parts of the Cenozoic San Joaquin Basin). From Wakabayashi and Sawyer (2001).

The tectonic setting of the range has changed in the last 100 Ma. Until 85 Ma, an active magmatic arc existed in what has become the Sierra Nevada. Syn-plutonic erosion and exhumation were associated with transpressional tectonics (Renne et al., 1993; Tobisch et al. 1995). Material eroded from the Sierra was deposited in the Great Valley forearc basin. Transpressional deformation migrated from west to east with time (Tobisch et al. 1995) and the most deeply exhumed rocks are in the western part of the range, with the exception of some much more deeply exhumed rocks in the southernmost Sierra and Tehachapi Mountains (Ague and Brimhall, 1988). The pattern of exhumation and tectonic evolution contrasts with the late Cenozoic tectonic regime in which the greatest exhumation occurs toward the eastern part of the range, associated with transtensional faulting that is encroaching westward into the range (Wakabayashi and Sawyer, 2001). Magmatism shut off in the Sierra at about 85 Ma (e.g., Stern et al., 1981; Chen and Moore, 1982), possibly in response to low-angle subduction (e.g., Dickinson and Snyder, 1978).

Magmatism did not resume in the vicinity of the Sierra until about 34 Ma, and actual arc magmatism did not occur until about 14 Ma (Christensen and Yeats, 1992). This arc magmatism resulted in nearly continuous volcanic cover of the Sierra Nevada from the Stanislaus River drainage northward by about 4-5 Ma. These andesites, andesitic mudflows and associated volcanic sedimentary rocks (the Mehrten Formation and related rocks) flowed westward from their sources across the Sierra. The southernmost paleodrainage traversed by such trans-Sierra volcanic rocks was the San Joaquin (Huber, 1981). Scattered Cenozoic volcanic rocks crop out south of the San Joaquin River drainage, and these volcanic rocks are local phenomena in contrast to the magmatic arc rocks to the north (Moore and Dodge, 1980). From 20 Ma to the present, the eastern boundary of the Sierran tectonic block or microplate has encroached westward; the width of the Sierran microplate has been progressively reduced.

Although this process, and associated Basin and Range extensional tectonics have been operative since 20 Ma, no effect on stream incision in the Sierra occurred until about 5 Ma when late Cenozoic uplift of the Sierra is estimated to have begun. This suggests that from 20 Ma to 5 Ma Basin and Range tectonism, including that occurring along the eastern Sierran microplate margin, did not result in significant uplift of the microplate.

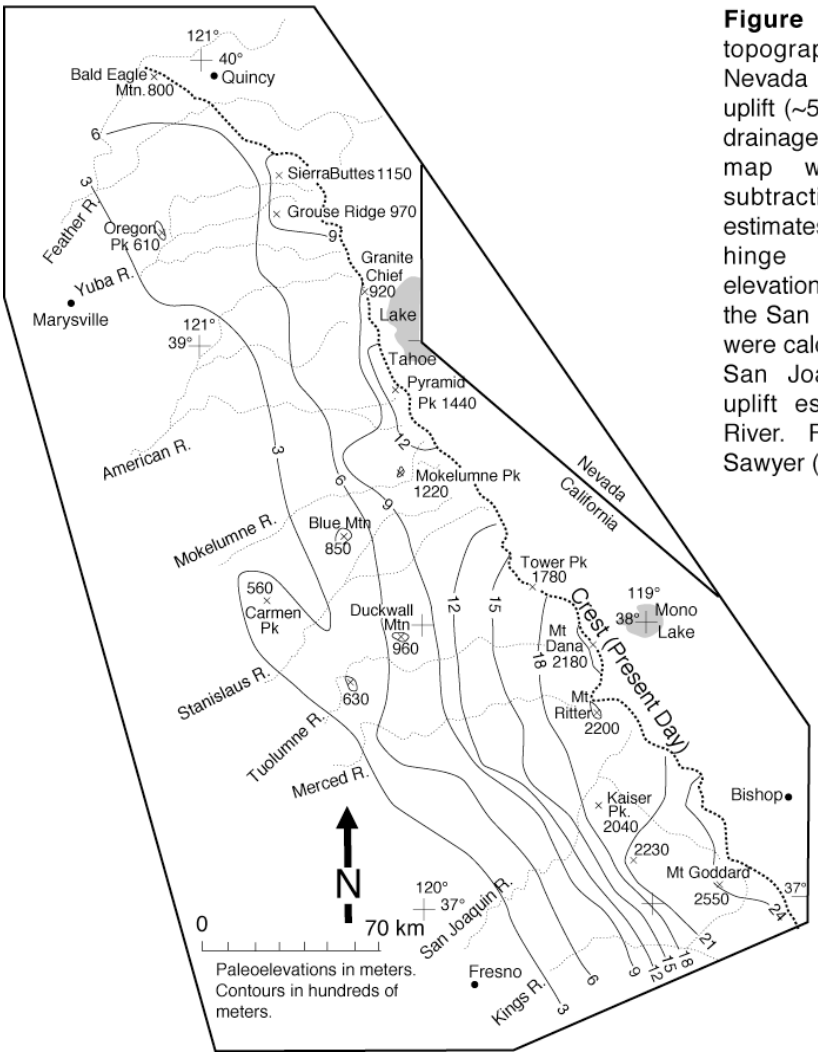

Figure 1-4. Generalized topography of the Sierra Nevada prior to late Cenozoic uplift (~5 Ma) with smoothing of drainages as in Figure 1-1. The map was constructed by subtracting preferred uplift estimates, scaled from crest to hinge line, from present elevations. Elevations south of the San Joaquin River drainage were calculated by extrapolating San Joaquin River drainage uplift estimates to the Kings River. From Wakabayashi and Sawyer (2001).

LATE CENOZOIC UPLIFT AND TOPOGRAPHIC HISTORY

For over a century, the modern high elevations and topography of the Sierra Nevada have been postulated to be the result of late Cenozoic uplift by westward tilting, coupled with faulting along the Frontal Fault system. Early workers observed that the broad, alluviated river systems of Eocene-Miocene age now had steeper gradients than their modern bedrock counterparts (e.g., Lindgren, 1911); these steeper gradients were presumably due to uplift of the range by tilting (Fig 1-5). Subsequent detailed study of ancient river channels, volcanic flows, and tilted Central Valley strata along the western slope provide refined estimates of the timing and magnitude of rock uplift at the crest (Huber, 1981; Unruh, 1991; Wakabayashi and

Sawyer, 2001). Projection of these tilted markers along a rigid block suggests 1.5 to 2 km of crestal rock uplift over the last 10 Myr, with most of the uplift occurring in the last 3 to 5 Myr (Huber, 1981; Unruh, 1991; Wakabayashi and Sawyer, 2001). Renewed river incision in the range (Wakabayashi and Sawyer, 2001) and accelerated sedimentation in the adjacent Central Valley (Fig. 1-3) around this time support these conclusions.

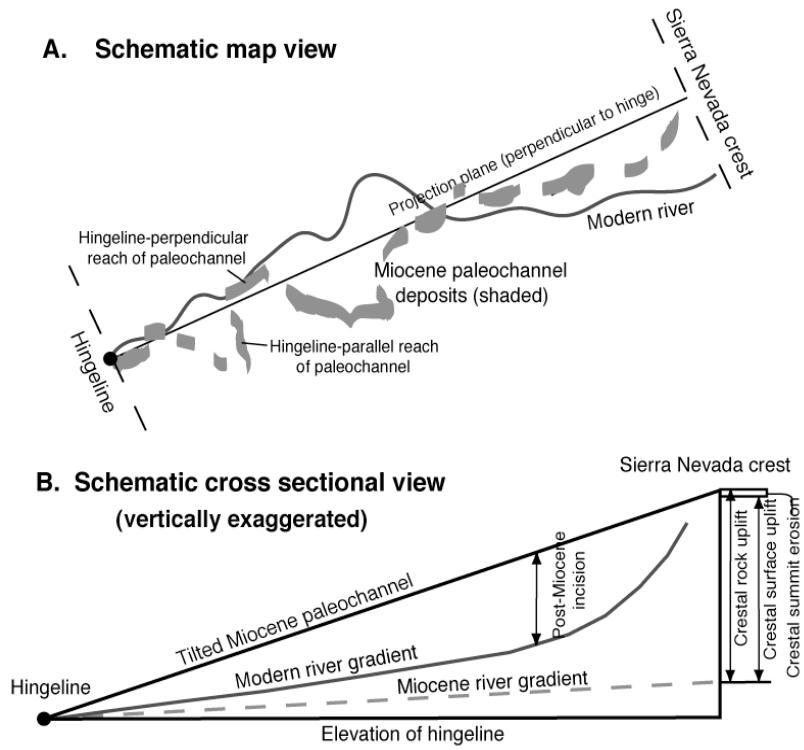

Figure 1-5. Methods used to estimate late Cenozoic rock uplift of the Sierra Nevada from tilted Cenozoic strata. A. Map view of Miocene paleochannel features used to estimate rock uplift. B. Diagram showing the relationship of tilted Miocene paleochannels, Miocene river gradients, and erosion to surface and rock uplift of the Sierra Nevada. From Wakabayashi and Sawyer (2001).

From both tectonic and isostatic perspectives, late Cenozoic rock uplift of the Sierra Nevada is unexpected. Researchers have therefore sought to explain late Cenozoic uplift by mechanisms independent of regional tectonics. Two mechanisms calling on significantly different forcing are particularly intriguing.

The first mechanism calls upon the flexural-isostatic response to accelerated erosion impelled by late Cenozoic climate change. Erosional unloading of the range, concentrated in the canyons, and simultaneous deposition of sediment in the adjacent Central Valley to the west, could drive rock uplift. Modeling suggests that approximately half to all of the observed tilt could be explained by this mechanism (Small and Anderson, 1995). In this scenario, mean elevation of the range decreases due to canyon lowering, enhanced by rapid glacial erosion, while summit elevations, limited to low bare bedrock erosion rates, increase.

The second proposed uplift mechanism is a tectonic rather than a climatic one. Recent geophysical research clearly demonstrated that the southern Sierra Nevada lacks a deep crustal root and suggested that the modern topography must instead be dynamically compensated by density variations in the mantle (e.g., Jones et al., 1994; Wernicke et al., 1996). Petrologic studies indicate that as silica-rich granitic rocks were distilled from sub ducted oceanic slab, a dense eclogite residue remained beneath the range following cessation of subduction (Ducea, 2001). This batholithic root was denser than the surrounding upper mantle. Rapid changes in xenolith composition and the pressure-temperature conditions of crystallization (Ducea and Saleeby, 1996; 1998) suggest that the dense root beneath the Sierra Nevada crest was convectively removed, or delaminated, sometime between 3 and 12 Ma. A short, potassium-rich pulse of magmata's may have accompanied this event (Manley et al., 2000; Farmer et al., 2002). Flexural-isostatic calculations indicate that the loss of a 10-40 km

thick eclogite root ($\rho \approx 3450$ kg/m^3) and its replacement with lower density asthenosphere ($\rho \approx 3300$ kg/m^3) would drive 1-2 km of rock uplift at the crest (Ducea and Saleeby, 1996; Stock and Anderson, unpublished modeling data). Crestal rock uplift of 1-2 km is consistent with the estimates of uplift based on extrapolation of tilted markers as discussed above.

Note that these two proposed uplift mechanisms (climatic and tectonic) are not mutually exclusive. Any tectonically induced tilting would likely accelerate erosion, resulting in further flexural isostatic rock uplift.

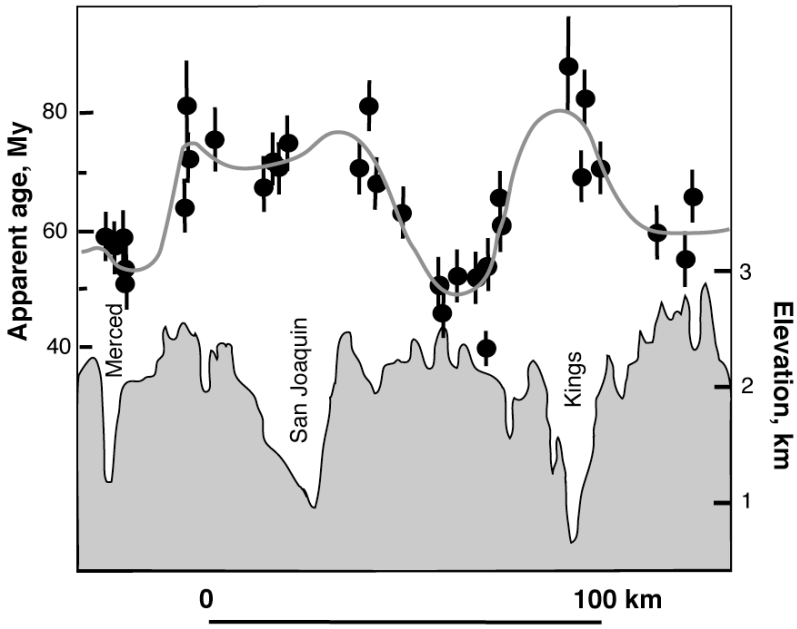

Figure 1-6. Results of U/Th(He) dating of apatite in Sierra Nevada granitic rocks. Older ages correlate approximately with modern canyons, while younger ages correlate with modern interfluves. These results were used to suggest significant local relief during the late Mesozoic and early Cenozoic that declined in the late Cenozoic, implying little or no late Cenozoic uplift (House et al., 1998)

(U-Th)/He apatite cooling ages may record high elevations and deep canyons in the Sierra Nevada as early as the late Cretaceous when the range was an active volcanic arc (Fig. 1-6; House et al., 1998; 2001). Greater local relief (the vertical distance between canyon bottoms and adjacent canyon rims) at 60-80 Ma than at present suggest that range elevations were higher at that time. Apatite cooling ages have also been used to argue for a monotonic decline in mean elevation and local relief during the Cenozoic. This implies no late Cenozoic uplift. In addition, $\delta^{18}O$ in antigenic minerals in volcanic deposits east of the Sierra Nevada crest suggest a persistent rain shadow throughout the Miocene (Poage and Chamberlain, 2002), implying crestal elevations were also high at that time. An apparent trend toward a decreasing rain shadow effect been interpreted as further evidence for a lack of late Cenozoic uplift (Poage and Chamberlain, 2002). Finally, recent pale botanical data suggest that the Sierra Nevada and adjacent Basin and Range had high elevations throughout the Miocene (Wolfe, 1997).

These new studies have called into question the long-held notion of late Cenozoic uplift and have renewed interest in the history of the Sierra Nevada topography. We hope to show over the course of this trip that the various conceptual models of late Cenozoic topographic evolution need not be in direct conflict. For example, the presence of substantial elevation and relief during the early Cenozoic need not preclude renewed uplift in the late Cenozoic. Westward tilting of the range, such as that incited by delamination of the batholithic root, would rejuvenate incision in pre-existing canyons, resulting in further flexural isostatic rock uplift. The depth history of Sierra Nevada river canyons is key to clarifying models of Cenozoic topographic evolution. New estimates of river incision and

paleotopography in the southern Sierra Nevada from cave deposits will be covered extensively during Stops 3, 6, and 7.

REFERENCES CITED

Ague, J.J., and Brimhall, G.H. 1988. Magmatic arc asymmetry and distribution of anomalous plutonic belts in the batholiths of California: Effects of assimilation, crustal thickness, and depth of crystallization. Geological Society of America Bulletin, v. 100, p. 912-927.

Argus, D. F., and Gordon, R. G., 1991, Current Sierra Nevada-North America motion from very long baseline interferometry: Implications for the kinematics of the western United States: Geology, v. 19, p. 1085-1088.

Bartow, J.A. 1985. Map and cross sections showing Tertiary stratigraphy and structure of the northern San Joaquin Valley, California. U.S. Geological Survey Misc. Field Studies Map MF-1761.age

Bateman, P.C., and Wahrhaftig, C. 1966, Geology of the Sierra Nevada, *In* Bailey, E.H., ed., Geology of northern California, California Division of Mines and Geology Bulletin 190, p. 107-172.

Berggren, W.A.; Kent, D.V.; Swisher, C.C., III; and Aubry, M.-P. 1995. A revised Cenozoic geochronology and chronostratigraphy. *In* Berggren, W.A.; Kent, D.V.; Aubry, M.-P.; and Hardenbol, J., eds. Geochronology time scales and global stratigraphic correlation. SEPM Spec. Pub. 54, p. 129-212

Chen, J.H., and Moore, J.G. 1982. Uranium-lead isotopic ages from the Sierra Nevada batholith. Journal of Geophysical Research, v. 87, p. 4761-4784.

Christiansen, R.L., and Yeats, R.S. 1992. Post-Laramide geology of the U.S. Cordilleran region. *In* Burchfiel, B.C.; Lipman, P.W.; and Zoback, M.L., eds. The Cordilleran orogen: Conterminous U.S. Geological Soc.iety of America, Geology of North America. G-3, p. 261-403.

Dickinson, W. R., and Snyder, W. S., 1978, Plate tectonics of the Laramide orogeny. *In* Matthews, V., III, ed., Laramide folding associated with basement block faulting in the western United States. Geological Society of America Memoir 151: 355-366.

Ducea, M. N., 2001, The California Arc: Thick granitic batholiths, eclogite residues, lithosphere-scale thrusting, and magmatic flare-ups: GSA Today, v. 11, p 4-10.

Ducea, M. N., and Saleeby, J. B., 1996, Buoyancy sources for a large, unrooted mountain range, the Sierra Nevada, California: evidence from xenolith thermobarometry: Journal of Geophysical Research, v. 101, p. 8229-8244.

Ducea, M. N., and Saleeby, J. B., 1998, A case for delamination of the deep batholithic crust beneath the Sierra Nevada: International Geology Review, v. 40, p. 78-93.

Dumitru, T.A. 1990. Subnormal Cenozoic geothermal gradients in the extinct Sierra Nevada magmatic arc: consequences of Laramide and post-Laramide shallow-angle subduction. Journal of Geophysical Research, v. 95, p. 4925-4941.

Farmer, G. L., Glazner, A. F., Manley, C. R., 2002, Did lithospheric delamination trigger late Cenozoic potassic volcanism in the southern Sierra Nevada, California?: Geological Society of America Bulletin, v. 114, p. 754-768.

Gradstein, F.M.; Agterberg, F.P.; Ogg, J.G.; Hardenbol, J.; VanVeen, P.; Thierry, J.; and Huang, Z. 1995. A Triassic, Jurassic, and Cretaceous time scale. *In* Berggren, W.A.; Kent, D.V.; Aubry, M.-P.; and Hardenbol, J., eds. Geochronology time scales and global stratigraphic correlation. SEPM Special Publication 54, p. 95-126.

House, M. A., Wernicke, B. P., and Farley, K. A., 1998, Dating topography of the Sierra Nevada, California, using apatite (U-Th)/He ages: Nature, v. 396, p. 66-69.

House, M. A., Wernicke, B. P., and Farley, K. A., 2001, Paleo-geomorphology of the Sierra Nevada, California, from (U-Th)/He ages in apatite: American Journal of Science, v. 301, p. 77-102.

Huber, N. K., 1981, Amount and timing of Late Cenozoic uplift and tilt of the central Sierra Nevada, California – evidence from the upper San Joaquin river basin: U.S. Geological Survey Professional Paper 1197, 28 p.

Jones, C. H., Hanimori, K., and Roeker, S. W., 1994, Missing roots and mantle "drips": Regional P_n and teleseismic arrival times in the southern Sierra Nevada and vicinity, California: Journal of Geophysical Research, v. 99, p. 4567-4601.

Lindgren, W., 1911, The Tertiary gravels of the Sierra Nevada of California: U.S. Geological Survey Professional Paper 73, 226 p.

Manley, C. R., Glazner, A. F., Farmer, G. L., 2000, Timing of volcanism in the Sierra Nevada of California: Evidence for Pliocene delamination of the batholithic root? Geology, v. 28, p. 811-814.

Moore, J.G., and Dodge, F.C.W. 1980. Late Cenozoic volcanic rocks of the southern Sierra Nevada, California I: Geology and petrology. Geological Society of America Bulletin, v. 91, p. 515-518.

Moxon, I., 1988, Sequence stratigraphy of the Great Valley in the context of convergent margin tectonics. *In* Graham, S. A., ed. Studies of the geology of the San Joaquin Basin. Pacific Section, SEPM 60, p. 3-28.

Renne, P. R., Tobisch, O. T., and Saleeby, J. B., 1993, Thermochronologic record of pluton emplacement, deformation, and exhumation at Courtright shear zone, central Sierra Nevada, California: Geology, v. 21, p. 331-334.

Small, E. E., and Anderson, R. S., 1995, Geomorphically driven Late Cenozoic rock uplift in the Sierra Nevada, California: Science, v. 270, p. 277-280.

Small, E. E., Anderson, R. S., Repka, J. L., and Finkel, R.,1997, Erosion rates of alpine bedrock summit surfaces deduced from in situ ^{10}Be and ^{26}Al: Earth and Planetary Science Letters, v. 150, p. 413-425.

Stern, T.W.; Bateman, P.C.; Morgan, B.A.; Newell, M.F.; and Peck, D.L. 1981. Isotopic U-Pb ages of zircon from granitoids of the central Sierra Nevada, California. U.S. Geological Survey Professional Paper 1185, 17 p.

Tobisch, O.T.; Saleeby, J.B.; Renne, P.R.; McNulty, B.; and Tong, W. 1995. Variations in deformation fields during the development of a large-volume magmatic arc, central Sierra Nevada, California. Geological Society of America Bulletin, v. 107, p. 148-166.

Unruh, J. R., 1991, The uplift of the Sierra Nevada and implications for Late Cenozoic epeirogeny in the western Cordillera: Geological Society of America Bulletin, v. 103, p. 1395-1404.

Wakabayashi, J., and Sawyer, T. L., 2001, Stream incision, tectonics, uplift, and evolution of topography of the Sierra Nevada, California: Journal of Geology, v. 109, p. 539-562.

Wernicke, B., Clayton, R., Ducea, M., Jones, C. H., Park, S., Ruppert, S., Saleeby, J., Snow, J. K., Squires, L., Fliedner, M., Jiracek, G., Keller, R., Klemperer, S., Luetgart, J., Malin, P., Miller, K., Mooney, W., Oliver, H., Phinney, R., 1996, Origin of high mountains in the continents: The southern Sierra Nevada: Science, v. 271, p. 190-193.

APPENDIX 2: STRATIGRAPHIC SEQUENCES OF THE KINGS RIVER ALLUVIAL FAN FORMED IN RESPONSE TO SIERRA NEVADA GLACIAL CYCLICITY

Gary S. Weissmann *Michigan State University, East Lansing, MI 48824*
weissman@msu.edu
George L. Bennett, V *Michigan State University, East Lansing, MI 48824*
benne183@msu.edu
Graham E. Fogg *University of California, Davis, Davis, CA 95616*
gefogg@ucdavis.edu

INTRODUCTION

Pleistocene glaciations in the Sierra Nevada produced significant amounts of sediment, much of which was deposited on alluvial fans and in basinal lacustrine or axial fluvial systems in the San Joaquin Valley. Cycles of high aggradation during periods of glaciation and low aggradation or erosion during interglacial periods have long been recognized from soil mapping (e.g., Janda, 1966; Arkley, 1962; Marchand, 1977; Marchand and Allwardt, 1981; Huntington, 1971, 1980; Harden, 1987) and subsurface analysis (Lettis, 1982, 1988; Atwater et al 1986).

Recently, Weissmann et al. (2002a) recognized stratigraphic sequences related to Pleistocene glaciations in the Kings River alluvial fan, located south of Fresno, California. In this work, they proposed a sequence stratigraphic conceptual model for deposition in large, stream-dominated alluvial fans (fluvial fans?) of the eastern San Joaquin Valley. The significance of the sequence stratigraphic model is that it provides a framework for regional- and local-scale analysis of groundwater flow and solute transport (e.g., Weissmann et al, 2002b, in press).

This paper outlines the alluvial fan sequence stratigraphic conceptual model and identifies stratigraphic sequences in the Kings River alluvial fan. Applications of this conceptual model as a framework for geostatistical modeling and in groundwater studies are beyond the scope of this paper, however details on such applications can be found in Weissmann and Fogg (1999) and Weissmann et al. (1999, 2002b, in press).

BACKGROUND

The advancement of concepts related to sequence stratigraphy has revolutionized geoscientist's views of stratigraphic development. Sequence stratigraphy provides a framework for prediction of facies distributions, enhancing our ability to predict and model subsurface fluid flow (e.g., petroleum and groundwater). In this approach, the stratigraphic section is divided into chronostratigraphic sequences, where a sequence is defined as "… a relatively conformable succession of genetically related strata bounded at its top and base by unconformities, or their correlative conformities" (Mitchum, 1977, p. 210). Although most applications of sequence stratigraphy have focused on marine or near shore settings, sequence stratigraphic concepts can likely lead to improved predictive modeling of facies in continental settings (Shanley and McCabe, 1994; Weissmann and Fogg, 1999; Weissmann et al., 2002a, 2002b).

Controls on sequence development in fluvial depositional systems, however, differ from those of marine depositional systems. Accommodation space, or space available for

sediment accumulation, in marine systems is primarily defined by relative sea level (controlled by eustatic sea level and local tectonics). In fluvial systems, Blum and Törnqvist (2000) suggest that accommodation should be viewed as a combination of accumulation space and preservation space. Accumulation space is controlled by variability in sediment supply and discharge, where the balance between these controlling factors determines whether a fluvial system is in aggradation, degradation, or at grade. Positive accumulation space exists when relatively long-term fluvial aggradation occurs at a site, while negative accumulation space exists in areas of degradation.

On alluvial fans, the intersection point separates regions on the fan that experience positive accumulation space from regions that experience negative accumulation space (Weissmann et al., 2002a). Above the intersection point, the alluvial fan river is held within an incised valley, thus indicating degradation and negative accumulation space. Below the intersection point, a depositional lobe exists where aggradation is occurring, thus indicating the presence of positive accumulation space. During periods of relatively high accumulation space, the intersection point lies at a position near the fan apex, with open-fan deposition occurring across most of the alluvial fan surface. During periods of low accumulation space, the intersection point shifts to a relatively distal position, the river is held in an incised valley, and the upper to mid-fan areas are exposed to soil development, erosion, and/or eolian reworking. These soils and the bases of incised valleys developed during the low accumulation space times mark the unconformities that eventually form the alluvial fan sequence boundaries.

Preservation space in a fluvial system is produced "… when subsidence lowers these deposits below possible depths of incision and removal" (Blum and Törnqvist, 2000, p. 20). Cycles in accumulation space form the stratigraphic sequences in a fluvial system, while production of preservation space allows the sequences to be preserved in the stratigraphic record.

SEQUENCE DEVELOPMENT ON ALLUVIAL FANS

Sequences on the Kings River alluvial fan were formed in response to glacial cyclicity in the Sierra Nevada (Figure 2-1). Development of sequence boundaries began on the Kings River alluvial fan at the end of glacial periods and the beginning of interglacial periods, when fan incision and a basinward shift in the fan intersection point occurred due to declines in the sediment supply to discharge ratio in the Kings River. This fan incision created an incised valley in the middle and upper portions of the fan. Throughout the interglacial period, deposition was confined to the distal portions of the fan while the upper alluvial fan was exposed to erosion, soil development, or modification by eolian processes. The base of the incised valley and the soils formed during the interglacial periods mark the sequence boundaries on the Kings River alluvial fan.

Rapid aggradation (e.g., accumulation space gain) occurred in response to higher sediment supply during the glacial events (Lettis, 1982, 1988; Weissmann et al., 2002a). Though discharge also increased significantly, the large sediment volume released from glaciers was sufficient to cause this aggradational event. Initially, the incised valley filled with a fining-upward succession of relatively coarse-grained channel and overbank deposits. Continued deposition due to high sediment supply to discharge ratios eventually filled the incised valley. Upon filling of the incised valley, the intersection point stabilized near the fan apex, leading to relatively unconfined deposition across the entire alluvial fan surface, or

open-fan deposition. These open-fan deposits consist of a mix of discrete coarse-grained, channel-fill deposits within fine-grained, silt-dominated overbank deposits. Sediments in the middle to upper portions of the Kings River alluvial fan are predominantly open-fan deposits. The end of glaciation led to repetition of this stratigraphic cycle with subsequent decrease in the sediment supply to discharge ratio (e.g., accumulation space loss), fan incision, basinward shift in deposition, and soil development on the upper alluvial fan.

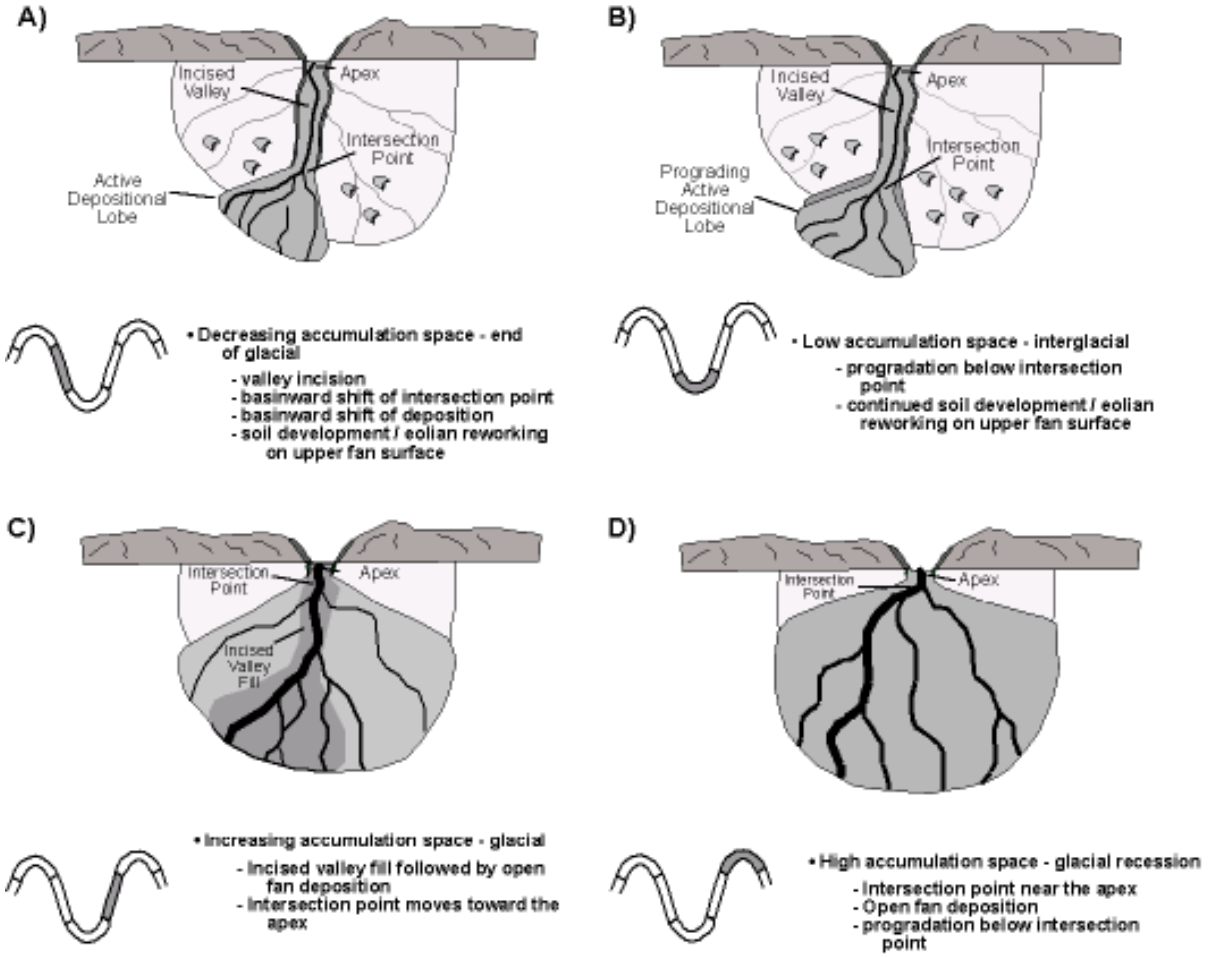

Figure 2-1. Sequence cycles on a stream-dominated alluvial fan. Darker shading indicates active areas of the alluvial fan. A) Decrease in accumulation space, B) Low accumulation space, C) Increase in accumulation space, D) High accumulation space. From Weissmann et al., 2002a.

KINGS RIVER ALLUVIAL FAN STRATIGRAPHY

Methods and Data Sources

Several data sources provide evidence supporting this stratigraphic model for the Kings River alluvial fan. Excellent soil series maps, compiled and interpreted by Huntington (1971, 1980), allowed for geomorphic assessment of sequence distributions and facies trends. Subsurface analysis of the fan stratigraphy was based on core from seven stratigraphic test wells (Burow et al, 1997; Weissmann, 1999; Weissmann et al., 2002a), from lithologic descriptions from hundreds of driller's well logs, and from approximately 120 km of ground penetrating radar surveys (Bennett et al., 2002). Anyone who has used driller's well log data

understands the high uncertainty involved in interpreting these data, however, we found that drillers that used cable tool drilling methods were relatively accurate in their lithologic descriptions. Recent ground penetrating radar data collection provides information that shows the lateral distribution and continuity of the shallowest paleosol on the Kings River alluvial fan (Bennett et al, 2002). The subsurface data were compiled into cross sections, and sequence geometries were determined from these cross sections. This stratigraphic framework was used for detailed geostatistical modeling of facies distributions (Weissmann et al, 1999; Weissmann and Fogg, 1999), which was in-turn applied in groundwater modeling (Weissmann et al., 2002b, in press).

Observations and Stratigraphy

The modern interglacial topography of the Kings River alluvial fan shows that the Kings River is currently held in a 3 meter deep incised valley (Figure 2-2). The modern intersection point is located in a distal position, approximately 2 km south of Kingsburg. The valley is sufficiently deep to contain flooding of any magnitude from the current climatic regime, therefore, the upper fan surface no longer receives sediment (except for minimal eolian deposition) and was exposed to soil development prior to intensive reworking through modern agriculture. Below the intersection point, aggradation on a depositional lobe (Laguna de Tache) occurred until the construction of Pine Flat Reservoir, located in the Sierra Nevada foothills on the Kings River.

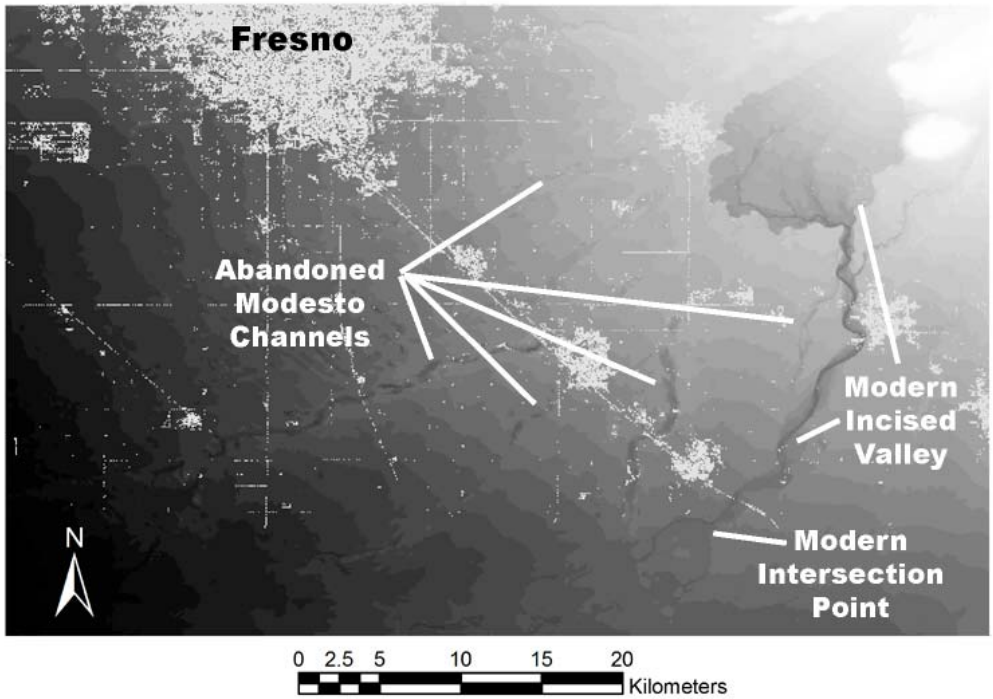

Figure 2-2. A digital elevation model for the upper Kings River alluvial fan (higher elevations shown as lighter shades) showing the modern incised valley and Modesto abandoned channels.

Also apparent on topographic maps, aerial photographs, satellite images, and soil surveys are a series of abandoned channels on the exposed upper fan surface that radiate outward from an old intersection point located near the fan apex approximately 4.5 km east of Sanger (Figure 2-2; Huntington, 1971, 1980; Weissmann et al., 2002a). Soil development and surrounding lithologies (e.g., relatively 'fresh' silt that appears to be similar to glacial flour) indicate these channels were active during the most recent glacial event (Huntington, 1971; 1980). Thus, open fan deposition appears to have occurred on the upper fan surface during glacial events. Regional correlation puts these most recent deposits in the Modesto Formation (Figure 2-3). The widths of these channels are consistent with significantly greater discharge in the Kings River expected during glacial episodes, however the thick succession of fan deposits indicates that the sediment load was sufficient to cause aggradation.

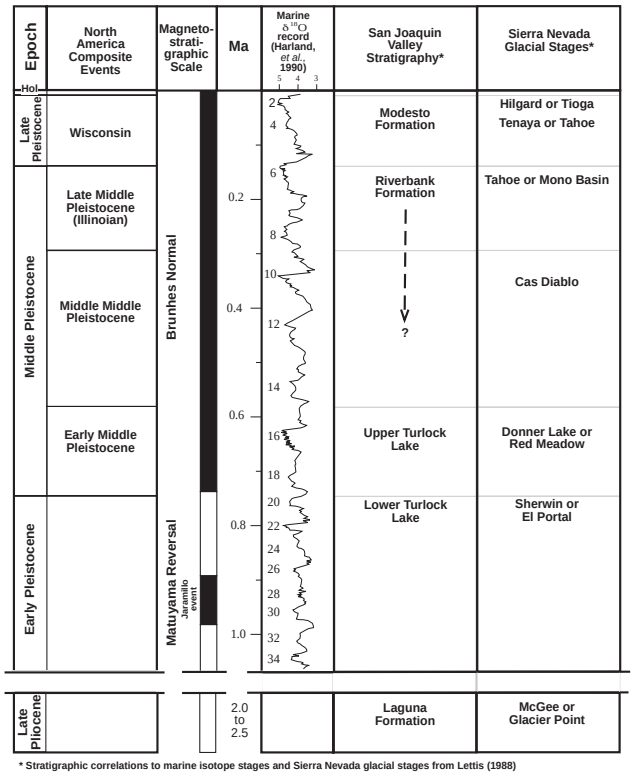

Figure 2-3. The stratigraphic column for the Kings River alluvial fan (based on Marchand and Allwardt, 1981; Harden, 1987; Lettis, 1988). Each stratigraphic unit consists primarily of stream-dominated alluvial fan deposits (From Weissmann et al., 2002a).

Soil morphologies can also be used to identify older, open fan deposits (e.g., Riverbank Formation, Turlock Lake Formation; Huntington, 1971, 1980). Relatively long-term exposure of these deposits has led to development of duripans. Because these units were deposited near the fan apex, the intersection point during these past glaciations must have also been near the apex, indicating that accumulation space was broadly available.

The hard B-horizon of the Riverbank Formation soils can be traced across the shallow subsurface on much of the Kings River alluvial fan. Soil surveys (Figure 2-4), extensive ground penetrating radar surveys (Bennett et al., 2002), and well log correlation (Figure 2-5) indicate that this soil is buried under a relatively thin veneer of Modesto Formation deposits.

This soil (paleosol) forms one of the sequence boundaries on the Kings River alluvial fan, separating the Riverbank Formation from the Modesto Formation.

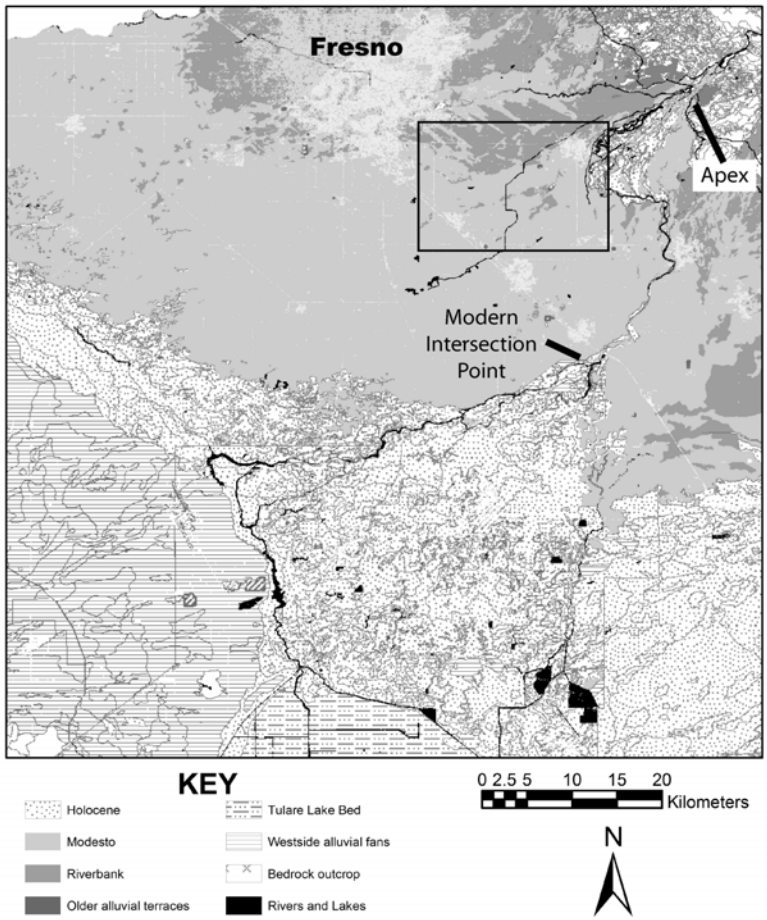

Figure 2-4. Interpreted soil survey of the Kings River alluvial fan showing the surface distribution of sequences (modified from Huntington, 1971).

The Riverbank soil, along with two paleosols that were correlated to the Turlock Lake, can be traced into the subsurface using driller's well logs and core (Figure 2-5). These soils appear as reddish clay-rich units. In the case of the paleosols that cap the Riverbank and upper Turlock Lake units, the paleosols appear as beds that dip at low angle into the basin, 'outcropping' close to areas mapped by Huntington (1971) for each of these units.

In the conceptual model, we propose that an incised valley must exist on the fan during interglacial periods in order to keep aggradation from occurring across the upper fan, thus allowing for soil development on the sequence bounding surfaces. The most recent incised valley (developed during the interglacial period between the Modesto and Riverbank times) was identified south of Sanger based on soil character and subsurface facies indications from driller's logs. The soil surveys indicate a sharp break in the Riverbank soils along a line south of Sanger (Figure 2-6). Additionally, driller's log data indicated the presence of cobbles at a depth of approximately 30 meters. These logs also lacked evidence for expected paleosols (capping the Riverbank and Upper Turlock Lake units) above this gravel unit.

Subsequent drilling and core collection showed that sediments in this area were significantly coarser grained than surrounding open fan deposits, consisting of an 8-m thick basal cobble unit that is overlain by a fining upward succession of very coarse to medium sand (Weissmann et al., 2002a, in press). Some overbank silts are present, but in significantly lower proportions relative to surrounding open fan deposits (Weissmann et al., 2002a, 2002b).

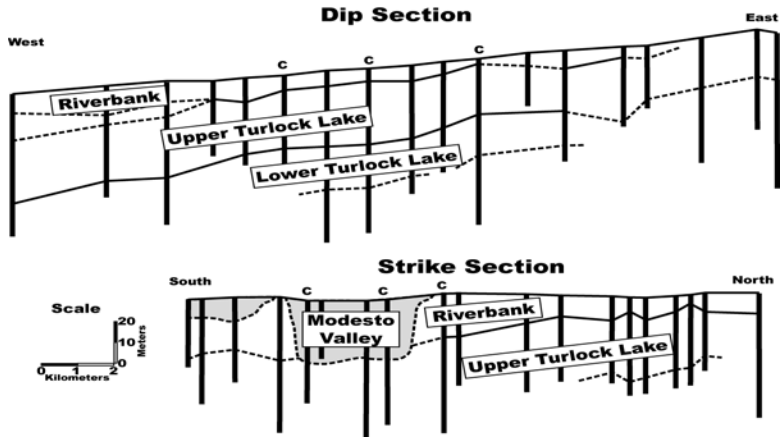

Figure 2-5. Cross sections through the Kings River alluvial fan. Correlations mark the paleosol sequence boundary markers. Wells labeled with a "C" indicate core collected. Modified from Weissmann et al., 2002a, *in press*.

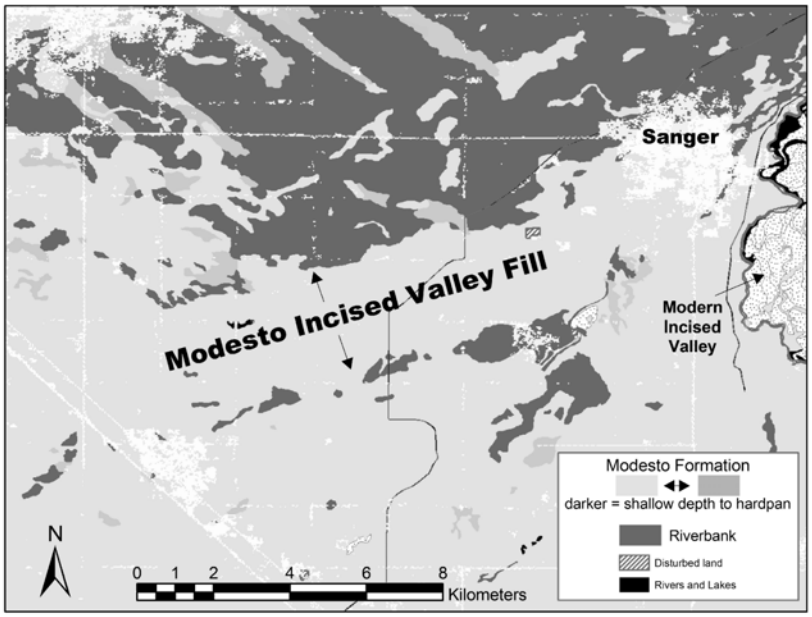

Figure 2-6. Detail of the soil survey around the incised valley fill. The incised valley fill is surrounded by Riverbank Formation outcrops (modified from Weissmann et al., 2002a).

Correlation of paleosols and the incised valley fill allow development of a 3-D stratigraphic framework that can be used for prediction of facies distributions in the alluvial fan (Figure 2-7). Models that have been developed in this framework honor the differences

between open fan and incised valley fill deposits, thus providing a reasonable characterization of the complex alluvial fan aquifer (Weissmann and Fogg, 1999; Weissmann et al., 1999, in press).

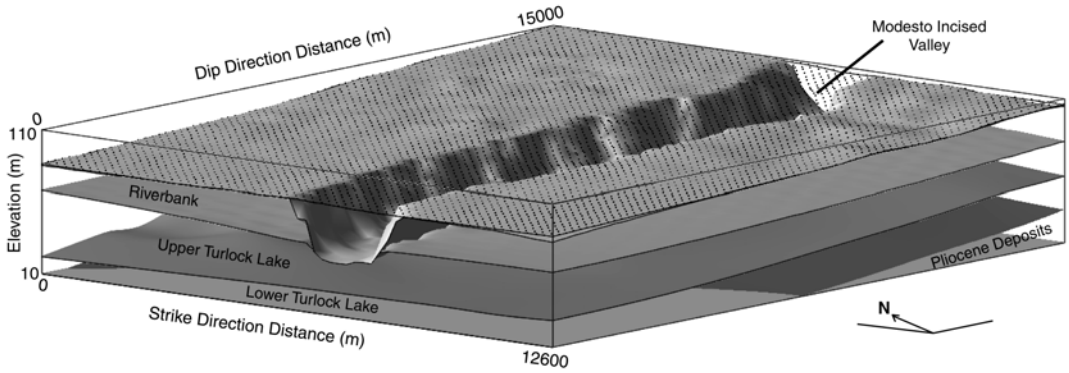

Figure 2-7. A block diagram showing the sequence surfaces in the upper Kings River alluvial fan as defined by paleosol correlation and the Modesto incised valley fill geometry (modified from Weissmann et al., *in press*).

CONCLUDING REMARKS

Stratigraphic sequences on the Kings River alluvial fan, related to past glacial cyclicity in the Sierra Nevada, contain a predictable distribution of facies related to processes that were active at different stages of glacial outwash. Sequences observed in the middle to upper fan are bounded by relatively mature paleosols. These sequences formed in response to changes in sediment supply and discharge, and consist of both open fan and incised valley fill deposits. Open fan deposits, consisting of relatively wide and straight channel sands and gravels surrounded by overbank silt, dominate the upper to middle fan stratigraphic section. Incised valley fill deposits consist of a relatively coarse-grained, fining upward succession. In standard sequence stratigraphic terminology, the open fan and incised valley fill units might represent systems tracts in the sequences.

Importantly, the sequence stratigraphic model allows for prediction of facies distributions on the fan. For instance, we expect to find an incised valley fill unit associated with each sequence bounding paleosol. Preliminary work on the Tuolumne alluvial fan, located in Modesto, California, indicates the presence of a large incised valley fill deposit located below the city. The sequence stratigraphic model allowed identification of this unit and offers information about the geometry of the coarse grained deposit.

The importance of identifying the incised valley fill and other facies patterns in these alluvial fans was shown by Weissmann et al. (in press). In this work, the authors modeled the influence of the coarse-grained incised valley fill on regional groundwater recharge and flow. Because this unit is coarser than surrounding deposits, it essentially acts as a ‘conduit’ for both groundwater recharge and contaminant migration into deeper and adjacent aquifer units. We expect future work to continue building our understanding of the stratigraphic influence on groundwater flow and contaminant transport as well as continued development of models for the Quaternary San Joaquin Basin fill.

ACKNOWLEDGMENTS

This research was supported by the Cooperative State Research Service, U.S. Department of Agriculture, under Agreement No. 93-38420-8792. This material is also based on work supported by the National Science Foundation under Grant No. EAR-98-70342 and N.I.E.H.S. Superfund Program (ES#04699). Additionally, acknowledgment is made to the donors of The Petroleum Research Fund, administered by the ACS, for partial support of this research (ACS PRF#37731-G8). We also thank significant discussions and data sharing with individuals at the US Geological Survey, Water Resources Division, especially Karen Burow. Much of this work could not have been completed without input from Jeffrey Mount, Michael Singer, Gordon Huntington, and Thomas Harter.

REFERENCES CITED

Arkley, R. J., 1962, The geology, geomorphology, and soils of the San Joaquin Valley in the vicinity of the Merced River, California. California Division of Mines and Geology, Bulletin 182, p. 25-31.

Atwater, B. F., Adam, D. P., Bradbury, J. P., Forester, R. M., Mark, R. K., Lettis, W. R., Fisher, G. R., Gobalet, K. W., and Robinson, S. W., 1986, A fan dam for Tulare Lake, California, and implications for the Wisconsin glacial history of the Sierra Nevada. Geological Society of America, Bulletin, v. 97, p. 97-109.

Bennett, G. L.,V., Weissmann, G.S., and Hyndman, D.W., 2002, Evaluating paleosol continuity using ground penetrating radar for more accurate regional-scale groundwater modeling on the Kings River Alluvial Fan, GSA National Meeting, Abstracts with Program, October 27-30.

Blum, M. D., and Törnqvist, T.E., 2000, Fluvial responses to climate and sea-level change: a review and look forward: Sedimentology, v. 47, p. 2-48.

Burow, K. B., Weissmann, G.S., Miller, R.D., and Placzek, G., 1997, hydrogeologic facies characterization of an alluvial fan near Fresno, California, using geophysical techniques, U.S. Geological Survey Open File Report 97-46, 15p.

Harden, J. W., 1987, Soil Development in Granitic Alluvium near Merced, California, US Geological Survey Bulletin 1590-A, 65p.

Huntington, G. L., 1971, Soil Survey, Eastern Fresno Area, California: U.S. Department of Agriculture, Soil Conservation Service, U.S. Government Printing Office, 323 p.

Huntington, G. L., 1980, Soil-Land Form Relationships of Portions of the San Joaquin River and Kings River Alluvial Depositional Systems in the Great Valley of California: unpublished Ph.D. Dissertation, University of California at Davis, 147 p.

Janda, R. J., 1966, Pleistocene history and hydrology of the upper San Joaquin River, California: unpublished Ph.D. Dissertation, University of California, Berkeley, 293 p.

Lettis, W. R., 1982, Late Cenozoic stratigraphy and structure of the western margin of the central San Joaquin Valley, California. U. S. Geological Survey Open-File Report 82-526, 203p.

Lettis, W. R., 1988, Quaternary geology of the Northern San Joaquin Valley, in Graham, S.A., ed., Studies of the Geology of the San Joaquin Basin: SEPM Pacific Section, v. 60, p. 333-351.

Marchand, D. E., 1977, The Cenozoic history of the San Joaquin Valley and the adjacent Sierra Nevada as inferred from the geology and soils of the eastern San Joaquin Valley, in Singer, M.J., ed., Soil Development, Geomorphology, and Cenozoic History of the Northeastern San Joaquin Valley and Adjacent Areas, California: University of California Press. Guidebook for Joint Field Session, Soil Science Society of America and Geological Society of America, p. 39-50.

Marchand, D. E., and Allwardt, A., 1981, Late Cenozoic Stratigraphic Units, Northeastern San Joaquin Valley, California: U.S. Geological Survey, Bulletin 1470, 70 p.

Mitchum, Jr., R. M., 1977, Part Eleven, Glossary of Terms Used in Seismic Stratigraphy, in Vail, P. R., Mitchum, Jr., R. M., Todd, R. G., Widmier, J. M., Thompson III, S., Sangree, J. B., Bubb, J. N., and Hatlelid, W. G., in Payton, C.E., (ed), Seismic Stratigraphy – applications to hydrocarbon exploration, AAPG Memoir 26, p. 205-212.

Shanley, K.W., and McCabe, P.J., 1994, Perspectives on the sequence stratigraphy of continental strata. American Association of Petroleum Geologists, Bulletin, v. 78, p. 544-568.

Weissmann, G. S., 1999, Toward New Models of Subsurface Heterogeneity: An Alluvial Fan Sequence Stratigraphic Framework with Transition Probability Geostatistics. Unpublished Ph.D. Dissertation, University of California, Davis, 279p.

Weissmann, G. S., Carle, S. F., and Fogg, G. E., 1999, Three-dimensional hydrofacies modeling based on soil surveys and transition probability geostatistics: Water Resources Research, v. 35, p. 1761-1770.

Weissmann, G. S., and Fogg, G. E., 1999, Multi-scale alluvial fan heterogeneity modeled with transition probability geostatistics in a sequence stratigraphic framework: Journal of Hydrology, v. 226, p. 48-65.

Weissmann, G. S., Mount, J. F., and Fogg, G. E., 2002a, Glacially driven cycles in accumulation space and sequence stratigraphy of a stream-dominated alluvial fan, San Joaquin Valley, California, U.S.A., Journal of Sedimentary Research, v. 72, p. 270-281.

Weissmann, G. S., Yong, Z., LaBolle, E. M., and Fogg, G. E., 2002b, Modeling environmental tracer-based groundwater ages in heterogeneous aquifers, Water Resources Research, v. 38, p. 1198-1211.

Weissmann, G. S., Yong, Z., Fogg, G. E., and Mount, J. F., in press, Influence of incised valley fill deposits on hydrogeology of a glacially-influenced, stream-dominated alluvial fan, in Bridge, J., and Hyndman, D.W., Aquifer Characterization, SEPM Special Publication 80, publication expected Spring 2004.

APPENDIX 3: CAVE FORMATION, GEOCHRONOLOGY, AND RATES OF RIVER INCISION IN A SOUTHERN SIERRA NEVADA STREAM CANYON: GEOMORPHIC STUDIES OF CRYSTAL CAVE

Greg M. Stock *University of California, Santa Cruz, Santa Cruz, CA 95060*
gstock@es.ucsc.edu

INTRODUCTION

Crystal Cave is one of the largest and most accessible caves in the Sierra Nevada. Though it has long been of scientific interest, it has seen renewed research activity in the past few years as new advancements in geochronology have allowed detailed dating of deposits within the cave. This stop will provide an example of the types of caves and cave deposits used to determine river incision rates across the central and southern Sierra Nevada. It will also highlight both the advantages and limitations of the newly developed technique of cosmogenic nuclide dating of buried sediment.

CAVE GENESIS AND MORPHOLOGY

Solutional caves are formed when mildly acidic groundwater dissolves carbonate rock (primarily limestone or marble). In the many cases where caves from along the water table, passages tend to resemble pipes full of water, with rounded cross-sections and low gradients (Ford and Williams, 1989; Palmer, 1991). These tubular passages are termed phreatic passages. In cases where the groundwater flow has not yet reached the local base level, cave passages resemble slot canyons or fissures, with steep-walled cross sections and steeply descending gradients. These are termed vadose passages. In most cases, caves are made up of a combination of phreatic and vadose passages, with the upstream sections forming in the vadose zone and the downstream sections forming in the phreatic zone. The largest caves in the Sierra Nevada are examples of complex cave morphologies with both phreatic and vadose development.

Because water tables in mountainous terrain can fluctuate widely, a single cave passage can alternately be subject to flooded conditions below the water table and dry conditions above the water table. As a result, most phreatically formed passages have some vadose overprinting. In fact, torrential floods from heavy rainfall and from spring snowmelt play an important role in forming and modifying Sierra Nevada caves. During these periods, sediment-laden streams become a greater force in mechanically eroding, as well as chemically dissolving, cave passages. Many simple passages are modified to become complex anastomotic mazes probably as a result of these floodwaters (Palmer, 1991). However, the erosional power of floods is a double-edged sword; as an example, during significantly elevated river discharges in January 1997, Wild Child cave, situated just above the Marble Fork of the Kaweah River, was transformed from a large walking-size passage to a low crawlway when floodwaters filled the cave with fluvial sediment.

CAVES OF THE SIERRA NEVADA

There are approximately 400 caves in the Sierra Nevada, with several new caves discovered each year. The longest known cave is Lilburn Cave in Redwood Canyon, currently showing 32 km (20 miles) of surveyed passages (see Appendix 4A). At least five

other caves (Church Cave, Crystal Cave, Soldiers Cave, Hurricane Crawl, and California Caverns) exceed 2 km (7,000 ft) in length. Caves and karst (landscapes characterized by sinking streams, sinkholes, caves, and springs) are found from the Feather River in the northern part of the range to the Kern River in the south. However, caves and karst are generally concentrated in two areas: the Mother Lode region of the central Sierra Nevada, and the Sequoia-Kings Canyon region of the southern Sierra Nevada.

Caves and karst of the southern Sierra Nevada have formed in narrow, elongate marble lenses. These marble lenses are associated with a belt of metamorphic rocks flanking the western edge of the batholith (see Appendix 6, Fig. 6-1). Marble lenses generally strike northwest, parallel to the range, and are often exposed in the deepest sections of river canyons cutting across the structural trend. In the southern Sierra, caves range from 550 to 3,350 m in elevation. Though the numerous alpine caves are fascinating topics for study, we have focused on the larger caves formed well downstream of glacial limits, where canyon cutting has been accomplished by river incision. Cave locations delineate a northwest trending transect across the central and southern Sierra Nevada, through the middle reaches of the major river canyons (see Appendix 6, Fig. 6-1). We have used caves along this transect to determine rates of river incision and landscape evolution in the southern Sierra Nevada.

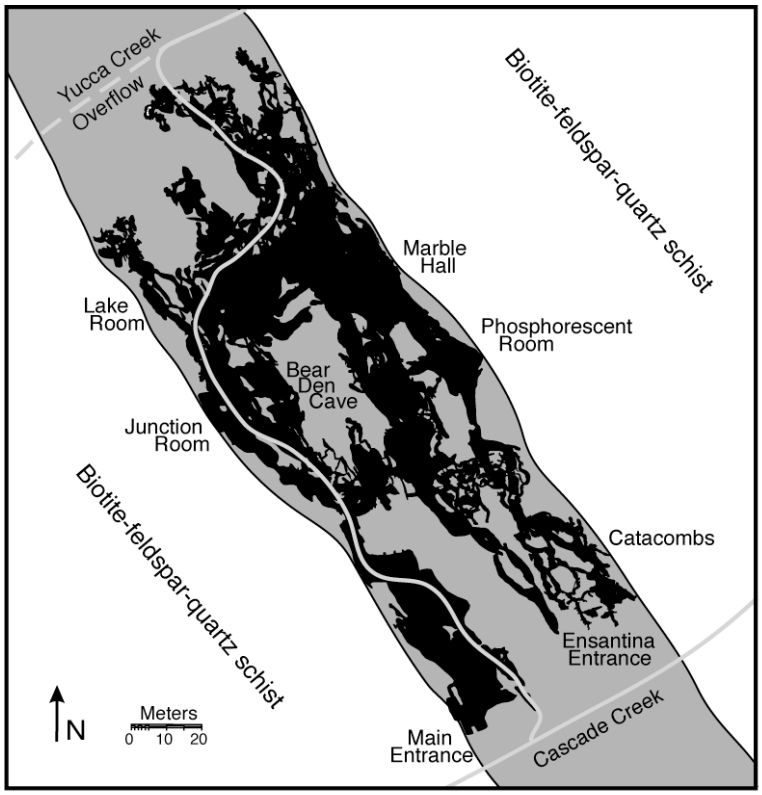

Figure 3-1. Plan view of Crystal Cave, Sequoia National Park. 4.2 km of mapped passages, shown in black, are contained within a narrow lens of marble, shown in gray, flanked on either side by biotite-feldspar-quartz schist (Sisson and Moore, 1994).

CRYSTAL CAVE

Crystal Cave has formed in a vertically-bedded lens of marble flanked by on either side by biotite-feldspar-quartz schist (Sisson and Moore, 1994). The block of marble containing the cave is some 60 m wide, 200 m long, and 100 m thick. Within this narrow lens there are 4.2 km of surveyed cave passages, making Crystal Cave the fourth longest cave in California. A significant portion of the available marble bedrock has been dissolved by groundwater, and many walls of the cave are composed of the insoluble schist beds in contact with the marble (Fig. 3-1).

Presently, Yucca Creek to the north of the cave encounters the marble lens containing the cave and is pirated into the cave. It then flows southward through the lowest level of the cave before emerging as a spring below the Main Entrance along Cascade Creek (Fig. 3-1). The discharge of Yucca Creek through the cave is remarkably steady across seasonal variation

in precipitation. During times of low discharge during summer and fall, the entire creek is diverted through the cave, while during times of high discharge in the winter and spring, much of the creek is not diverted into the cave, but "overflows" down the main Yucca Creek channel (Fig. 3-1). Sedimentary evidence (primarily large cobbles not transportable by the present streamflow) suggests that discharges through the cave were significantly greater in the past.

Crystal Cave is composed of several distinct levels over 60 m vertical extent (Fig. 3-2A). The main levels are generally composed of large, low gradient, modified phreatic passages, and are connected vertically by narrow, steeply-descending vadose canyons. Passage gradients, wall scallop orientations (Curl, 1974), and sediment imbrication all indicate that groundwater has consistently flowed from Yucca Creek to Cascade Creek through time, sequentially forming cave levels as the water table dropped due to bedrock incision of Cascade Creek (Despain and Stock, in prep). The major levels of Crystal Cave, perched within the hillside, mark former levels of Cascade Creek.

CAVES AS RECORDERS OF RIVER INCISION

Caves can record river incision because many are former river levels etched into bedrock. As the elevation of the most deeply incised river defines the local water table, sinking streams flowing through fractured carbonate rock dissolve caves that are graded to river level. Alternatively, a portion of the river itself is sometimes diverted into the canyon wall, forming cave passages parallel to the river. Bedload sediment is often deposited in either type of passage. Subsequent incision of the river through bedrock lowers the river relative to the caves, leaving sediment-laden passages perched high in riverside cliffs. A vertical sequence of cave passages is therefore analogous to a flight of strath terraces scribed into a canyon wall. In fact, cave sediments shielded within bedrock hillslopes can be much longer-lived than such terraces; cave deposits millions of years old are often exquisitely preserved. Sierra Nevada caves, many of which are fortuitously situated in the walls of the major westward-flowing river canyons, represent important archives of river incision.

COSMOGENIC NUCLIDE BURIAL DATING

Recently, a technique has been developed for dating buried quartz-rich sediment based on the ratio of concentrations of ^{26}Al and ^{10}Be (Lal, 1991; Granger et al., 1997; Granger et al, 2001; Granger and Muzikar, 2001). These cosmogenic nuclides are produced in quartz within the top few meters of the earth's surface by secondary cosmic rays. Sediment accumulates ^{26}Al and ^{10}Be primarily during exhumation from hillslopes. The ^{26}Al/^{10}Be ratio $(N_{26}/N_{10})_0$ in a steadily eroding outcrop will change with erosion rate (ε) according to equation 3-1:

$$\left(\frac{N_{26}}{N_{10}}\right)_0 = \frac{P_{26}\left(\frac{1}{\tau_{10}} + \frac{\varepsilon}{\Lambda}\right)}{P_{10}\left(\frac{1}{\tau_{26}} + \frac{\varepsilon}{\Lambda}\right)} \qquad (3\text{-}1)$$

where N_{26} and N_{10} are nuclide concentrations, P_{26} and P_{10} are nuclide production rates, and Λ is the cosmic ray penetration depth ($\Lambda \approx 60$ cm in rock of density 2.6 g cm^{-3}). The total nuclide concentration is therefore dependent on the rates of nuclide production and rock

erosion. While nuclide production rates vary in space and time, ^{26}Al is always produced ~6 times faster than ^{10}Be. The inherited ^{26}Al/^{10}Be ratio at the surface is therefore known to be ~6 (Stone, 2000). If the sediment is then buried deeply enough (typically >10 m) that cosmic rays are shielded, nuclide production drastically slows or ceases and the products decay exponentially:

$$N_{26} = \left(N_{26}\right)_0 e^{-t\left(\frac{1}{\tau_{26}}\right)} \quad \text{and} \quad N_{10} = \left(N_{10}\right)_0 e^{-t\left(\frac{1}{\tau_{10}}\right)} \tag{3-2}$$

where t is time of burial. Because ^{26}Al [τ_{26}=1.02 ± 0.04 (Norris et al., 1983)] decays approximately twice as fast as ^{10}Be [τ_{10}=2.18 ± 0.09 (Hofmann et al., 1987)], the inherited ^{26}Al/^{10}Be ratio decreases exponentially over time according to equation 3-3:

$$\frac{N_{26}}{N_{10}} = \left(\frac{N_{26}}{N_{10}}\right)_0 e^{-t\left(\frac{1}{\tau_{26}} - \frac{1}{\tau_{10}}\right)} \tag{3-3}$$

where $(N_{26}/N_{10})_0$ represents the inherited ^{26}Al/^{10}Be ratio as determined from equation 3-1 (Granger et al., 1997). Equations 3-1, 3-2, and 3-3 are solved iteratively for both burial age and pre-burial erosion rate. ^{26}Al/^{10}Be ratios in buried sediments may be used to determine the time at which sediments were deposited within a cave over a range of about 0.1 to 5 Ma (Granger et al., 1997; 2001; Granger and Muzikar, 2001). Burial ages depend only on the ratio of ^{26}Al and ^{10}Be and not on their absolute concentrations, so they are not sensitive to variations in the rate of exhumation. They are also immune to variations in nuclide production rates, driven by changes in the Earth's magnetic field that complicate surface exposure dating (Dunai, 2000).

Sierra Nevada caves present an ideal setting for cosmogenic burial dating, as quartz-rich sediments are eroded primarily from the granitic batholith upstream and are carried rapidly into caves. We collected well-rounded gravel and cobbles, predominantly of granitic composition, from coarse, well-sorted, clast-supported deposits. Such deposits are indicative of river bedload, and ensure that deposition did not occur significantly after passage development (as might occur by eolian processes, for example). Furthermore, we sampled only from isolated cave passages with clear relations to former river levels, ensuring that the sediment contained within the passages was derived only from bedload transport and not from slumping or sifting of sediment from upper levels. By dating bedload material, we most accurately record when caves were at river level.

Although cosmogenic nuclide burial ages provide only minimum cave ages (resulting in maximum river incision rates), they provide better estimates of cave ages than other available methods. Although we do not report our results here, both sediment paleomagnetism and ^{234}U/^{230}Th basal ages on speleothems from Crystal Cave consistently underestimated the ages of cave levels, by as much as an order of magnitude. This is primarily because sediment accumulation is not constant, a necessary assumption for paleomagnetism, and because initiation of speleothem growth may significantly lag cave development. Granger et al. (2001) reached similar conclusions in a study of Mammoth Cave deposits.

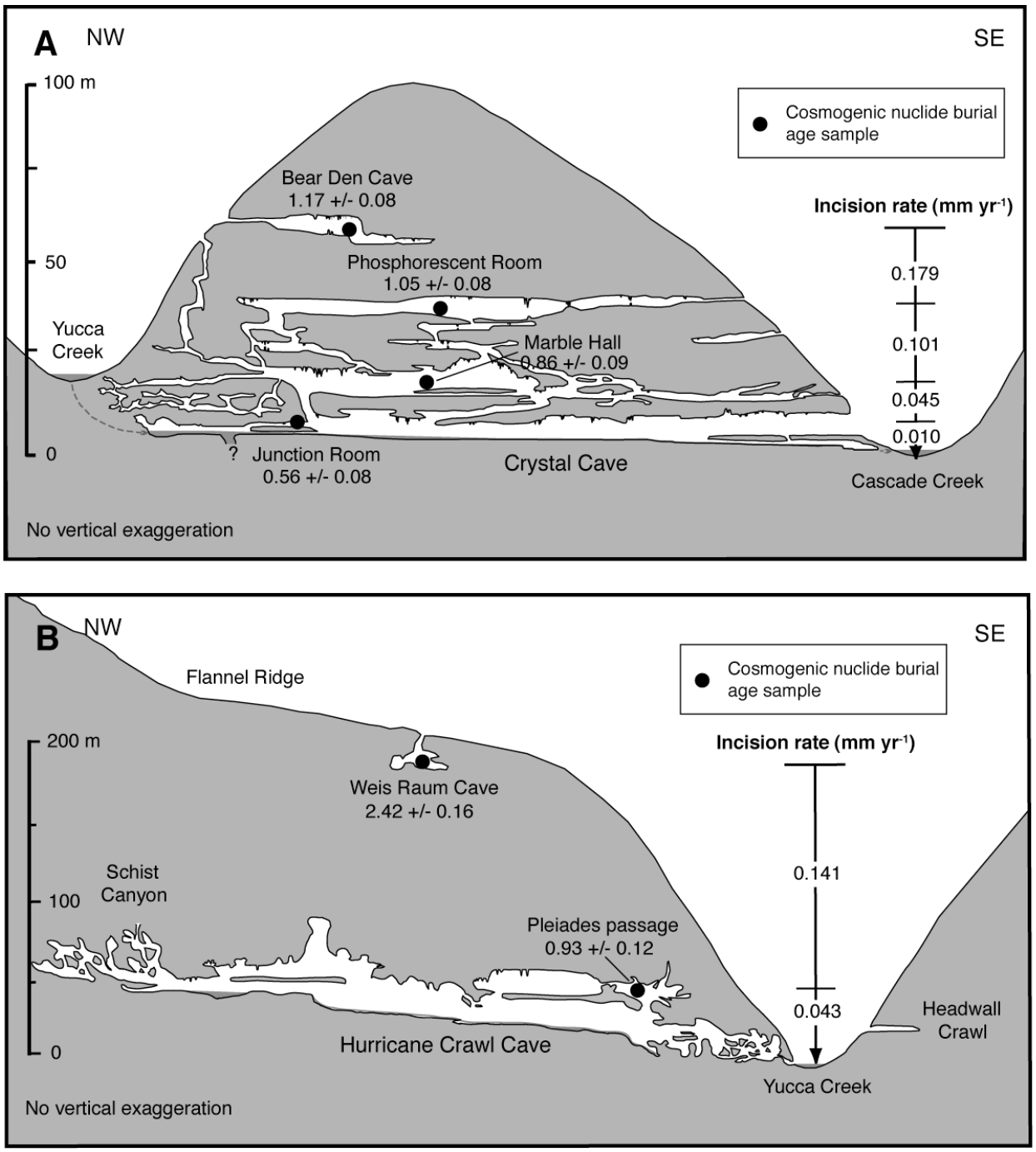

Figure 3-2. Cave profiles and cave-derived rates of incision for Cascade and Yucca Creeks, tributaries of the North Fork Kaweah River. A. Profile view of Crystal Cave, showing cave levels formed as groundwater, flowing from Yucca Creek through the cave, moved downward in response to incison of Cascade Creek. B. Downstream, below the junction of Cascade Creek and Yucca Creek, Weis Raum and Hurricane Crawl caves have formed in a separate ridge of marble. Cosmogenic nuclide burial ages for fluvial sediments from the major levels within Crystal Cave, and from Wies Raum and Hurricane Crawl caves, yield incision rates for Cascade and Yucca creeks, respectively. These rates range from 0.01 to 0.18 mm yr^{-1}, and show a trend toward lower rates of incision in the late Quaternary. Note different vertical scales for A and B.

BURIAL DATING RESULTS

Figure 3-2A shows cosmogenic nuclide burial dating results for four samples from the major levels within Crystal Cave. Sediment burial ages range from 1.17 Ma (considered a preliminary age) for the uppermost level of the cave (Bear Den Cave) to 0.56 Ma for the lowermost level (Junction Room). As expected, burial ages are in correct stratigraphic order, i.e., the higher cave levels are older than the lower levels. These burial ages suggest that Crystal Cave formed from about 1.2 to 0.5 Ma, and that little enlargement of cave passages has occurred since 0.5 Ma. Roughly 60 m of canyon incision occurred in 0.7 Myr, leading to a long-term incision rate of 0.08 mm yr^{-1} for Cascade Creek. However, multiple dated levels provide further detail, and show a marked decrease in the rate of incision from 0.18 to 0.015 mm yr^{-1} over the 0.7 Myr represented by the burial ages. This pattern of decreasing incision is reflected in many other drainages in the southern Sierra Nevada, including nearby Yucca Creek (Fig 3-2B). A detailed discussion of range-wide burial dating results is presented in Appendix 6, and possible causes for the trends of incision is presented in Appendix 7. As we shall see later at Stops 6 and 7, Crystal Cave is just one of several Sierra Nevada caves that appear to capture broad, range-scale changes in river incision associated with regional changes in both uplift rate and climate (Stock et al., in review).

REFERENCES CITED

Curl, R. L., 1974, Deducing flow velocity in cave conduits from scallops: National Speleological Society Bulletin, v. 36, p. 1-5.

Despain, J., and Stock, G. M., (in prep), Geomorphology and geochronology of Crystal Cave, Sequoia National Park, California.

Dunai, T.,J., 2000, Scaling factors for production rates of in situ produced cosmogenic nuclides: a critical reevaluation: Earth and Planetary Science Letters, v. 176, p. 157-169.

Ford, D.C., and Williams, P.W., 1989, Karst Geomorphology and Hydrology: London, England, Unwin Hyman, 601 p.

Granger, D. E., Kirchner, J. W., Finkel, R.C., 1997, Quaternary downcutting rate of the New River, Virginia, measured from differential decay of cosmogenic ^{26}Al and ^{10}Be in cave-deposited alluvium: Geology, v. 25, p. 107-110.

Granger, D. E., Fabel, D., and Palmer, A. N., 2001, Pliocene-Pleistocene incision of the Green River, Kentucky, determined from radioactive decay of cosmogenic ^{26}Al and ^{10}Be in Mammoth Cave sediments: Geological Society of America Bulletin, v. 113, p. 825-836.

Granger, D. E., and Muzikar, P. F., 2001, Dating sediment burial with in situ-produced cosmogenic nuclides: theory, techniques, and limitations: Earth and Planetary Science Letters, v. 188, p. 269-281.

Hofmann, H. J., Beer, J., Bonani, G., von Gunten, H. R., Raman, S., Suter, M., Walker, R. L., Wolfli, W., and Zimmerman, D., 1987, ^{10}Be: Half-life and AMS-standards: Nuclear Instruments and Methods in Physics Research, v. B29, p. 32-36.

Lal, D., 1991, Cosmic ray labeling of erosion surfaces: In situ nuclide production rates and erosion models: Earth and Planetary Science Letters, v. 104, p. 424-439.

Norris, T. L., Gancarz, A. J., Rokop, D. J., and Thomas, K. W., 1983, Half-life of ^{26}Al: Proceedings of the Fourteenth Lunar and Planetary Science Conference, Part I: Journal of Geophysical Research, v. 88, p. B331-B333.

Palmer, A. N., 1991, Origin and morphology of limestone caves: Geological Society of America Bulletin, v. 103, p. 1- 21.

Sisson, T., W., and Moore, J. G., 1994, Geologic map of the Giant Forest Quadrangle, Tulare County, California: U.S. Geological Survey Map GQ-1751

Stock, G. M., Anderson, R. S., and Finkel, R. C., in review, Pace of landscape evolution in the Sierra Nevada, California, revealed by cosmogenic dating of cave sediments

Stone, J. O., 2000, Air pressure and cosmogenic isotope production: Journal of Geophysical Research, v. 105, p. 23,753-23,759

APPENDIX 4A: LILBURN CAVE AND THE KARST OF REDWOOD CANYON: A FLEETING OVERVIEW

John C. Tinsley *U. S. Geological Survey, Menlo Park, CA 94025 jtinsley@usgs.gov*

INTRODUCTION

Redwood Canyon is chiefly known for containing the largest remaining giant sequoia grove in the world. However, it also contains world-class speleological features, specifically the sinkholes and swallets comprising the Redwood Canyon Karst, including Lilburn Cave, and the system's resurgence at Big Spring, a rare ebb and flow spring. The National Park Service long has recognized the merits of this cave system for scientific study, and has managed the cave as an underground research laboratory since about 1967. Since 1977, the research here has been conducted under auspices of the Cave Research Foundation (CRF). Lilburn Cave is gated and is open to those principal investigators holding NPS-approved research permits (and those who assist the researchers). The current CRF Sequoia-Kings Canyon coordinator is John Tinsley. Ongoing research includes survey, inventory, and monitoring of the cave, including aspects of its hydrology, sedimentology, biology, and cave restoration.

The principal consumer of cavers' volunteer labor is the cartography project, now entering its 21st year. Two decades of compass-and-tape surveys of the complex, multiple-level maze cave now show more than 32 km (20 mi) of surveyed passage (Fig. 4A-1), placing Lilburn Cave (barely) within the top 100 of the world's long caves.

Not only is Lilburn is California's longest cave, it is probably also California's most studied cave. Three MS theses and one (almost) Ph.D. thesis have been written on aspects of the karst, its geochemistry, hydrology, and structure. Many amazing insights about Lilburn Cave have come from scuba dives by diver William Farr into the sumped (water-filled) passages at both ends of the cave, and also at the stream resurgence at Big Spring. Conducted at high altitudes and in very cold water, these technical and committing dives have thus far reached depths exceeding 75 m (240 ft) below the point of entry.

LILBURN CAVE HYDROLOGY AND SEDIMENTOLOGY

Lilburn Cave and the Redwood Canyon Karst include three separate caves, about 80 sinkholes, Sequoia-Kings Canyon's largest spring (a single-orifice Vauclusian ebb-and-flow spring, Big Spring) and remarkable active hydrologic and sedimentologic regimes that continue to amaze those who study karst processes from both above- and below-ground perspectives. The sinks and caves are developed in a black-and-white-striped marble lens situated within the amphibolite-grade metasedimentary rocks of the Redwood Mountain roof pendant (part of the Triassic Kings Terrane) (Sisson and Moore, 1994). This pendant lies between two Cretaceous batholiths, the Giant Forest and Big Baldy plutons. The karst basin extends down canyon from roughly the Hart Tree Trail/Redwood Creek junction to Big Spring, a distance of about 5.5 km. Lilburn Cave is developed within the lower 20% of the available marble in this basin. Two distinct contrasting provenances represent Redwood Creek (60% metamorphic clasts) and the west-flowing tributaries (95-100% granitic clasts). These contrasts interplay within the karst and enable mapping of sedimentary formations in the 3-dimensional cave maze.

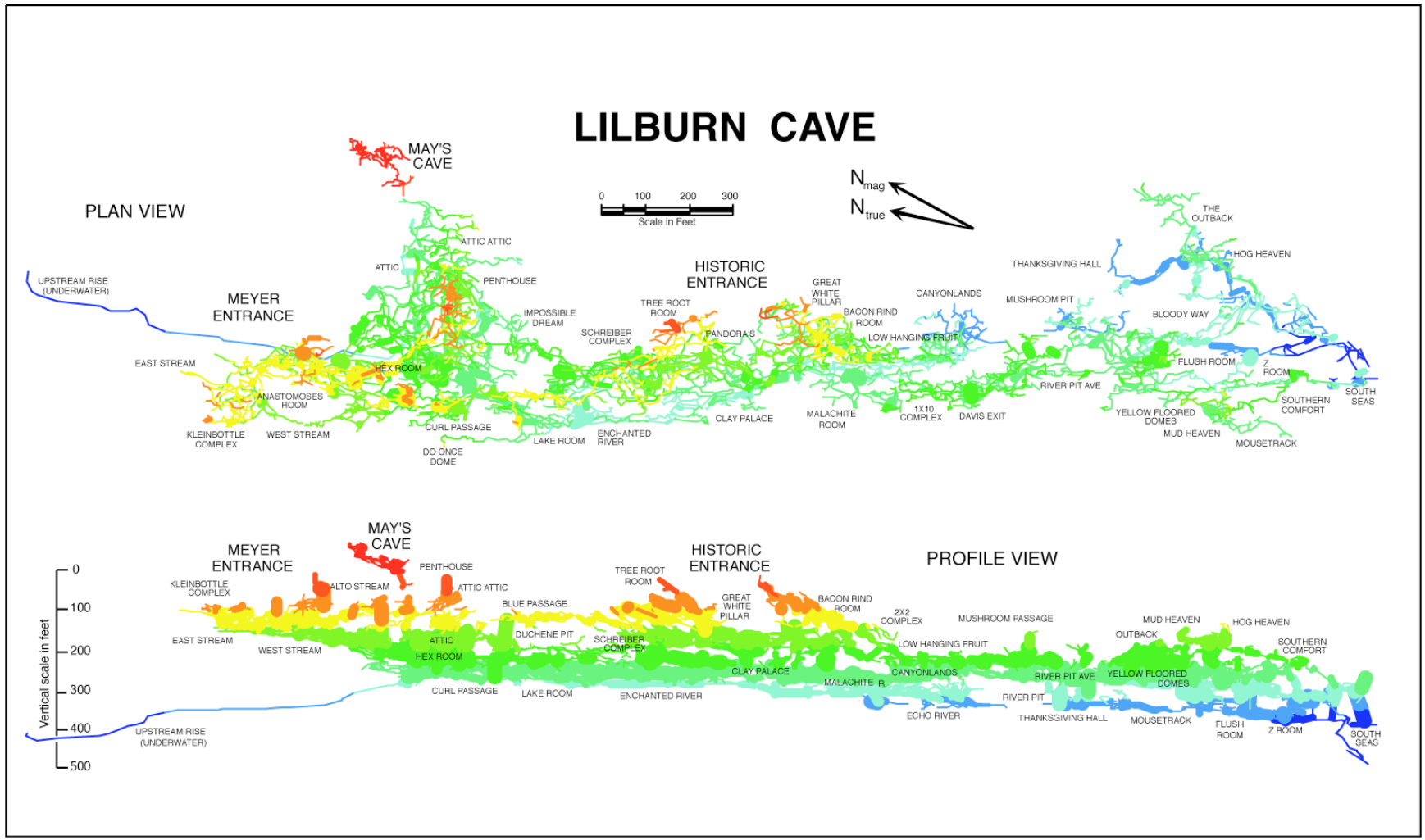

Figure 4A-1. Plan and profile views of Lilburn Cave, depicting >32 km (20 mi) of cave passages. Color shows depth of various passages below ground in 50 ft increments; cooler colors identify passages located deeper subsurface. Modified by Bosted et al. (2003).

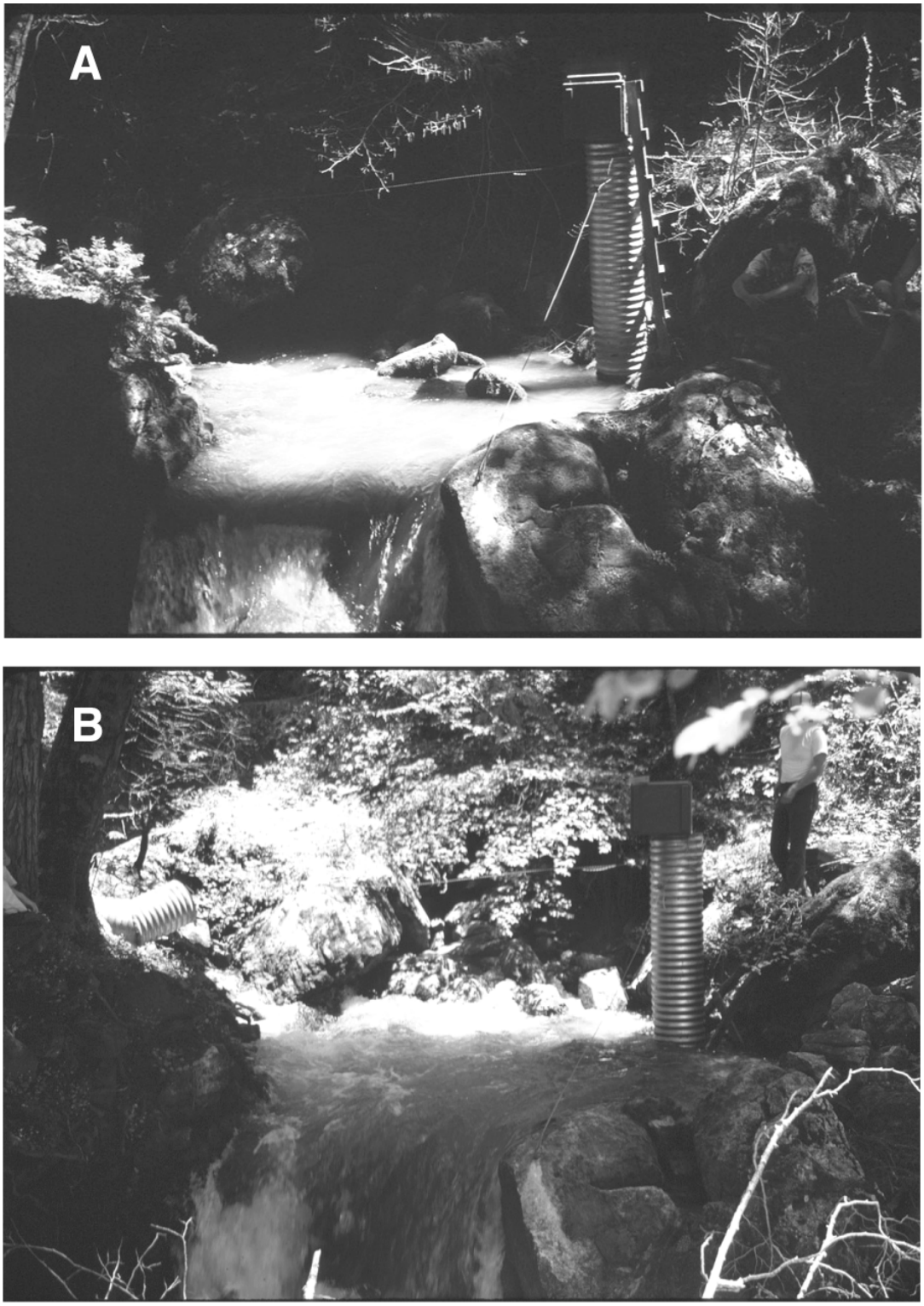

Figure 4A-2. Photographs of Big Spring at base flow conditions (A) and soon thereafter during a flush (B). Amplitude of flush is about 1 foot as measured by the stage recorder. The discharge cascades over a broad-crested weir. Corrugated culvert contains instrumentation. Photographs by John Tinsley, Cave Research Foundation.

A volcanic ash erupted ca. 0.7 ka from Deadman Dome in the Inyo Craters chain east of the Sierra Nevada crest is found in Redwood Canyon sinkholes and enables researchers to gauge sediment volumes delivered to the sinkholes during the past ~700 years.

The Lilburn Cave system swallows the entire discharge of Redwood Creek for much of the year, but the mantled karst condition limits rate of input of surface waters to the cave. Peak discharges send the excess surface water down Redwood Creek west of Cave Hill and thence past Big Spring to the North Fork of the Kaweah River. The point where Redwood Creek resurges from the cave, Big Spring, is a rare ebb and flow spring. Lilburn Cave is the one place in the world where researchers can get access to both ends of an ebb and flow system. Monitoring of stage, sediment transport within the cave, and observations by divers within the spring's conduit have enabled researchers to appreciate the role of intermittent sediment plugs in controlling the ebb and flow behavior here. Hydraulic head builds within the cave as the cave stream is backed up by sediment plugging the bottom of a U-shaped tube that connects the cave to Big Spring. Once this head exceeds some critical threshold, the sediment is dissipated and the backed up water quickly "flushes" through the tube, rapidly increasing the discharge at Big Spring (Fig 4A-2, 4A-3). See Sara (1977), Moore and Sullivan (1978), and Urzendowski (1993) for additional discussions of ebb and flow spring behavior specific to Big Spring.

Lilburn is also an excellent place to study cave sedimentary processes, as a prodigious load of clastic detritus washes through the cave. During El Nino winters, when atmospheric circulation patterns funnel warm moist air masses from Hawaii into this latitude of California (the "Pineapple Express", of local weather parlance) any early season snowpack melts and a double dose of precipitation plus snowmelt hits the sinkholes and swallets. Maximum changes in hydraulic head ranging from 40 to 55 m (30 to 180 ft) drive large volumes of pebbly sand into and through the cave system. Static sediment samplers and field mapping of flood deposits establish that sediment waves exceeding 10 m (33 ft) in amplitude move through the cave's canyon passages during these flood events. When these deposits get blown through the conduits and out Big Spring. During major runoff events, paired fill terraces form briefly in Redwood Creek owing to the temporary increase in bed load. Detritus eventually goes to Lake Kaweah, that aquatic attraction where we camped earlier during this field trip.

REFERENCES CITED

Bosted, Peter, Hacker, Brad, Despain, Joel, Tinsley, John, 2003, Lilburn Cave Atlas, Tulare County, California: Cave Research Foundation, Menlo Park, California, 90 p.

Moore, G. W. and Sullivan, G. N., 1978, Speleology: The study of caves, Cave Books, St. Louis, MO.

Sara, M. N., 1977, Hydrology of Redwood Canyon, Tulare County, California, MS Thesis, Geology, University of Southern California.

Sisson, T., W., and Moore, J. G., 1994, Geologic map of the Giant Forest Quadrangle, Tulare County, California: U.S. Geological Survey Map GQ-1751.

Urzendowski, Linda, 1993, Spectral analysis of the flow behavior of Big Spring, Kings Canyon National Park, California. MS Thesis, Department of Geoscience, University of Nevada, Las Vegas.

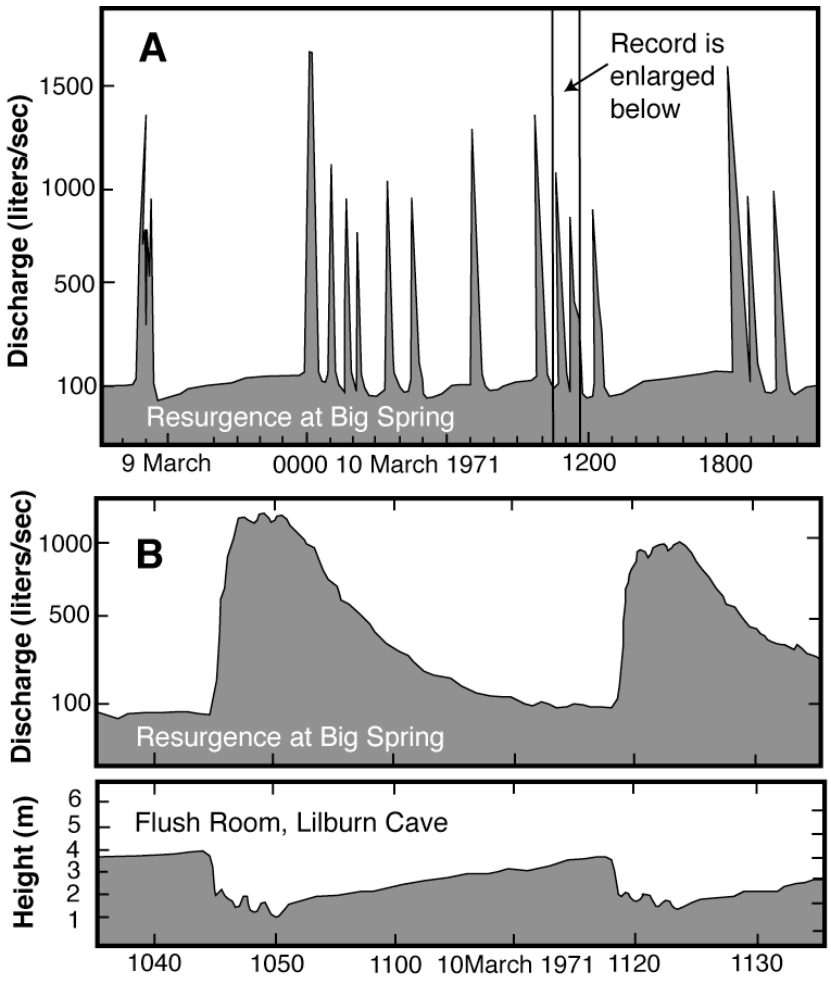

Figure 4A-3. Ebb and flow behavior of Big Spring. (A). Ebb and flow spring hydrograph of Big Spring recorded during March 1971. (B). Twin hydrographs collimated to illustrate Lilburn Cave's ebb and flow spring behavior at timescale expanded from (A). The upper hydrograph shows two flush cycles as measured at Big Spring. The lower hydrograph shows stage heights in the Flush Room inside Lilburn Cave. Note fine scale synchronicity interpreted as sloshing or resonance typical of a water-filled U-shaped tube. Sedimet plug dissipates under a sufficient increase in head, releasing the pulse of water observed as a flush at Big Spring.

APPENDIX 4B: HOLOCENE FIRE AND CLIMATE HISTORY FROM SIERRA NEVADA TREE RINGS

Tony Caprio *National Park Service, Sequoia-Kings Canyon National Park, CA 93271 Tony_Caprio@nps.gov*

INTRODUCTION

Old living trees are relatively abundant in the southern Sierra Nevada and vicinity. There are at least six species within the region that have been used in developing long millennial length tree-ring chronologies (>1000 years). Probably no other location within North America has this diversity or concentration of old trees. Individual living tree ages range up 4,780 years for bristlecone pines (oldest known living tree). Of special importance for chronology construction is the existence of remnant wood (pieces of wood from long dead trees) for most of the species except giant sequoia. Remnant material, usually found in rare protected locations, frequently allows dendrochronologists to double the length of chronologies. In the Sierra Nevada this wood is generally found in situations where fire does not occur. The oldest crossdated chronologies come from bristlecone pines in the White Mountains of California, located just east of the Sierra Nevada.

Trees species with long chronologies in the Sierra Nevada and vicinity

Giant Sequoia (*Sequoiadendron giganteum*)	~3,375 years
Foxtail Pine (*Pinus balfouriana*)	~4,000 years
Western Juniper (*Juniperus occidentalis*)	~3,507 years
Whitebark Pine (*Pinus albicaulis*)	~1,000+ years
Limber Pine (*Pinus flexilis*)	~2,675 years
Bristlecone Pine (*Pinus longaeva* - White Mtns)	~8,700 years (+3,000 floating)

Another important characteristic of these long-lived species is that they are found across a variety of ecological settings and elevations. Thus, they can provide a wide array of information about differing habitats, physical locations, and climate characteristics. Over the last several decades these species have contributed a wealth of information about past processes and events, some with global significance. An important feature of this information is that it is annually resolved with each tree ring dated to the actual calendar year in which it was formed. The process of dating tree rings is known as "crossdating" and primarily depends on comparing unique patterns of large and small rings among samples. These patterns are dependent on a regional climate signal(Fig. 4B-1) that result in a similar pattern (small and large rings) among trees across a region. Long chronologies, older than any living tree, can be developed by matching the tree-ring series from the outer portions of dead wood to the inner portion of live tree-ring series. The ability to crossdate dead wood also has sampling advantages (live trees in a national park don't need to be cut) and in dating events that may have killed the trees. Spatial characteristics of past events can also be compared with fewer errors because of the precise temporal resolution. The downside to a dendrochronological dated sample is that crossdating is frequently difficult (sometimes impossible) and nearly always time consuming.

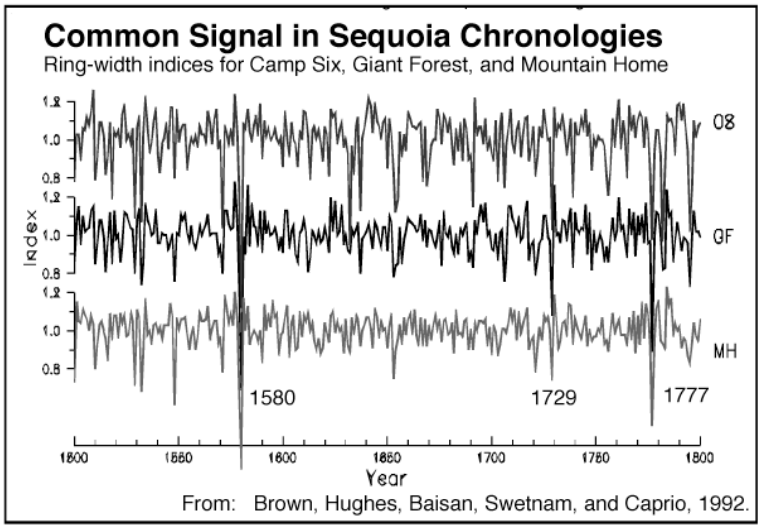

Figure 4B-1. Common signal in sequoia chronologies.

Why do these trees get so old?

The general adage among dendrochronologist is "longevity under adversity" (coined by E. Schulman), although giant sequoias, growing in a mesic environment, appear to an exception to the rule. More specifically, habitat, climate, and growth characteristics of a tree species are all important in determining the potential age an individual can reach. Old bristlecone pines inhabit high elevations with an extremely arid environment in the rain shadow of the Sierra Nevada. They and foxtail pine (PIBA), limber pine (PIFL) pine, western juniper (JUOC) can develop a strip bark growth form as they age. The apparent advantage of this growth form in these harsh environments is that a large amount of crown foliage does not need to be maintained, nor does new wood need to be grown around the whole circumference of the tree. Other local species such as white-bark pine (PIAL) develop a kromholtz (stunted wind-flattened) growth form while giant sequoias (SEGI) seem to survive through sheer mass with thick fire-resistant bark and rot resistant wood.

A considerable amount historical research on giant sequoia tree rings was carried out in the first half of the twentieth century and provided the foundation for many recent studies. Early work by E. Huntington scientifically documented the great age of giant sequoias and found many of the oldest trees (Huntington, 1914). Additional sampling by A.E. Douglass (see Webb 1983 for more information about his life and work), using many of Huntington's stumps, used the species to develop the first multi-millennial length precisely crossdated tree-ring chronologies from the species by the 1930s (Douglass, 1945). Both used the stumps remaining from the many trees felled by logging activities in the late nineteenth and early twentieth centuries. Their chisel and v-cuts can still be seen today on many of the stumps they sampled. The large data set Huntington published was recently utilized by Stephenson and Demetry (1995) to develop size/age equations used to better understand sequoia demographics and Douglass' sequoia chronologies

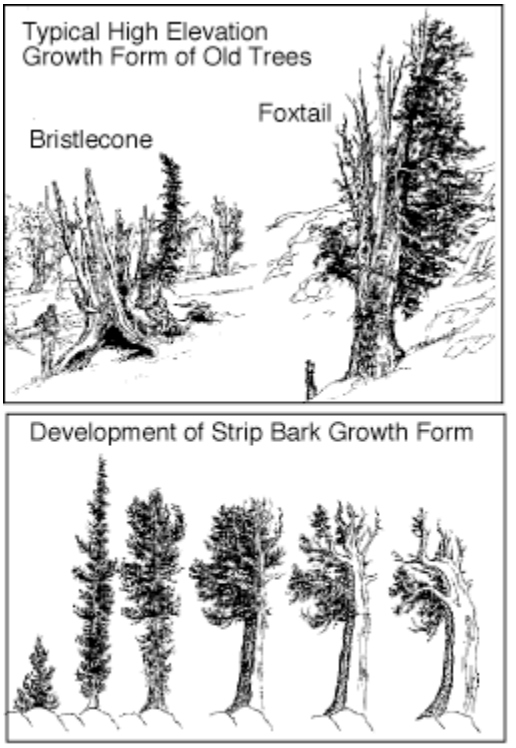

Figure 4B-2. Morphology and development of growth forms for old trees

still are the basis for crossdating most sequoia samples today (such as the recent fire history research by Swetnam et al., 1992). The first really important use of the long tree-ring chronologies from the region was the calibration of radiocarbon dating methods (carbon-14) using giant sequoias and bristlecone pine in the 1960s and 70s (LaMarche and Harlan, 1973).

TREE-RING CHRONOLOGIES AND CLIMATE

Tree-Line Fluctuations and Inferred Climate Change

Trees respond to year-by-year temperature and precipitation changes. Year-to-year changes in ring widths are predominantly influenced by rainfall, particularly at the lowest elevations a species grows. In contrast, the response to temperature is usually seen at decadal scales and is most pronounced in trees growing at upper tree line. Figure 4B-3 shows differences in chronologies of foxtail pine growing at their lower elevational limit (bottom plot) and at a tree-line site (upper plot). Low frequency variation is most obvious at the tree-line site and high frequency at the low site.

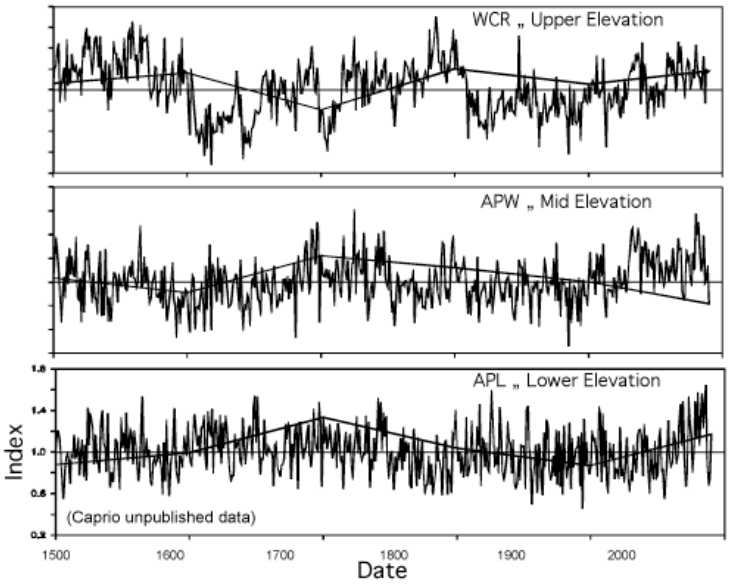

Figure 4B-3. Foxtail chronology characteristics at differing elevations.

These differences between upper and lower elevation chronologies from bristlecone pines in the White Mountains have been used to infer long-term fluctuations in precipitation and temperature (Fig. 4B-4) (LaMarch, 1974; 1978).

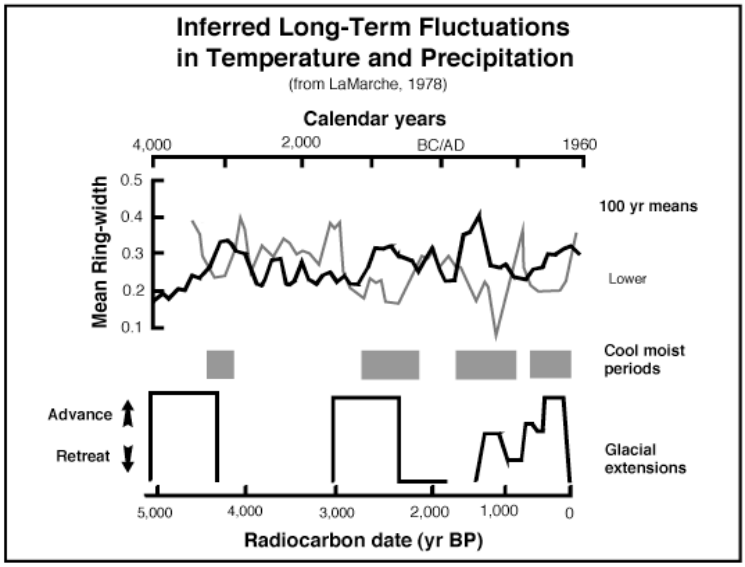

Figure 4B-4. Inferred long-term fluctuations in temperature and precipitation from White Mountain bristlecone pines.

Mortality patterns of upper elevation trees found in "ghost forests" (sites where trees can no longer survive but where subfossil wood from former stands exists) have also been used to infer periods of climatic change. Figure 4B-5 shows two periods of decline in foxtail stands on the west slope of the Sierra Nevada that are now ghost forests.

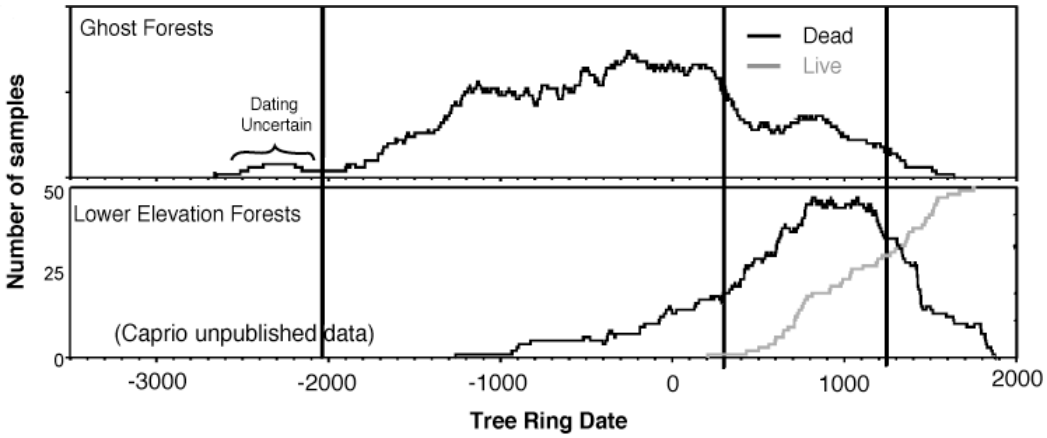

Figure 4B-5. Sample depth plot showing tow preiods of decline in foxtial pine stands on the western slope of the Sierra Nevada

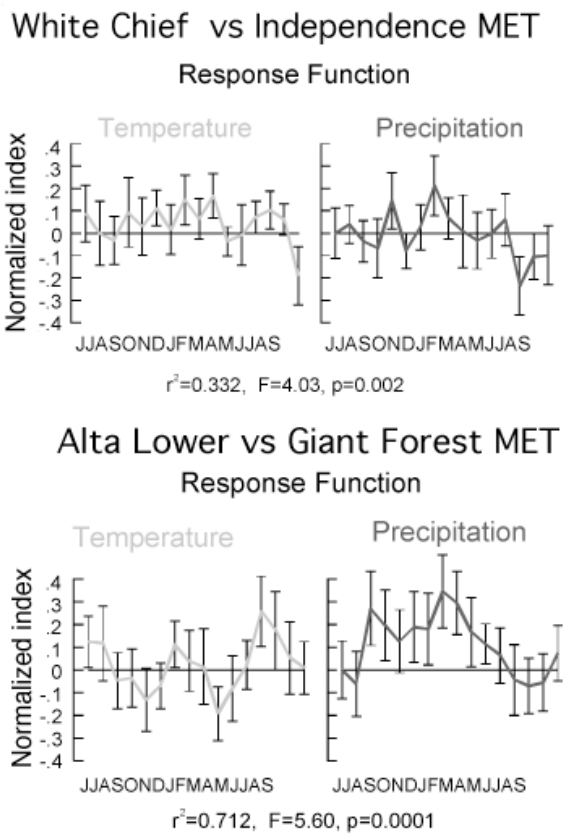

Figure 4B-6. Response function of tree ring chronologies to montly meteorological station

Climate Reconstructions

Where moisture or temperature limit tree-growth, tree-ring records can give information on the timing, duration and magnitude of fluctuations in climate or river flow. The response function of Figure 4B-6 provides an idea of the relative response of specific chronologies to monthly MET station data. The lower elevation foxtail series shows a strong response to rainfall but not temperature. Temperature reconstructions at higher elevations are hindered by the lack of long-term MET records at these elevations.

A reconstruction of the variations in the annual flow of the San Joaquin River is shown below (from Meko et al., 2002). The reconstruction was derived from a network of tree-ring sites (foxtail, giant sequoia, and western juniper) in the Sierra Nevada south of 39° N. Other important precipitation and temperature reconstructions have been developed for the area by Graybill and Funkhouser (1999); Graumlich (1993); and Hughes and Graumlich (1996).

Calibration/verification of the climate and tree-ring data are carried out for the period

of overlap (Fig. 4B-7). The statistical model for the reconstruction is multiple linear regression, and the predictors are tree-ring indices averaged over groups of sites identified by principal components analysis as having similar growth variations. The predictand is the log-transformed total of natural or "unimpaired" flow for the "water year" (Oct-Sept). For the example, predictors were entered stepwise from a pool of seven potential predictors with the model cross-validation at each step. Accuracy was high for a river-flow reconstruction in the Southwest.

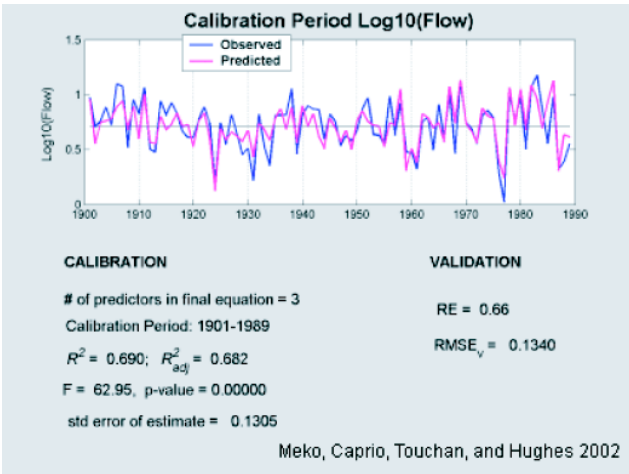

Figure 4B-7. Tree-ring based reconstruction of San Joaquin River flows going back to 1900.

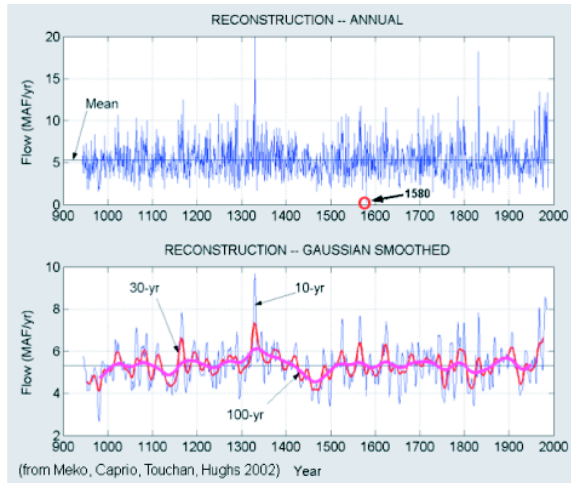

Figure 4B-8. Tree-ring based reconstruction of San Joaquin River flow from 942 to 1989 A.D.

Figure 4B-8 shows the reconstructed San Joaquin flow from 942 to 1989 AD. Low frequency variations are displayed in the plot of the annual series smoothed with low-pass gaussian filters. The mid-1400's emerge as the driest period at the 100-year wavelength. The smoothed series trend sharply downward into this drought from extremely high flows in the mid-1300s a time that lake levels apparently rose and killed hundred-year old pine trees rooted in what is now the bottom of Mono Lake (Stine,1994).

For one-year to three-year droughts, the long-term record has examples of low flow much more severe than any in the gauged record. The instrumental record for the 1987-92 drought is fairly representative of the six-year extreme low flow. Hundred-year means of San Joaquin river flow have departed by at most by about 15% from the modern (1901-2001) mean.

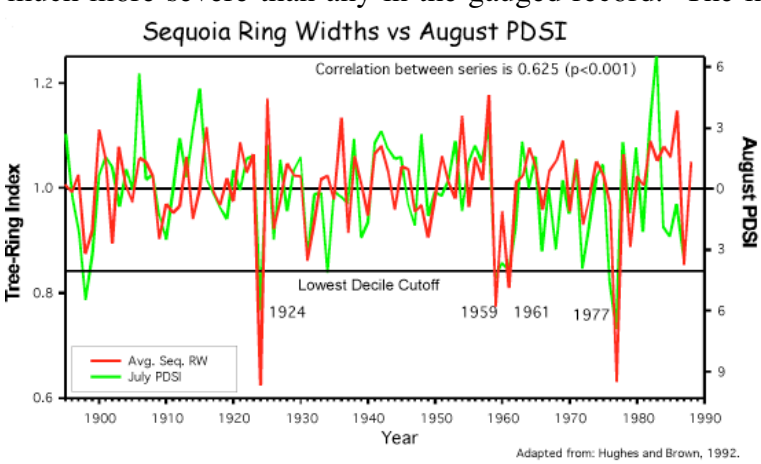

Figure 4B-9. Sequoia ring widths vs. August PDSI

Although giant sequoias growing in a mesic environment show an overall weak climate signal, low-growth years correspond to regional droughts. Hughes and Brown (1992) reconstructed drought years

(101 B.C. to A.D. 1988) using August PDSI and the lowest decile cutoff (Fig. 4B-9). Their results suggest that from 1850 to 1950 drought frequency was lower than during any other period.

Frost Rings and Rare Climatic Events

A feature observed in many high elevation chronologies are latewood "frost rings". These are distorted rings (Fig. 4B-10) in which the latter portion of the ring has been mechanically disrupted by the formation of ice before the growing season has ended. A strong correlation has been found between these rings and volcanic eruptions that have ejected dust and gas into the stratosphere. LaMarche and Hirschboeck (1984) examined frost rings in bristlecone pines and determined that the late season events were indicators of large scale climatic events and correlated well with major volcanic eruptions. That these impacts were at least hemispheric in nature has been verified when these same events were found to be recorded in more recently developed long chronologies from Irish and English oaks (Baillie, 1995).

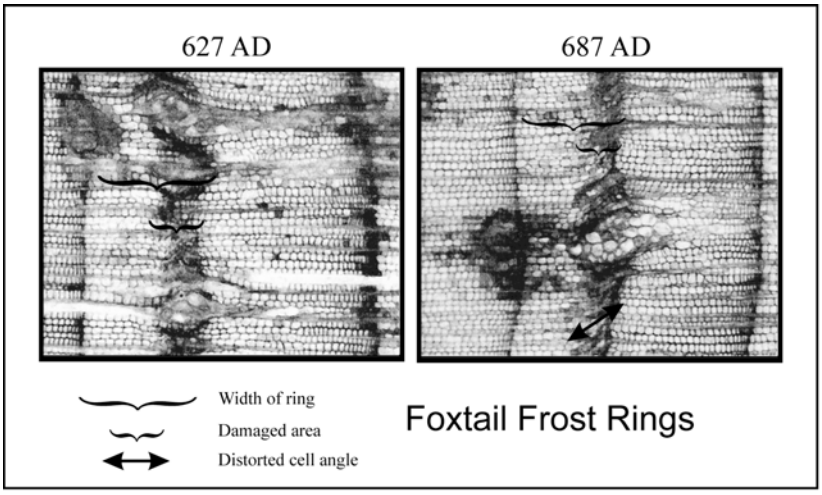

Figure 4B-10. Foxtail frost rings

The much cited frost ring in 1627 B.C. has been attributed to the eruption of Santorini in the Aegean and the destruction of the Minoan civilization (LaMarche and Hirschboeck, 1984). Similar patterns of frost ring occurrence are being found as long chronologies are developed from foxtail pine in the Sierra (Fig. 4B-11, 4B-12).

Figure 4B-11. Foxtail snag in the upper Mineral King Valley, Sequoia National Park.

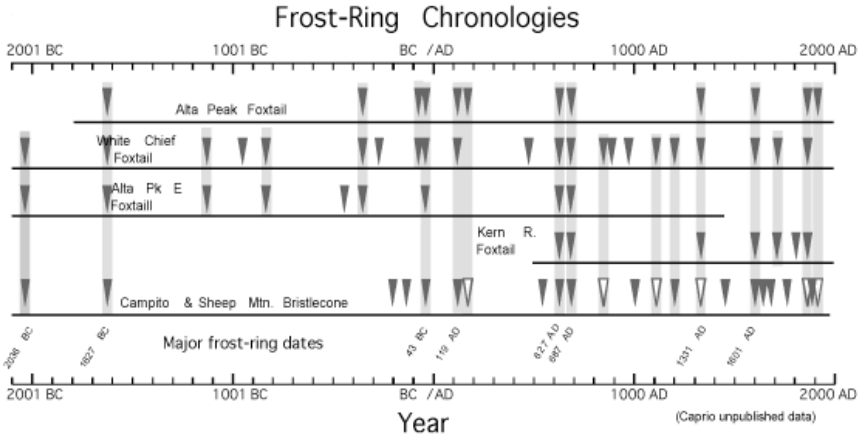

Figure 4B-12. Frost-ring chronologies for Sierra Nevada foxtail pines.

TREE-RING CHRONOLOGIES AND FIRE

Giant Sequoias: Fire and Climate

Giant sequoia fire scars have provided a rare annually resolved fire history for the last 2,000 years. Samples in the parks have been obtained from stumps and logs and provided an excellent record of fire (Fig. 4B-13 shows the lower left corner of the slab on display in Sherman Tree parking lot that had 80+ scars from 257 B.C. to A.D. 1955).

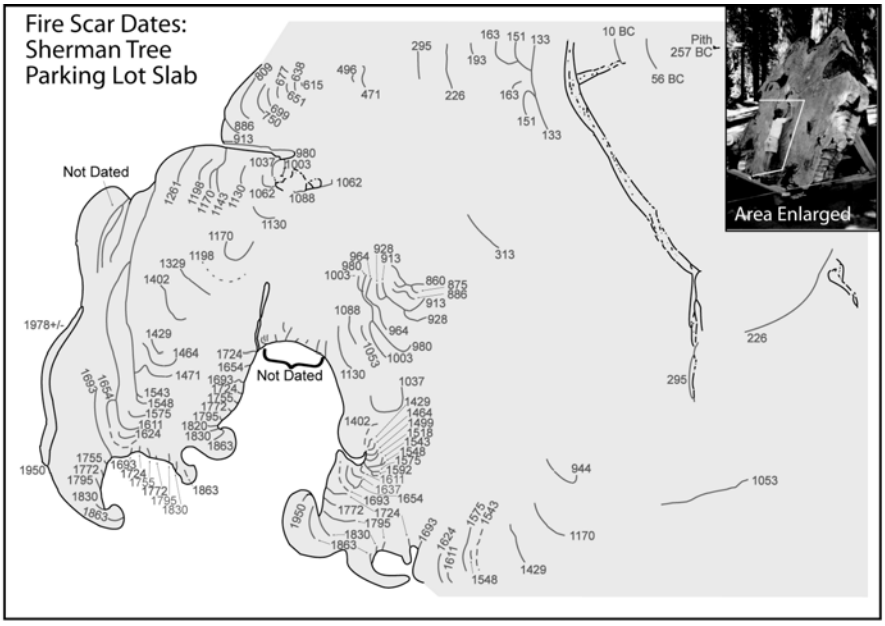

Figure 4B-13. Fire scar dates from a sequoia slab at the Sherman Tree Parking Lot.

A chronology of fire events from the Atwell Grove (one of five sites sampled) is shown below. Each tree is represented by a horizontal line, and each fire indicator as a vertical line (red=fire scars, blue=other such as growth releases). Figure 4B-14 is a composite record from all trees that show variation through time.

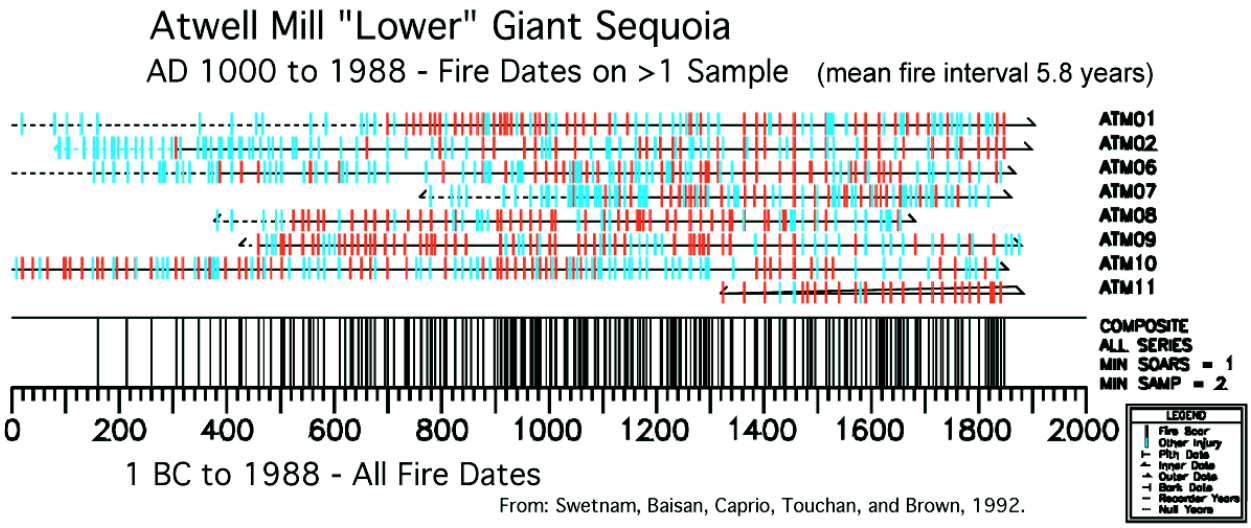

Figure 4B-14. Chronology of fire events from Atwell Grove, Sequoia National Park.

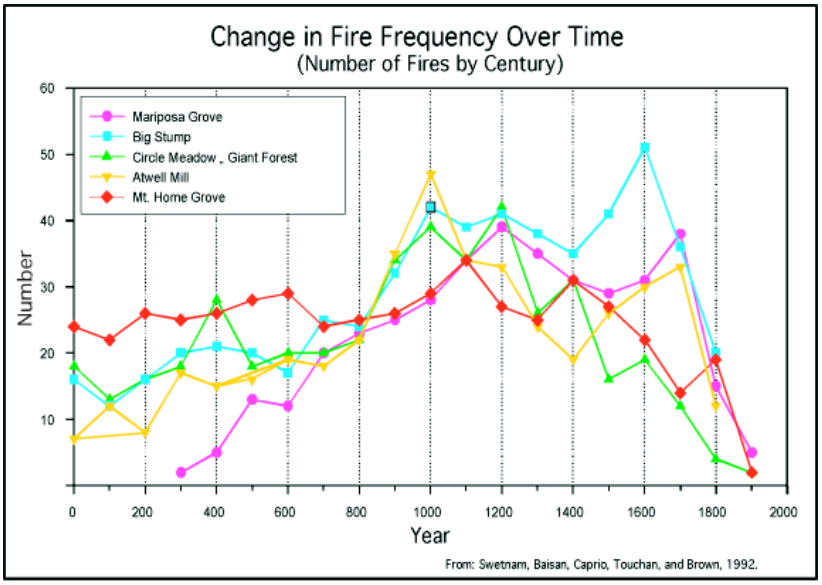

Figure 4B-15. Change in Sierra Nevada fire frequency over time.

Shifts in fire frequency over the last two millennia are apparent when data from the five sequoia groves are examined (Fig. 4B-15). The long-term pattern of fire corresponds to long-term climate changes (temperature – Fig. 4B-16) with increased frequency and smaller fires during the so-called "Medieval Warm Period", ~ AD 900-1300, and decreased frequency during the "Little Ice Age", ~AD 1400-1840 (Swetnam 1993). The decrease in fire occurrence in mid-to-late nineteenth century corresponds to extirpation of Native Americans and intense livestock grazing in the Sierra Nevada that resulted in fine fuel consumption that limited fire spread. Widespread organized fire suppression activities were not important or effective until well into the twentieth century.

High frequency variation in fire occurrence was associated with reconstructed precipitation patterns (Fig. 4B-17) (Brown et al., 1992; Swetnam, 1993). Superimposed epoch analysis shows that the most extensive fire events that were synchronous among the five sequoia groves sampled and had the strongest drought signal while years with few or no fires were wet.

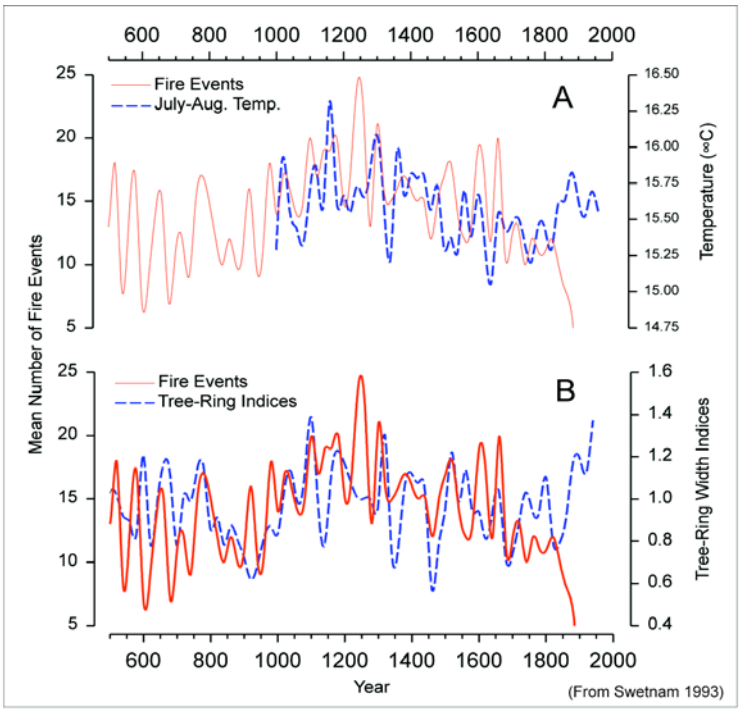

Figure 4B-16. Correspondence of long-term fire patterns and long-term climate changes

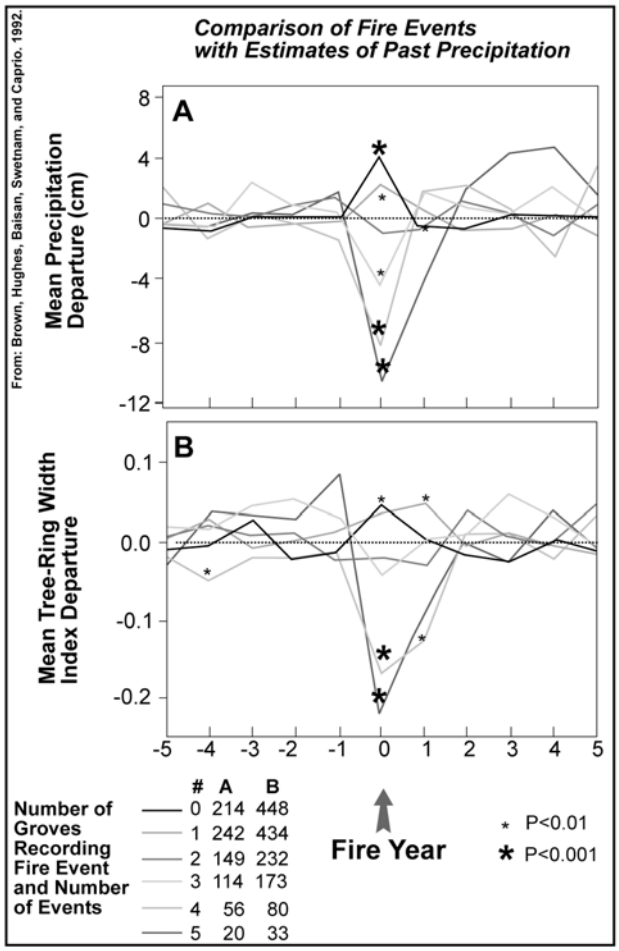

Figure 4B-17. Comparison of fire events with estimates of past precipitation.

FIRE AND LANDSCAPES

Recent fire history studies have focused on provided a more spatially explicit picture of fire occurrence in the southern Sierra Nevada. Sampling has been conducted along transects and using networks of sites throughout conifer forests (such as the East Fork of the Kaweah River a 20,000 ha watershed). These are being used to assess past variations in fire occurrence across elevations (Caprio and Swetnam, 1995) and aspects, among differing vegetation types, and to coarsely reconstruct fire size reconstruct fire size at a watershed scale. An inverse relationship between fire and elevation (Fig. 4B-18, showing number of fires from 1700-1860 by aspect) with a comparatively high frequency on lower south aspect is observed. The fire chronology of Figure 4B-19 shows the differences in fire frequency among three elevationally distinct vegetation types. Fire climate relationships (Fig. 4B-20) are also being explored among these landscape attributes.

These data have become an important source of information for Sequoia-Kings Canyon National Park's fire management program. It is being used to understand fire return interval departures (FRID) and to help plan where on the landscape prescribed burning might be most effective or needed ecologically (Caprio et al., 1997). They also provide a conservative baseline estimate of how much fire occurred within Sierra

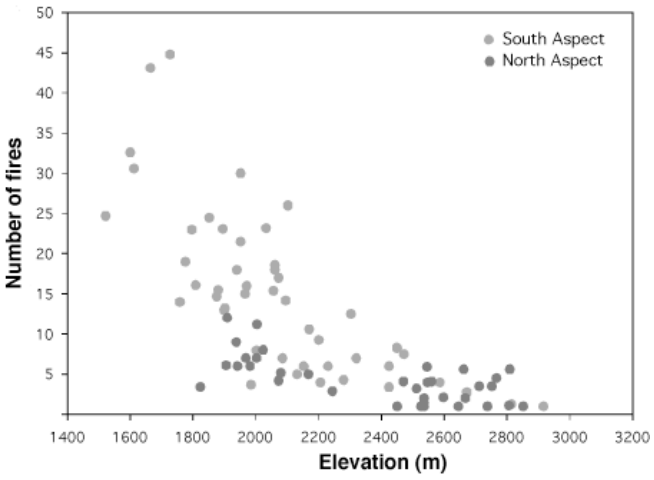

Figure 4B-18. Inverse relationship between fire and elevation.

Nevada ecosystems in the past. This is being utilized to gage whether we are being effective at restoring to fire to our systems (Caprio and Graber, 2000).

Although Sequoia-Kings Canyon National Parks has had an aggressive fire management program over the last 30 years, this information still suggests that we are not being entirely successful at returning fire as a process in the parks (Fig. 4B-21).

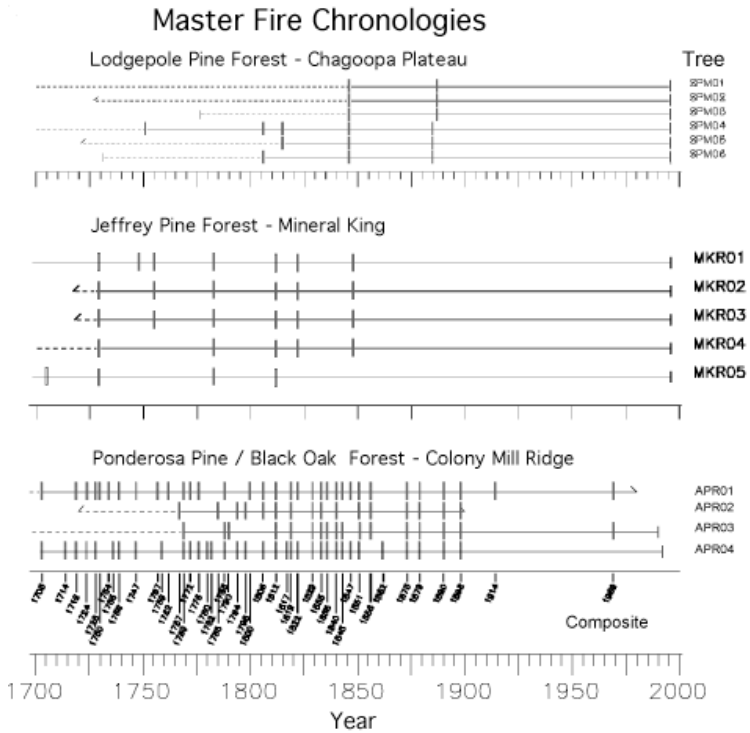

Figure 4B-19. Fire chronology for three elevationally distinct vegetation types in Sequoia National Park.

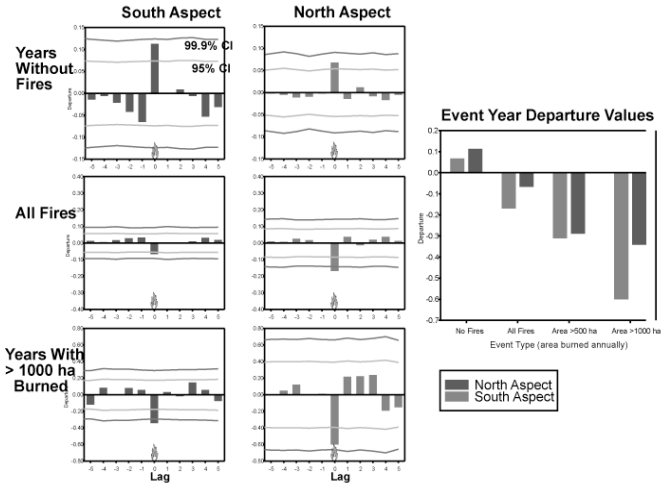

Figure 4B-20. Fire climate relationships in Sequoia and Kings Canyon National Parks

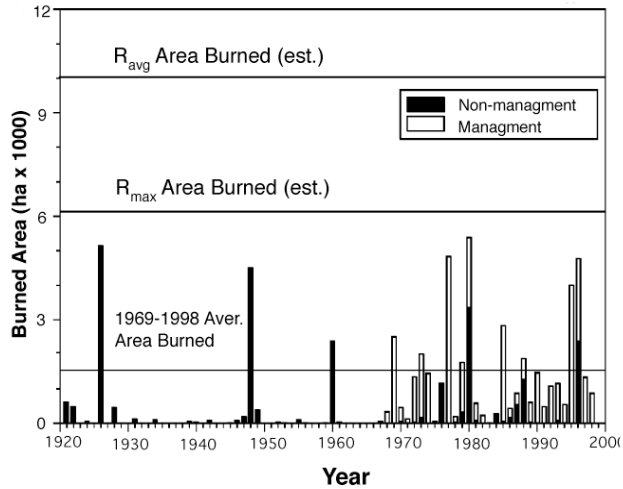

Figure 4B-21. Managed vs. non-managed fires in Sequoia and Kings Canyon National Parks.

REFERENCES CITED

Baillie, M.G.L., 1995, A Slice Through Time: Dendrochronology and Precision Dating. B.T. Batsford, London. 176 pp.

Caprio, A.C. and D.M. Graber, 2000, Returning fire to the mountains: can we successfully restore the ecological role of pre-euroamerican fire regimes to the Sierra Nevada? pp 233-241. In: Cole, David N.; McCool, Stephen F.; Borrie, William T.; O'Loughlin, Jennifer (comps). Proceedings: Wilderness Science in a Time of Change-- Vol. 5 Wilderness Ecosystems, Threats, and Management; 1999 May 23-27; Missoula, MT. Ogden, UT: U.S. Department of Agriculture, Forest Service, Rocky Mountain Research Station. Proceedings RMRS-P-15-VOL-5

Caprio, A.C., C.M. Conover, M. Keifer, and P. Lineback, 1997, Fire management and GIS: a framework for identifying and prioritizing fire planning needs. In: Proceedings of the Conference on Fire in California Ecosystems: Integrating Ecology, Prevention, and Management. Nov. 17-20, 1997, San Diego, CA.

Caprio, A.C. and Swetnam, T.W., 1995, Historic fire regimes along an elevational gradient on the west slope of the Sierra Nevada, California, In: J.K. Brown, R.W. Mutch, C.W. Spoon, R.H. Wakimoto (tech. coord.) Proceedings: Symp. On Fire in Wilderness and Park Management, 1993 March 30-April 1; Missoula, MT, USDA For. Serv. Gen. Tech. Rep. INT-GTR-320

Douglas, A. E. 1945. Survey of Sequoia Studies: Tree-Ring Bulletin, Vol. 11, No.4, University of Arizona.

Graumlich, L.J. 1993, A 1,000-year record of temperature and precipitation in the Sierra Nevada: Quaternary Research, v. 39, p. 249- 255.

Graybill, D.A. and G.S. Funkhouser. 1999, Dendroclimatic reconstructions during the past millennium in the southern Sierra Nevada and Owens Valley, California, pp. 239-269, In: M.R. Rose and P.E. Wigand (eds.) Proceedings of Southern California Climate Symposium on Trends and Extremes of the Past 2,000 Years, October 25, 1991. Natural History Museum of Los Angeles County, Tech. Rep., No. 11.

Hughes, M.K. and P.M. Brown, 1992, Drought frequency in central California since 101 B.C. recorded in giant sequoia tree rings: Climate Dynamics, v. 6, p. 161-167.

Hughes, M.K., Graumlich, L.J., 1996, Multimillennial dendroclimatic records from western North America, In: Bradley RS, Jones PD, Jouzel J, Editors, Climatic variations and forcing mechanisms of the last 2000 years. Berlin: Springer Verlag. p 109-24.

Huntington, E. 1914, The climate factor as illustrated in arid America, Carnegie Inst. Washington Publ. 192.

LaMarche, V.C. Jr., 1974, Paleoclimatic inferences from long tree-ring records: Science, v. 183, p. 1043-1048.

LaMarch, V. C., 1978, Tree-ring evidence of past climatic variability: Nature, v. 276, p. 334-338.

LaMarche, V.C. and T.P. Harlan, 1973, Accuracy of tree ring dating of bristlecone pine for calibration of the radiocarbon time scale: Journal of Geophysical Research, v. 78, p. 8849-8858.

LaMarche, V.C. Jr. and Hirschboeck, K.K., 1984, Frost rings in trees as indicators of major volcanic eruptions: Nature, v. 307, p. 121-126.

Stephenson, N.L. and A. Demetry, 1995, Estimating ages of giant sequoias: Canadian Journal of Forestry Research, v. 25, p. 223-233.

Stine, S., 1994, Extreme and persistent drought in California and Patagonia during mediaeval time: Nature, v. 369, p. 546-549.

Swetnam, T. W., C. H. Baisan, A. C. Caprio, R. Touchan, and P. M. Brown. 1992. Tree-Ring Reconstruction of Giant Sequoia Fire Regimes: Final report on Cooperative Agreement No. DOI 80181-0002 to National Park Service, Sequoia and Kings Canyon National Parks, California.

Swetnam, T.W, 1993, Fire History and Climate Change in Giant Sequoia Groves: Science, v. 262, p. 885-889.

Webb, G.E., 1983, Tree Rings and Telescopes: The Scientific Career of A.E. Douglass. U of A Press, Tucson, AZ. 242 pp.

APPENDIX 4C: GIANT SEQUOIA ECOLOGY AND RECENT GLACIAL RETREAT: EVIDENCE FOR HOLOCENE CLIMATE CHANGE IN THE SOUTHERN SIERRA NEVADA

Nathan Stephenson *U. S. Geological Survey, Western Ecological Research Center, Sequoia-Kings Canyon Field Station, Sequoia and Kings Canyon National Parks, CA 93271 nstephenson@usgs.gov*

CLIMATE, FIRE, AND GIANT SEQUOIAS

Abundant giant sequoia pollen in sediment from the Tulare Lake basin suggests that during the most recent Pleistocene glacial advance, sequoias were much more abundant in the southern Sierra Nevada than today. However, there is little evidence to tell us exactly where in the Sierra they were. The best evidence to date comes from sequoia foliage found in a few Pleistocene woodrat middens in caves near Boyden Cave in the South Fork Kings River canyon (Stop 7; Appendix 7). Found at an elevation of 1,000 to 1,400 m (3,300 to 4,600 ft), a landscape now dominated by mixed chapparal and oak woodland, these middens show evidence of sequoias in this region during the Last Glacial Maximum (Cole, 1983). During the warm, dry early Holocene sequoias apparently retreated to their current, higher elevations.

Working with pollen in meadow sediment, R. Scott Anderson (Northern Arizona University) has shown that during the early- to mid-Holocene, sequoias were present in the areas of the current major groves, but in extremely low numbers – in fact, they may have been near extinction (Anderson, 1994; Anderson and Smith, 1994). During the gradual cooling that started about 4,500 years ago, sequoias began to expand out to their current grove boundaries (Fig. 4C-1). The groves as we know them today may be only two sequoia lifespans old. Look at the trees around you and imagine – some of them may be just the second generation of colonists!

To reproduce and thrive, sequoias require certain environmental conditions. Specifically, they require fires that burn hot enough to open holes in the forest canopy that are larger than about 0.1 ha (0.25 acre), thus reducing competition for light and water and allowing their seedlings to take root. Following such fires, sequoias also apparently require mild enough summers to allow the drought-sensitive seedlings to establish their root systems. Though climate and fire regimes have varied over the last few thousand years, conditions ripe for sequoia regeneration seem to have occurred several times per century, and sequoias have experienced something of a heyday. That is, until Euro-American settlers arrived.

With the arrival of Euro-American settlers in the late 1800s, fires that once roamed the landscape freely began to taper off, probably due to some combination of disruption of Native American burning practices, livestock grazing that reduced fine fuels, and active fire suppression. Consequently, sequoia reproduction during the last century effectively fell to zero – a condition without precedent in at least the last few millennia. Additionally, more fire-sensitive species like white fir began to establish in abundance (Fig. 4C-2), increasing the hazard of unusually severe and uncontrollable wildfires. However, with the advent of prescribed burning in the 1970s, hazardous fuels in sequoia groves are being reduced, and sequoia reproduction has returned in abundance.

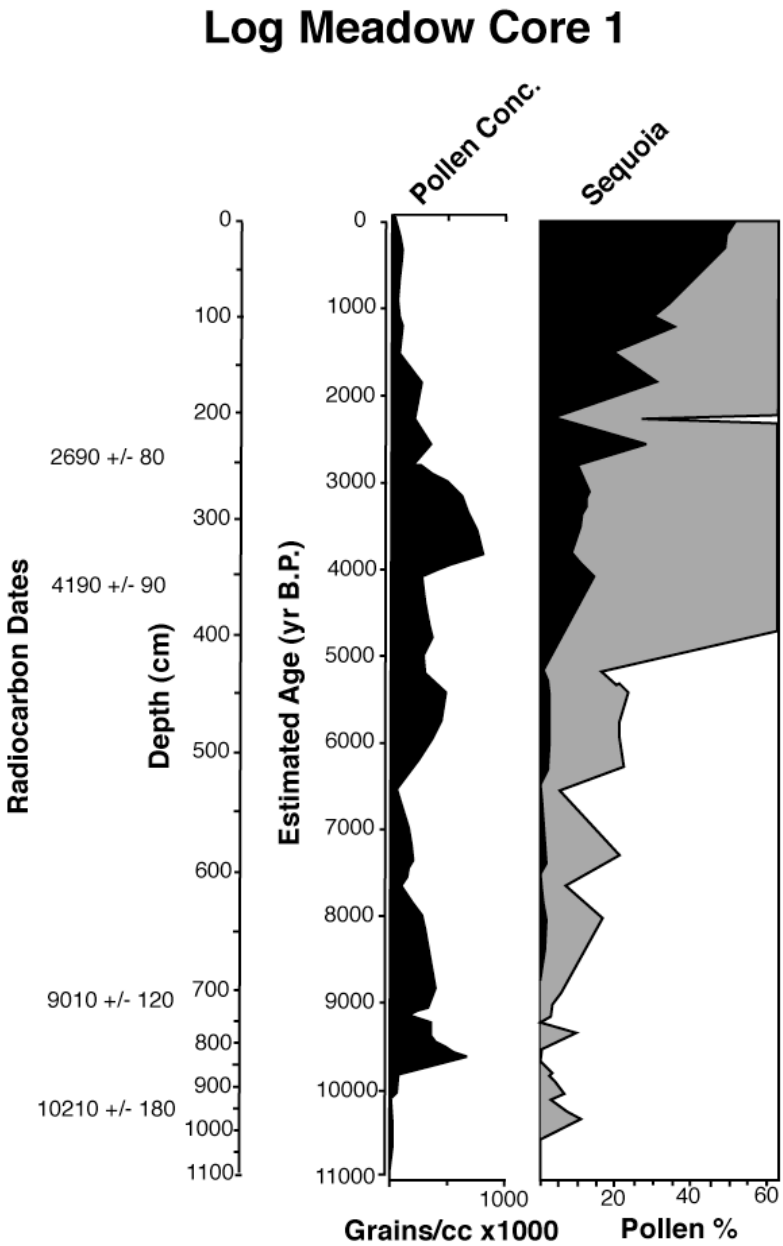

Figure 4C-1. Pollen percentage diagram for Log Meadow Core 1. Pollen abundance suggests an expansion of Giant Sequoias around 4500 B.P., in response to cooling climate. Modified from Anderson (1994).

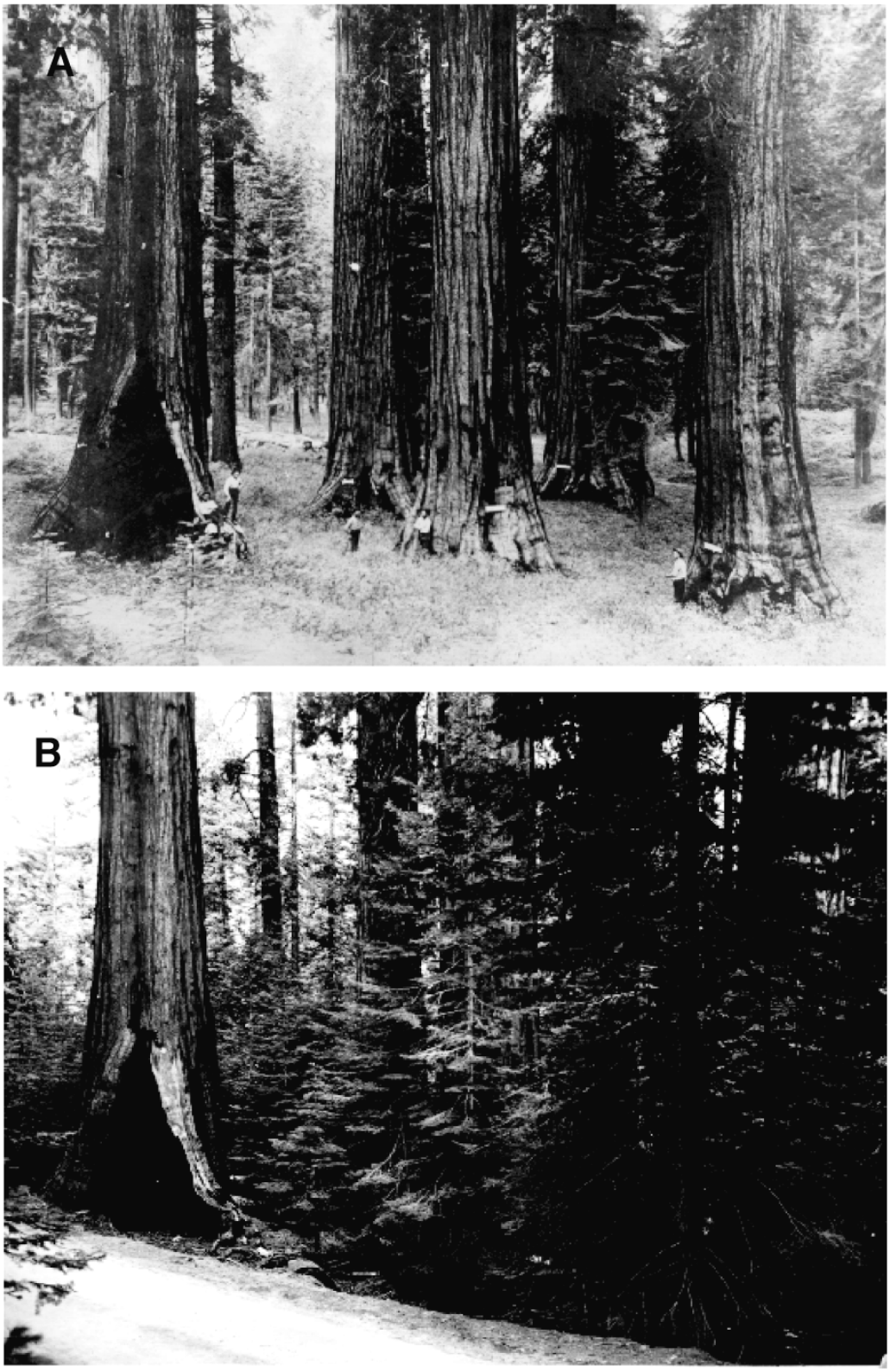

Figure 4C-3. Example of vegetation change due to fire exclusion in the SIerra Nevada. **A**. Photograph of the Mariposa Grove near Yosemite ca. 1890. **B.** Photograph from the same location in 1970, showing abundant growth of fire sensitive conifer species.

RECENT RETREAT OF SOUTHERN SIERRA NEVADA GLACIERS

In recent decades, alpine glaciers have been retreating nearly everywhere on earth. To determine whether the same trend holds in the southern Sierra Nevada, this summer National Park Service and USGS employees teamed up to re-photograph some of the larger glaciers in northern Kings Canyon National Park. Early photographs taken by G. K. Gilbert in 1908 were reproduced as accurately as possible (Fig. 4C-3, 4C-4). These photographs clearly show that, indeed, these glaciers also have been retreating. Photographs from different time periods during the last century suggest that the retreat has been occurring since at least the early 1900s, and is not a phenomenon limited to the last few decades.

REFERENCES CITED

Anderson, R. S., 1994, Paleohistory of a giant sequoia grove: The record from Log Meadow, Sequoia National Park, p. 49-56, in Aune, P. S., ed., Proceedings of the Symposium on Giant Sequoias: Their Place in the Ecosystem and Society", USDA Forest Service, General Technical Report PSW-GTR-151.

Anderson, R.S., and Smith, S.J., 1994, Paleoclimate interpretations of meadow sediment and pollen stratigraphies from California: Geology, v. 22, p. 723-726.

Cole, K., 1983, Late Pleistocene vegetation of Kings Canyon, Sierra Nevada, California: Quaternary Research, v. 19, p. 117-129.

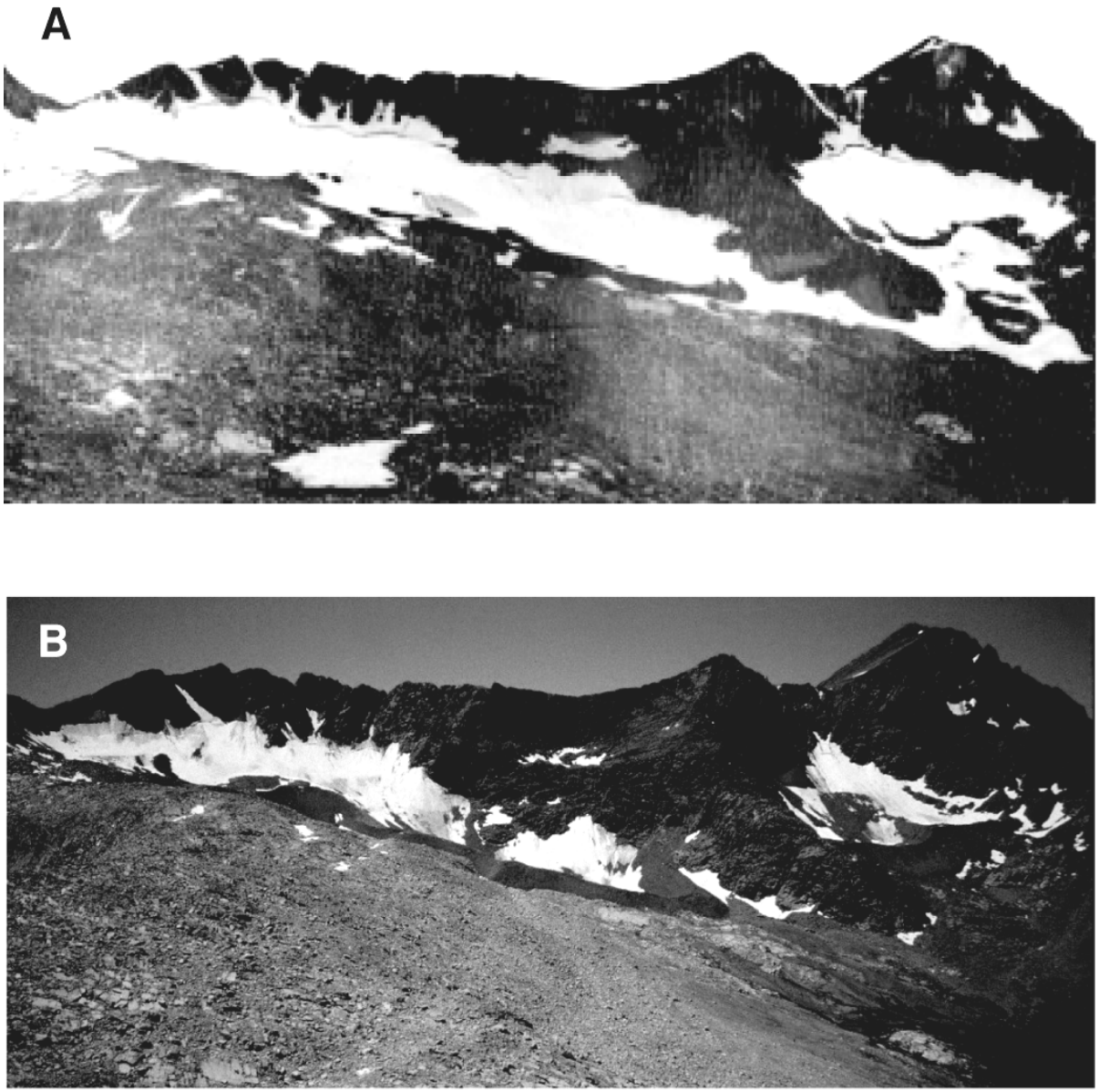

Figure 4C-3. Recent retreat of the Goddard Glacier, located on the northeast side of Mount Goddard (4136 m; 13,568 ft), northern Kings Canyon National Park. **A.** Photograph of the Goddard Glacier on August 13, 1908. **B.** Photograph of the Goddard glacier from the same location on August 4, 2003.

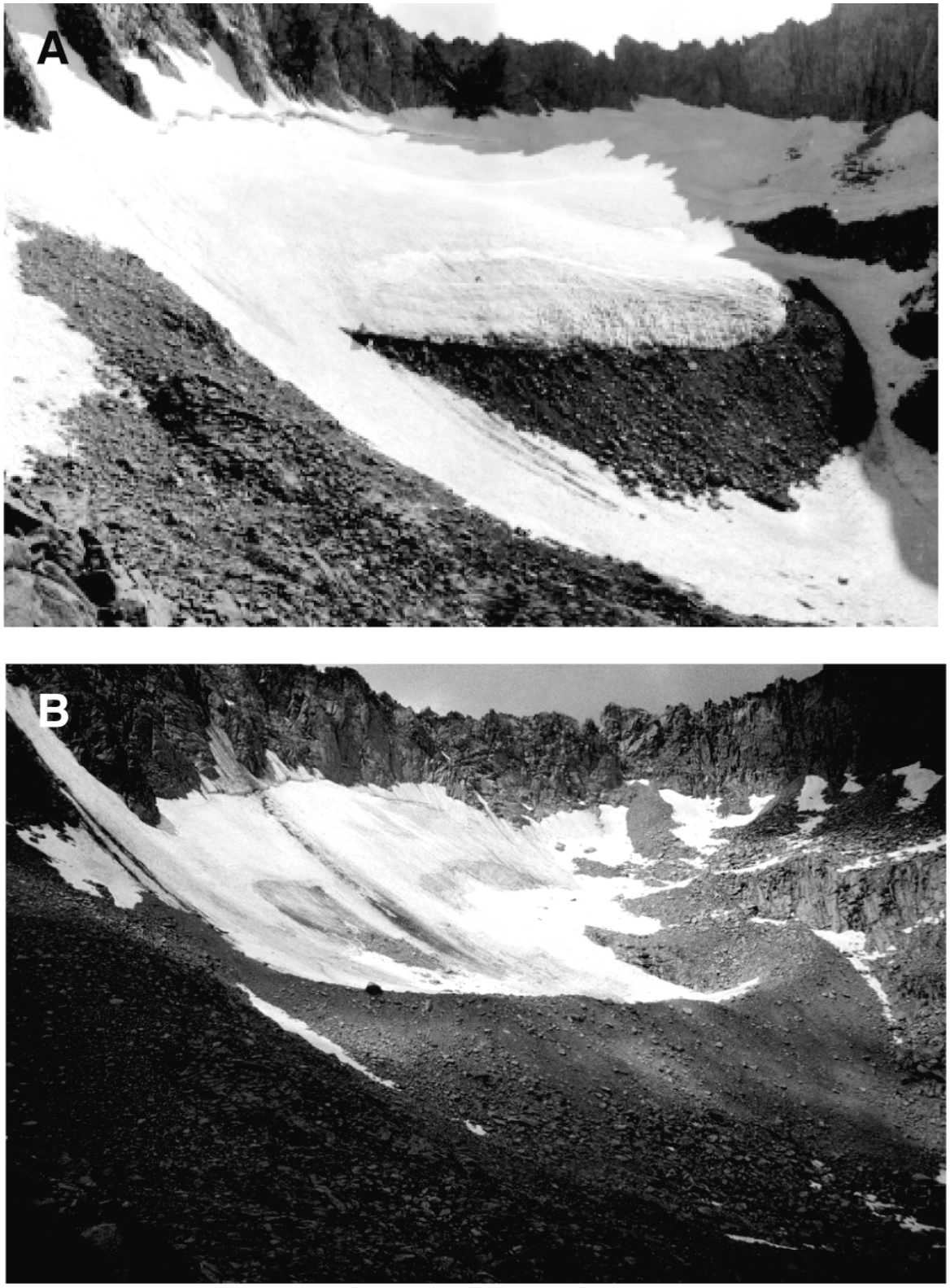

Figure 4C-4. Recent retreat of the Darwin Glacier, located on the northwest side of Mount Darwin (4216 m; 13,830 ft), northern Kings Canyon National Park. **A.** Photograph of the Darwin Glacier on August 14, 1908. **B.** Photograph of the Darwin glacier from the same location on August 2, 2003.

APPENDIX 5: VOLCANIC EVIDENCE FOR PLIOCENE DELAMINATION OF THE SIERRA NEVADA BATHOLITHIC ROOT

Allen Glazner *University of North Carolina, Chapel Hill, NC, 27599 afg@unc.edu*

INTRODUCTION

The Sierra Nevada range from Yosemite south was largely devoid of magmatism in the Cenozoic except for a brief, intense, and compositionally unusual episode about 3.5 Ma. This anomalous volcanic event was more-or-less coincident with a Miocene-to-Pliocene shift in the nature of mantle xenoliths carried by the lavas and with development of at least some of the topography in and around the range. It is possible that all these events were caused by delamination of lithosphere beneath the Sierra Nevada (e.g., Ducea and Saleeby, 1998; Manley et al., 2000).

DELAMINATION OF THE BATHOLITHIC ROOT

A variety of seismic, magnetotelluric, and petrologic evidence indicates that the southern Sierra Nevada presently lacks a deep crustal root (e.g., Wernicke et al., 1996; Ruppert et al., 1998). However, petrologic studies predict that such a root resided beneath the range following cessation of subduction; the lowermost portion of this root was likely eclogitic in composition and more dense than the surrounding mantle (Ducea, 2001). Presence of an eclogite root beneath the Sierra Nevada in the Miocene is supported by xenolith data (Ducea and Saleeby, 1998) and may have been caused by abnormal cooling of the deep lithosphere during Laramide subduction (Dumitru, 1990; Dumitru et al., 1991). Rapid changes in Pliocene xenolith composition, and the pressure-temperature conditions of crystallization (Ducea and Saleeby, 1996; 1998), suggest that the dense root beneath the Sierra Nevada crest was convectively removed, or delaminated, sometime between 3 and 12 Ma.

Delamination might occur for two reasons. First, Bird (1979) noted that mantle lithosphere might delaminate because it is cooler and therefore denser than deeper mantle. Second, compositional contrasts can make shallow lithosphere denser than the underlying mantle. In particular, mafic igneous rocks cooled into the eclogite stability field, in which low-density olivine+plagioclase assemblages convert to higher-density garnet+pyroxene assemblages, can be significantly denser than peridotitic mantle (Kay and Kay, 1993).

PLIOCENE VOLCANISM IN THE SOUTHERN SIERRA NEVADA

Although fluvial and glacial erosion have destroyed much of the Cenozoic volcanic record of the Sierra Nevada, there is clear evidence for a short-lived, intense burst of unusual volcanism at about 3.5 Ma. Evidence for this event consists of small, discontinuous outcrops of potassic volcanic rocks scattered across the range (Moore and Dodge, 1980; Van Kooten, 1980; Bergquist and Diggles, 1986; Fig. 5-1). Most Cenozoic volcanism in the range occurred in two pulses—in the Miocene from 12 to 8 Ma and in the Pliocene from 4 to 3 Ma (Moore and Dodge, 1980; Manley et al., 2000). Volcanism resumed in the Quaternary (0.1-0.01 Ma) at the Golden Trout volcanic field south of Mt. Whitney, contemporaneous with activity east of the range in the Big Pine, Coso, and Long Valley volcanic fields.

The potassic basalt outcrop southeast of Hume Lake, backdrop for Stop 5, is one of the Pliocene basalt flows belonging to the San Joaquin - Kings volcanic field. It contains phenocrysts of biotite and clinopyroxene (Moore and Dodge, 1980), and has a $^{40}Ar/^{39}Ar$ age of ~3.5 Ma (Manley et al, 2000).

The Pliocene (ca. 3.5 Ma) volcanic outburst is clearly evident in the data compiled in Figure 5-1. Data in Figure 5-1 are from a preliminary compilation (Manley et al., 2000); a more comprehensive dataset is being developed for the NAVDAT project (navdat.geo.ku.edu; see also www.earthchem.org). Prior to 4 Ma volcanism was almost absent from the Sierra Nevada south of Yosemite except for some Miocene lava flows in the lower San Joaquin drainage and in the southernmost part of the range. From 4 to 3 Ma volcanism was widespread across the range in the San Joaquin - Kings volcanic field (Moore and Dodge, 1980), in the Coso Range (Duffield et al., 1980), and in isolated spots east of the Sierra Nevada. After 3 Ma volcanism left the Sierra Nevada except for the Golden Trout field and became focused along the eastern side of the range. These patterns are clearly visible in the animation posted at navdat.geo.ku.edu.

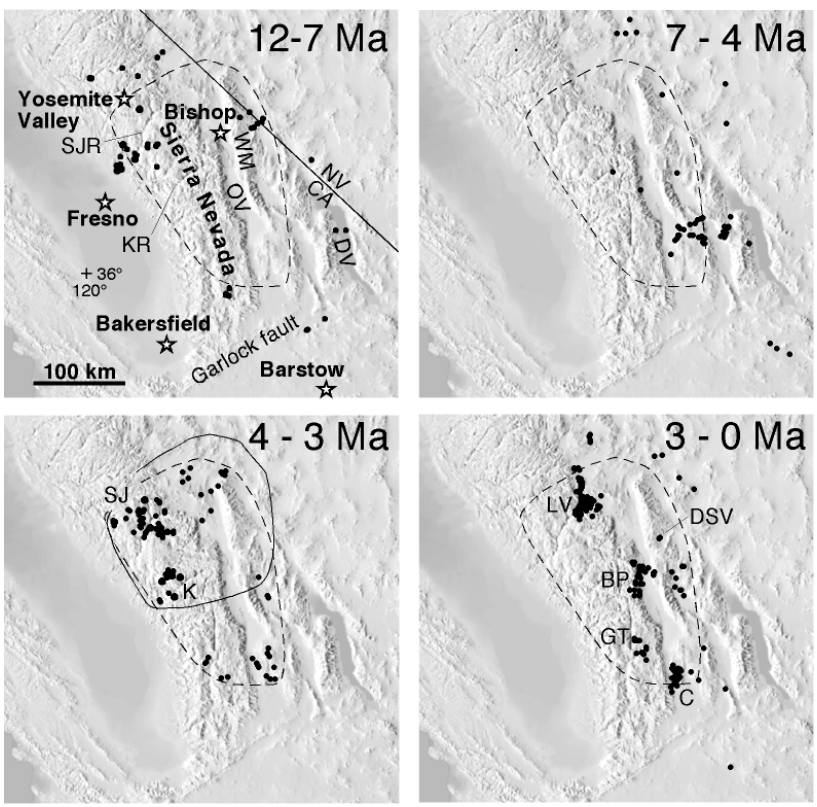

Figure 5-1. Distribution of volcanism in the southern Sierra Nevada region as a function of time. Dashed line outlines area within which Pliocene (chiefly 4-3 Ma) volcanism was prevalent; note that Quaternary (1.5-0 Ma) volcanic fields (LV–Long Valley, BP–Big Pine, GT–Golden Trout, C–Coso) all lie within area of Pliocene event. Solid line in 4-3 Ma panel outlines area of highly potassic lavas (K1>1; see Figure 2). DV–Death Valley, OV–Owens Valley, WM–White Mountains, SJR–San Joaquin River, SJ–San Joaquin volcanic field, KR–Kings River, K–Kings volcanic field, DSV–Deep Springs Valley. Area east of Death Valley was not included in this study.

These data reveal several unusual aspects of the Pliocene pulse of magmatism. First, it was preceded and followed by low levels of activity and, in the Sierra Nevada itself, by almost 5 m.y. without volcanism. Second, it was abrupt, short-lived, and contemporaneous across the southern half of the Sierra Nevada and the adjacent Owens Valley. The dashed line in Figure 5-1 shows the area affected; within this area there is no resolvable sweep of volcanism. Third, many of the lavas erupted during the pulse were mafic and highly potassic

(e.g., >3 wt% K_2O at 55 wt% SiO_2), unlike volcanism before or after (Fig. 5-2). In the Kings and San Joaquin volcanic fields, Pliocene volcanism was dominated by ultrapotassic compositions (Van Kooten, 1980; Moore and Dodge, 1980; Huber, 1981; Feldstein and Lange, 1999; Farmer et al., 2002) with several wt% more K_2O at a given level of SiO_2 than anything erupted before or after. In contrast, Miocene and Quaternary rocks generally follow standard subalkalic to alkalic trends.

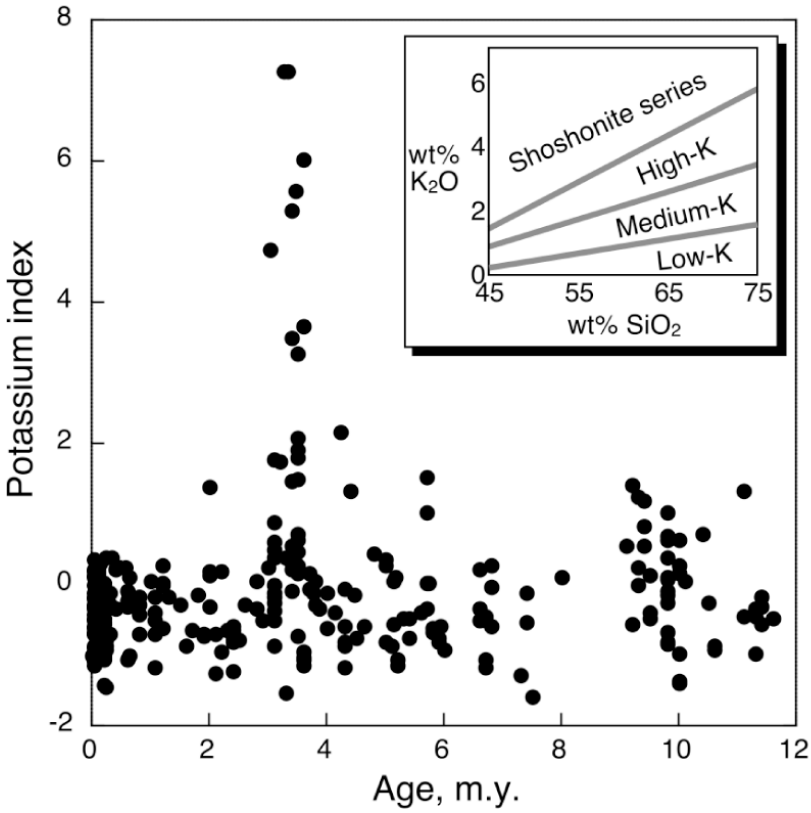

Figure 5-2. Potassium index (K1) plotted against time, showing that many lavas in the 4-3 Ma window are highly potassic. Potassium index is given by K1 = K_2O + 5.135 – 0.145(SiO_2) and is a measure of how far a given sample plots above the line defining the upper limit of high-K field of Gill (1981, p. 6). Inset box shows the K_2O-SiO_2 classification and definition of the shoshonite series. Rocks in this field (K1 > 0) belong to the shoshonite series. Figure includes data from NAVDAT database in a latitude/longitude box defined by (–120, 40) and (-114, 34). Data extracted September 20, 2003.

Ducea and Saleeby (1998) suggested, on the basis of xenolith studies, that the garnet-rich root of the Sierra Nevada delaminated in the late Miocene or Pliocene, because Miocene xenoliths in Sierran lavas are locally garnet-rich, but xenoliths in Pliocene and Quaternary lavas are typically garnet-free spinel peridotite. Manley et al. (2000) and Farmer et al. (2002) proposed that the 3.5 Ma pulse of magmatism was caused by the delamination event.

The 4-3 Ma pulse of volcanism in the Sierra Nevada strikingly resembles Cenozoic magmatic pulses in the Andes and Himalayas that have been attributed to mantle delamination. Kay and Kay (1993) and Kay et al. (1994) explained a 3-2 Ma pulse of mafic, potassic magmatism in the central Andes as indicating mantle delamination beneath the southern Puna plateau of Argentina. Delamination was also invoked by England and Houseman (1989) to explain Miocene uplift, extension, and volcanism on the Tibetan plateau. Turner et al. (1993) and Chung et al. (1998) showed that after 90 Ma, the plateau was generally devoid of volcanic activity until ca. 40 Ma, when pulses of small-volume eruptions began. Erupted products include potassic basaltic andesites (shoshonites) and minor felsic

rocks; trace element concentrations and Sr and Nd isotopic characteristics imply a lithospheric mantle source for the mafic magmas (Turner et al., 1993).

POSSIBLE TRIGGERS OF DELAMINATION

If delamination in the Sierra Nevada occurred in the Pliocene, it may have been triggered by tectonism. For example, faulting may reduce lithospheric strength enough to allow foundering. Significant regional Pliocene events in California include folding along the coast (Page and Brocher, 1993), spreading in the Gulf of California (Curry and Moore, 1984; Axen and Fletcher, 1998), and major extension between Death Valley and the Sierra Nevada (Wernicke and Snow, 1998). In Death Valley, significant extension began at ca. 7 or 6 Ma (McKenna and Hodges, 1990) and progressed westward. Valleys just east of the Sierra Nevada began to fill with sediment in the late Miocene and Pliocene (e.g., Bacon et al., 1982; Burchfiel et al., 1987; Lueddecke et al., 1998). These data indicate that the onset of significant extension along the eastern front of the Sierra Nevada coincided with the Pliocene pulse of magmatism and may have triggered delamination. Alternatively, spontaneous delamination may have weakened the lithosphere enough to allow faulting.

In summary, the widespread pulse of volcanism that occurred across the Sierra Nevada at 3.5 Ma was brief (<500 ka), compositionally distinctive (potassic and ultrapotassic; low Nd isotope ratios), and affected an area that was otherwise almost devoid of magmatism during the Neogene. Independent studies of xenoliths carried by these lavas indicate that delamination of the lithosphere under the Sierra Nevada may have occurred in the late Miocene or Pliocene. Manley et al. (2000) suggested, by analogy with the Andes and Himalaya, that the Pliocene magmatic pulse is a signature of this delamination event and provides a good estimate of its timing. Extensional faulting in eastern California may have been the trigger for the delamination of the Sierra Nevada lower lithosphere.

REFERENCES CITED

Axen, G.J., and Fletcher, J.M., 1998, Late Miocene-Pleistocene extensional faulting, northern Gulf of California, Mexico and Salton Trough, California: International Geology Review, v. 40, p. 217-244.

Bacon, C.R., Giovannetti, D.M., Duffield, W.A., Dalrymple, G.B., and Drake, R. E., 1982, Age of the Coso Formation, Inyo County, California: U.S. Geological Survey Bulletin 1527, 18 p.

Bergquist, J.R., and Diggles, M.F., 1986, Potassium-argon ages of volcanic rocks from the Domeland, southern Sierra Nevada, California: Isochron/West, v. 46, p. 6-8.

Bird, P., 1979, Continental delamination and the Colorado Plateau: Journal of Geophysical Research, v. 84, p. 7561-7571.

Burchfiel, B.C., Hodges, K.V., and Royden, L.H., 1987, Geology of Panamint Valley - Saline Valley pull-apart system, California: Palinspastic evidence for low-angle geometry of a Neogene range-bounding fault: Journal of Geophysical Research, v. 92, p. 10422-10426.

Chung, S.-L., Lo, C.-H., Lee, T.-Y., Yuquan, Z., Yingwen, X., Xianhua, L., Wang, K.-L., and Wang, P.-L., 1998, Diachronous uplift of the Tibet Plateau starting 40 Myr ago: Nature, v. 394, p. 769-773.

Curry, J.R., and Moore, D.G., 1984, Geologic history of the mouth of the Gulf of California, *in* Crouch, J.K., and Bachman, S.B., eds., Tectonics and sedimentation along the California margin: Pacific Section, Society of Economic Paleontologists and Mineralogists, v. 38, p. 17-36.

Ducea, M., and Saleeby, J., 1998, A case for delamination of the deep batholithic crust beneath the Sierra Nevada, California: International Geology Review, v. 40, p. 78-93.

Duffield, W. A., Bacon, C. R., and Dalrymple, G. B., 1980, Late Cenozoic volcanism, geochronology, and structure of the Coso Range, Inyo County, California: Journal of Geophysical Research, v. 85, p. 2381-2404.

Dumitru, T. A., 1990, Subnormal Cenozoic geothermal gradients in the extinct Sierra Nevada magmatic arc: Consequences of Laramide and post-Laramide shallow-angle subduction: Journal of Geophysical Research, v. 95, p. 4925-4941.

Dumitru, T. A., Gans, P. B., Foster, D. A., and Miller, E. L., 1991, Refrigeration of the western Cordilleran lithosphere during Laramide shallow-angle subduction: Geology, v. 19, p. 1145-1148.

England, P.C., and Houseman, G., 1989, Extension during continental convergence, with application to the Tibetan plateau: Journal of Geophysical Research, v. 94, p. 17561-17579.

Farmer, G. L., Glazner, A. F., and Manley, C. R., 2002, Did lithospheric delamination trigger late Cenozoic potassic volcanism in the southern Sierra Nevada, California?: Geological Society of America Bulletin, v. 114, p. 754–768.

Feldstein, S.N., and Lange, R.A., 1999, Pliocene potassic magma from the Kings River region, Sierra Nevada, California: Evidence for melting of a subduction-modified mantle: Journal of Petrology, v. 40, p. 1301-1320.

Gill, J., 1981, Orogenic andesites and plate tectonics: New York, Springer-Verlag, 390 p.

Huber, N.K., 1981, Amount and timing of late Cenozoic uplift and tilt of the central Sierra Nevada, California -- Evidence from the upper San Joaquin River basin: U.S. Geological Survey Professional Paper 1197, 28 p.

Kay, R. W., and Kay, S. M., 1993, Delamination and delamination magmatism: Tectonophysics, v. 219, p. 177-189.

Kay, S.M., Coira, B., and Viramonte, J., 1994, Young mafic back arc volcanic rocks as indicators of continental lithospheric delamination beneath the Argentine Puna plateau, central Andes: Journal of Geophysical Research, v. 99, p. 24323-24339.

Lueddecke, S.B., Pinter, N., and Gans, P., 1998, Plio-Pleistocene ash falls, sedimentation, and range-front faulting along the White-Inyo Mountains front, California: Journal of Geology, v. 106, p. 511-522.

Manley, C. R., Glazner, A. F., and Farmer, G. L., 2000, Timing of volcanism in the Sierra Nevada of California: evidence for Pliocene delamination of the batholithic root?: Geology, v. 28, p. 811-814.

McKenna, L.W., and Hodges, K.V., 1990, Constraints on the kinematics and timing of late Miocene-recent extension between the Panamint and Black Mountains, southeastern California, in Wernicke, B.P., ed., Basin and Range extensional tectonics near the latitude of Las Vegas, Nevada: Geological Society of America Memoir 176, p. 363-376.

Moore, J.G., and Dodge, F.C.W., 1980, Late Cenozoic volcanic rocks of the southern Sierra Nevada, California: I. Geology and petrology: Geological Society of America Bulletin, Part II, v. 91, p. 1995-2038.

Moore, J. G., and Nockleberg, W. J., 1991, Geologic map of the Tehipite Dome Quadrangle, Fresno County, California: U.S. Geological Survey map GQ-1676.

Page, B.M., and Brocher, T.M., 1993, Thrusting of the central California margin over the edge of the Pacific plate during the transform regime: Geology, v. 21, p. 635-638.

Ruppert, S., Fliedner, M. M., and Zandt, G., 1998, Thin crust and active upper mantle beneath the southern Sierra Nevada in the western United States: Tectonophysics, v. 286, p. 237-252.

Turner, S., Hawkesworth, C., Liu, J., Rogers, N., Kelley, S., and van Calsteren, P., 1993, Timing of Tibetan uplift constrained by analysis of volcanic rocks: Nature, v. 364, p. 50-53.

Van Kooten, G.K., 1980, Mineralogy, petrology, and geochemistry of an ultrapotassic basaltic suite, central Sierra Nevada, California, USA: Journal of Petrology, v. 21, p. 651-684.

Wernicke, B., and Snow, J.K., 1998, Cenozoic tectonism in the central Basin and Range: Motion of the Sierran-Great Valley block: International Geology Review, v. 40, p. 403-410.

Wernicke, B., Clayton, R., Ducea, M., Jones, C. H., Park, S., Ruppert, S., Saleeby, J., Snow, J. K., Squires, L., Fliedner, M., Jiracek, G., Keller, R., Klemperer, S., Luetgart, J., Malin, P., Miller, K., Mooney, W., Oliver, H., Phinney, R., 1996, Origin of high mountains in the continents: The southern Sierra Nevada: Science, v. 271, p. 190-193.

APPENDIX 6: LATE CENOZOIC EVOLUTION OF SOUTHERN SIERRA NEVADA TOPOGRAPHY FROM COSMOGENIC DATING OF CAVE SEDIMENTS

Greg M. Stock *University of California, Santa Cruz, Santa Cruz, CA 95060 gstock@es.ucsc.edu*

Robert S. Anderson *Institute of Artic and Alpine Research, University of Colorado, Boulder, CO 80309-0450 andersrs@colorado.edu*

Robert C. Finkel *Lawrence Livermore National Laboratory, Livermore, California 94550 finkel1@llnl.gov*

INTRODUCTION

As discussed in Appendix 3, numerous caves dot the southern Sierra Nevada landscape. These caves have formed in narrow marble lenses contained within the fragmented metamorphic belt that flanks the western edge of the Sierra Nevada Batholith. Virtually all of the westward flowing rivers in the Sierra Nevada flow across this belt, carving narrow gorges through the marble units. Many of these gorges contain caves preserved in the steep canyon walls that may be considered analogous to strath terraces. Caves therefore provide a means of determining rates of river in the central and southern parts of the range where late Cenozoic volcanic deposits are absent from the landscape. They also provide additional constraints on the amount of local relief (the vertical distance between canyon bottoms and adjacent canyon rims) present when the caves formed. Finally, the cave-derived incision rates can be compared with measured erosion rates of the interfluve surfaces to clarify the history of Quaternary relief production.

BURIAL DATING AND RATES OF RIVER INCISION

We dated 15 sediment samples from 10 caves in five Sierra Nevada river canyons along a transect delineated by the positions of caves within the metamorphic belt (Fig. 6-1). We determined cave ages using cosmogenic nuclide burial dating (Granger and Muzikar, 2001) of predominantly granitic bedload sediment (Stock et al., in review). We isolated ^{26}Al and ^{10}Be using the techniques of Granger et al. (2001) and measured ^{26}Al and ^{10}Be ratios by accelerator mass spectrometry at Lawrence Livermore National Laboratory.

Cave sediment burial ages range from 0.3 to 2.7 Myr (Fig. 6-2; Table 6-1). These ages provide late Pliocene and Quaternary incision rates for Sierra Nevada canyons that previously lacked estimates of incision, particularly the Kings and Kaweah river canyons. Importantly, the caves also provide detail not resolvable in previous studies. Figure 6-2 shows that the rate of incision has not been steady of the past 2.7 Ma, either in any one drainage, or for the range as a whole. Rather, incision appears to have been rapid from 2.7 to approximately 1.5 Ma, and has since slowed considerably. In the South Fork Kings (Fig. 6-4) and Yucca Creek (Fig 3-2B), tiered caves in the canyon walls reveal that high incision rates of 0.2 mm yr^{-1} from 2.7 to1.5 Ma markedly decline to 0.02 mm yr^{-1} thereafter (Fig. 6-2). In all other canyons, caves younger than 2 Ma also show trends toward low incision rates of 0.02 to 0.05 mm yr^{-1}, considerably lower than the range-wide long-term rate (Wakabayashi and Sawyer, 2001).

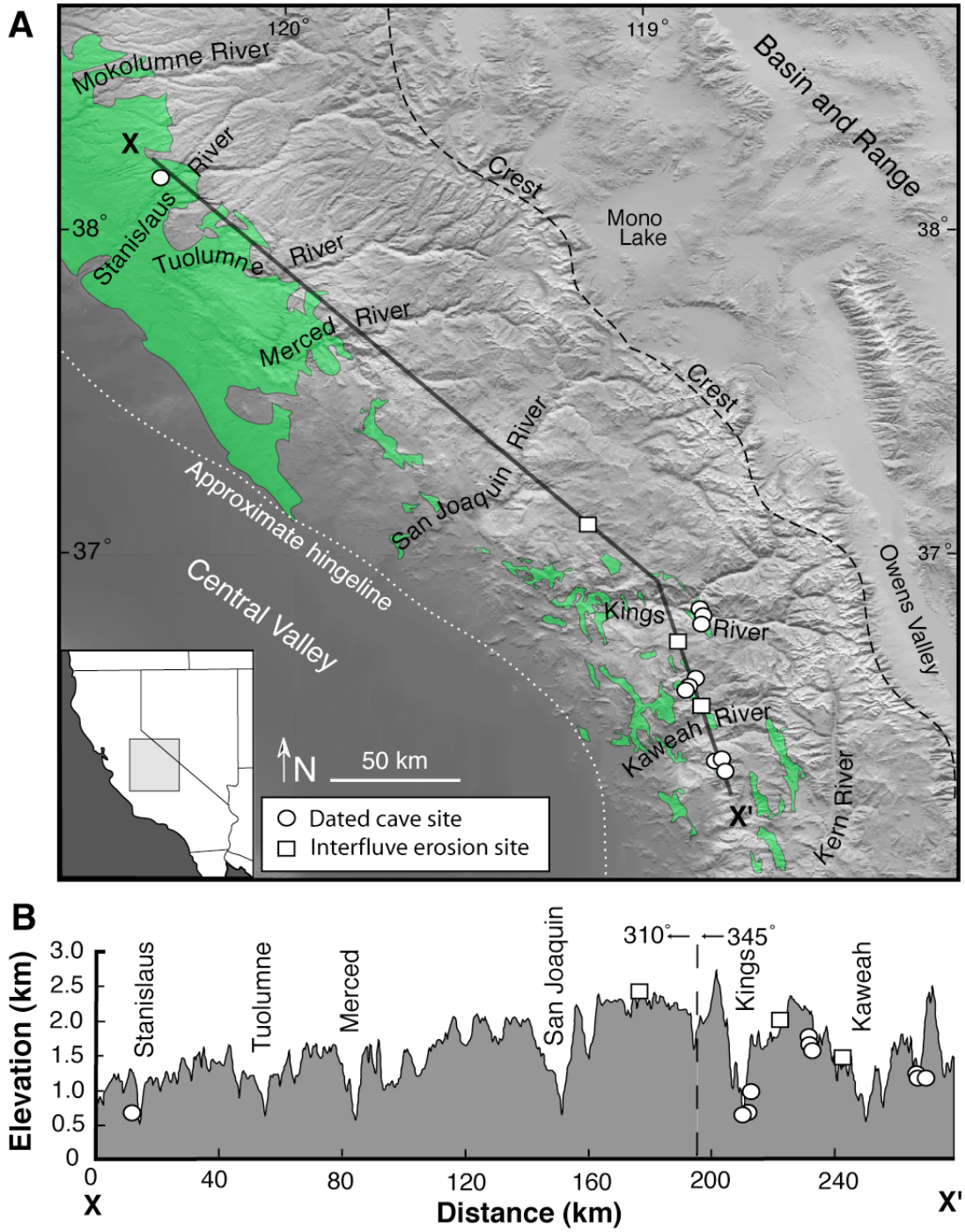

Figure 6-1. (A). Geologic and topographic setting of the central and southern Sierra Nevada. The Sierra Nevada is a west-tilted block with a relatively uniform western slope and a steep normal-faulted escarpment east of the crest. The highly fragmented Paleozoic and Mesozoic age metamorphic belt containing cave-bearing marble (shown in green) bounds predominantly Cretaceous age granitic rocks of the Sierra Nevada Batholith. The thick dark line X-X' delineates the study transect, which is dictated by cave locations. A lack of marble and suitable caves between the Tuolumne and San Joaquin rivers limits incision estimates in this region. **(B)** Topographic profile along transect X-X'. Mean elevation and local relief increase systematically south of the Stanislaus River, reaching a maximum in the vicinity of the Kings River.

Table 6-1. Cosmogenic nuclide data, burial ages, pre-burial erosion rates, and river incision rates from Sierra Nevada caves

Cave	River	Elev. (m)*	^{26}Al (10^4 atmg^{-1})	^{10}Be (10^4 atmg^{-1})	^{26}Al/^{10}Be	Burial age (Ma)†	Pre-burial erosion (mmyr^{-1})†‡	Incision (mmyr^{-1})
Crystal Stanislaus	Middle Fork Stanislaus	92 ± 5	26.56 ± 0.98	10.28 ± 0.21	2.59 ± 0.11	1.63 ± 0.08 (0.16)	0.046 ± 0.003 (0.010)	0.058
Bat	South Fork Kings	395 ± 2	11.15 ± 0.93	6.64 ± 0.16	1.48 ± 0.16	2.70 ± 0.21 (0.38)	0.079 ± 0.006 (0.016)	0.271
Boyden	South Fork Kings	42.5 ± 1	36.41 ± 1.36	12.43 ± 0.30	2.93 ± 0.13	1.40 ± 0.08 (0.15)	0.078 ± 0.005 (0.017)	0.021
Bear	South Fork Kings	8 ± 1	56.24 ± 2.61	10.92 ± 0.28	5.15 ± 0.22	0.32 ± 0.10 (0.18)	0.163 ± 0.012 (0.035)	0.023
Weis Raum	Yucca Creek	212 ± 2	9.46 ± 0.75	5.50 ± 0.12	1.72 ± 0.14	2.42 ± 0.16 (0.28)	0.055 ± 0.005 (0.012)	0.115
Hurricane Crawl	Yucca Creek	39.5 ± 1	35.23 ± 1.93	9.44 ± 0.24	3.73 ± 0.23	0.93 ± 0.12 (0.24)	0.064 ± 0.005 (0.014)	0.042
Crystal (Bear Den)	Yucca Creek	58 ± 1	97.53 ± 4.10	29.81 ± 0.70	3.27 ± 0.16	1.17 ± 0.09 (0.16)	0.021 ± 0.001 (0.005)	0.179
Crystal (Phosph. Room)	Cascade Creek	36.5 ± 1	311.9 ± 8.7	91.8 ± 2.6	3.39 ± 0.14	1.05 ± 0.08 (0.15)	0.007 ± 0.0004 (0.001)	0.108
Crystal (Marble Hall)	Cascade Creek	22.5 ± 1	79.17 ± 3.41	20.47 ± 0.49	3.87 ± 0.19	0.86 ± 0.09 (0.16)	0.035 ± 0.002 (0.007)	0.046
Crystal (Junction Room)	Cascade Creek	8.5 ± 1	107.2 ± 3.5	23.79 ± 0.56	4.51 ± 0.18	0.56 ± 0.08 (0.15)	0.034 ± 0.003 (0.009)	0.015
Clough	South Fork Kaweah	53.5 ± 2	7.33 ± 0.61	2.09 ± 0.07	3.51 ± 0.31	1.06 ± 0.17 (0.30)	0.354 ± 0.026 (0.075)	0.050
New	South Fork Kaweah	34 ± 2	54.44 ± 2.44	13.85 ± 0.33	3.93 ± 0.20	0.83 ± 0.10 (0.18)	0.059 ± 0.004 (0.013)	0.040
Soldiers (Entrance passage)	South Fork Kaweah	83 ± 2	50.24 ± 3.24	15.94 ± 0.38	3.15 ± 0.22	1.25 ± 0.13 (0.20)	0.038 ± 0.003 (0.008)	0.155
Soldeirs (Waiting Room)	South Fork Kaweah	41 ± 2	71.36 ± 2.97	19.63 ± 0.49	3.64 ± 0.18	0.98 ± 0.09 (0.17)	0.035 ± 0.002 (0.005)	0.049
Soldiers (Lower Corridor)	South Fork Kaweah	12.5 ± 2	73.93 ± 3.21	15.03 ± 0.36	4.92 ± 0.24	0.40 ± 0.09 (0.17)	0.059 ± (0.004) (0.010)	0.031
Modern river sediment	South Fork Kings	0 ± 0	22.68 ± 1.17	3.61 ± 0.07	6.26 ± 0.35	-0.06 ± 0.11 (0.21)	0.508 ± 0.038 (0.108)	—
Modern river sediment	Middle Fork Kaweah	0 ± 0	35.25 ± 1.65	5.90 ± 0.16	5.97 ± 0.32	0.04 ± 0.10 (0.18)	0.202 ± 0.015 (0.043)	—

* Reported elevations are sample elevations above local modern rivers. Where multiple caves exist in canyon walls, we use the elevation between caves to calculate incision rates; for example, the distance between Weis Raum Cave and Hurricane Crawl Cave (168.5 m) is used to calculate the incision rate for the period 2.42 to 0.93 Ma.

† We calculated burial ages and pre-burial erosion rates using equations in (Granger et al., 2001). Uncertainties represent one standard error measurement uncertainty, with systematic uncertainties in production rates (20%), ^{26}Al/^{10}Be production ratio (Stone, 2000) and radioactive decay constants (Norris et al., 1983; Hofmann et al., 1987) added in quadrature and shown in parentheses.

‡ Unlike the ^{26}Al/^{10}Be burial age, pre-burial erosion rates are sensitive to production rates that scale with altitude and latitude. We used sea level, high-latitude production rates for ^{26}Al and ^{10}Be of 31.1 and 5.1 atoms g^{-1} yr^{-1}, respectively (Stone, 2000), and corrected for latitude and altitude (Dunai, 2000). Because the caves draw sediment from drainage basins with hundreds to thousands of meters of local relief, and because we have no knowledge of where within these basins sediment originated, we scaled production rates using the mean altitude of the modern basin upstream of the caves. Accounting for the possible range of source altitudes leads to additional total uncertainty in pre-burial erosion rates.

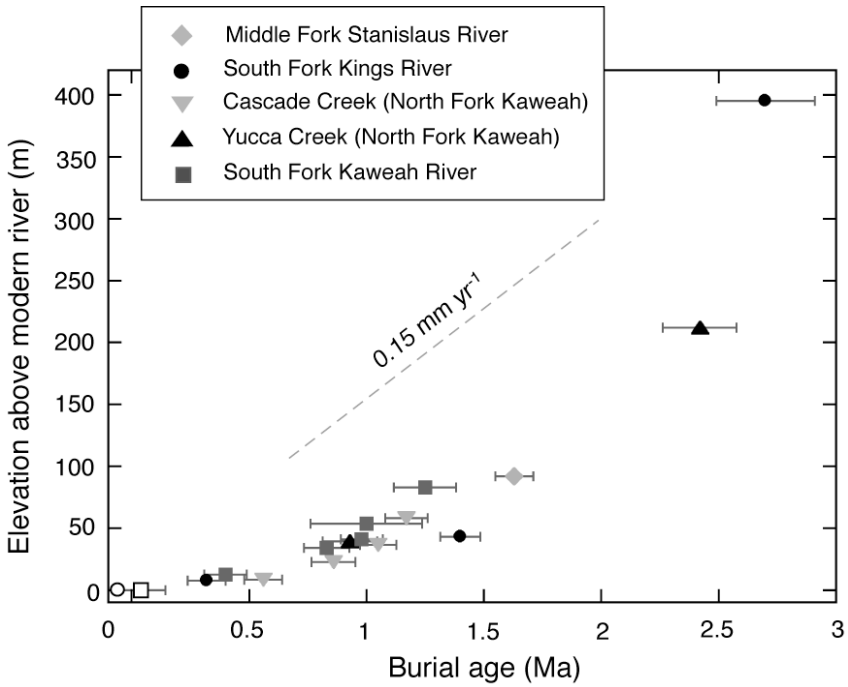

Figure 6-2. River incision history from Sierra Nevada caves. Granitic sediment from modern rivers, shown by open symbols, yield burial ages indistinguishable from zero, so we have no reason to expect an inherited burial signal in cave sediments. A change in incision rate at ~1.5-2 Ma is evident from caves across the study transect. Slope of dashed line denotes the 5 Ma average range-wide incision rate of 0.15 mm yr^{-1} (Wakabayashi and Sawyer, 2001). Error bars represent 1σ analytical uncertainty.

REPRODUCIBILITY OF BURIAL DATING RESULTS

A few key points in Fig 6-2 dictate much of the trend from high late Pliocene-early Quaternary incision rates to low late Quaternary rates. Therefore, we felt compelled to test the reproducibility of these ages, while at the same time testing the validity of the burial dating technique. We collected additional sediment samples from the two caves showing the largest analytical uncertainty (Bat and Clough caves; Fig 6-2) and ran multiple AMS targets from these additional samples. Internal (analytical variation) and external (geologic variation) burial ages for these samples agree within 30%, and all samples plot within error of each other (Fig. 6-3). Burial ages tend to cluster around those samples showing the lowest analytical error. These results demonstrate that burial ages are reproducible within analytical error, which is typically around 0.1 Myr.

Geologic evidence also leads us to believe that the cave ages are accurate. As expected, all burial ages are in correct stratigraphic order, i.e. cave passages high above modern river levels are older than those closer to the rivers. Furthermore, the long-term average incision rates of approximately 0.15 mm yr^{-1} deduced from cave ages are similar to those reported from northern and central Sierra Nevada rivers based on incision below the ~5 Ma Mehrten formation (Wakabayashi and Sawyer, 2001) (see dashed line, Fig 6-2). Furthermore, an incision rate of 0.15 mm yr^{-1} averaged over 2.7 Ma from the South Fork Kings canyon closely matches the 5 Myr average rate of 0.13 mm yr^{-1} from an equivalent upstream position in the San Joaquin canyon. Low cave-derived rates of incision in the late Quaternary must have been faster prior to this time to match the long-term rates derived from late Cenozoic volcanic deposits.

We conclude that the apparent trend toward decreasing river incision rates in the late Quaternary is not an artifact of either sampling protocol (see Appendix 3) or analyses, and is therefore likely real. Possible causes for this somewhat surprising result will be the topic of the next stop and are discussed in Appendix 7.

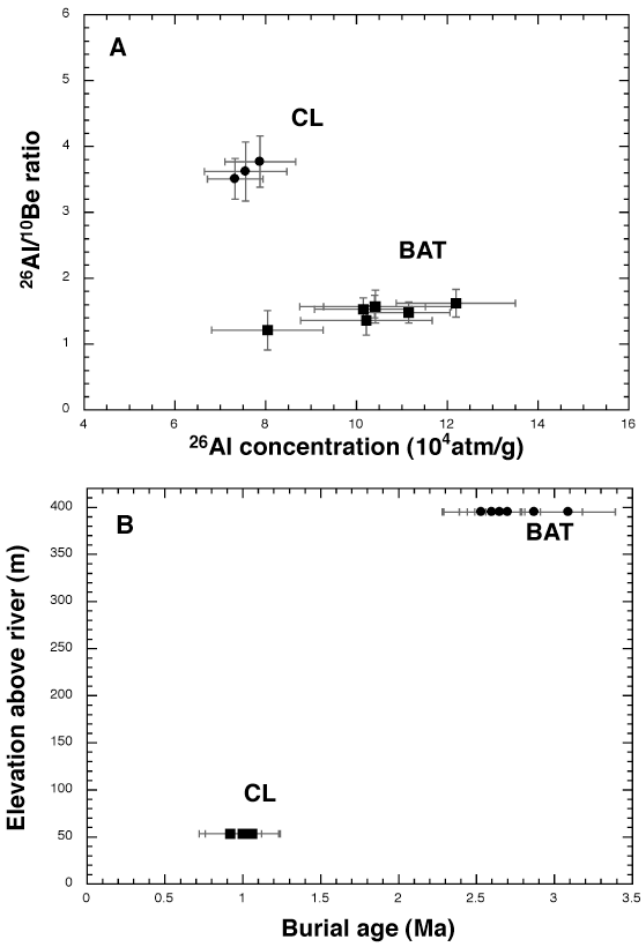

Figure 6-3. Internal (measured) and external (geologic) reproducibility results for the two cave samples showing the greatest uncertainty. BAT samples are from Bat Cave, CL samples are from Clough Cave. For Bat cave samples, six ^{26}Al and three ^{10}Be targets from two different sediment samples were analyzed. For Clough Cave samples, three ^{26}Al and two ^{10}Be targets from two different sediment samples were analyzed. (**A**) ^{26}Al/^{10}Be ratio vs. ^{26}Al concentration plot. ^{26}Al concentrations are expected to vary depending on pre-burial erosion rate experienced by the sediment, but the ^{26}Al/^{10}Be ratios for samples from the same cave should be consistent. Ratios vary by a factor of 1.5, and all samples plot within error of each other. Ratios from the two different sediment samples are indistinguishable within error. (**B**) Burial age vs. elevation above modern river level plot for the analyses shown in (A) (compare with results shown in Figure 6-2). Uncertainty in the BAT samples show that the true burial age could range between 2.3 and 3.4 Ma, but the most precise ^{26}Al/^{10}Be ratios yield ages of 2.6 to 2.8 Ma. CL samples could range in age from 0.7 to 1.3 Ma, but cluster at 1.0 Ma.

PALEOTOPOGRAPHY OF THE SOUTHERN SIERRA NEVADA

Dated caves in canyon walls provide snapshots of the Sierra Nevada landscape as it evolved toward its present form. For example, the depth of the South Fork Kings canyon prior to 2.7 Ma was ~1600 m, the distance from the highest dated cave to the adjacent north rim of the canyon near Wren Peak (Fig. 6-4). Caves in other Sierra Nevada canyons also show that substantial (400-1100 m) local relief was present when the caves formed (Table 6-2). This finding is in accord with previous work reporting relief in the southern Sierra Nevada prior to the late Pliocene (Dalrymple, 1964; Huber, 1981; Wakabayashi and Sawyer, 2001; House et al., 1998; 2001).

We do not know when rapid incision began at the cave sites, only that it had started by 2.7 Ma. Late Cenozoic rock uplift is an obvious driving mechanism for rapid river incision. If late Cenozoic rock uplift commenced at ~10 Ma (Huber, 1981), the maximum incision rates we document from the South Fork Kings River (0.27 mm yr^{-1}) can accommodate cutting of the entire South Fork Kings canyon prior to the decline in

rate we document at 1.5 Ma. On the other hand, if the uplift event is as young as 3.5 Ma (Manley et al., 2000; Farmer et al., 2002) or 5 Ma (Unruh, 1991; Wakabayashi and Sawyer, 2001), then very rapid incision (0.7 to 2 mm yr^{-1}, respectively) prior to 2.7 Ma must be invoked to produce the present local relief. Though such rapid rates are documented in a few of the most active mountain belts around the world (e.g., the Himalaya; Burbank et al., 1996), they are not seen in other estimates of Sierra Nevada incision rates based on 3-10 Ma volcanic deposits (Huber, 1981; Wakabayashi and Sawyer, 2001). If such rapid rates of incision are deemed unlikely, then only a small fraction of the local relief present in the South Fork Kings River canyon was produced in response to late Cenozoic uplift. Given the compelling evidence for 3-5 Ma uplift, many canyons in the southern Sierra Nevada likely displayed substantial (>1 km) relief prior to this time. Low river incision rates from the Eocene to Miocene (Wakabayashi and Sawyer, 2001) suggest that much of the present relief may well be relict from the late Cretaceous (House et al., 1998; 2001).

Table 6-2. Estimates of local paleorelief for southern Sierra Nevada river canyons

River	Oldest cave (Ma)	Relief prior to oldest cave (m)*
Middle Fork Stanislaus	1.63 ± 0.08	600
South Fork Kings	2.75 ± 0.21	1600
Cascade Creek (North Fork Kaweah)	1.17 ± 0.08	420
Yucca Creek (North Fork Kaweah)	2.42 ± 0.16	400
South Fork Kaweah	1.25 ± 0.13	1060

*** Local paleorelief is the distance from the oldest (and therefore highest) cave to the adjacent canyon rim. Interfluve erosion rates are low (order 10 m Myr^{-1}), suggesting that present rim elevations have changed little over millions of years relative to the total local relief. Estimates are approximate because rim elevations are not uniform – we chose the most representative rim elevation for these estimates.**

INTERFLUVE EROSION AND RELIEF PRODUCTION

Some researchers have posited that high local relief present in the late Cretaceous declined monotonically throughout the Cenozoic (House et al., 1998; 2001), implying no late Cenozoic rock uplift. Such a decrease in relief requires that interfluve erosion outpace river incision. On the other hand, late Cenozoic rock uplift would drive a pulse of incision that would likely increase local relief (defined here as the distance between canyon bottoms and adjacent canyon rims). In order to discriminate between these scenarios, incision rates from the canyons and erosion rates from the adjacent interfluves are needed. The caves provide river incision rates for the last 2.7 Myr. In order to constrain interfluve erosion rates, we measured concentrations of ^{26}Al and ^{10}Be in granitic rocks exposed along the study transect (Fig. 6-1). Cosmogenic nuclide concentrations may be used to calculate erosion of bare bedrock surfaces (e.g., Lal, 1991; Small et al., 1997; Bierman and Caffee, 2001). On average, we find that interfluve surfaces in the southern Sierra Nevada are eroding at 0.012 mm yr^{-1} averaged over ~75 kyr (Table 6-3), comparable to rates measured east of the Sierra Nevada crest and in other alpine environments over equivalent timescales (Small et al., 1997). Interfluve erosion rates are more than an order of magnitude lower than the late Pliocene to early Quaternary canyon incision rates derived from caves, and remain slightly less, by a factor of 2 to 3, than the late Quaternary incision rates.

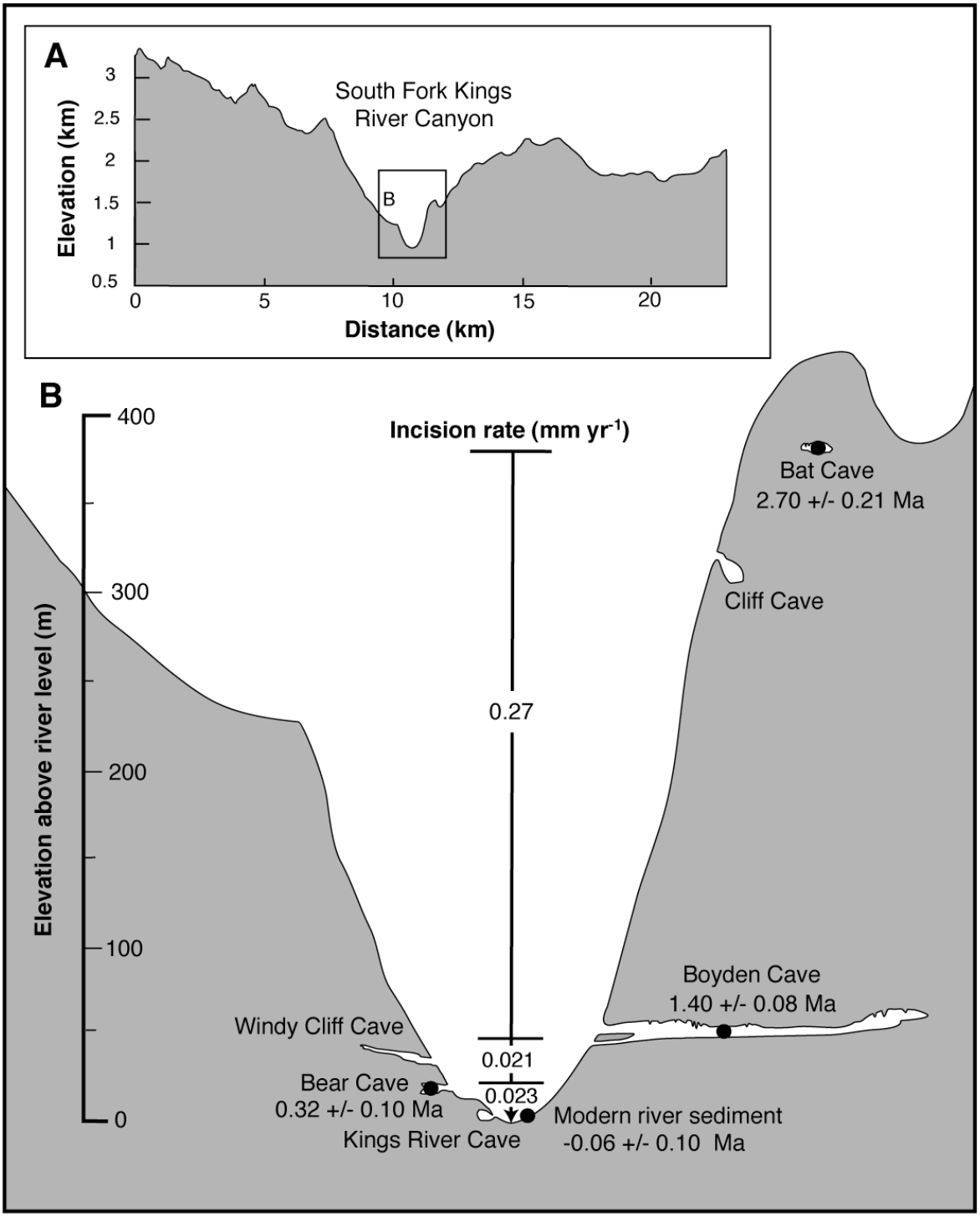

Figure 6-4. Cave-derived river incision rates in the South Fork Kings River canyon. **(A)** Topographic profile across the South Fork Kings River canyon in the vicinity of Boyden Cave. Note ~2 km local relief. **(B)** The inner gorge of the South Fork Kings River canyon, containing a suite of dated caves well preserved by the exceptionally steep canyon walls. These caves reveal an order of magnitude decline in incision rate toward the present. While the oldest cave demonstrates 400 m of canyon cutting in the last 2.7 Myr, the larger context shown in (A) reveals that this represents only ~20% of the present local relief.

We argue that erosion rates of these interfluve surfaces are roughly steady over millions of years. Our interfluve sample sites are far enough from the adjacent canyons that they are effectively decoupled from incision (Anderson, 2002); any change in erosion rate through time must therefore be driven by changes in the weathering climate. As our erosion rate measurements are averaged across glacial-interglacial transitions, they are likely representative of rates throughout the Quaternary. Furthermore, climatic effects on granitic weathering rates in the Sierra Nevada appear to be negligible (Riebe et al., 2001). Finally, preservation of 12-3.5 Ma volcanic flows on the broad Kings-San Joaquin interfluves suggest that these surfaces have not experienced significant erosion in the last few Myr. If this reasoning is correct, it appears that local relief along our study transect, already substantial in the middle Pliocene, was enhanced by rapid incision in the late Pliocene and early Quaternary. The inner gorges that characterize many southern Sierra Nevada river canyons probably formed during this time. Since then, local relief has increased only slowly, as incision outpaced interfluve erosion by factors of 2-4 (Stock et al., in review).

Table 6-3. Cosmogenic nuclide data, erosion rates, and exposure ages for interfluve surfaces

Sample	Elev. (m)	^{26}Al* (10^6 atm g^{-1})	^{10}Be* (10^6 atm g^{-1})	^{26}Al/^{10}Be	^{26}Al erosion† (mm yr^{-1})	^{10}Be erosion† (mm yr^{-1})	^{26}Al age† (kyr)	^{10}Be age† (kyr)
HR-1	1975	42.85 ± 1.58	8.12 ± 0.18	5.28 ± 0.23	0.014 ± 0.0029	0.013 ± 0.0026	41.7 ± 8.6	45.7 ± 9.3
BR-1	1948	143.14 ± 4.96	28.17 ± 0.59	5.08 ± 0.21	0.004 ± 0.0009	0.003 ± 0.0008	144.6 ± 31.5	163.2 ± 34.1
BVD-1	2294	38.74 ± 1.35	6.85 ± 0.19	5.66 ± 0.25	0.020 ± 0.0041	0.019 ± 0.0039	29.3 ± 6.0	30.7 ± 6.2
Mean					0.012 ± 0.0051	0.012 ± 0.0049	71.9 ± 33.2	79.9 ± 35.9

*We used ^{26}Al and ^{10}Be production rates of 31.1 and 5.1 atoms g^{-1} yr^{-1}, respectively (Stone, 2000), and corrected for latitude, altitude (Dunai, 2000) and topographic shielding (Dunne et al., 1999).
† Uncertainties in erosion rates and exposure ages are propagated from measurement uncertainty, plus systematic uncertainties in production rates (10%), attenuation coefficients, and radioactive decay constants (Norris et al., 1983; Hofmann et al., 1987).

IMPLICATIONS FOR LATE CENOZOIC UPLIFT MECHANISMS

Our findings help to clarify some of the proposed models of late Cenozoic uplift. Significant pre-Quaternary relief and low interfluve erosion rates place new limits on the amount of flexural isostatic compensation expected in response to late Cenozoic erosion. Within a range of realistic effective elastic thicknesses for the crust underlying the Sierra Nevada, it seems unlikely that late Cenozoic erosion alone is sufficient to drive all of the observed rock uplift inferred from tilted markers (Small and Anderson, 1995). This diminishes the contribution of late Cenozoic climate change on rock uplift, thereby strengthening the case for a tectonically-driven uplift mechanism. Although our cave data do not point directly to any particular tectonic mechanism, they are consistent with the expected landscape response to rock uplift incited by root delamination approximately 3 to 10 Ma (e.g., Ducea and Saleeby, 1996; 1998; Manley et al., 2000; Farmer et al., 2002). Whatever the driving mechanism, late Cenozoic rock uplift almost certainly caused an increase in the rate of river incision, inciting further rock uplift through the flexural isostatic compensation to this erosion. Thus, both tectonic and climatic mechanisms worked together to drive rock uplift in the Sierra Nevada over the last 3 to 10 Myr.

ACKNOWLEDGEMENTS

We thank Darryl Granger for initial training in cosmogenic nuclide separation techniques, and also for early encouragement of this work. Joel Despain and Steve Bumgardner provided field assistance and discussions. This paper benefited from a critical review by John Wakabayashi. This research was supported by grants from the National Science Foundation (EAR-0126253), the Institute of Geophysics and Planetary Physics, and the Geological Society of America.

REFERENCES CITED

Anderson, R. S., 2002, Modeling the tor-dotted crests, bedrock edges, and parabolic profiles of high alpine surfaces of the Wind River Range, Wyoming: Geomorphology, v. 46, p. 35-58.

Bierman, P. R., and Caffee, M., 2002, Cosmogenic exposure and erosion history of Australian bedrock landforms: Geological Society of America Bulletin, v. 114, p. 787-803.

Burbank, D.W., Leland, J., Fielding, E., Anderson, R.S., Brozovic, N., Reid, M.R., and Duncan, C., 1996, Bedrock incision, rock uplift, and threshold hillslopes in the northwestern Himalayas: Nature, v. 379, p. 505-510.

Dalrymple, G. B., 1964, Cenozoic chronology of the Sierra Nevada, California: University of California Publications in Geological Sciences, v. 47, p. 1-41.

Ducea, M. N., and Saleeby, J. B., 1996, Buoyancy sources for a large, unrooted mountain range, the Sierra Nevada, California: evidence from xenolith thermobarometry: Journal of Geophysical Research, v. 101, p. 8229-8244.

Ducea, M. N., and Saleeby, J. B., 1998, A case for delamination of the deep batholithic crust beneath the Sierra Nevada: International Geology Review, v. 40, p. 78-93.

Dunai, T.,J., 2000, Scaling factors for production rates of in situ produced cosmogenic nuclides: a critical reevaluation: Earth and Planetary Science Letters, v. 176, p. 157-169.

Dunne, J., Elmore, D., and Muzikar, P., 1999, Scaling factors for the rates of production of cosmogenic nuclides for geometric shielding and attenuation at depth on sloped surfaces: Geomorphology, v. 27, p 3-11

Farmer, G. L., Glazner, A. F., Manley, C. R., 2002, Did lithospheric delamination trigger late Cenozoic potassic volcanism in the southern Sierra Nevada, California?: Geological Society of America Bulletin, v. 114, p. 754-768.

Granger, D. E., and Muzikar, P. F., 2001, Dating sediment burial with in situ-produced cosmogenic nuclides: theory, techniques, and limitations: Earth and Planetary Science Letters, v. 188, p. 269-281.

House, M. A., Wernicke, B. P., and Farley, K. A., 1998, Dating topography of the Sierra Nevada, California, using apatite (U-Th)/He ages: Nature, v. 396, p. 66-69.

House, M. A., Wernicke, B. P., and Farley, K. A., 2001, Paleo-geomorphology of the Sierra Nevada, California, from (U-Th)/He ages in apatite: American Journal of Science, v. 301, p. 77-102.

Huber, N. K., 1981, Amount and timing of Late Cenozoic uplift and tilt of the central Sierra Nevada, California – evidence from the upper San Joaquin river basin: U.S. Geological Survey Professional Paper 1197, 28 p.

Lal, D., 1991, Cosmic ray labeling of erosion surfaces: In situ nuclide production rates and erosion models: Earth and Planetary Science Letters, v. 104, p. 424-439.

Manley, C. R., Glazner, A. F., Farmer, G. L., 2000, Timing of volcanism in the Sierra Nevada of California: Evidence for Pliocene delamination of the batholithic root? Geology, v. 28, p. 811-814.

Riebe, C. S., Kirchner, J.W., Granger, D. E., and Finkel, R. C., 2001, Minimal climatic control of erosion rates in the Sierra Nevada, California: Geology, v. 29, p. 447-450.

Small, E. E., and Anderson, R. S., 1995, Geomorphically driven Late Cenozoic rock uplift in the Sierra Nevada, California: Science, v. 270, p. 277-280.

Small, E. E., Anderson, R. S., Repka, J. L., and Finkel, R. C., 1997, Erosion rates of alpine bedrock summit surfaces deduced from in situ ^{10}Be and ^{26}Al: Earth and Planetary Science Letters, v. 150, p. 413-425.

Stock, G. M., Anderson, R. S., and Finkel, R. C., in review, Pace of landscape evolution in the Sierra Nevada, California, revealed by cosmogenic dating of cave sediments

Stone, J. O., 2000, Air pressure and cosmogenic isotope production: Journal of Geophysical Research, v. 105, p. 23,753-23,759

Unruh, J. R., 1991, The uplift of the Sierra Nevada and implications for Late Cenozoic epeirogeny in the western Cordillera: Geological Society of America Bulletin, v. 103, p. 1395-1404.

Wakabayashi, J., and Sawyer, T. L., 2001, Stream incision, tectonics, uplift, and evolution of topography of the Sierra Nevada, California: Journal of Geology, v. 109, p. 539-562.

APPENDIX 7: CAVE-DERIVED RIVER INCISION RATES FROM THE SOUTH FORK KINGS RIVER: COMPLEX RIVER RESPONSE TO TECTONIC AND CLIMATIC FORCING

Greg M. Stock *University of California, Santa Cruz, Santa Cruz, CA 95060 gstock@es.ucsc.edu*
Robert S. Anderson *Institute of Artic and Alpine Research, University of Colorado, Boulder, CO 80309-0450 andersrs@colorado.edu*

INTRODUCTION

The inner gorge of the South Fork of the Kings River near Boyden Cave presents one of the most interesting sites for determining and evaluating cave-derived rates of river incision. The South Fork Kings River canyon is one of the deepest canyons in the Sierra Nevada, and has been implicated as having high local relief since the late Cretaceous (House et al., 1998). The South Fork Kings River has carved a dramatic inner gorge through vertically-bedded marble within the Boyden Cave metamorphic pendant. Many caves are preserved within the exceptionally steep walls of this gorge (Fig. 7-1). Cosmogenic nuclide burial ages for fluvial sediment within these caves show an intriguing pattern of river incision for the last 2.7 Myr.

TEMPORAL PATTERNS OF RIVER INCISION

Cave sediment burial ages for the South Fork Kings River gorge range from 0.3 to 2.7 Ma and, as expected, increase with elevation above the present river level (Fig. 6-2; Table 6-1). Granitic sediment collected from the modern river just downstream of the bridge over the South Fork Kings River at Boyden Cave yields a burial age indistinguishable from zero, indicating that there is no inherited burial signal in sediment entering the caves. The long-term incision rate of the South Fork Kings River (averaged over 2.7 Myr) is 0.15 mm yr^{-1}, identical to the long-term average rate for northern and central Sierra Nevada rivers based on incision through the ~5 Ma Mehrten Formation (Wakabayashi and Sawyer, 2001). Furthermore, this rate closely matches a 5 Myr average rate of 0.13 mm yr^{-1} from an equivalent upstream position in the San Joaquin canyon (calculated from Huber, 1981; Wakabayashi and Sawyer, 2001). Similarity among incision rates derived from different sources indicates that the cave sediment burial ages are reliable recorders of river incision.

However, cave-derived incision rates provide additional detail on the history of the incision that was not resolvable in previous studies. Caves in the South Fork Kings River gorge reveal relatively high rates of incision from 2.7 to ~1.5 Ma, followed by reduced rates from ~1.5 Ma to the present. Similar patterns are found in tributaries of the Kaweah River. In three other canyons, caves younger than 1.6 Ma consistently yield low incision rates of 0.02 to 0.05 mm yr^{-1} (Fig. 7-1). Cave-derived incision rates for the last 1.5 Myr are therefore considerably lower than the range-wide long-term rate of 0.15 mm yr^{-1} (Wakabayashi and Sawyer, 2001), suggesting that river incision in the Sierra Nevada was rapid in the Pliocene and early Quaternary, but has slowed considerably in the late Quaternary.

Figure 7-1. Looking out of a newly discovered cave entrance high in a canyon wall above the South Fork Kings River. A 180 m high wall was scaled to reach this cave. Photograph by Greg Stock.

The temporal pattern of incision derived from the caves could reflect any combination of 1) climate history that drives changes in river discharge and sediment supply, 2) a transient erosional response to late Cenozoic rock uplift, and 3) evolution of the rock uplift pattern itself. River incision into bedrock is commonly taken to be proportional to stream power, the product of river slope and river discharge (e.g., Whipple and Tucker, 1999). It is commonly presented as the stream-power equation:

$$\frac{dz}{dt} = kQ\frac{dz}{dx} \tag{7-1}$$

where dz/dt is river incision, dz/dx is river slope, Q is river discharge, and k is a constant that scales the erosional efficiency. Both tectonically induced changes in slope and climatically induced changes in discharge can change stream power and incite changes in river incision rate. Though this notion is fairly intuitive, positive feedbacks linking uplift and climate ensure that river response to uplift is complex. For example, surface uplift of the Sierra Nevada crest would increase orographic precipitation on the western slope (Roe et al., 2002), increasing river discharge, and accelerating bedrock incision. Accelerated incision would in turn drive further rock uplift and tilting through the flexural-isostatic compensation of this erosional unloading (Fig. 7-2A).

LANDSCAPE EVOLUTION MODELING

In order to examine the complex response of the South Fork Kings River to perturbations in uplift and climate, we constructed numerical models of river profile

evolution (Stock et al., in review). Preliminary numerical models incorporating the feedbacks outlined above indicate that 1-2 km of crestal rock uplift initiates a wave of erosion that begins at the mountain front and propagates upriver (Fig. 7-2C). Discrete points along the profile, such as those marked by caves, experience a period of rapid incision as the knick zone sweeps by, followed by a return to slower incision (Fig. 7-2C inset). As caves occur only in the narrow metamorphic belt, which is oriented perpendicular to the river, they tightly constrain the timing of the passage of this knick zone. The time after initiation of uplift at which the knick zone passes the caves depends on the upstream distance of the caves and the lithology-dependent efficiency of the river incision process. While the temporal pattern of late Pliocene and Quaternary incision as recorded by the caves in the South Fork Kings Canyon is well modeled as a transient response to tectonic tilting, the modeled late Quaternary incision rates are higher than those we have documented from the caves. This suggests that an additional mechanism acts to inhibit late Quaternary incision.

One possible mechanism may be the initiation of major global glaciation ~2 to 3 Ma (Fig. 7-2B), which undoubtedly influenced Sierra Nevada rivers. During periods of glaciation, glacial erosion in the headwaters sent pulses of sediment down the fluvial system, mantling the riverbeds (e.g., Whipple and Tucker, 2002; Pratt et al., 2002). Studies of alluvial fan deposits in the San Joaquin Valley indicate that rapid aggradation occurred in response to higher sediment supply during glacial maxima (Marchand and Allwardt, 1981; Lettis, 1982; Weissmann et al., 2002; see Appendix 2). Within the Sierra Nevada river canyons, such aggradation would effectively armor the riverbeds against incision. Excavation of sediment during interglacial times (Hancock and Anderson, 2001) would be required before bedrock incision could resume. The gradual onset of Pliocene-Pleistocene glacial cycles might therefore be expected to reduce long-term bedrock incision rates. In addition, the transition at ~1 Ma from predominantly 41 kyr glacial cycles to predominantly 100 kyr cycles (Clark et al., 1999) was associated with an increase in the magnitude of glaciations (Fig 7-2B). This transition likely represents the onset of major glaciation in the Sierra Nevada. Larger glaciers after ~1 Ma would presumably have contributed more sediment to the canyons, further reducing the incision rate. Incorporating in our model a progressive increase in bed armoring during the Quaternary can explain the low incision rates we derived from cave ages (Fig. 7-2C inset). Our preliminary model results therefore suggest that the present river profiles and the profile evolution recorded by the caves reflect both a transient response to late Cenozoic uplift and sediment armoring of the bed during Quaternary glaciations. Further modeling work is underway, but, not surprisingly, it appears that both tectonic and climatic events have worked in concert to drive the late Cenozoic evolution of the Sierra Nevada landscape.

CENOZOIC LANDSCAPE EVOLUTION IN THE SIERRA NEVADA

The detailed 2.7 Myr incision history revealed by the caves, along with the measured interfluve erosion rates, serve to link many of the previous conceptual models of Cenozoic topographic evolution. What follows is our attempt to incorporate the new incision data within the framework of previously published data to come up with a semi-coherent view of late Cenozoic landscape evolution in the southern Sierra Nevada.

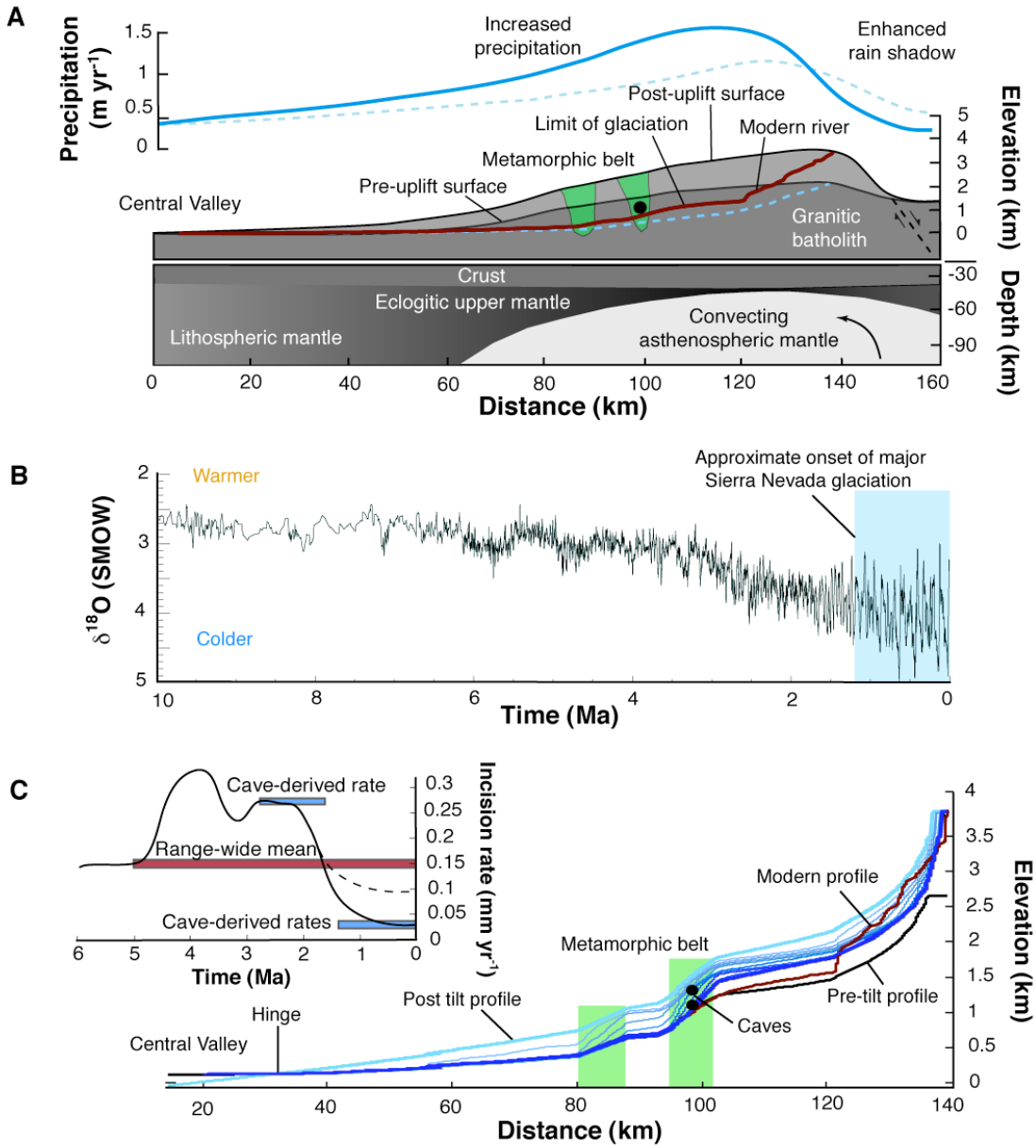

Figure 7-2. Response of the South Fork Kings River to late Cenozoic tectonic and climatic events. **(A)** Conceptual model of late Cenozoic uplift. Pre-uplift surface and river profile are uplifted 1.5 km by westward tilting, steepening river gradients. Surface uplift increases orographic precipitation on the western slope of the range and enhances rain shadow to the east. Thin crust beneath the range crest (Wernicke et al., 1996) likely reflects delamination of the batholithic root (Ducea and Saleeby, 1998). **(B)** Global deep-sea oxygen isotope record for the late Cenozoic showing pronounced global cooling (Zachos et al., 2001). Higher amplitude glacial cycles beginning ~1 Ma likely mark the onset of major Sierra Nevada glaciation. **(C)** Example of numerical simulation of river response to tilting and glaciation. A steady river profile with steps corresponding to quartzite in two metamorphic belts is subjected to ~1.5 km of crestal uplift. 1 Myr profiles show that over the next 9 Myr a wave of rapid incision begins at the hinge line and propagates up the profile. Inset shows the last 6 Myr of incision history at the cave site; a wave of rapid incision passes between ~5 and 2 Ma, followed by a return to low pre-uplift rates (dashed curve after 2 Ma). Further reduction in late Quaternary rates (solid curve after 2 Ma) reflects sediment mantling of the bed associated with large glaciers in the headwaters; this is mimicked in the model by reduction in incision efficiency that follows $\delta^{18}O$ curve of (B). Final modeled river profile (dark blue) fits the modern profile (red) to just upstream of the cave site, above which glacial erosion has dominated the last few Myr.

The Sierra Nevada grew during arc volcanism in the Cretaceous (e.g., Bateman and Wahrhaftig, 1966). As volcanism waned in the late Cretaceous, erosion reigned and the range began to decay. Rapid erosion in the early Cenozoic led to rapid sedimentation in the adjacent Central Valley during this time (Wakabayashi and Sawyer, 2001). As the range decayed, significant canyons developed, and the southern Sierra Nevada likely displayed substantial (>1.5 km) local relief during this time (Wakabayashi and Sawyer, 2001; House et al., 1998; 2001). Low interfluve erosion rates likely served to preserve much of the early Cenozoic topography. Remnant high-elevation topography persisted in this region well into the Miocene, casting a rain shadow into the western Basin and Range (Poage and Chamberlain, 2002).

Following a long period of quiescence during the early and mid-Cenozoic, marked by negligible Eocene-Miocene incision and Central Valley sedimentation (Wakabayashi and Sawyer, 2001), the dense batholithic root beneath the eastern Sierra Nevada fell away around 3-10 Ma (Ducea and Saleeby, 1998; Manley et al., 2000; Farmer et al., 2002). This geophysical event incited rock and surface uplift (Huber, 1981; Unruh, 1991; Wakabayashi and Sawyer, 2001) in a pattern that steepened the gradients of the westward-flowing rivers. These rivers responded in a wave of incision that propagated up the river profile, beginning at the hinge line along the eastern edge of the Central Valley. River incision in the cave-bearing marble belt reached its maximum rate as the wave of rapid incision passed roughly 5-2 Ma. In the southern Sierra Nevada, local relief increased during this time as river incision outpaced interfluve erosion. Following passage of the knick zone, incision rates slowed considerably. As major late Quaternary glaciers etched the high Sierra Nevada, the sediment they produced mantled the riverbeds, further reducing incision rates. We hypothesize that at present most Sierra Nevada rivers are in the process of transporting sediment delivered to them during the Last Glacial Maximum, and little bedrock incision is taking place.

REFERENCES CITED

Bateman, P.C., and Wahrhaftig, C. 1966, Geology of the Sierra Nevada, *In* Bailey, E.H., ed., Geology of northern California, California Division of Mines and Geology Bulletin 190, p. 107-172.

Clark, P. U., Alley, R. B., and Pollard, D., 1999, Northern Hemisphere ice-sheet influences on global climate change: Science, v. 286, p. 1104-1111.

Ducea, M. N., and Saleeby, J. B., 1998, A case for delamination of the deep batholithic crust beneath the Sierra Nevada: International Geology Review, v. 40, p. 78-93.

Farmer, G. L., Glazner, A. F., Manley, C. R., 2002, Did lithospheric delamination trigger late Cenozoic potassic volcanism in the southern Sierra Nevada, California?: Geological Society of America Bulletin, v. 114, p. 754-768.

House, M. A., Wernicke, B. P., and Farley, K. A., 1998, Dating topography of the Sierra Nevada, California, using apatite (U-Th)/He ages: Nature, v. 396, p. 66-69.

House, M. A., Wernicke, B. P., and Farley, K. A., 2001, Paleo-geomorphology of the Sierra Nevada, California, from (U-Th)/He ages in apatite: American Journal of Science, v. 301, p. 77-102.

Hancock, G. S., and Anderson, R. S., 2002, Numerical modeling of fluvial strath-terrace formation in response to oscillating climate: Geological Society of America Bulletin, v. 114, p. 1131-1142.

Huber, N. K., 1981, Amount and timing of Late Cenozoic uplift and tilt of the central Sierra Nevada, California – evidence from the upper San Joaquin river basin: U.S. Geological Survey Professional Paper 1197, 28 p.

Lettis, W. R., 1982, Late Cenozoic stratigraphy and structure of the western margin of the central San Joaquin Valley, California. U. S. Geological Survey Open-File Report 82-526, 203p.

Marchand, D.E., and Allwardt, A., 1981, Late Cenozoic Stratigraphic Units, Northeastern San Joaquin Valley, California: U. S. Geological Survey, Bulletin 1470, 70 p.

Pratt, B., Burbank, D. W., Heimsath, A., and Ojha, T., 2002, Impulsive alluviation during early Holocene strengthened monsoons, central Nepal Himalaya: Geology, v. 30, p. 911-914.

Roe, G. H., Montgomery, D. R., and Hallet, B., 2002, Effects of orographic precipitation variations on the concavity of steady-state river profiles: Geology, v. 30, p. 143-146.

Stock, G. M., Anderson, R. S., and Finkel, R. C., in review, Pace of landscape evolution in the Sierra Nevada, California, revealed by cosmogenic dating of cave sediments

Wakabayashi, J., and Sawyer, T. L., 2001, Stream incision, tectonics, uplift, and evolution of topography of the Sierra Nevada, California: Journal of Geology, v. 109, p. 539-562.

Weissmann, G. S., Mount, J. F., and Fogg, G. E., 2002, Glacially driven cycles in accumulation space and sequence stratigraphy of a stream-dominated alluvial fan, San Joaquin Valley, California, U.S.A., Journal of Sedimentary Research, v. 72, p. 270-281.

Wernicke, B., Clayton, R., Ducea, M., Jones, C. H., Park, S., Ruppert, S., Saleeby, J., Snow, J. K., Squires, L., Fliedner, M., Jiracek, G., Keller, R., Klemperer, S., Luetgart, J., Malin, P., Miller, K., Mooney, W., Oliver, H., Phinney, R., 1996, Origin of high mountains in the continents: The southern Sierra Nevada: Science, v. 271, p. 190-193.

Whipple, K. X., and Tucker, G. E., 1999, Dynamics of the stream power river incision model: Implications for the height limits of mountain ranges, landscape response timescales, and research needs: Journal of Geophysical Research, v. 104, p. 17,661-17,674.

Whipple, K. X., and Tucker, G. E., 2002, Implications of sediment-flux dependent river incision models for landscape evolution, Journal of Geophysical Research, v. 107, 2039, doi: 10.1029/2000JB000044.

Zachos, J., Pagani, M., Sloan, L., Thomas, E., and Billups, K., 2001, Trends, rhythms, and aberrations in global climate 65 Ma to present: Science, v. 292, p. 686-693.

APPENDIX 8: GUIDE TO SIERRA NEVADA LICHENOMETRY

William B. Bull *University of Arizona, Tucson, AZ*
Bill@ActiveTectonics.com

ABSTRACT

Local and distant earthquakes cause synchronous landslides of regional extent in the Sierra Nevada of California. This allows development and testing of field measurement and analytical procedures for sizes of lichens growing on historical rockfall accumulations. Digital calipers were used to measure the maximum diameter of the largest lichen on numerous rockfall blocks. Rates of growth were calibrated for four genera of lichens using historical and tree-ring dated sites where substrate exposure times are known to the year or day. Lichen-size peaks for synchronous rockfall events are the same for sites with diverse climate, altitude, and substrate lithology. This regionally consistent lichen growth rate allows use of single growth-rate equations. Lichenometry is now a surface-exposure dating method with precision and accuracy uncertainties at the 95% confidence level that can be reduced to better than ±10 years. It dates the event, not the time of organic material that grew before or after the event. It can date landforms and geomorphic processes of the past 1,000 years. This new method can evaluate landslide, avalanche, and flood hazards; decipher the Little Ice Age; and make maps depicting patterns of seismic shaking for prehistorical earthquakes.

INTRODUCTION

This guide uses work in the Sierra Nevada of California to outline field methods and advantages of a new lichenometry procedure for geomorphologists and Quaternary geologists. This procedure was developed during a decade of work in New Zealand and testing in California and Sweden. A large sample of the lichen-size population is measured instead of the traditional largest five lichens (Locke, 1979; Porter, 1981, Innes, 1985, O'Neal and Schoenenberger, 2003). Precision and accuracy are easily tested in mountain ranges subject to seismic-shaking events that create rockfalls of regional extent. This advantage allows one to test the quality of new field and analytical procedures.

The main purpose here is to outline field aspects of the method. See Bull and Brandon (1998) for analysis of lichen-size data. Topics include site selection including an evaluation of which lichens to use, quality assessment of lichen-size measurements, how to calibrate lichen growth, and comparisons of the ages of lichen-size peaks from different sites.

Many examples use data from the Roaring River lichenometry site, which was used for a lichenometry short course in 2002 and was a trip stop for the 2003 Friends of the Pleistocene trip. This easily accessible site illustrates many aspects of the new lichenometry.

Although my model has substantial paleoseismology implications, this guide also illustrates two applications of special interest to the Friends of the Pleistocene. One of these is dating of late Holocene glacial moraines, and the other is the assessment of lichen snowkill events (Benedict, 1993) during the Little Ice Age.

Lichen dating of regional coseismic landslide events--or of young glacial moraines--complements studies that emphasize stratigraphic dating with radiocarbon. Advantages of this new approach to paleoseismology include:

1) Estimation of the time of the earthquake itself instead of dating organic material that grew before or after a particular earthquake.

2) Precision and accuracy of dating that is ± 10 years or better.

3) Ability to make maps depicting patterns of seismic shaking for prehistorical earthquakes that are as good as Mercalli intensity maps for historical earthquakes. Unstable and rapidly changing glaciated hillslopes of the Sierra Nevada allow detection of regional rockfall events generated by distant San Andreas fault earthquakes. This is easily demonstrated regionally for the sites shown in Figure 8-1 and at the Roaring River FOP 2003 trip stop site.

Deficiencies of earthquake-lichenometry studies include inability to measure amounts of coseismic slip, general lack of suitable slow growing crustose lichens at low altitudes in the Sierra Nevada, and deficiency of lichens older than 300 years at some sites. Lichens older than 1,000 years are rare but a few are present at the Roaring River site.

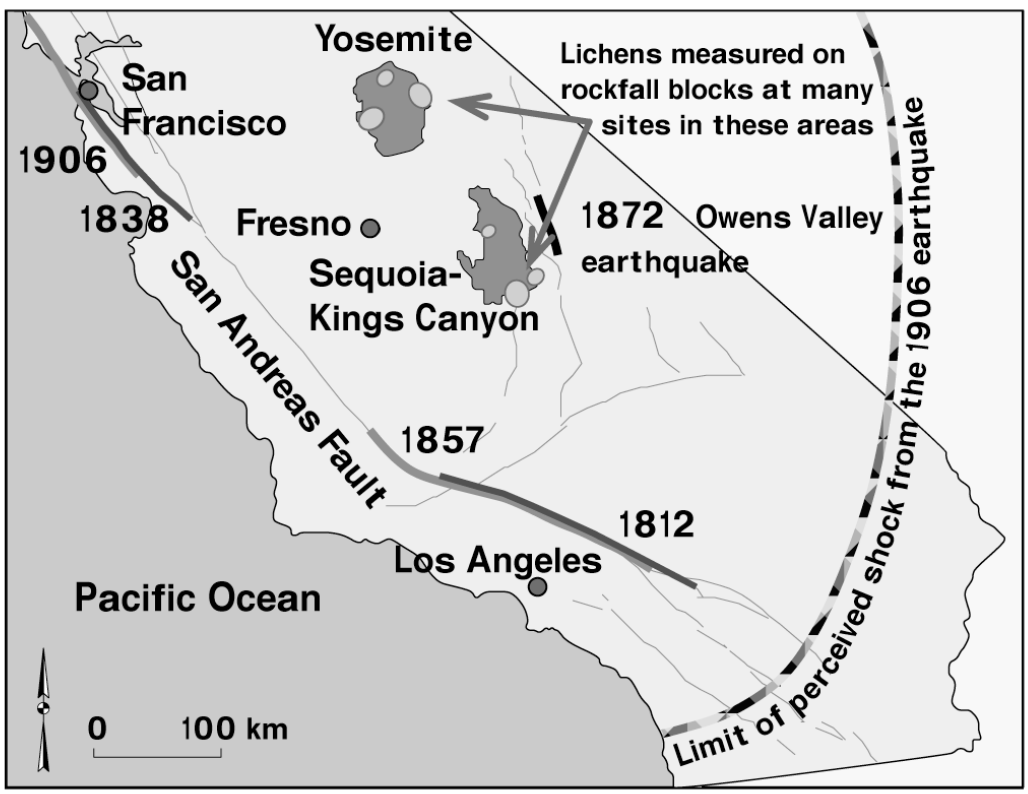

Figure 8-1. California location map showing locations of lichenometry sites in and near Yosemite and Sequoia-Kings Canyon National Parks used in this guide. Extents of historic magnitude Mw ~7.5 San Andreas fault earthquakes are shown by grey lines and the Owens Valley earthquake of 1872 with a black line. Limit of 1906 percieved shock is from Ellsworth (1990).

STARTING YOUR OWN LICHENOMETRY DATING PROJECT

Which Lichens Should You Use?

Key aspects include deciding which genera of lichens should be used, which thalli meet quality standards for inclusion in your data set, how to measure lichen size with minimal operator bias, and calibration of lichen-growth rates.

We started by measuring four genera of lichens with the intention of evaluating which species would be best for dating exposure times of rock surfaces. Crustose lichens are preferred. A surface cortex of dense, protective fungal tissue is underlain by photosynthetic green algae or cyanobacteria. Thalli (main lichen body) have well-defined marginal rims and are tightly attached to rock substrates. Only exposed lichens are measured so as to minimize the effects of a slightly faster growth rate in shady micro-climatic settings. Comparison of visually different lichens growing on a single-age rock surface is an easy way to discern relative rates of lichen growth. Use the slow-growing lichens; even they can provide a precision and accuracy of 5 to 10 years.

Each lichen has a preferred macro-climate and microclimatic setting, so only one of our four selected lichens might be growing at some sites. Later, in the analysis stage of the project, we realized that it was useful to cross check age estimates by using data from a different lichen genus. Lichens were simply labeled 1, 2, 3, and 4 for ease of notation in field notes and computer labels. Clifford Wetmore of the University of Minnesota and Thomas Nash of Arizona State University provided the following provisional identifications: lichen 1, *Acarospora chlorophana*, lichen 2 *Lecanora sierrae*, lichen 3 *Lecidea atrobrunnea, and* lichen 4 *Rhizocarpon* subgenus *Rhizocarpon*. Each probably includes many species, which fortunately grow at the same rate; *Lecidea* providing the only recognized case of one species growing faster than the one used for dating. Identification to the species level requires the skill of a lichenologist and is based on detailed microscopic and biochemical examination. Such identification is not likely to be done by a lichenometrist measuring thousands of lichens. Admittedly pretty crude, but the following hand-lens characteristics were useful for field identification. Go to http://www.lichen.com/index.html for illustrated terms and superb lichen photos.

Lichen 1 is conspicuous because its thallus is bright chartreuse. It has distinct margins but has no thallus rim. The outermost 4-5 mm on mature, large specimens has a foliose (leaf-like lobes) radiating structure (Fig. 8-2). Areoles (segments of cracked crust) in the interior of the lichen tend to be fairly circular and range in diameter from 0.6 to 1.1 mm. Septa divide each areole into five to ten parts. The apothecia (reproductive structures) are not obvious, but are quite common. They consist of 0.9 to 1.4 mm high and wide structures that stand slightly above the adjacent areoles. The tops of the apothecia are still chartreuse in color but have a grayish green tinge that makes them stand out from the adjacent areoles; they commonly have two to three septa. Lichen 1 grows on a variety of substrates in the dryer macroclimatic settings and commonly prefers north-facing sides of blocks. It appears to be susceptible to encroachment and colonization by other lichens, so it typically has a fretted interior where replaced by several other species, especially the Rhizocarpons.

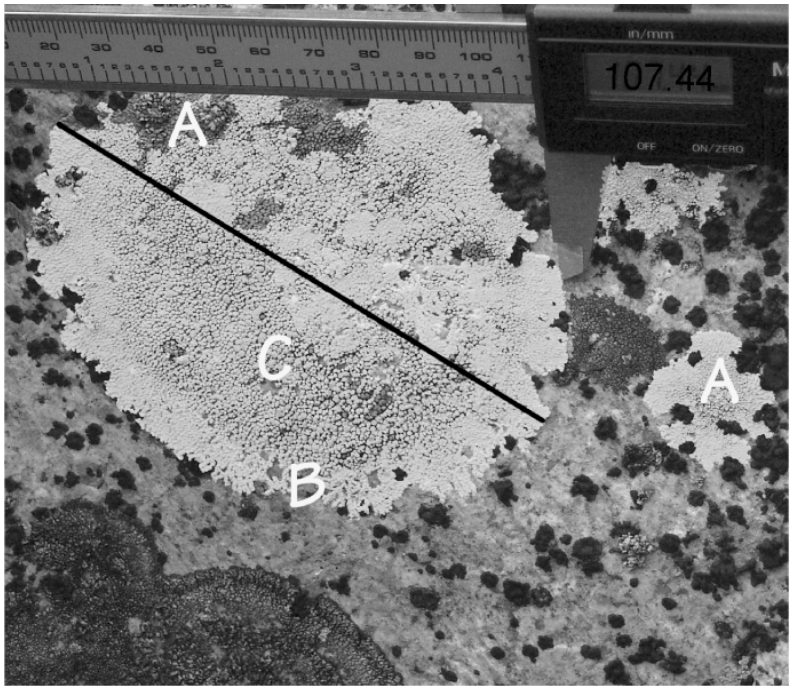

Figure 8-2. A 1000 year-old lichen growing at the Roaring River site, Kings Canyon, Sierra Nevada, California. A. Lichens are competitive. This mirco-environment is damp enough to allow two other types of lichens to grow on this *Acarospora chlorophana*. This process creates holes in the thallus and embayed margins. B. The strings of fungal cells near the margins have a different structure and color compared to the larger central areoles and apothecia that contain reproductive spore cases at C.

Patches of smooth fungi near the center may be newer growth that has repaired damage caused by competing lichens. This mass appears to be a single lichen because of the overall elliptical shape of the margins and the paralleling elliptical bands of internal cell structure. We obtain best statistical results by measuring the long axes of the ellipse shown by the black line. I am confident that the upper left measuring point is intact, but am less sure about the lower right end point. Most likely it is intact, but let's allow for the possibility of slight erosion by competing lichens. This would lower my quality assessment number that accompanies this particular lichen-size measurement.

Lichen 2 seems to have a wide range of color but similar morphology. Colors range from a pale greenish gray to a bluish green yellow to a dark greenish blue. Variations in color appear to be in part a function of microenvironment because large lichens that grow around the corner of a block may have markedly different hues on the two sides. Foliose margins are distinct, typically having a change in color to bright blue to dark greenish blue to dark bluish gray. Areoles tend to be more equant in the center of the lichens, but the typical habit is for short worm-like ridges; these areoles are 0.4 to 0.6 mm wide and 0.8 to more than 2 mm long. Apothecia appear to be absent in some lichens, even for fairly large specimens. Most have a sprinkling of apothecia in the central portions of the lichen; colors range from light tan to dark reddish brown. The sizes of the apothecia tend to be quite large, typically being 1.4 to 2.3 mm across and fairly equant in shape. Most apothecia can be detached fairly easily. Occasionally there is a septum dividing the top of the apothecia in two parts but most lack septa. The black algal mat between the areoles and apothecia is readily apparent.

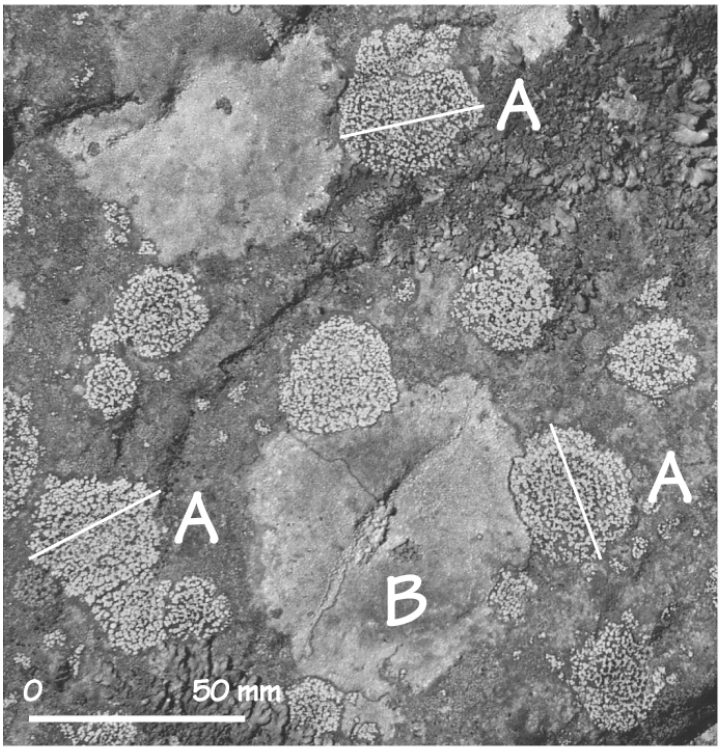

Figure 8-3. Lichens growing on a rockfall block in the Seaward Kaikoura Range, New Zealand. A wide range of sizes for *Rhizocarpon* subgenus *Rhizocarpon* is shown. These lichens have the typical salt-and-pepper texture of most yellow *rhizocarpons*. Three of the largest lichens at locations A are nearly the same size: 33.46, 34.09, and 34.32 mm. The white lines indicative of the longest axis maximum diameter include the black algal rim, which is part of the lichen. The top lichen is a composite of several yellow *rhizocarpons*, but the isolated nature of most lichens suggests that this is a first-generation community of lichens. The lichen at B is a fast-growing crustose lichen that would require a separate growth calibration.

Lichen 3 is a common brown lichen with distinct margins, but a gray to black thallus rim seems to be present on only about a third of the lichens. Where present, the thallus rim can be prominent, having widths of as much as 1.9 mm. Areoles are equant blisters, tan to dark blackish brown in color, and typically being 1.6 to 2.9 mm in size. Areoles have a white interior. As for lichen 2 many gradations of intermediate colors are present between the two end members. The black algal mat is visible between them. Apothecia are common in the central portions of thalli; they are black, flat-topped, and range in size from 1.2 to 2.1 mm.

Lichen 4 is present from the floor of Yosemite Valley to the crest of the Sierra Nevada, but not on the dryer eastern slopes. It too likes the north-facing sides of rockfall blocks and appears to be an aggressive member of the lichen community. Margins are distinct; thallus rims tend to be narrow or absent in some cases. The interior of lichen 4 has a distinctive salt-and-pepper texture (Fig. 8-3) because of the large number of apothecia evenly scattered through the areoles. Concentric rings of aureoles are may occur. The areoles are pale greenish yellow; they may have two to four poorly defined septa and vary widely in size, ranging from 0.5 to 1.6 mm. The apothecia are black, these are dull charcoal surfaces form domal structures that rise only slightly above the adjacent areoles.

In hindsight, which lichen would I now use? I still see an advantage of having several crustose lichens available because a genus that may be perfect at one site might not even grow at the next site. Lichen 2 was used less than the others, and the thalli margins are not as sharp as for lichens 1 and 3. Lichen 4 has the same problem and overall has the poorest quality thalli. But it is the slowest growing lichen used and can be found at the largest range of altitudes. Lichen 3 worked out quite well despite having to be careful not to measure faster growing, scaly, look-a-like lichens. Lichen 1,

Acarospora chlorophana, appears to have only one growth rate, its chartreuse color makes it easy to find, it has good thalli margins, and grows almost as slowly as lichen 4. It probably is the oldest lichen in the Sierra Nevada, and would be the lichen of choice if only it grew at all sites.

Selection of Quality Sites and Lichens

Pick sites that fit your goals. Avalanche-chute cones are best for dating blocks produced during winters of large snowfall. Talus derived from fragile cliffs, landslides, and scattered blocks on stream-terrace treads can provide sensitive records of earthquakes, even when the earthquake epicenter is distant (Keefer, 1984, 1994). Lichens on high-altitude blocks or outcrops can indicate times of exposure after burial during Little Ice Age snowpacks.

We seek large, trustworthy data sets. As a quality-control measure, you should make a subjective evaluation of the relative quality of each lichen measured. The main questions to be answered are:

1. Is this really a single thallus, or have several lichens grown together?
2. Is the lichen sufficiently well preserved to reveal the end points of the longest axis of growth? See Figure 8-2.
3. Are the margins at the two measurement points sharp and well defined?

Quality control numbers range from 1 to 4:

1. A superb lichen that has you reaching for your camera to take a picture of it.
2. Close to ideal for a reliable lichen-size measurement.
3. Nothing special but we feel quite comfortable in including it in the data set.
4. We hesitate about including this lichen size in the dataset; it has borderline characteristics.

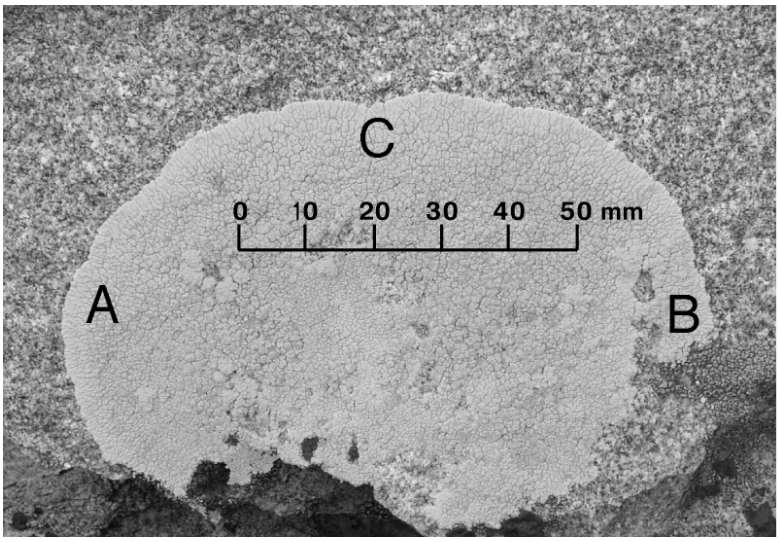

Figure 8-4. Evaluating the quality of a large *Acarospora chlorophana* at the Roaring River site between longest axis points near A and B, and taking indentation like that at C into account. See text for the reasoning process.

The lichen shown in Figure 8-4 is not complete because it is growing at the edge of a block and it has been partially cannibalized by competing lichens. Its nice elliptical shape is diminished by an indentation at C, but this does not bother me because the internal cells have a pattern suggestive of one instead of a composite of two lichens. The

margin at measurement point A is ideal. Fortunately, the other side of the lichen at B has not been removed. But I do not know how this margin would have appeared if the lower-right portion of the lichen had not been severely degraded. On balance this lichen seems good enough to measure and I give it a quality rating of 3. Your rating might be different because there is quite a bit of operator variance on this subjective evaluation. But each operator should strive to be consistent in her or his evaluations.

How many lichens must be on a rockfall block before you accept the measurement of the largest one? The answer is that a single lichen will suffice. Obviously we have more confidence when several lichens of about the same size are present (Fig. 8-3), and this is reflected in an assignment of a better lichen quality measurement number (for example, 3 would be raised to 2).

Size measurements are made with digital calipers in order to increase precision and reduce bias. The long axis of the largest lichen is evaluated for measurement on each block on a talus slope or glacial moraine. Long axes of elliptical thalli record optimal lichen growth and it is assumed that the largest lichen was the first to colonize a new rock surface. The presence of a second lichen that is nearly as large as the lichen that was measured increases ones confidence that the lichen-size measurement is indicative of the time of exposure of the rock surface (Fig. 8-3). The largest lichen is quickly spotted on blocks smaller than 1 m. Work is facilitated where more than two-thirds of the blocks have isolated instead of merged lichens and the blocks are adjacent to one another. It is important to carefully examine the thallus of the largest lichen to make sure that it does not consist of several lichens that have grown together, and that the margins are sufficiently sharp that replicate measurements are within ±0.1 mm. Such replicate measurements are precise (±1 year of growth for lichens 1 and 4, and ± 0.5 year for lichens 2 and 3), so measuring lichen sizes of is a trivial source of error. Large numbers of lichen-size measurements, 100 to 1,000 lichens, helps define individual lichen-size peaks and allows valid separation of events only a few years apart.

Calibrating Lichen Growth Rates

Calibration of the growth rate for each lichen genus was based on calibration at sites such as landslides and construction sites whose age is known to the year. The Figure 8-5 example supposes that your study area is Yosemite National Park and that you want to calibrate the rate of growth for *Rhizocarpon* subgenus *Rhizocarpon*. Three young points give you a possible rate of growth, which is confirmed by tree-ring dating of a much older site. Lichen sizes were measured next to a trail to Nevada Falls that was constructed in 1940. We also did this for a landslide that fell off of Liberty Cap in 1908 and identified the blocks for a witnessed 1872 coseismic landslide by analyzing the annual growth rings of trees damaged by granitic blocks. Lichens of this age have entered the uniform-growth stage of lichen growth as shown by the way in which this point falls on the regression line. The younger great-growth stage is characterized by exponentially declining lichen growth. These three calibration points span only 68 years, not sufficient for extrapolation into the distant past. A rock avalanche named The Slide (Huber, et al., 2002) had potential as an essential calibration site, but only if we could date it's time of formation to the year by tree-ring analysis.

Radiocarbon dating of wood buried by the landslide might seem to be ideal dating but has two deficiencies. First, any wood collected for this purpose grew before the

landslide event, so can only constrain the approximate time of the cataclysmic slide. Secondly, variations in production of carbon 14 in the atmosphere have varied so much during the past 300 years that one has to choose between several possible radiocarbon age ranges. The wood sampled from beneath the slide gave Bronson and Watters (1987) calendric radiocarbon age estimates of 1638-1680, 1753-1804, and 1937-1954 A. D.. Of course we can easily dismiss the 1937-1954 possibility, but have no basis for picking between the other two. Indeed this left dendrochronology as our best hope.

The Slide may have begun as a block slide, but it quickly became a rapidly moving mass of blocks as it shot downhill towards Piute Creek. The rapid speed at which the rock avalanche moved is suggested by crude transverse waves and a raised rim where it stopped abruptly in a forest of hemlock trees. By running up 37 m on the opposite side of the valley this rock avalanche achieved speeds in excess of 225 km per hour when it crossed Piute Creek. Tree-ring analyses by Bill Phillips cross-dated the patterns of annual growth for the hemlock trees and dated the time of damage as occurring between the end of the growing season in September 1739 and before the start of growth in June 1740. This fourth calibration point on Figure 5 at 1740 A.D. falls on the same line as the other points. Mountain hemlock in the Piute Creek area commonly live over 400 years as shown by the Bill Phillips tree-ring chronology; a rockslide in 1739-40 AD would incorporate many logs 60 to 100 years old, resulting in the 1638-1680 range of the radiocarbon date. Dating The Slide provided an essential calibration point for other lichens too, as summarized in the following equations.

Regression of mean lichen size in millimeters, D, and calendric years, t, describes uniform lichen growth as

$$D = 190 - 0.095\ t; \qquad (8\text{-}1)$$

n (number of control points) is 5 and r^2 (correlation coefficient) is 0.99.

The age for a specific size of lichen is the sum of colonization time, initial great-growth phase, and uniform-growth phase. Uniform-phase growth is about 9.5 mm per century. Thus lichens growing on substrates exposed in A.D. 1 would have a mean size of 190 mm in 1994 A. D.. Similar calibration procedures were used for the three other genera of lichens.

The calibration equation for *Acarospora chlorophana* is

$$D = 225 - 0.114\ t; \qquad (8\text{-}2)$$

n is 5 and r^2 is 1.0.

The calibration equation for *Lecidea atrobrunnea* is

$$D = 448 - 0.231\ t; \qquad (8\text{-}3)$$

n is 6 and r^2 is 0.998.

The calibration equation for *Lecanora sierrae* is

$$D = 377 - 0.189\ t; \qquad (8\text{-}4)$$

n is 7 and r^2 is 0.998.

Sizes for earthquake-generated lichen-size peaks of known age fall on existing calibration plots, like that of Figure 8-5. So, each lichen genus used here grows at virtually the same rate in the 600 to 3500 m altitude range of the Sierra Nevada study region.

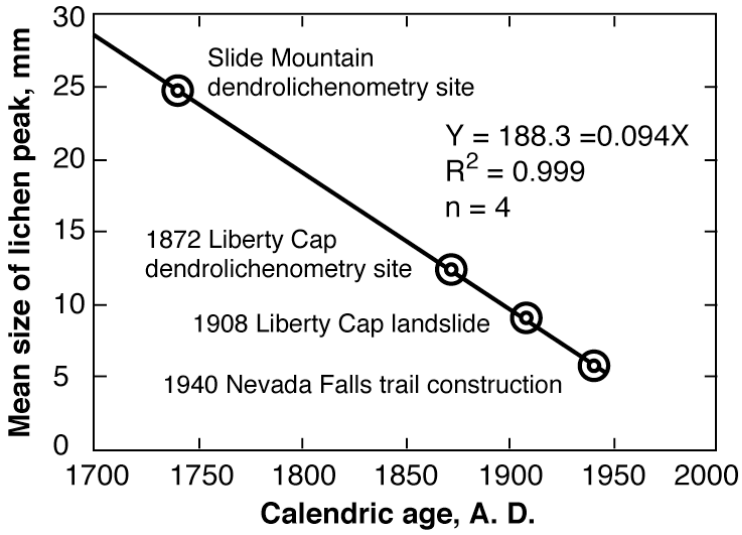

Figure 8-5. Example of calibration procedure to determine lichen growth rates, using lichen-size measurements only from sites in Yosemite National Park whose time of exposure is known to the year. Many lichen sizes were measured and dominant lichen-size peaks were identified, for *Rhizocarpon subgenus Rhizocarpon* in this case. The 68-year time span of the three historical sites was increased by 132 years when tree-ring dating of a big rock avalanche known as "The Slide" expanded the calibration data set.

Lecidea atrobrunnea is the fastest growing of the four lichens with a uniform phase growth rate of 23 mm/100 yr. This is a bit slower than the 33 mm/100 yr of Bob Curry's calibration (Curry, 1969) and much faster than the 4.6 mm/100 yr of Louis Scuderi's calibration (1984 University of California at Los Angeles Ph.D. dissertation; Holocene glaciation and dendroclimatology of the southern Sierra Nevada). Fortunately, as shown later, we can compare our age estimates for regional rockfall events against the nicely dated San Andreas fault earthquakes at Pallet Creek (Sieh et al., 1989).

Data sets collected in different years should be adjusted to a common year using the known annual growth rate. Combining data collected 10 years apart in the Sierra Nevada will introduce errors ranging from 1 to 2.3 mm thereby changing age estimates for lichen-size peaks.

Distinguishing Real from False Lichen-Size Peaks

Two types of histograms are used here to define lichen-size peaks. Identification of specific lichen-size peaks in probability density plots can be done with simple histograms or with the more robust decomposition of Gaussian kernel probability density plots as described by Bull and Brandon (1998). These plots are constructed by converting each measurement into a unit Gaussian function and averaging the densities of lichen sizes. This produces a probability density plot of overlapping Gaussians. The result is analogous to a simple histogram, but a unit Gaussian width instead of a vertical increment of a histogram bar represents each observation. Histogram class-interval size is replaced by a Gaussian kernel size. Lichen-size peak values are about the same for the two methods, but deconvolution of Gaussian probability density plots identifies peaks that might be hidden in standard histograms.

Lichenometric age estimates are obtained by inserting means of normally distributed lichen-size peaks into the above regional equations for lichen growth. Precision of dating is estimated by comparing ages of lichen-size peaks for a specific regional rockfall event at many sites in a region. Accuracy of dating is determined by comparing lichenometric ages of regional rockfall events with dates of historical earthquakes, or with tree-ring dated landslides.

The choice of an appropriate histogram class interval involves a trade-off between precision and resolution. Numerous, meaningless, small peaks are obvious noise if a class interval is too small. So one is tempted to use a large class interval. Resolution is not as good but gives the impression that the few large histogram peaks are real. This can be misleading. Merging of real peaks into false peaks with meaningless mean lichen sizes should also be avoided (See Figure 10 of Bull and Brandon, 1998).

Reliability of identification of real peaks (as compared to unrealistic noise) in probability density plots increases with density of lichen-size measurements. One or two measurements are worthless, but 10 to 100 measurements tightly clustered in a normal distribution supports the hypothesis of a lichen-size peak. So, density of lichen-size measurements affects choice of histogram class intervals, as illustrated later for the Roaring River site. Sizes of lichens from a repository of rockfall blocks typically record many rockfall events with the central part of the probability density plot rising far above low tails at very small or large lichen sizes. The usual approach is to use a class interval, or unit Gaussian kernel width, that introduces minimal noise into the central part (high-density) part of the display of lichen-size peaks. However the tradeoff is possible spurious lichen-size peaks in the tails of the distribution where density of lichen-size measurements commonly is mediocre.

Fortunately, the Bull-Brandon approach to paleoseismology has several ways to confirm the presence of real peaks. Real peaks also occur at many lichenometry sites in the study region because the shaking that caused the coseismic rockfalls is regional in extent. It can be assumed that peaks are real at an individual site when they match the ages of historical earthquakes. Significant peaks can also be defined as those that rise more than three standard errors above a uniform distribution of lichen sizes (defined by Bull and Brandon (1998, p. 67, 68) as lichens growing at a constant rate on blocks in a deposit fed by continuous rockfall events.

STATUS OF SIERRA NEVADA LICHENOMETRY DATING

Glacial Moraines

Do you seek better age control for young glacial moraines? If so, you'll be surprised at how lichenometry describes characteristics of moraines in ways not possible with traditional radiocarbon dating.

I initially thought that it would be easy to date a single, simple pulse of glacial end-moraine deposition. Measurement of lichens growing on blocks at the crest and sides of a moraine should provide a single, dominant lichen-size peak whose mean size could be used to date cessation of glacial advance. It soon became readily apparent that lichens date not only emplacement of the moraine, but also the times of rockfalls onto moving glaciers before moraine deposition. Then moraines change their shapes as blocks shift to more stable positions, thereby creating additional fresh rock surfaces for colonization by lichens. Lichen sizes record all this.

Earthquakes in the Sierra Nevada affect these processes. The result is numerous lichen-size peaks such as those shown in Figure 8-6. Indeed, it appears that moraines might be a delicate recorder of past earthquakes. Glaciation has virtually ceased in the Sierra Nevada, so we need to explore this matter further by going to the Southern Alps of New Zealand, which has larger and more active glaciers.

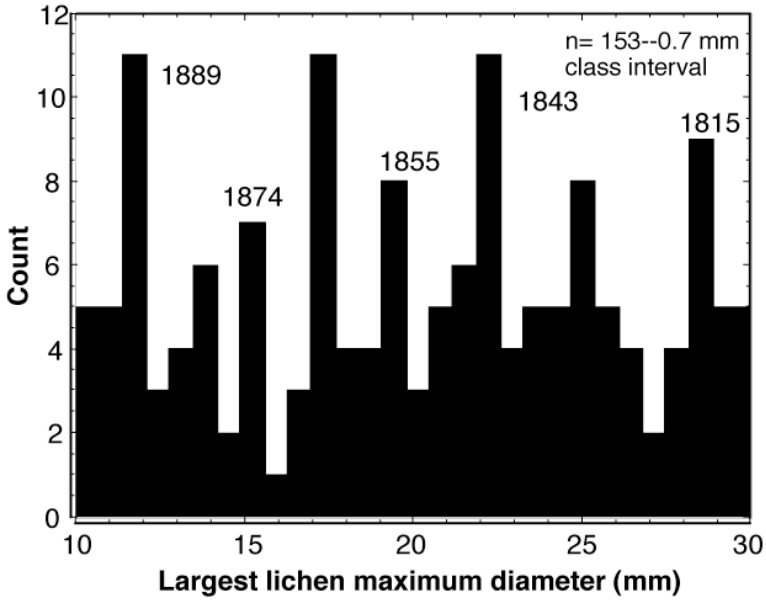

Figure 8-6. Attempt to date a young moraine at Cirque Peak using largest lichen maximum diameter on young moraine blocks. A single peak is not present. Instead, lichen size peaks for *Lecidea Atrobrunnea* have ages indicative of disturbances by the historical earthquakes of 1890, 1872, 1857, 1838, and 1812. Such readjustments of unstable glacial moraines make it difficult to use lichens to date the time of moraine formation.

In 1993 I made lichen-size measurements on the youngest moraines in the Cameron Valley of the Arrowsmith Range, New Zealand, which had been studied by Colin Burrows (Burrows, et al., 1990) and Trevor Chinn (1981). These lichen-size distributions were valuable for mapping young moraines and provided fascinating clues regarding origins of moraine detritus.

The A1 moraine consisted of a medial mound in the valley floor and a lateral portion plastered onto the side of an older moraine. So I measured lichens on both (Figures 8-7A and B). The data set for Figure 8-7A is small but the main peak at ~16-17 mm clearly coincides (within ± 6 years) with the time of fairly distant magnitude Mw 7.8 Murchison earthquake of June, 1929 and the even closer Mw 7.1 Arthurs pass earthquake of March 1929. The smaller peak at ~22 mm coincides with the time of the Mw 7 North Canterbury earthquake of 1888.

The nearby A1 lateral moraine (Fig. 8-7B) also has a pronounced 16 mm lichen-size peak. Substantial lichen-size peaks at ~ 21.5 and 26 mm coincide with the time of two other strong historical earthquakes. Mean lichen size increases from 17.8 mm for Figure 7A to 22.2 mm for Figure 8-7B. These would not have been mapped as the same moraine if Bull-Brandon style lichen-size data sets had been compared.

The A2a moraine has soil and plant cover indicative of an older moraine. It too has many distinct lichen-size peaks (Fig. 8-7C) that reflect either multiple times of deposition or episodes of surficial boulder movement after deposition of the moraine. Peaks that coincide with earthquake dates are present here too; the three peaks of Figure 7B plus several older ones. Still older Cameron moraines further illustrate a consistent pattern of lichen-size peaks matching dates of earthquakes, including those on the Alpine fault, which is only 38 km away.

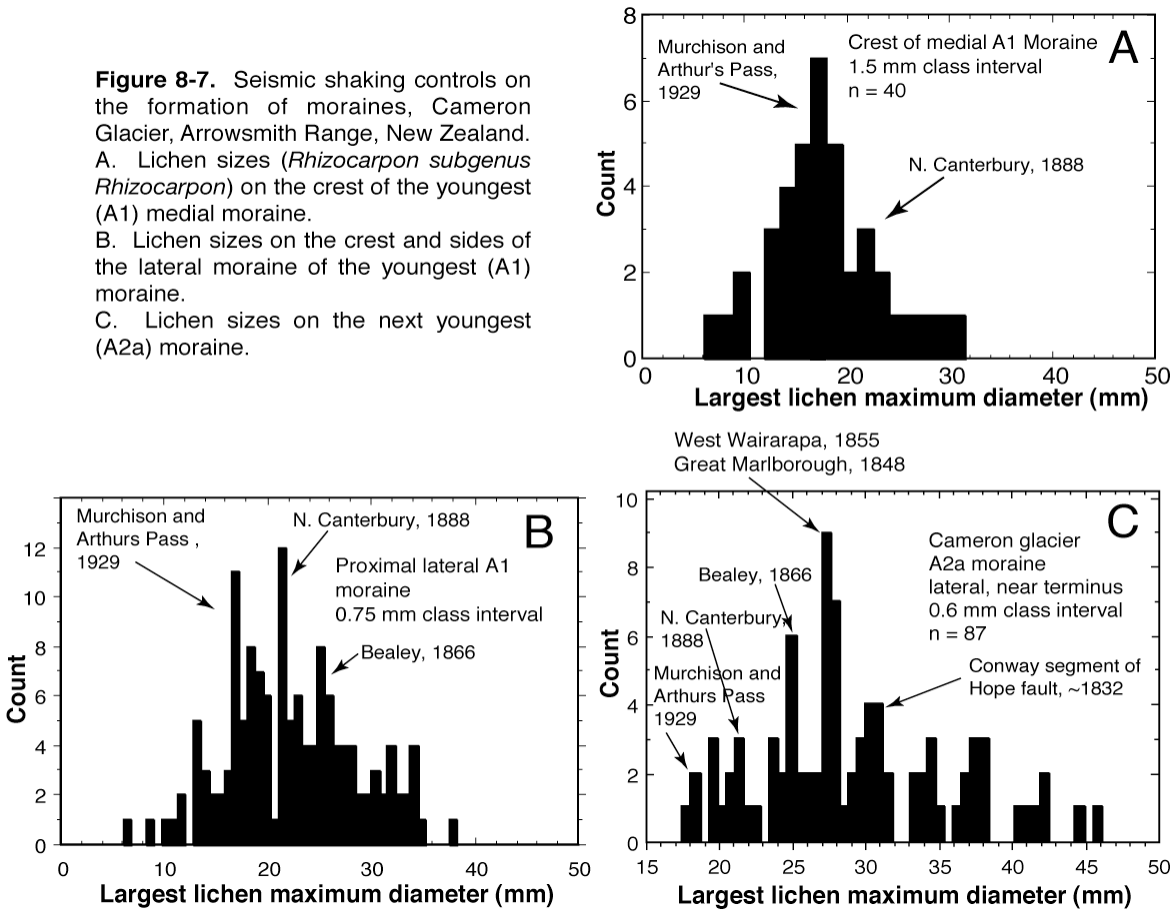

Figure 8-7. Seismic shaking controls on the formation of moraines, Cameron Glacier, Arrowsmith Range, New Zealand.
A. Lichen sizes (*Rhizocarpon subgenus Rhizocarpon*) on the crest of the youngest (A1) medial moraine.
B. Lichen sizes on the crest and sides of the lateral moraine of the youngest (A1) moraine.
C. Lichen sizes on the next youngest (A2a) moraine.

These lichen-size data suggest that even the youngest moraines may not be the result of a single pulse of deposition. The polymodal nature of the lichen-size distributions may record:

a) Numerous post-depositional movements of surficial boulders on a highly unstable freshly deposited moraine,

b) The possibility of more than one advance of the glacier terminus during deposition of a moraine, or

c) The possibility of rockfalls and other landslide detritus being deposited on the glacier and being carried to the terminus. Lichen growth could begin before moraine deposition.

Surface-exposure dating, be it weathering rinds, lichenometry, or cosmogenic isotopes is greatly affected by earthquakes. The consistent pattern of lichen-size peaks that matches earthquake dates suggests that coseismic landslides are an important source of detritus. Alternatively, the time of moraine formation may coincide with the oldest lichen-size peak, and all subsequent peaks are recording disturbances of surficial boulders. The less precise radiocarbon and weathering rind dating methods are not able to discern these fine details of moraine history. Neither is the traditional lichenometry method, which uses the mean of the five largest lichens on a moraine. It would be instructive to have similar moraine lichen-size measurements in an area that is not subject to frequent seismic shaking like that in the Sierra Nevada and Southern Alps.

Northern Sweden is virtually aseismic and has a long history of lichenometry investigations. We sought and found an ideal young moraine, because it appeared to have been deposited by a single pulse of glacier advance. Bull, et al., (1995) measured the sizes of lichens on what appeared to be the youngest "Little Ice Age" moraine of the Kärkerieppe cirque glacier, avoiding a lower and slightly more distal weathered accumulation of moraine material. The sizes of the largest lichens on blocks larger than 0.5 m clearly record prolonged, intermittent deposition (Fig. 8-8). Major pulses of glacier advance that resulted in the composite moraine, are recorded by the strong 71, 81, and 89 mm lichen-size peaks, and more recent minor advances may be recorded by the 58 and 63 mm lichen-size peaks. The 58 mm lichen-size peak would date (±10 yr) to 1850 A. D., the 89 mm peak to 1748 A. D., and the 107 mm peak to 1689 A. D. Lichenometry indicates that multiple glacier advances created a single fresh-appearing moraine before the Little Ice Age ended at about 1850 A. D.

Once again I was unable to identify a single glacial advance by examination of the characteristics of a young moraine in the field. You can imagine how those using radiocarbon dating, or only the five largest lichens, would have fared in estimating the age of this moraine. Lacking the precision of the Bull-Brandon method, they would have incorrectly concluded that the moraine was the product of a single advance, and their 'age estimate' would have added to the confusion about the synchronicity of timing of the Little Ice Age glacial advances in different study areas.

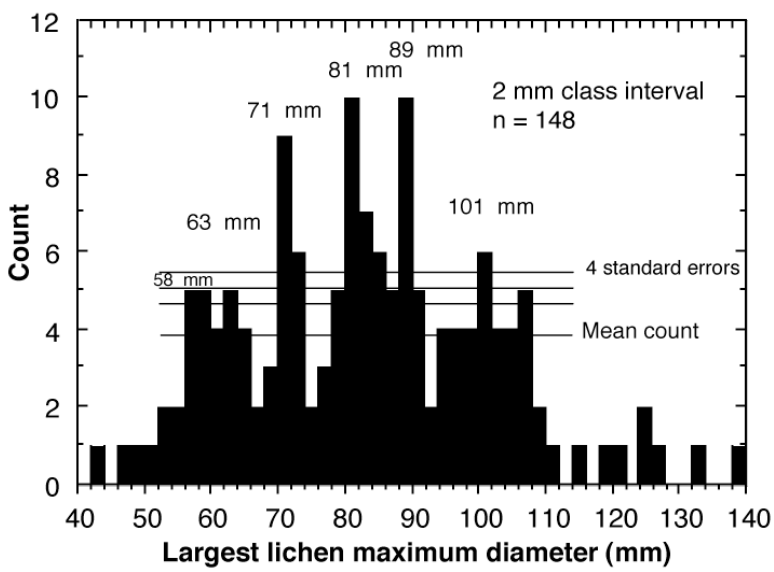

Figure 8-8. Frequency distribution of *Rhizocarpon subgenus Rhizocarpon* sizes on the blocks of the youngest Karkerieppe glacial moraine, northern Sweden. Largest lichens were measured within unit areas (boulders) of about 0.5 to 2 m^2. Significance of lichen-size peaks for 136 measurements between 50 and 110 mm is classed on the bases of how far a peak rises above the mean count value in the 2 mm class intervals: weak, 2 to 3 standard errors; moderate, 3 to 4 standard errors; and strong, >4 standard errors. From Bull et al., 1995, Figure 9.

Little Ice Age Snowkill Events

Times of Little Ice Age glacial conditions were also times when permanent snowfields killed pre-existing lichens. Then lichens would recolonize these surfaces when snowbanks melted and glaciers retreated.

A lichenometry transect across a glacial moraine in the Sierra Nevada suggests that at least two snowkill events occurred during the past 1,000 years (Figure 8-9). These data are largest lichen maximum diameters on each surficial block of granitic rock and the univariate scattergram is merely a plot of the sequence of lichen-size measurements.

A 200 mm *Lecidea atrobrunnea* would date back to about 1070 A. D., well before the onset of the Little Ice Age. The density of the first 200 lichen-size measurements is essentially constant to 150 mm, above which lichens are sparse. Establishment of a perennial snowbank would kill all lichens except those on blocks that rose above the snow. Then normal colonization would resume after the snow melted. It appears that the first snowkill event at this site ended approximately at 150 mm time (about 1290 A. D.). The even distribution of lichen sizes below the 150 mm line indicates that this part of the measurement transect was not subject to further snowkills. The next 220 measurements in the sequence of lichen-size are much smaller; none are larger than 76 mm and most are smaller than 20 mm. I infer a snowkill event that ended at 20 mm time (1853 A. D. ± 10 years). The many lichen sizes between 5 and 20 mm suggests that renewed colonization did not occur on all blocks at the same time. The moraine may not have been entirely free of persistent snow cover. This 19th century snowkill event is coeval with the "Little Ice Age" in the Sierra Nevada and the earlier event approximates the time suggested for the beginning of the Little Ice Age in Europe and North America.

Other Sierra Nevada lichenometry sites also reveal snowkill events at times between the dates suggested by the Chickenfoot Moraine site. The bright yellow of *Acarospora chlorophana* provides quick visual assessment of depressions where snowkill was likely. Much could be accomplished with little additional work because regional calibration of lichen growth rates is complete, except for the opportunistic set of cross-check data.

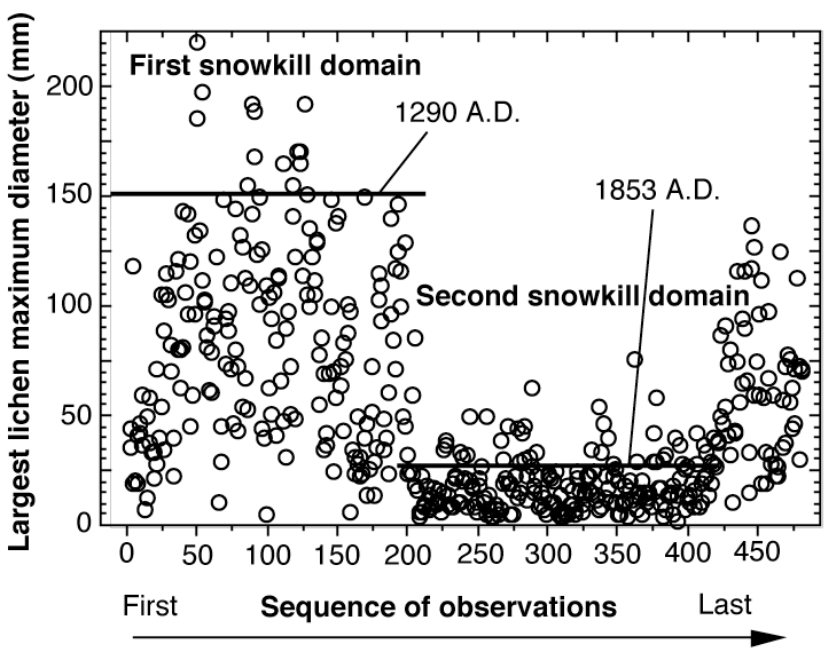

Figure 8-9. Univariate scattergram of *Lecidea atrobrunnea* at the Chickenfoot moraine lichenometry site, altitude of 3,540 m, in the Sierra Nevada of California reveals two domains of anomalous decrease in density of lichen sizes that suggest times when snowkill events ended. n = 481

Earthquake-Induced Rockfall Events

Growth-rate calibration of the four lichens sets the stage for a different approach to paleoseismology in the Sierra Nevada. The sensitivity of this landscape to seismic shaking from local and distant sources has been documented (Bull, et al., 1994; Bull, 1996), and is illustrated by the FOP trip stop described in the next section. So the main purpose of this introductory statement is to update two aspects of the published work.

The Friends of the Pleistocene trip of 2001 A. D. called attention to the potential for large earthquakes on the Honey Lake fault zone in the transition zone between the northern Sierra Nevada and Basin and Range Province (Adams, et al., 2001; Wakabayashi, and Sawyer, 2000). A bit of reconnaissance work by Jim Brune and myself found useful lichens on rock-fall blocks from a volcanic neck. This site is at the crest of Fort Sage Mountains at the Nevada state line in northeastern California and is 1 km S of the 2001 A. D. FOP Stop 4 campsite, altitude is 1600 m, and mean annual precipitation is ~250 mm.

The hot, dry crest of the northern Fort Sage Mountains is also exposed to wind, so only a few lichens grow in sheltered locations. Granitic blocks are nearly bare of lichens. Our brief reconnaissance found a few usable rock-fall blocks on the NW side debris slope, and a good repository of rockfalls in a chute on the NW side that was sheltered from sun and wind. Using digital calipers we measured the largest lichen on 39 rock-fall blocks and 5 outcrop joint faces. Even this small sample of *Acarospora chlorophana* illustrates the potential for lichenometry in earthquake studies in the northern Sierra Nevada.

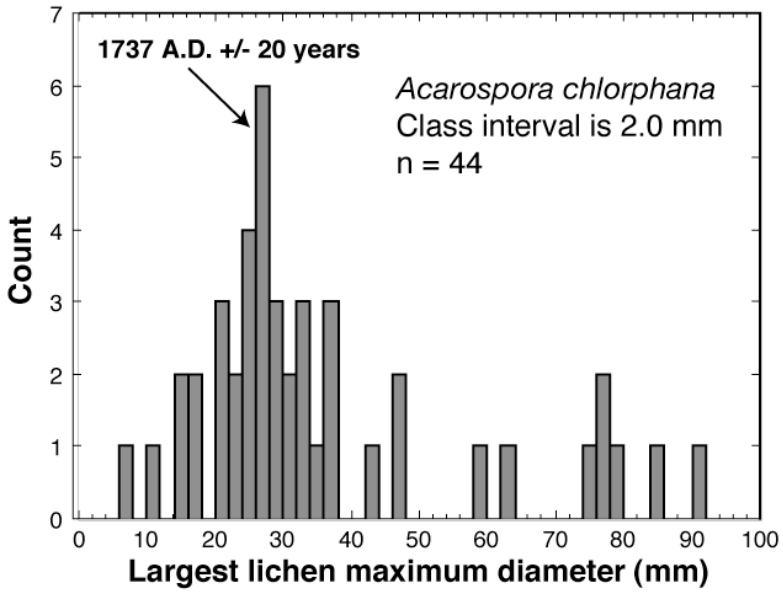

Figure 8-10. Histogram of the sizes of the larges *Acarospora Chlorophana* lichens on blocks that have fallen off a volcanic neck, or are growing on joint faces from where rock-fall blocks originated. This site in the Fort Sage Mountains in northeastern California is near the Honey Lake Fault zone. Date of prominent lichen-size peak agrees with stratigraphic radiocarbon dating of the most recent earthquake.

Lichen sizes in Figure 8-10 peak and then decline in a low tail because the older lichens are less likely to be preserved. An obvious peak at 27 mm and a likely peak at 77 mm have calendric ages close to 1737 and 1198 A. D. The large assigned uncertainty of ± 20 years could be reduced to less than ±10 years by;

1) getting 200 instead of 44 lichen-size measurements (with only 44 measurements we have to use a large bin size. See Bull and Brandon (1998, Fig. 20) for the relation of sample size and precision of dating).

2) modeling the means of component peaks in a probability density plot constructed by graphical summation of Gaussians representing individual lichen-size measurements.

3) showing that these peaks are real - they exist at other lichenometry sites.

Yes, the ~1737 A. D. lichen-size peak is present at many sites, including the Roaring River FOP trip stop. Most importantly, it matches the 1739-1740 A. D. tree ring

date of "The Slide"—that rock avalanche now appears to have been triggered by an earthquake on the Honey Lake fault zone. This possibility could be tested with a map depicting seismic shaking (rockfall abundance of this specific lichen-size peak) using data from many lichenometry sites.

The pervasive influence of earthquakes on Sierra Nevada rockfalls is nicely shown by a regional analysis of lichen sizes, in this case *Rhizocarpon* subgenus *Rhizocarpon*. Modeled lichen-size peaks for the combined data of 10 lichenometry sites clearly matches the times of historic earthquakes (Fig. 8-11). The second largest peak dates to about 1837 but all Bull (1996) could say about it was "The A.D. 1837 ± 10 yr lichen size peak records a regional rockfall event of unknown cause." Then Toppozada and Borchardt (1998) described the previously unregistered San Andreas fault earthquake of 1838. Its location is directly opposite our study region (Fig. 8-1), which contributed to the large size of the lichen-size peak for that particular rockfall event. We now know that all the lichen-size peaks of Figure 8-11 record regional seismic shaking events.

Our present listing of the more significant earthquakes known to have caused Sierra Nevada landslides is summarized in Table 8-1, together with sizes of lichen-size peaks observed at lichenometry sites. Many prehistorical earthquakes, recorded by regional lichen-size peaks, have yet to be defined in terms of their source faults.

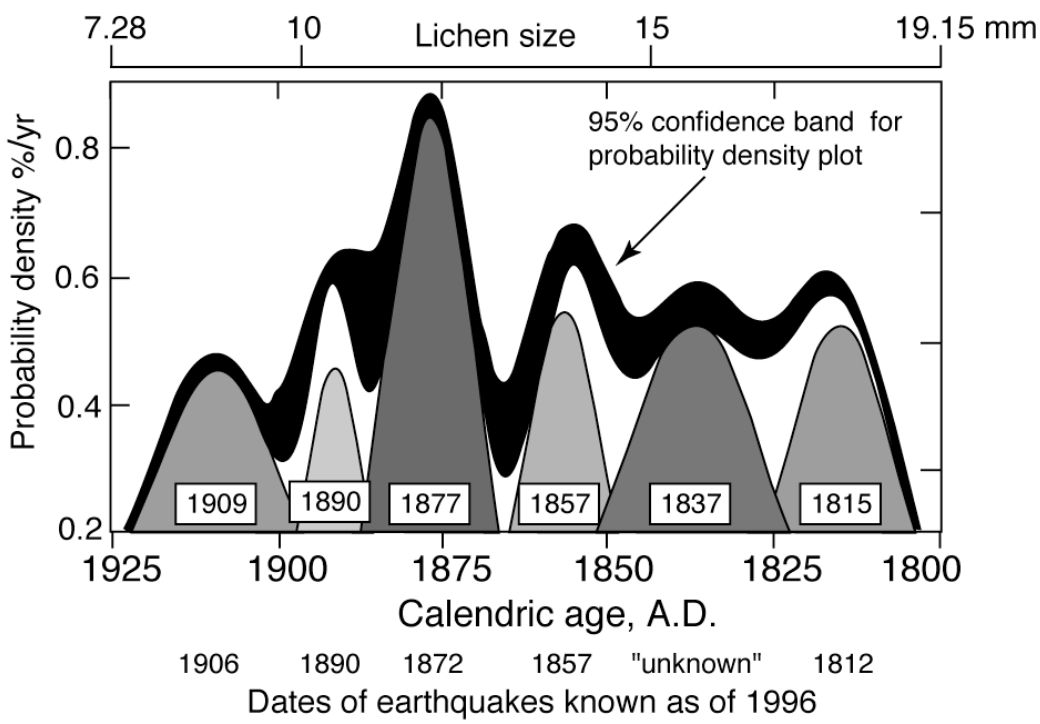

Figure 8-11. Times of rockfalls for 10 Sierra Nevada sites are clustered, which requires regional causes. 1872 and 1890 local earthquakes and 1812, 1857, and 1906 are San Andreas fault earthquakes. Five dates have a 2 sigma accuracy of 2.2 +/- 3.5 yr. The A.D. 1837 +/- 10 yr lichen-size peak records a regional rockfall event of "unknown cause", but turned out to be caused by the San Andreas earthquake of 1838 (Toppozada and Borchardt, 1998). From Bull 1996, Figure 4.

Table 8-1. Partial list of dates of seismic shaking in the Sierra Nevada based on historical accounts, tree-ring analyses, and radiocarbon dating at the Pallett Creek stratigraphic paleoseismology site of Kerry Sieh on the San Andreas Fault (Sieh et al., 1989).

Earthquake	Earthquake date Calendric, A. D.	*Acarospora chlorophana* Lichen-size peak, 2002
Kern County	1952.56	~3 mm (great growth)
San Francisco, San Andreas fault	1906.30	~8 mm (great growth)
Mono	1890.00	~9.5 mm
Owens Valley	1872.23	~11.5 mm
Southern California, San Andreas fault	1857.02	~13.5 mm
Hollister, San Andreas fault earthquake	1838.47	~15.5 mm
Southern California, San Andreas fault	1812.95	~18.5 mm
Liberty Cap rockfall was a regional event, some tree-ring control	1780± 10 yr	~22 mm
Slide Mountain dendro-lichen calibration site. Rock avalanche caused by earthquake on Honey Lake fault bordering northern Sierra Nevada	1739.9±0.4 yr	~26.5 mm
Mean lichenometry age for Southern California, San Andreas fault earthquake. ^{14}C dated as 1688 ±13 yrs (Fumal, et al.., 1993)	1692±3	~32 mm
Pallett Creek ^{14}C estimate 1610 +40 -110 yr. Pretty crude so several possible lichen-size peaks in the Sierra Nevada	1614±10 a possible event	~41 mm
Mean lichenometry age for San Andreas fault earthquake. ^{14}C dated at Pallett Creek in southern California by Sieh, et al., (1989) as 1480 ±15 yr	1485±5	~56 mm
Mean lichenometry age for San Andreas fault earthquake. ^{14}C dated at Pallett Creek (Sieh, et al., 1989) as 1346 ±17 yr	1344±5	~72 mm
Mean lichenometry age for San Andreas fault earthquake. ^{14}C dated at Pallett Creek (Sieh, et al., 1989) as 1100 ±65 yr	1096.00±9	~100 mm
Mean lichenometry age for San Andreas fault earthquake. ^{14}C dated at Pallett Creek (Sieh, et al., 1989) as 1048 ±33 yr	1049±8	~105.6 mm
Mean lichenometry age for San Andreas fault earthquake. ^{14}C dated at Pallett Creek (Sieh, et al., 1989) as 997 ±16 yr	996±12	~111.5 mm
Mean lichenometry age for San Andreas fault earthquake. ^{14}C dated at Pallett Creek (Sieh, et al.,1989) as 797 ±17 yr	797±16	~134 mm
Mean lichenometry age for San Andreas fault earthquake. ^{14}C dated at Pallett Creek (Sieh, et al., 1989) as 734 ±13 yr	742±12	~140.5 mm

ROARING RIVER FOP TRIP STOP

The previous sections provide background for an instructive lichenometry site that you can drive to in the South Fork of the Kings Canyon.

The instructional part of the site is right by the road just downvalley from the Roaring River Falls parking lot. All four lichens are present here and some are 1,000 years old. Look up at the cliffs to see the sources of recent rock falls, which are the whiter parts of the cliff whose overall grey color is caused by lichens. Rock-fall blocks that have run into the adjacent small grove of oak trees outline possible calibration scenarios using dendrochonology.

A nice paleoseismology site is only several minutes walk up the valley on the trail from the falls. The first large sheet of talus that you come to was used by the 2002 lichenometry short course, and the even larger adjacent talus sheet may be just as good. Large, old lichens are common here because of minimal recent influx of rock-fall blocks.

More active talus slopes are the norm. Lichen sizes tend to be quite small but are useful for defining the impact of recent earthquakes (Fig. 8-12). Peak size varies a lot from site to site, and not all cliff sources collapse during a given large earthquake. But rock-fall block abundance at a given distance from an earthquake epicenter increases with intensity of seismic shaking in a sufficiently regular manner to allow generation of seismic shaking index maps for historical and prehistorical earthquakes, such as that made by Bull (2000) for Southern Alps, New Zealand earthquake. Lichen-size peaks for the 1952 Kern County earthquake are only about 3 mm. Such peaks are not precisely dated by equations 1 - 4 because these lichens are still in the great-growth stage.

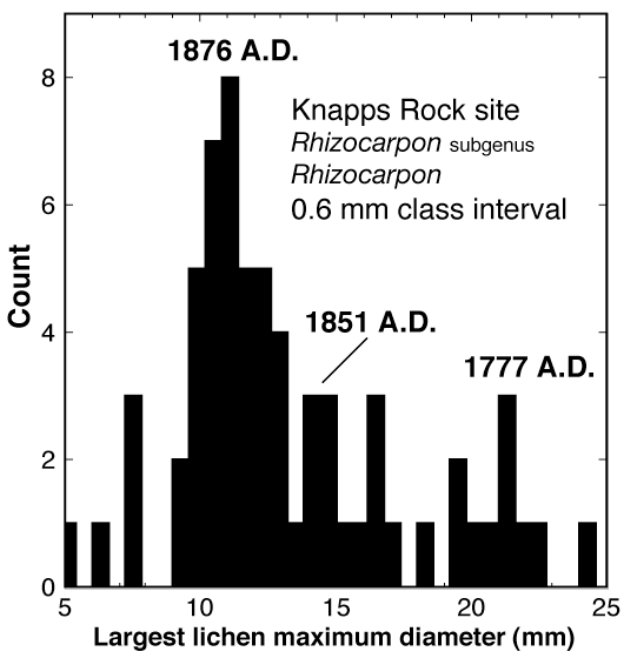

Figure 8-12. Kings Canyon peaks in lichen-size distributions of young lichens record seismic shaking caused by earthquakes. Histogram of lichen-size measurements of *Rhizocarpon* subgenus *Rhizocarpon* at Knapp's Rock rockfall site. Amplitude (and index of seismic-shaking for this time span) of 12 mm peak reflects magnitude 7.6 earthquake of 1872 (Lubetkin and Clark, 1988) whose epicenter was only 50 km away. Other labeled peaks date to the earthquakes of Table 8-1.

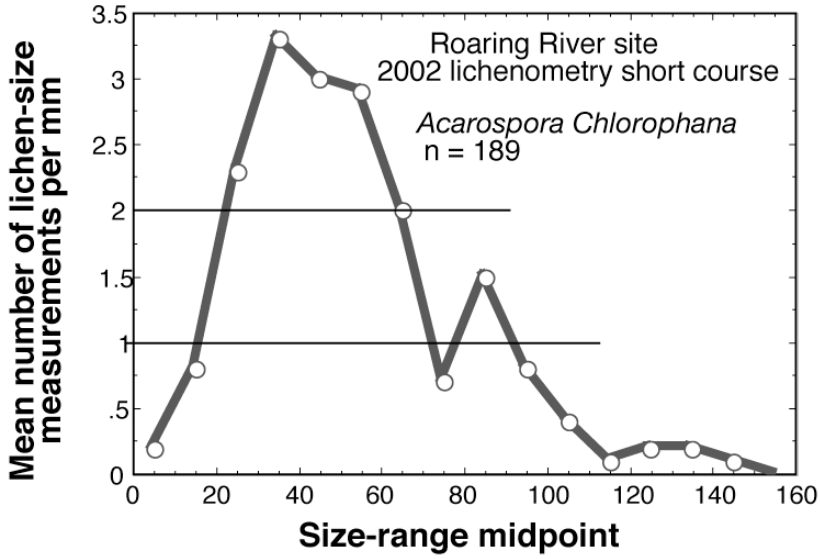

Figure 8-13. Variation of density of lichen-size measurements with sizes of *Acarospora chlorophana* measured by the 2002 lichenometry short-course participants at the Roaring River site.

The 2002 lichenometry short course results at the Roaring River lichenometry site fit the regional picture. Data density affects choice of class interval, or Gaussian kernel size, when defining lichen-size peaks. The 189 *Acarospora* measurements occur mainly between 20 and 60 mm (Fig. 8-13), which allows us to surmise that:
<1.0 lichen-size measurements/mm is pretty risky, so get more data
1 to 2 measurements/mm is OK if quality of lichen thalli is above average
>2 lichen-size measurements/mm is preferred

A class interval of 0.7 mm reveals nicely separated, prominent lichen-size peaks in the 35 to 65 mm size range where we had the greatest abundance of lichen-size measurements (Fig. 8-14A). As nice as these appear, we should ask "are these peaks real? " and “do these peaks record local or regional events?”. Peaks that match the dates for the Table 1 earthquakes have been flagged. We have fewer measurements of *Lecidea* (Fig. 8-14B), but enough to give results similar to those for the *Acarospora* data set. Note that both plots show the 1740 A. D. event generated by an earthquake on the Honey Lake fault and tree-ring dated at “The Slide” rock avalanche in Yosemite National Park.

CONCLUSIONS

The prospects for future lichenometry studies in the Sierra Nevada and elsewhere are exceptional. Future studies might address the following topics:

1. Assess the distribution and types of historical mass movements in the Sierra Nevada that have been triggered by local and distant earthquakes. This would complement the nice hazards work done by Wieczorek et al., 1992; Wieczorek and Stefan, 1996.
2. Evaluate rockfall abundance in different topographic and structural settings, in response to seismic waves generated by earthquakes east, south, and west of the Sierra Nevada.

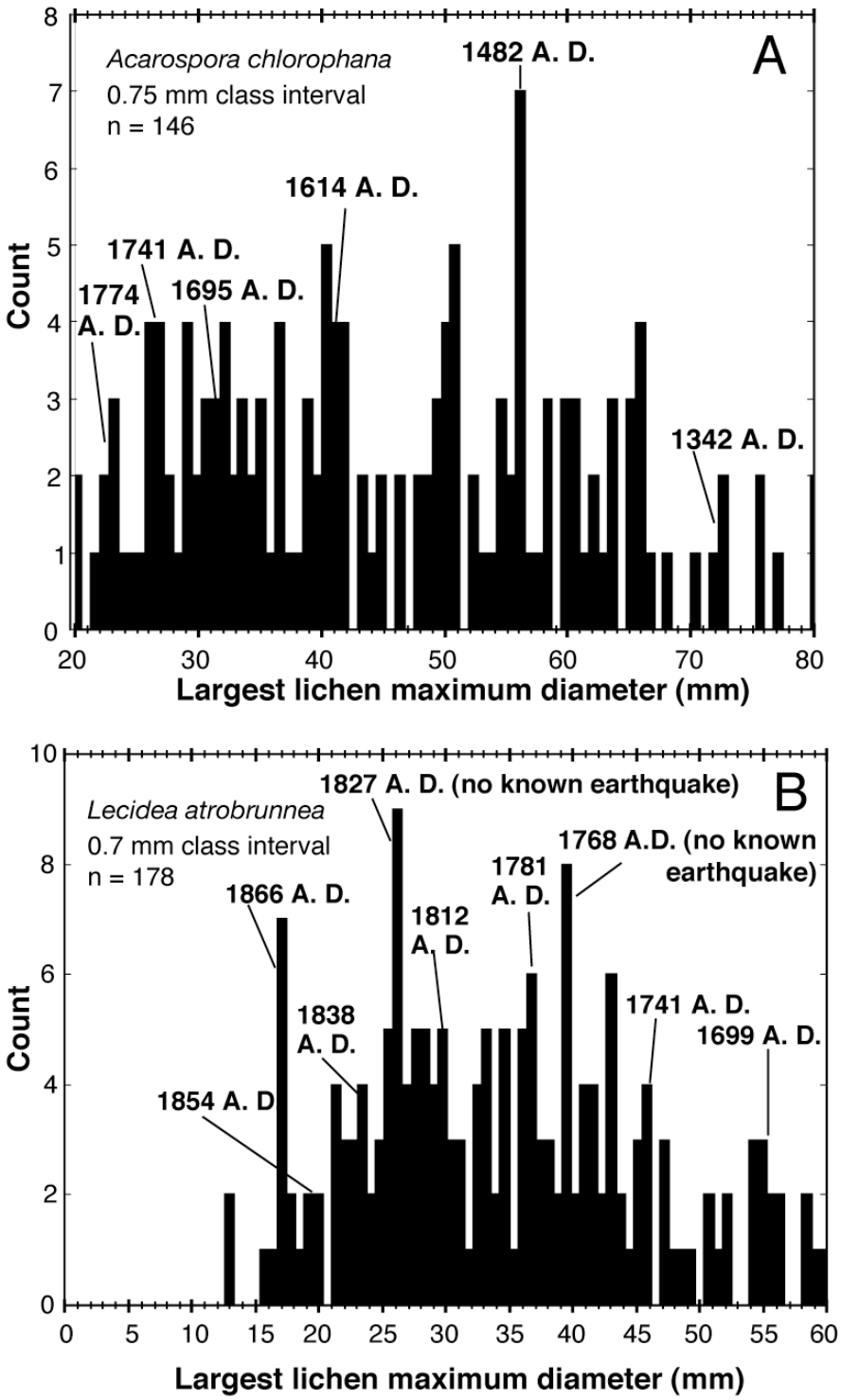

Figure 8-14. Distribution of largest lichen maximum diameters on rock-fall blocks at the Roaring River site, as measured by the 2002 lichenometry short-course participants. Lichenomtery age estimates that coincide with prehistorical San Andreas fault earthquakes are shown in bold font. Labeled peaks date to the earthquakes of Table 8-1.
A. *Acarospora chlorophana*
B. *Lecidea atrobrunnea*

3. Make seismic-shaking index maps to describe extent and intensity of regional rockfall events associated with historical earthquakes in order to better estimate approximate sizes of prehistorical earthquakes determined by similar maps. This study would address San Andreas fault as well as more local earthquakes. Maps indicative of seismic shaking patterns should reveal which lichen-size peaks for rockfall events record prehistorical earthquakes emanating from the adjacent Basin and Range Province.
4. Assess the intensity and duration of Little Ice Age snowkill events in different parts of the Sierra Nevada.

ACKNOWLEDGEMENTS

Financial support for this work was provided by the Geophysics and the Geology Programs of the U. S. National Science Foundation, the Royal Swedish Academy of Sciences, and the Swedish Environmental Protection Board. U. S. National Park Service personnel went out of their way to assist us in Sequoia Kings and Yosemite National Parks. Students and faculty from the University of California at Santa Barbara and the University of California at Santa Cruz measured the lichens at the 2002 lichenometry short course.

I thank Tim Blunt, Mark Brandon, Sara Brogaard, Jim Brune, Jonathan Davis, John King, Fanchen Kong, Tom Moutoux, Elise Pendall, Bill Phillips, Peter Schlyter, Nancy Sprague, Kirk Vincent, and Jeremy Webb for assistance in obtaining lichen-size measurements and analyzing them, for tree-ring studies at lichen-growth calibration sites, and for essential discussions regarding methods and results.

REFERENCES CITED

Adams, K. , Briggs, R., Bull, W., Brune, J., Granger, D., Ramelli A, Riebe, C, Sawyer, T. , Wakabayashi, J., and Wills, C., 2001, Guidebook to the northern Walker Lane and northeast Sierra Nevada: Friends of the Pleistocene Pacific Cell field trip, October 12-14, 2001.

Benedict, J. B., 1993, A 2000-year lichen-snowkill chronology for the Colorado Front Range, USA: The Holocene, v. 3, p. 27-33.

Bronson, B. R., and Watters, R. J., 1987: The effects of long term slope deformations on the stability of granitic rocks of the Sierra Nevada, California. Proceedings of the 23rd Symposium on Engineering Geology and Soils Engineering [Utah State University, Logan, Utah], p. 203-217.

Bull, W. B., 1996, Dating San Andreas fault earthquakes with lichenometry: Geology, v. 24, p. 111-114.

Bull, W. B., 2000 Lichenometry; A New Way of Dating and Locating Prehistorical Earthquakes: *in* Noller, J. S, Sowers, J. M., and Lettis, W. R., editors, Quaternary Geochronology: Methods and Applications; American Geophysical Union Reference Shelf Series, Vol. 4, 582 p.

Bull, W. B., and Brandon, M. T., 1998, Lichen dating of earthquake-generated regional rockfall events, Southern Alps, New Zealand": Geological Society of America Bulletin. v. 110, p. 60-84.

Bull, W. B., King, J. Kong, F. Moutoux, T., and Phillips, W. M, 1994, Lichen dating of coseismic landslide hazards in alpine mountains: Geomorphology, v. 10, p. 253-264.

Bull, W. B., Schlyter, P., and Brogaard, S., 1995, Lichenometric analysis of the Kaerkerieppe slush-avalanche fan, Kaerkevagge, Sweden: Geografiska Annaler, v. 77A, p. 231-240.

Burrows, C.J., Duncan, K.W., and Spence, J.R., 1990, Aranuian vegetation history of the Arrowsmith Range, Canterbury. II. Revised chronology for moraines of the Cameron Glacier: New Zealand Journal of Botany, v. 28, p. 455-466.

Chinn, T. J. H. 1981: Use of rock weathering-rind thickness for Holocene absolute age-dating in New Zealand: Arctic and Alpine research v. 13, p. 33–45.

Curry, R.R., 1969, Holocene climatic and glacial history of the central Sierra Nevada, California, *in* Geological Society of America Special Paper 123 (edited by S.A. Schumm and W.C. Bradley), p. 1-47.

Fumal, T., Pezzopane, S., Weldon, R., Schwartz, D., 1993, "A 100-Year Average Recurrence Interval for the San Andreas Fault at Wrightwood, California", Science, v. 259, p.199-203.

Ellsworth, W. L., 1990, Earthquake history, 1769-1989 *in* Wallace R. E. , ed.,The San Andreas fault system, California: U.S. Geological Survey Professional Paper 1515, p. 153-187.

Huber, N. K., Phillips, W. M., and Bull, W. B., 2002, The Slide, Yosemite National Park, CA, Yosemite Association, YOSEMITE, v. 64, no. 3, p. 2-4.

Innes, J. L., 1985, Lichenometry: Progress in Physical Geography, v. 9, p.187-254.

Keefer, D. K., 1984, Landslides caused by earthquakes: Geological Society of America Bulletin, v. 95, p. 406-421.

Keefer, D. K., 1994, The importance of earthquake-induced landslides to long term slope erosion and slope-failure hazards in seismically active regions: Geomorphology, v. 10, p. 265-284.

Locke, W. W., III, Andrews, J. T., and Webber, P. J., 1979, A manual for lichenometry: British Geomorphological Research Group Technical Bulletin 26, 47 p.

O'Neal, M. A., and Schoenenberger, K.B., 2003, A Rhizocarpon geographicum growth curve for the Cascade Range of Washington and Northern Oregon, USA: Quaternary Research, v. 60, p. 233-241.

Porter, S.C., 1981, Lichenometric studies in the Cascade Range of Washington; establishment of *Rhizocarpon geographicum* growth curves at Mount Rainier: Arctic and Alpine Research, v. 13, p. 11-23.

Sieh, K. E., Stuiver, M., and Brillinger, D., 1989, A more precise chronology of earthquakes produced by the San Andreas fault in southern California: Journal of Geophysical Research, v. 94, p. 603-623.

Toppozada, T. R., and Borchardt, G., 1998, Re-evaluation of the 1836 "Hayward Fault" and the 1838 San Andreas Fault Earthquakes: Bulletin of the Seismological Society of America,1998 v 88, n 1 , p. 140- ?

Wakabayashi, J., and Sawyer, T.L., 2000, Neotectonics of the Sierra Nevada and the Sierra Nevada-Basin and Range Transition, California, with field trip stop descriptions for the northeastern Sierra Nevada: in Brooks, E.R., and Dida, L.T., eds., Field guide to the geology and tectonics of the northern Sierra Nevada, California Division of Mines and Geology Special Publication 122, p. 173-212.

Wieczorek, G. F., and Jäger, Stefan, 1996, Triggering mechanisms and depositional rates of postglacial slope-movement processes in the Yosemite Valley, California: Geomorphology, v. 15, p. 17-31.

Wieczorek, G. F., Snyder, J. B., Alger, C. S. and Issaacson, K. A., 1992, Rock falls in Yosemite Valley, U. S. Geological Survey Open-File Report 92-387, 136 p.

APPENDIX 9A: A NOTE ON THE GLACIAL HISTORY OF THE SEQUOIA – KINGS CANYON NATIONAL PARKS REGION

Raymond "Bud" Burke *Humboldt State University, Arcata, CA*
rmb2@axe.humboldt.edu

INTRODUCTION

The glaciation of the Sierra Nevada was first recognized by the scientific community in 1863 when J. D. Whitney, the California State Geologist, noted in a letter that he observed glacial polish and moraines in Tuolumne Valley. Extensive studies have been ongoing since and there is still not agreement of the glacial history of the Sierra Nevada. By the 1970's the stratigraphic terminology presently in use had been fairly well established on the bases of relative dating and limited numerical ages. More recent work has focused on applying refined dating techniques in an effort to establish landform ages related to past glaciations. In the absence of adequate numerical age control, the efforts to establish a chronology related to former climatic variations has led many workers to attempt telecorrelations with the Marine Oxygen Isotope Stages (MIS) or even the ice core data from Greenland or Antarctica. However, efforts to correlate deposits from glaciations along the range, let alone across the range, continue to be extremely difficult. In the absence of any extensive recent work on the glacial chronology of the Sequoia - Kings Canyon National Parks region, we herein present a historical overview of work within the Sierra Nevada, a review of the confusing and clouded Sierra Nevada glacial chronology, and then present a review of regional work on the better known LGM and Holocene climate shifts.

HISTORICAL OVERVIEW

The prose of John Muir (1872, 1874, 1880) enthusiastically describe the role that prior glaciations had on the present topography, and his debates with J.D. Whitney over the various roles of glacial, fluvial, and tectonic processes in shaping the topography are quite famous. LeConte (1873) put Muir's verbiage into a more tempered description of the effects of glacial modification of a fluvially carved mountain block. Lawson (1904) first delineated the southern extend of Sierra Nevada glaciation in the Kern and Kaweah drainages less than 50 km to the south of the Kings River drainage.

The "modern" era of studies on the Sierra Nevada glacial history began in the 1930's with Eliot Blackwelder and Francois Matthes. While Blackwelder concentrated his research on the eastern slopes of the Sierra Nevada, Matthes worked mostly along the western slopes of the Sierra Nevada.

GLACIAL CHRONOLOGY

At present there are only a few cirque glaciers within the Sierra Nevada. However, there is ample evidence that there have been multiple advances of more extensive ice throughout the Pleistocene. The asymmetry of the Sierra Nevada mountain range, along with the orographic variation in precipitation created glaciers on the east side which were less than 20 km long while those on the west side were as much as 100 km in length (Wahrhaftig and Birman, 1965).

On the eastern slopes of the Sierra Nevada, W. D. Johnson (who had been a topographic surveyor for I.C. Russell) had delineated three distinct (2 young and 1 old) glacial advances by 1907, but died before publishing his findings. It was then Blackwelder who first published the stratigraphy of the eastern Sierra Nevada, working at the time that Francois Matthes was working on the western slopes of the Sierra Nevada. Matthes best-known work is the *Geologic History of Yosemite Valley* (Matthes, 1930) and it was in this publication that the first detailed mapping of Sierra Nevada glacial deposits appeared. After his Yosemite work, Matthes moved south to the San Joaquin and Sequoia-Kings regions. Both of these studies were published posthumously (Matthes, 1960; 1965) and his 1965 report remains the most complete study of the glacial history of the Sequoia-Kings region. Matthes recognized multiple Pleistocene glaciations and was the first to apply the term "Little Ice Age" to the reappearance of glaciers after late Wisconsin time. Matthes established a threefold sequence of pre Little Ice Age glaciation for the western slope: from youngest to oldest these were termed the Wisconsin, El Portal, and Glacier Point. The Wisconsin deposits were defined as well-developed lateral moraines with little-weathered bouldery surfaces. The El Portal was defined as bulky lateral moraines that are noticeably more weathered. The Glacier Point deposits are restricted to scattered erratics above the elevation of the two younger tills. Meanwhile, Blackwelder had defined the Tioga, Tahoe, Sherwin, and McGee glaciations on the eastern slopes of the Sierra Nevada. Although Matthes and Blackwelder could never personally agree on a correlation of glaciations across the Sierra Nevada crest, Blackwelder published his personal preference as the Wisconsin being equivalent to his Tioga and Tahoe, and the El Portal being equivalent to his Sherwin. Blackwelder further felt that the Glacier Point was not established on the eastern slopes, and that there was no evidence of the McGee on the western slopes (Blackwelder, 1931, p. 909).

The works of many investigators since Matthes and Blackwelder have advanced the idea of organizing the glacial events into alloformations. More recent efforts have attempted to supply numerical ages to these alloformations. Putnam (1949, 1962), Sharp and Birman (1963), Birkeland (1964), Birman (1964), Janda (1966), Curry (1968), Clark (1967), Sharp (1968, 1972), Burke and Birkeland (1979), Gillespie (1982), Phillips et al. (1990,1996), and Berry (1994) stand as ample evidence of the scrutiny that the Quaternary record of the Sierra Nevada has undergone. Most of these studies have relied to some degree upon relative dating techniques for the development of local stratigraphies.

The terminology of the Sierra Nevada glacial events remains confusing at best (see Clark et al., 2003), and while efforts to resolve the confusion are underway (Gillespie et al., 2003), solutions appear to be in the future. In addition, much of the Sierra Nevada glacial terminology has originated from deposits along the eastern slopes where most workers recognize at least the Tioga, Tenaya, Tahoe, Mono Basin, Sherwin, and pre-Sherwin (from youngest to oldest). Allan James, who is presently working on the glacial records of the Yuba and American Rivers, along the western Sierra Nevada slopes some 250-300 km to the north of the Kings River Drainage feels that glacial erosion features may be quite useful in the future interpretation of former glacial processes (James, 2003a).

He notes that unlike glacial features of the semi-arid eastern Sierra Nevada, glacial deposits of the western Sierra Nevada are often within deeply eroded valleys,

thickly forested, and difficult to locate (James, 2003b). James has accepted a practice of assigning local names to glaciations beyond the age of Tioga until better dating is available for correlation purposes. He finds two major glacial groups Tioga and pre-Tioga, but he cautions that their mapping methods force a "lumping " of glacial fluctuations and there may be a more detailed stratigraphy in the future. An addition to the Kings Canyon chronology came from Birman (in Wahrhaftig and Birman, 1965) who felt the floor of Kings canyon contained rather obscure moraines of Tenaya age while the Tioga deposits were confined to the higher portions of the canyons.

THE LATEST PLEISTOCENE AND HOLOCENE RECORD

Unlike the older glacial records of the Sierra Nevada, the latest Pleistocene (Tioga and Recess Peak glaciations) and Holocene (Little Ice Age or Matthes glaciation) records are fairly well constrained by numerical ages, and the extent of Tioga ice is well known (Fig. 9A-1). The Tioga glaciation is now thought to date from ca. 30 ka, and to have been gone from most of the Sierra Nevada by at least 14 ka (Phillips et al., 1996; Clark, 1995; Clark and Gillespie, 1997).

Birman (1964) initially defined the Recess Peak as Holocene in age. Lichen ages by Curry suggested there might be late Holocene (2 ka - 3 ka) deposits correlative with the Recess Peak. However, relative dating and radiocarbon dating by Yount et al. (1992) at the type locality suggested the Recess Peak was probably latest Pleistocene in age. Detailed studies by Clark (1995) and by Clark and Gillespie (1996) have demonstrated that the Recess Peak ended before ~13,100 cal. Years B.P. Their efforts included 23 high-precision AMS dates from 3 different bogs along the Sierra Nevada crest.

The "Little Ice Age" glaciation within the Sierra Nevada is now named for Matthes and is well constrained by tephra dating and ^{14}C ages as being less than ~ 650 cal. Years B.P. Clark (1995) makes a good case that the only Holocene glaciations within at least part of the Sierra Nevada are Matthes in age.

Clark (1995) Clark and Gillespie (1997) further provide an estimate of climate change for the Tioga, Recess Peak, and Matthes glaciations. Along a transect from Olancha peak in the south to Lake Tahoe in the north (a distance of about 400 km), they have calculated the past Equilibrium Line Altitudes (ELA) for each of these glaciations. The ELA gradient is shown for the 400 km profile along the crest of the Sierra Nevada (figure 5 of Clark and Gillespie, 1997) and is about 100 m lower to the north. The average depression of the ELA is about 900m during Tioga time (Clark et al., 2003), but is a few hundred meters lower at Armstrong Canyon opposite the headwaters of the Kings River gorge. The ELA depression of the Recess Peak and the Matthes was about 20% and 10% of the Tioga depression.

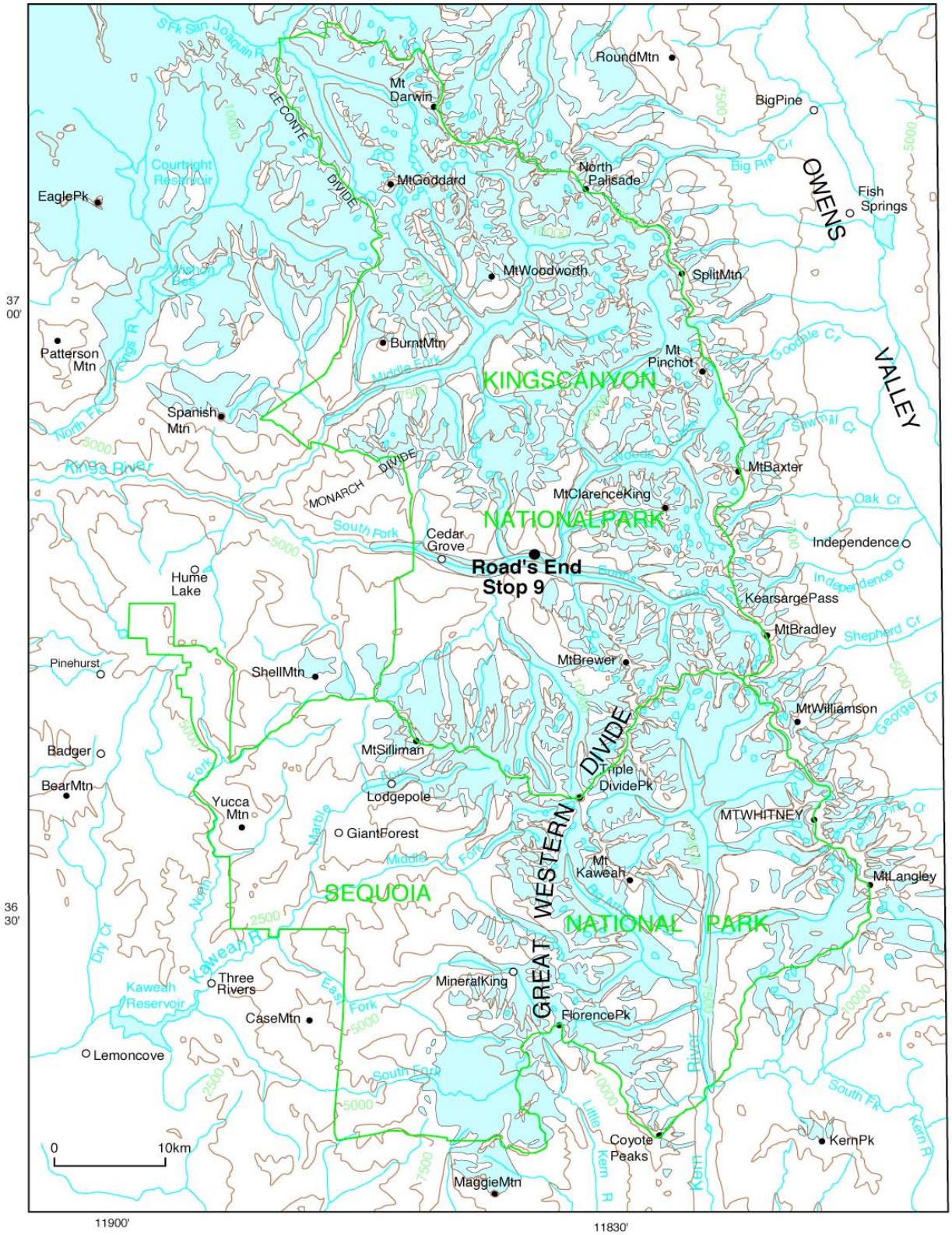

Figure 9A-1. Map of maximum extent of Tioga ice (ca. 30-14 ka) in the southern Sierra Nevada. Modified from Moore (2000), courtesy of NPS.

REFERENCES CITED

Bateman, P.C., and Wahrhaftig, C., 1966, Geology of the Sierra Nevada, pp. 107-172, *in* Geology of Northern California, Calif. Div. Mines and Geology, Bull. 190.

Birkeland, P.W., 1964, Pleistocene glaciation of the northern Sierra Nevada, north of Lake Tahoe, California, Journal of Geology, v. 72, p. 810-825.

Berry, M.E., 1994, Soil-geomorphic analysis of late-Pleistocene glacial sequences in the McGee, Pine, and Bishop creek drainages, east-central Sierra Nevada, California, Quaternary Research, v. 42, p. 49-59.

Birman, J.H., 1964, Glacial geology across the crest of the Sierra Nevada, Geological Society of America Special Paper 75, 80 p.

Blackwelder, Eliot, 1931, Pleistocene glaciation in the Sierra Nevada and the Basin Ranges, Geological Society of America Bulletin, v. 42, p. 865-922.

Burke R.M., and Birkeland, P. W., 1979, Re-evaluation of multiparameter relative dating techniques, and their application to the glacial sequence along the eastern escarpment of the Sierra Nevada, California: Quaternary Research, v. 11, p. 21-51.

Clark, D. H., 1995, Extent, timing, and climatic significance of latest Pleistocene and Holocene glaciation in the Sierra Nevada: Ph.D. thesis, University of Washington, Seattle, WA, 193 p.

Clark, D. H., and Gillespie, A.R., 1997, Timing and significance of late-glacial and Holocene cirque glaciation in the Sierra Nevada, California: Quaternary International, v. 38/39, p.21-38.

Clark, D., Gillespie, A.R., Clark, M., Burke, R.M., 2003, Mountain glaciations of the Sierra Nevada, *in*, D.J. Easterbrook ed., Quaternary Geology of the United States, INQUA 2003 Field Guide Volume, XVI INQUA Congress, Reno, NV: Desert Research Institute, p. 287-311.

Clark, M. M., 1967, Pleistocene glaciation of the drainage of the West Walker River, Sierra Nevada, California: Ph.D. thesis, Stanford University, Stanford, CA, 170 p.

Curry, R.R., 1968, Quaternary climatic and glacial history of the Sierra Nevada, California: Ph.D. thesis, University of California, Berkeley, CA, 107 p.

Curry, R.R., 1969, Holocene Climate and glacial history of the central Sierra Nevada, California, *In* Schumm, S.A., and Bradley, W. C. (eds), United States Contributions to Quaternary Research, Geological Society of America Special Paper 123, p. 1-47.

Gillespie, A.R., 1982, Quaternary Glaciation and Tectonism in the Southeastern Sierra Nevada, Inyo County, California: Ph.D. thesis, Caltech, Pasadena, CA., 695 p.

Gillespie, A.R., Porter, S.C.., Atwater, B.F., in press, 2003, The Quaternary Period in the United States, Developments in Quaternary Science, v. 1.

Janda, R. J., 1966, Pleistocene history and hydrology of the San Joaquin River, California: Ph.D. thesis, University of California, Berkeley, University Microfilms, Inc., no. 67-5086, Ann Arbor Michigan, 425 p.

James, A. L., 2003a, Glacially eroded landforms in the Northwestern Sierra Nevada, California, XVI INQUA Congress, International Quaternary Association, Programs with Abstracts, Reno, Nevada, USA, p. 115.

James, A. L., 2003b, Late Pleistocene Glaciations in the Northwestern Sierra Nevada, Field Trip Guide and Road Log, XVI INQUA Congress, International Quaternary Association, Reno, Nevada, USA, 15 p.

Lawson, A.C., 1904, The geomorphology of the upper Kern Basin, University of California Department, Geological Science Bulletin, v. 3., p. 291-376.

LeConte, J., 1873, On some of the ancient glaciers of the Sierra: American Journal of Science, 3rd series, v. 5, p. 325-339.

Matthes, F., 1930 Geologic history of the Yosemite Valley: U.S. Geological history of the Yosemite Valley: U.S. Geological Professional Paper 504-Am p. A1-A-58.

Matthes, F.E., 1960, Reconnaissance of the geomorphology and glacial geology of the San Joaquin basin, Sierra Nevada, California: U.S. Geological Survey Professional Paper 329, 62 p.

Matthes, F.E., 1965, Glacial Reconnaissance of Sequoia National Park, California: U.S. Geological Survey Professional Paper 504-A, 58 p.

Muir, John, 1872, Living glaciers of California, Overland, v. 9, p. 547-579.

Muir, John, 1874, Studies in the Sierra: Overland, v. 12, p. 393-403, 489-500; v. 13, p.67-79, 174-184, 393-401, 530-540; v. 14, p. 64-73.

Muir, John, 1880, Ancient glaciers of the Sierra: California, v. 2, p. 550-557.

Phillips, F.M., Zreda, M.G., Smith, S.S., Elmore, D., Kubick, P.W., and Sharma, P, 1990, Cosmogenic chlorine-36 chronology for glacial deposits at Bloody Canyon, eastern Sierra Nevada: Science, v. 248, p. 1529-1532.

Phillips, F.M., Zreda, M. G., Benson, L.V., Plummer, M.A., Elmore, D., Sharma, P., 1996, Chronology for fluctuations in late Pleistocene Sierra Nevada glaciers: Science, v. 274, no. 5288, p. 749-751.

Putnam, W.C., 1949, Quaternary geology of the June Lake district, California: Geological Society of America Bulletin, v. 60, p. 1281-1302.

Putnam, W.C., 1962, Late Cenozoic geology of McGee Mountain, Mono County, California: University of California Publications, Geological Science, v. 40, p. 181-218.

Sharp, R. P., 1968, Sherwin Till-Bishop Tuff relationship, Sierra Nevada, California: Geological Society of America Bulletin, v. 79, p. 351-364.

Sharp, R.P., 1972, Pleistocene glaciation, Bridgeport Basin: Geological Society of America Bulletin, v. 83, p. 2233-2260.

Sharp, R. P., and Birman, J.H., 1963, Additions to the classical sequence of Pleistocene glaciations, Sierra Nevada, California, Geological Society of America Bulletin, v. 74, p. 1079-1086..

Wahrhaftig, Clyde, and Birman, J.H., 1965, The Quaternary of the Pacific mountain system in California *in* Wright, H. E., Jr., and Frey, D. G., eds., The Quaternary of the United States: Princeton, Princeton University Press, p. 299-340.

Yount, J.C., Birkeland, P.W., and Burke, R.M., 1982, Holocene glaciation Mono Creek, central Sierra Nevada, California: Geological Society of America Abstracts with Program, v. 14, p. 246.

APPENDIX 9B: SPELEOTHEM RECORDS OF GLACIAL-INTERGLACIAL TRANSITIONS IN THE SIERRA NEVADA

Greg Stock *University of California, Santa Cruz, Santa Cruz, CA 95060*
gstock@es.ucsc.edu
James Zachos *University of California, Santa Cruz, Santa Cruz, CA 95060*
jzachos@es.ucsc.edu

INTRODUCTION

As discussed in Appendix 9A, the nature and timing of Pleistocene glaciations in the Sierra Nevada, and the coincidence of these events with globally-recognized climate events, remains an open question. Much effort has been made to correlate the observed events, most obviously recorded in glacial moraines, with recognized global climate events (e.g., Phillips et al., 1996; Benson et al., 1997), but the suggested correlations remain controversial primarily because of inadequate age control. Although a number of dating methods have been applied to glacial deposits (e.g. K/Ar dates on lava flows within till [Dalyrmple, 1964], ^{14}C dating of organic moraine debris and lake sediments [Clark and Gillespie, 1997], and cosmogenic ^{36}Cl dating [Phillips et al.,1996]), precise ages on glacial events in the Sierra remain elusive.

Of the potential terrestrial climate archives, speleothems (cave calcite deposits) show great promise for resolving decadal to millennial frequency climate variability over the late Pleistocene and Holocene (e.g., McDermott et al., 2001). Climate indicators such as temperature, precipitation, vegetation change, and soil productivity may be derived from geochemical studies of these deposits (e.g., Gascoyne, 1992; Dorale et al., 1992; Musgrove et al., 2001). As such, they are potential archives of climate change associated with glacial-interglacial transitions. Speleothems occupy an important niche in paleoclimate records for several reasons: 1) they are often continuously deposited, 2) they preserve records over long periods of the Quaternary, and 3) they may be precisely dated by mass spectrometric $^{234}U/^{230}Th$ dating.

We are presently investigating four speleothems from the central and southern Sierra Nevada using stable isotopes, trace element concentrations, and $^{234}U/^{230}Th$ dating (Fig. 9B-1). We present here new age and stable isotope data for these samples. Though still underway, this research suggests that these speleothems record glacial-interglacial transitions, potentially offering a means of precisely dating some of the late Pleistocene glacial events in the Sierra Nevada.

SPELEOTHEM STABLE ISOTOPES AS PALEOCLIMATE PROXIES

The oxygen isotope composition of speleothem calcite ($\delta^{18}O_c$) is a function of both cave temperature and of the isotopic composition of precipitation. $\delta^{18}O_c$ variations are therefore linked to changes in surface temperature through the average $d\delta^{18}O_p/dT$ relation in modern precipitation (~0.6‰ °C^{-1}; Dansgaard, 1964), and the water-calcite fractionation that accompanies speleothem deposition (~-0.24‰ °C^{-1}; Friedman and O'Neil, 1977). Speleothem $\delta^{18}O_c$ is therefore a product of two distinct signals: temperature and precipitation (this is not unlike the combination of temperature and ice

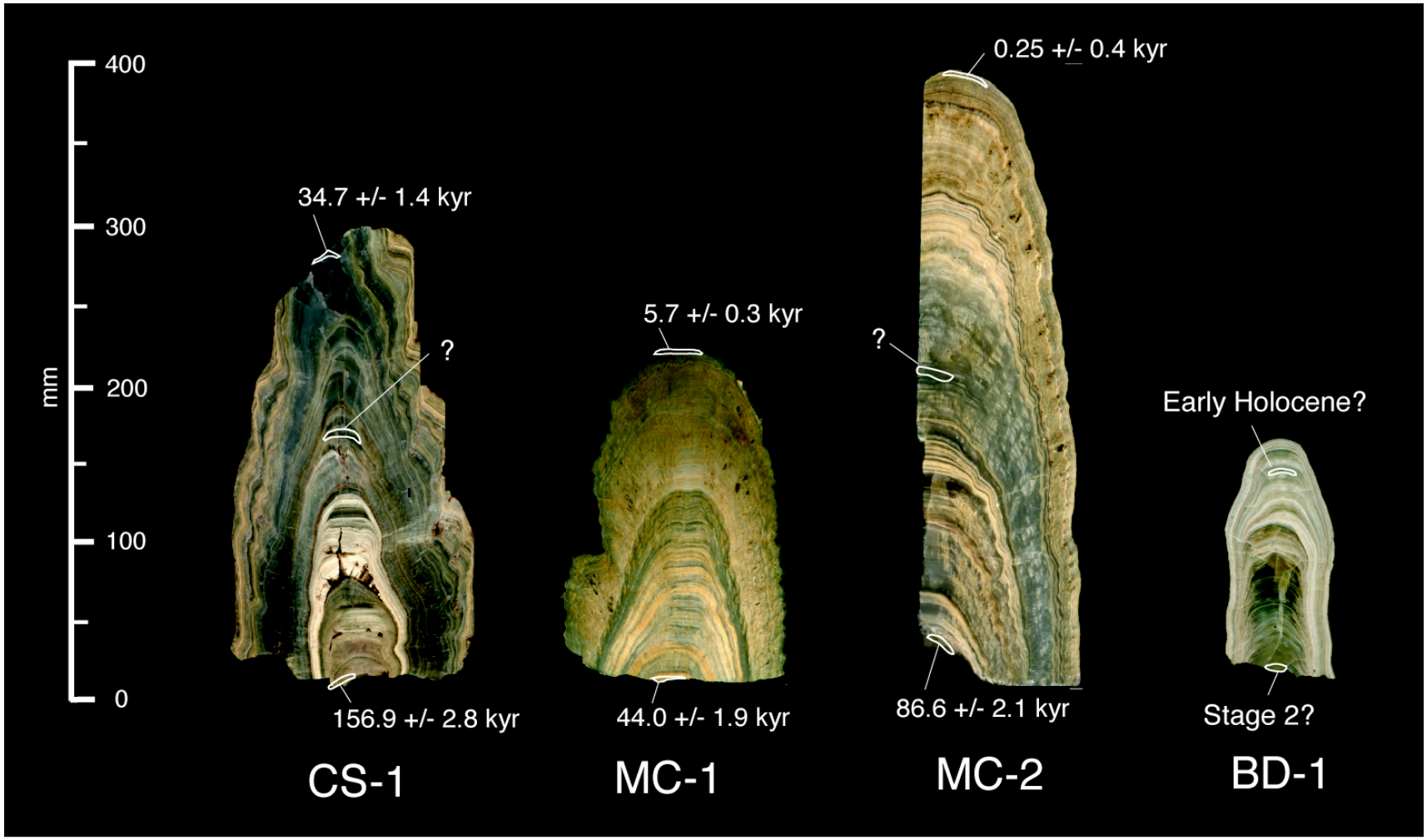

Figure 9B-1. Sierra Nevada speleothems used to investigate late Pleistocene glacial-interglacial transitions. Samples show considerable variation in color and growth band thickness, likely relating to growth rate changes which scale with amounts of precipitation falling on the surface above the cave. Samples for stable isotope analyses were taken at 1 mm intervals. $^{234}U/^{230}Th$ ages demonstrate that collectively the four samples cover the last ~157 kyr. Question marks indicate samples currently in prep; data may be available by field trip time. Estimates for age of sample BD-1 based on stable isotope profile.

volume recorded in the $\delta^{18}O$ of foraminifera in ocean sediment cores, though in the case of speleothems the two effects have opposite polarities). However, changes in depositional conditions, and in the amount and $\delta^{18}O$ of precipitation ($\delta^{18}O_p$), also influence the $\delta^{18}O_c$, and in some situations may obscure the temperature-controlled signal. Direct paleotemperature calculations from $\delta^{18}O_c$ variations is therefore questionable. However, $\delta^{18}O_c$ and growth rate records from multiple samples may potentially be used to isolate the precipitation amount effect, deconvolving the temperature and precipitation signals .

The carbon isotope composition of speleothem calcite ($\delta^{13}C_c$) is thought to primarily reflect the $\delta^{13}C$ values of soil CO_2, as well as the partial pressure of CO_2 in solution (Gascoyne, 1992). Both vary as a function of soil respiration rates (Quade et al., 1989). Variations in $\delta^{13}C_c$ values are also generally indicative of surface vegetation types present during speleothem deposition, defined by vegetation utilizing either C_3 or C_4 photosynthetic pathways (e.g., Dorale et al., 1992). There is an additional isotopic contribution from the carbonate bedrock (~2‰ for Sierra Nevada marble).

CAVE MICROCLIMATES

$\delta^{18}O$ and $\delta^{13}C$ signals of meteoric water are most accurately preserved in a speleothem if isotopic equilibrium is achieved between water and dissolved calcite prior to CO_2 degassing, and if evaporation does not occur during deposition. Cave passages with seasonally stable interior temperatures, high relative humidity (>90%), and minimal airflow favor isotopic equilibrium (Gascoyne, 1992). Deep caves with minimal airflow are generally thought to maintain temperatures approximating the mean annual surface temperature (Wigley and Brown, 1971; Gascoyne, 1992). Although buffered significantly from day-to-day changes in temperature and humidity, cave environments are conceivably subject to seasonal fluctuations that may affect the isotopic composition of calcite during speleothem deposition.

In an effort to document fluctuations in cave microclimates over a seasonal cycle, we installed ten temperature/humidity data loggers in caves throughout the Sierra Nevada. Deployment sites were specifically chosen to evaluate seasonal fluctuations in both deep and shallow conditions with variable airflow. Measurements were taken every four hours, and collected after one year. Most caves reveal remarkably stable microclimates, particularly when compared with surface fluctuations from temperature loggers placed on the surface above the caves (Fig. 9B-1). These results demonstrate the general stability of cave microclimates, verify the assumption that cave temperatures reflect the mean annual surface temperature, and imply that evaporative effects during speleothem deposition may be limited due to high relative humidity within the caves (95-100%). We therefore expect limited kinetic effects. However, preliminary dripwater analyses indicate that the modern cave climates are not free of kinetic fractionation. We have therefore adopted a semi-quantitative approach to these speleothem studies; we use the stable isotope profiles and a conceptual model of isotope variation over glacial-interglacial cycles to interpret the paleoclimate record, and then date these transitions with highly accurate and precise $^{234}U/^{230}Th$ dating.

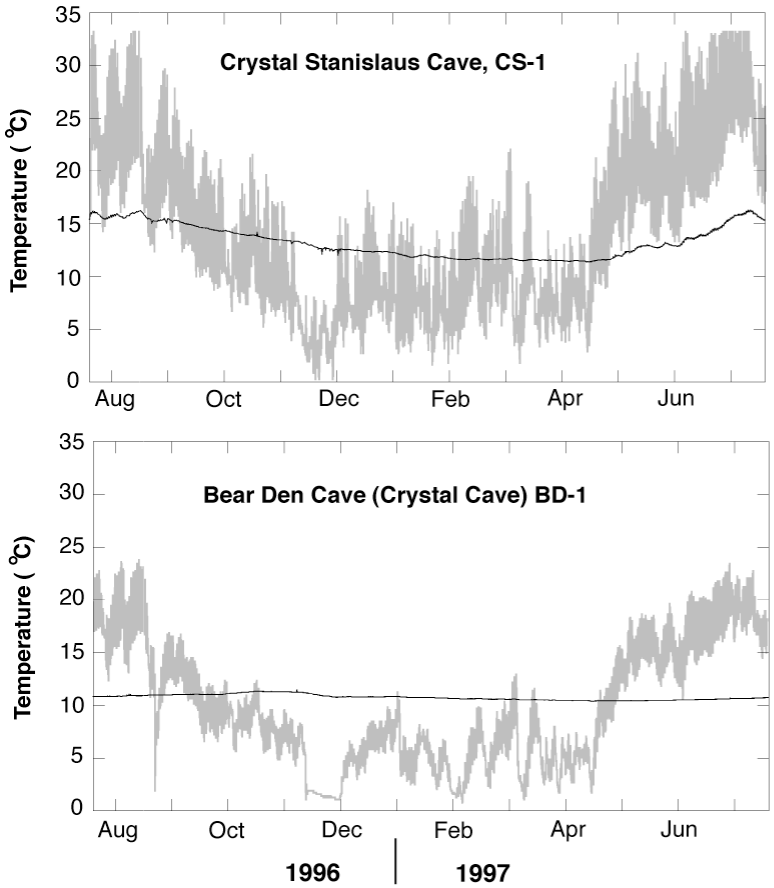

Figure 9B-2. Microclimate data for two Sierra Nevada caves from which speleothem paleoclimate records have been obtained. Surface and cave temperatures were collected for one year (summer 2002-summer 2003). Surface temperatures above the caves are shown in gray, and cave temperatures are shown in black. Both caves show minimal response to seasonal temperature fluctuations. Crystal Stanislaus Cave has two entrances, leading to greater variation than Bear Den Cave, which only has one. The temperature measurements also support the notion that cave temperatures approximate mean annual surface temperatures.

CONCEPTUAL MODEL OF THE EFFECTS OF GLACIAL CYCLES ON SIERRA NEVADA SPELEOTHEMS

California climate is characterized by a pronounced north-south climate gradient. The central California boundary between the wet, cool Pacific Northwest climate regime and the warm, dry Mediterranean climate regime is prone to latitudinal shifts with changes in climate boundary conditions. For instance, climate models of the LGM indicate a southward shift of the jet stream and mid-latitude storms due to expansion of the Laurentide ice sheet and mountain glaciers, resulting in precipitation increases over much of western North America (Bartlein et al., 1998). This concept is supported by the ages of pluvial lake highstands from the Basin and Range (e.g., Benson, 1991) and by mass-balance modeling of Sierra Nevada glaciers (Hostetler and Clark, 1997). It is also consistent with speleothem records from the southwestern U.S. (Musgrove et al., 2001).

During glacial periods, cave dripwater would likely have lower (more negative) $\delta^{18}O_c$, resulting both from the increase in precipitation amount (e.g. Ayalon et al., 1998) and from the reduction in mean air temperature. The shift toward lighter isotope values would be amplified by a reduction in evaporation due to increased year-round humidity in the caves. Conversely, during interglacial periods, warmer air temperatures, reduced precipitation, and lowered cave humidity would tend to increase $\delta^{18}O_c$. Carbon isotopes, though more complex, ought to show similar shifts. Soil productivity is highly dependent

on precipitation amounts, and so increases in precipitation ought to shift $\delta^{13}C$ values toward lighter values.

STABLE ISOTOPE RECORDS

Figure 9B-3 shows complete stable isotope profiles for three Sierra Nevada samples (BD-1, MC-1, and BD-1). Age constraint for these samples is presently limited, so stable isotopes are shown as a function of distance from the tip of each speleothem. Note that distance is a proxy for age, though age and distance are not linearly related due to expected changes in growth rates.

Both $\delta^{18}O$ and $\delta^{13}C$ values in these speleothems appear to show glacial-interglacial patterns, with low values ($\delta^{18}O$ ~-10.5‰) apparently occurring during glacial stages, and high values ($\delta^{18}O$ ~-5.5‰) apparently occurring during interglacials (Fig. 9B-3). These patterns fit the conceptual model sketched out above.

Specifically, sample MC-2, whose age is bracketed at ~86 to 0.2 ka, shows an increase in $\delta^{18}O$ values from ~-10‰ near the base and throughout much of its length to ~ 6‰ toward the tip. This values matches well the modern cave calcite values of –5 to –6‰ (Fig. 9B-3). As outlined above, we interpret this shift as representing a warming and/or drying trend in the Holocene. A peak in the trend toward isotopically heavier values may relate to the mid-Holocene warm period. Sample BD-1, thought to represent the LGM and early Holocene, shows a similar pattern.

Perhaps the most compelling record comes from sample CS-1, whose age is bracketed to be ~157 to ~34 ka (Fig. 9B-1). As such, the basal portion of this sample should preserve isotope substage 5e, the previous interglacial and the most recent time in which temperatures were warmer and sea level higher than at present. In fact, slightly above the base of sample CS-1, isotope values are similar to, or slighter heavier than, those interpreted in other samples as Holocene values (Figure 9B-3). After attaining these heavy values, indicative of warm and/or dry periods, the $\delta^{18}O$ record for sample CS-1 falls toward lighter values in a stairstep pattern reminiscent of global records (Fig. 9B-3). For the remainder of the record, $\delta^{18}O$ values are relatively low (~-9.5), indicating relatively cooler and/or wetter conditions, as we would expect for isotope stages 2 and 4. These values are nearly identical to presumed glacial values from the other two samples.

The 5‰ shift in $\delta^{18}O$ between glacial and interglacial times would require temperature changes of 14°C, an unlikely scenario. We therefore attribute the shift to both decreased air temperatures and increased precipitation amounts during glacials, a combination ultimately lowering the $\delta^{18}O$ of cave dripwater. In addition, speleothem growth rates appear to slow during interglacials and accelerate during glacials. Thinner, opaque growth bands are found nearer the tip (Holocene) and base (isotope substage 5e) of the samples, while thicker, more translucent bands are found throughout the remaining portions (Last Glacial Maximum and stage 3 and 4) (Fig. 9A-1). This suggests higher precipitation in the Sierra Nevada during glacial periods, and indicates that the isotope profiles are compressed during interglacials with respect to time, and expanded during glacials. $^{234}U/^{230}Th$ dating of growth bands will ultimately provide age models for these speleothem and rescale the isotope profiles shown here.

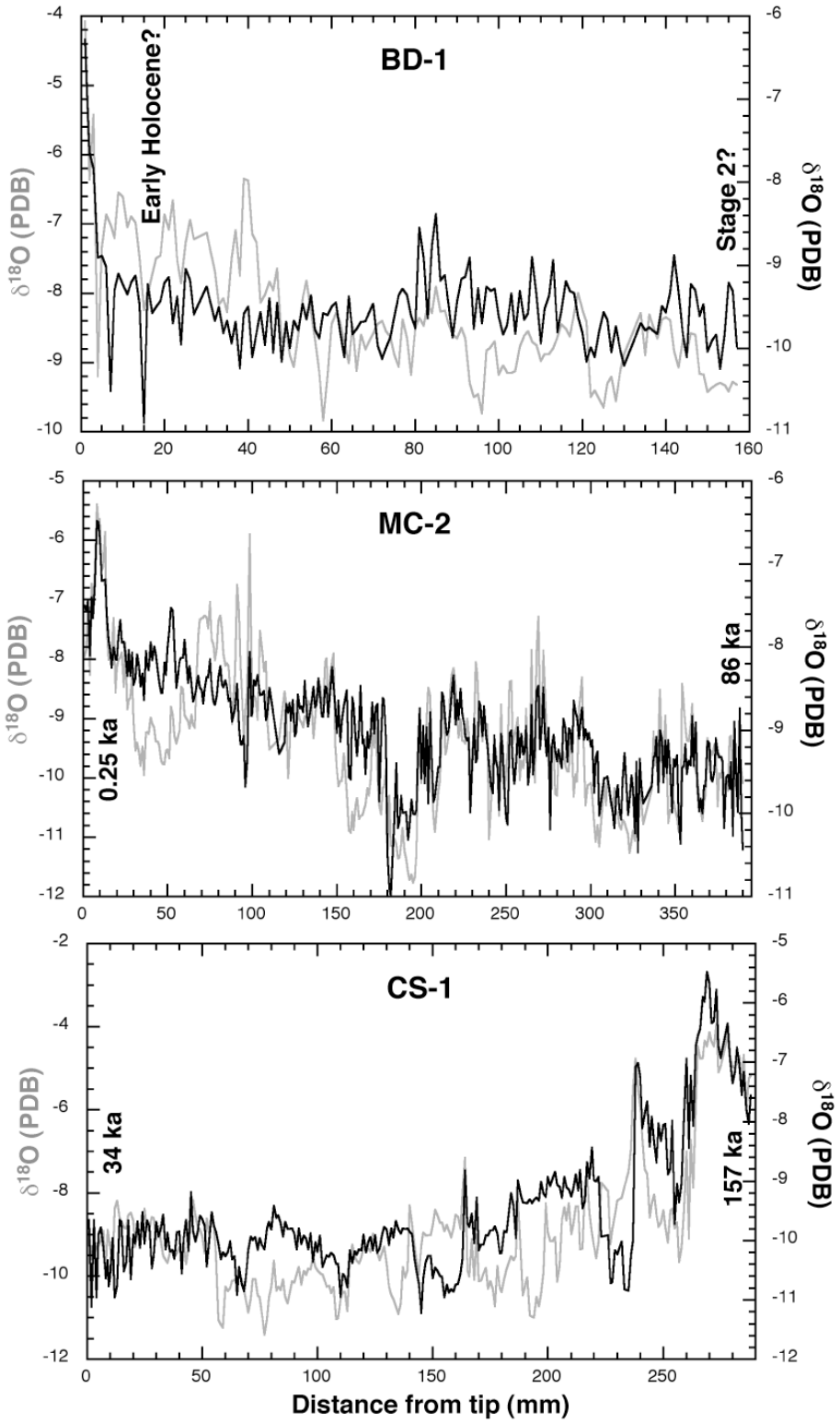

Figure 9B-3. Stable isotope values for three Sierra Nevada speleothems as a function of distance from the tip. $\delta^{18}O$ values are shown in black, and $\delta^{13}C$ values in gray. Isotopically heavy (less negative) values near the tips of samples BD-1 and MC-2 and near the base of sample CS-1 are interpreted to represent interglacial values, while isotopically light (more negative) values are intepreted to represent glacial values. $^{234}U/^{230}Th$ ages are provided where available.

CONCLUSIONS

Similar isotope values and growth trends preserved in several speleothems from across the Sierra Nevada lead us to believe that the speleothems record regional climate change. We attribute large shifts in speleothem $\delta^{18}O$ to changes in both temperature and precipitation amount, and similar shifts in $\delta^{13}C$ to changes in soil productivity and drip rate. Qualitative growth rate observations and preliminary $^{234}U/^{230}Th$ ages suggest that changes in growth rates and stable isotope values reflect cooler and wetter climates during glacial periods and warmer and dryer climates during interglacials. Identified transition periods of $\delta^{18}O$ values may be precisely dated using $^{230}Th/^{234}U$, potentially providing robust age constraint on the timing of glacial maxima and glacial-interglacial transitions in the Sierra Nevada. This dating is currently underway.

REFERENCES CITED

Ayalon, Avner, Bar-Matthews, Miryam, and Sass, Eytan, 1998, Rainfall-recharge relationships within a karstic terrain in the Eastern Mediterranean semi-arid region, Israel: $d^{18}O$ and dD characteristics: Journal of Hydrology, v. 207, p. 18-31

Bartlein, P.J., Anderson, K.H., Anderson, P.M., Edwards, M.E., Mock, C.J., Thompson, R.S., Webb, R.S., Webb III, T., and Whitlock, C., 1998, Paleoclimate simulations for North America over the past 21,000 years: Features of the simulated climate and comparisons with paleoenvironmental data: Quaternary Science Reviews, v. 17, p. 549-585.

Benson, L.V., Burdett, J.W., Lund, S., Kashgarian, M., and Mensing, S., 1997, Nearly synchronous climate change in the Northern Hemisphere during the last glacial termination: Nature, v. 388, p. 263-265

Clark, D.H., and Gillespie, A.R., 1997, Timing and significance of Late-Glacial and Holocene cirque glaciation in the Sierra Nevada, California: Quaternary International, v. 38/39, p. 21-38.

Dansgaard, W., Stable isotopes in precipitation: Tellus, v. 16, p. 436-468.

Dorale, J.A., Gonzalez, L.A., Reagan, M.K., Pickett, D.A., Murrell, M.T., and Baker, R.G., 1992, A high resolution record of Holocene climate change in speleothem calcite from Cold Water Cave, northeast Iowa: Science, v. 258, p. 1626-1630.

Friedman, I., and O'Neil, J.R., 1977, Compilation of stable isotope fractionation factors of geochemical interest: U.S. Geological Survey Professional Paper P-0440-KK, 1-12.

Gascoyne, M., 1992, Paleoclimate determination from cave calcite deposits: Quaternary Science Reviews, vol. 11, p. 609-632

Hostetler, S.W., and Clark, P.U., 1997, Climatic controls of Western U.S. Glaciers at the Last Glacial Maximum: Quaternary Science Reviews, v. 16, p. 505-511.

Ingraham, N.L., and Taylor, B.E., 1991, Light stable isotope systematics of large-scale hydrologic regimes in California and Nevada: Water Resources Research, v. 27, no. 1, p. 77-90.

McDermott, F., Mattey, D.P., and Hawkesworth, C., 2001, Centennial-scale Holocene climate variability revealed by a high-resolution speleothem $\delta^{18}O$ record from SW Ireland: Science, v. 294, p. 1328-1331.

Musgrove, M., Banner, J.L., Mack, L.E., Combs, D.M., James, E.W., Cheng, H., and Edwards, R.L., 2001, Geochronology of late Pleistocene to Holocene speleothems from central Texas: Implications for regional paleoclimate: Geological Society of America Bulletin, v. 113, p. 1532-1543

Phillips, F.M., Zreda, M.G., Benson, L.V., Plummer, M.A., Elmore, D., and Sharma, P., 1996, Chronology for fluctuations in Late Pleistocene Sierra Nevada glaciers and lakes: Science, v. 274, p. 749-751.

Quade, J., Cerling, T.E., and Bowman, J.R., 1989, Systematic variations in the carbon and oxygen isotopic compositions of pedogenic carbonate along elevation transects in the southern Great Basin, United States: Geological Society of America Bulletin, v. 101, p. 464-475.

Wigley, T.M.L., and Brown, M.C., 1971, Geophysical applications of heat and mass transfer in turbulent pipe flow: Boundary Layer Meterology, v. 1, p. 300-320.

APPENDIX 10: BURIED TOPOGRAPHY AND LACK OF TERTIARY STRATA IN THE SOUTHERN SIERRA NEVADA FOOTHILLS

Greg Stock *University of California, Santa Cruz, Santa Cruz, CA 95060*
gstock@es.ucsc.edu

INTRODUCTION

This final stop of the 2003 FOP field trip is in a peculiar southwestern foothills setting east of Fresno. The Sierra Nevada foothills mark the transition from the Central Valley to the Sierra Nevada. For over 300 km between latitude ~37° and ~40°N, the western foothills display a remarkably consistent stratigraphic and geomorphic expression. In this region, predominantly Tertiary age sediments rest unconformably on Sierra Nevada basement rocks and dip gently westward underneath Quaternary alluvium of the Central Valley. However, in the southwestern foothills, in the vicinity of the Kings and Kaweah rivers, this situation changes significantly. Here, Tertiary sediments are not exposed, and instead Quaternary alluvium surrounds isolated basement outcrops, suggesting bedrock topography buried by recent sedimentation.

This stop serves to highlight the buried topography, distinct in the Sierra foothills, and to review proposed explanations for this anomalous topography. I want to emphasize that these explanations are fundamentally the work of others, primarily Jason Saleeby and his colleagues. As they have recently proposed, the southwestern foothills may well be in the midst of a dynamic crustal drawdown relating to an upper mantle "drip" structure imaged beneath the southwestern Sierra Nevada and southern San Joaquin valley (Saleeby et al., 2003; Foster and Saleeby, 2003).

STRATIGRAPHIC AND GEOMORPHIC SETTING

The shift in the stratigraphic and geomorphic setting of the western foothills from north to south is best expressed in the setting of the Superjacent Series (Bateman and Wahrhaftig, 1966). The Superjacent Series consists of widespread, predominantly Tertiary age strata that lie unconformably on metamorphic and granitic basement rocks. Between latitudes ~37° and ~40°N the Superjacent Series dips gently westward off the basement, with increasing dip of the strata with age, reflecting basin subsidence to the west in concert with crestal uplift of the Sierra Nevada (Unruh, 1991). Eventually, Superjacent Series strata dip beneath overlapping Quaternary alluvium of the Central Valley. Except for major river drainages, the locus of Quaternary sedimentation above the Superjacent Series between ~37° and ~40°N starts about one-third of the distance across the Central Valley (Fig. 10-1; Jennings, 1977).

The stratigraphic and geomorphic expression of the western Sierra Nevada foothills change dramatically south of latitude ~37°N (Fig. 10-1). Here, Tertiary strata of the Superjacent Series are not exposed, and Quaternary alluvium extends much further eastward, lapping up onto basement exposures. Subsurface data for the southeastern San Joaquin Valley show that the Tertiary strata of the Superjacent Series lie buried beneath these sediments (Bartow, 1991). This indicates that the hingeline about which the Sierra Nevada moves relative to the Central Valley is shifted eastward in this region. South of

the Tule River, Superjacent Series strata are again exposed on the surface, and the stratigraphic and geomorphic setting resembles that to the north (Jennings, 1977).

The eastward encroachment of Quaternary alluvium into the southwestern foothills is accompanied by apparently "buried" topography of the southwestern foothills, seen most extensively in the vicinity of the outlets of the Kings and Kaweah rivers. Basement rocks, primarily granitic in composition, extend out into the San Joaquin Valley as large, isolated hills and ridges surrounded by Quaternary alluvium (Fig 10-2). These steep-sided hills and ridges generally lack colluvial debris around their bases; presumably this material is buried beneath the alluvium that surrounds them. It seems that these bedrock "islands" represent the ridges and peaks of a formerly high-relief topography that is subsiding beneath Central Valley sediments.

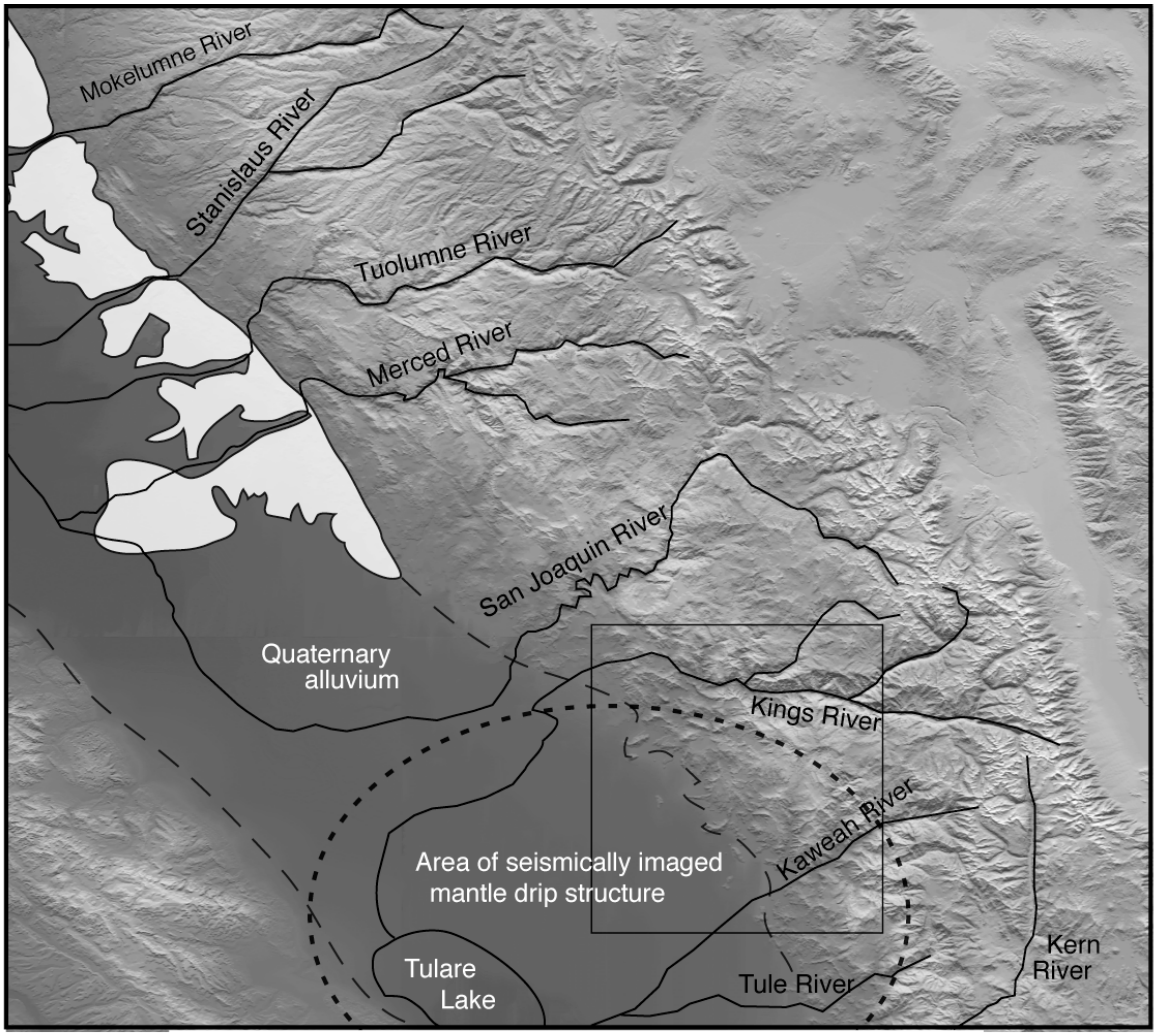

Figure 10-1. Stratigraphic and geomorphic setting of the southwestern foothills of the Sierra Nevada. Outcrops of Tertiary strata of the Superjacent Series are shown in white. The dashed line marked the extent of Quaternary alluvium of the Central Valley. Note that south of the San Joaquin River the unconformity between the Tertiary strata and Sierra Nevada basement bends eastward and the Tertiary strata disappears beneath Qautarnary alluvial deposits, burying basement topography. The boxed area is shown in Figure 10-2. The circular area approximates the area of the seismically-imaged upper mantle drip structure, positioned roughly beneath the Tulare Lake Basin. Before agricultural diversion, southern Sierra Nevada rivers flowed into this closed basin, never reaching the Pacific Ocean.

A final important and unusual aspect of the southwestern foothills relates to range scale drainage patterns. Southern and central Sierra Nevada rivers north of, and including, the San Joaquin River flow westward out of the Sierra and turn north upon reaching the Central Valley, ultimately reaching the Pacific Ocean via San Fancisco Bay. South of the San Joaquin River, however, the Kings, Kaweah, Tule, and Kern rivers are instead diverted into the closed Tulare sub basin (Fig. 10-1). Until the rise of industrial agriculture and major water diversion in the Central Valley, this basin contained wide, shallow Tulare Lake. Though development of Tulare sub basin and deflection of the Kings River southward into it is likely in part climatically-controlled (Atwater et al., 1986), a structural control is favored for its general development (Davis and Green, 1962).

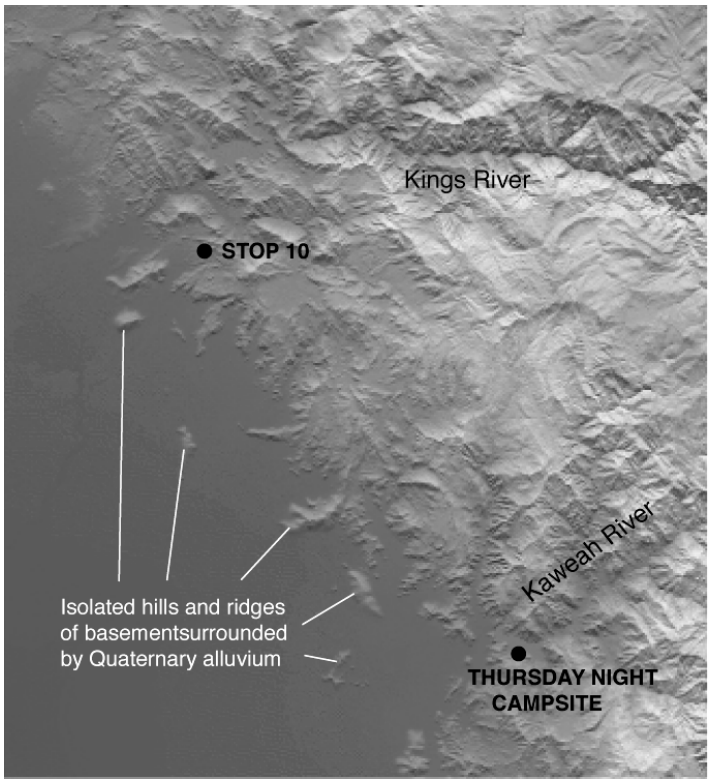

Figure 10-2. Expanded view of buried topography in the vicinity of the Kings and Kaweah rivers. Isolated hills and ridges composed of Sierra Nevada basement (primarily granitic) rocks are surrounded by Quaternary alluvium of the San Joaquin Valley. The broad exposures of Tertiary strata (Superjacent Series) separating basement rocks from Quaternary alluvium in the northern and central Sierra Nevada are buried by Quaternary alluvium in this region.

MANTLE "DRIP" BENEATH THE SOUTHWESTERN SIERRA NEVADA

Appendix 5 outlines evidence for Pliocene delamination of the batholithic root from beneath the southern Sierra Nevada crest. Much of this evidence comes from seismic and magnetotelluric data indicating that the crust is thin (~35 km) beneath the crest of the Sierra Nevada and is underlain by convecting asthenosphere (e.g. Jones et al., 1994; Wernicke et al., 1996; Ruppert et al., 1998). In contrast, along the southwestern margin of the range the crust thickens to ~42 km (Ruppert et al., 1998). In this region, a domain of high P-wave seismic velocities is resolved (Jones et al., 1994; Ruppert et al., 1998). This domain has been imaged as a "drip" structure in the mantle (Jones et al., 1994), and is interpreted as having a greater density than the surrounding mantle by about 100 kg/m^3. The density difference is thought to be due to its eclogitic composition,

which is well represented in xenoliths within Miocene volcanic rocks (e.g., Ducea and Saleeby, 1998).

Saleeby et al., (2003) interpret the high-density mantle drip structure and the adjacent upwelling asthenosphere as a Rayleigh-Taylor convective instability. As the drip descends into the mantle, modeling predicts that the downward flow field ought to dynamically draw down the surface above it (Davies, 1999). As seismic imaging places the drip structure beneath the southwestern foothills, such dynamic drawdown presents an appealing explanation for the buried topography and lack of Tertiary strata in this region. Foster and Saleeby (2003) hypothesize that Pliocene-recent subsidence in the Tulare sub-basin has accompanied the most vigorous phase of drip formation - we may presently be in the midst of the most vigorous phase.

CONCLUSIONS

The anomalous stratigraphic setting, buried topography, and structural Tulare sub-basin in the southwestern Sierra Nevada suggest subsidence of this region in the Pliocene-present. This subsidence may relate to the seismically imaged mantle "drip" structure beneath the region, in which high-density mantle lithosphere is being convectively removed (Saleeby et al., 2003). Dynamic drawdown of the surface topography during drip formation may be actively subsiding the southern Sierra Nevada foothills beneath the level of Quaternary alluvium in the Central Valley, burying the basement rock topography and Tertiary strata in this region (Foster and Saleeby, 2003). Tilted Central Valley strata may record both crestal uplift of the Sierra Nevada and basin subsidence due to this dynamic drawdown.

REFERENCES CITED

Atwater, B. F., Adam, D. P., Bradbury, J. P., Forester, R. M., Mark, R. K., Lettis, W. R., Fisher, G. R., Gobalet, K. W., and Robinson, S. W., 1986, A fan dam for Tulare Lake, California, and implications for the Wisconsin glacial history of the Sierra Nevada. Geological Society of America, Bulletin, v. 97, p. 97-109.

Bartow, J. A., 1991, The Cenozoic evolution of the San Joaquin Valley, California: U. S. Geological Survey Professional Paper 1501, 40 p.

Bateman, P. C., and Wahrhaftig, C., 1966, Geology of the Sierra Nevada, in Bailey, E. H., ed., Geology of northern California, California Division of Mines and Geology Bulletin, v. 190, p. 107-172.

Davis, G. H., and Green, J. H., 1962, Structural control of the interior drainage, southern San Joaquin Valley, California: U. S. Geological Survey Professional Paper 450D, p. D89-D91.

Ducea, M. N., and Saleeby, J. B., 1998, A case for delamination of the deep batholithic crust beneath the Sierra Nevada: International Geology Review, v. 40, p. 78-93.

Foster, Z., and Saleeby, J., 2003, Topographic response to mantle lithosphere removal in the southern Sierra Nevada region, California: GSA Abstracts with programs, Annual Fall Meeting, Seattle, WA.

Jennings, C., 1977, Geologic map of California: California Division of Mines and Geology, scale 1:750,000.

Jones, C. H., Hanimori, K., and Roeker, S. W., 1994, Missing roots and mantle "drips": Regional P_n and teleseismic arrival times in the southern Sierra Nevada and vicinity, California: Journal of Geophysical Research, v. 99, p. 4567-4601.

Ruppert, S., Fliedner, M. M., and Zandt, G., 1998, Thin crust and active upper mantle beneath the southern Sierra Nevada in the western United States: Tectonophysics, v. 286, p. 237-252.

Saleeby, J., Ducea, M., and Clemens-Knott, D., 2003, Production and loss of high-density batholithic root, southern Sierra Nevada, California: Tectonics (in press)

Unruh, J. R., 1991, The uplift of the Sierra Nevada and implications for Late Cenozoic epeirogeny in the western Cordillera: Geological Society of America Bulletin, v. 103, p. 1395-1404.

United States Department of the Interior

NATIONAL PARK SERVICE
Sequoia and Kings Canyon National Parks
47050 Generals Highway
Three Rivers, California 93271-9651
(559) 565-3341

IN REPLY REFER TO:

A8219
8/8/03

Greg Stock
Earth Sciences Department
University of California, Santa Cruz
Santa Cruz, CA
95064

Dear Mr. Stock,

We are happy to learn of your interest in Sequoia and Kings Canyon National Parks. We will expect your group of geologists on Oct. 3-5, 2003, for access through the Hwy. 198 and Hwy. 180 entrance stations. Please present a copy of this letter for each vehicle that enters and leaves the parks. Fees are waived for bona fide, chartered educational institutions conducting an organized trip in the park for educational or scientific purposes related to the resources of the area.

If you wish to visit one of our visitor centers, please contact park staff at Ash Mountain (559) 565-3719. We hope you have a rewarding, enjoyable, and educational experience.

Sincerely,

Erik Öberg
Park Ranger

Visit us on the internet at: http://www.nps.gov/seki